A MATHEMATICAL MODEL FOR THE SUSPENSION POLYMERISATION OF VINYL CHLORIDE

by

DAVID GERALD KELSALL

A thesis submitted for the degree of
Doctor of Philosophy of the University of London
and for the
Diploma of Membership of Imperial College

MARCH 1985

Department of Chemical Engineering
Imperial College of Science and Technology
London SW7 2BY

ABSTRACT

A number of models have been developed before to describe the bulk heterogeneous polymerisation of vinyl chloride; they are often applied to suspension polymerisations. However, they are restricted and idealised in their approach. The aim of this research has been to develop a realistic model for poly vinyl chloride suspension polymerisation which (i) describes accurately the chemical kinetics, (ii) is based on the observed morphological development of precipitated PVC particles, (iii) incorporates mass transfer of molecular species between the various phases present, and (iv) can take account of changes in the process conditions.

In order to develop the model, a set of conservation equations was written for all the molecular species taking part in the polymerisation (ie, initiator, monomer, growing radicals and formed polymer) allowing for morphological development in the multi-phase system. A generating function was then used to reduce the number and complexity of the equations requiring solution. Equations for the moments of the polymer molecular weight distribution were thus derived. These were solved numerically on a computer.

The system of differential equations developed was very 'stiff': small integration timesteps were required to obtain satisfactory model solutions. Various ways of reducing the stiffness were considered in order to minimise the computer time used. Numerical inversion of the generating function was also considered in an attempt to derive the full molecular weight distributions: it is shown to be unsatisfactory.

An analytic solution was derived for a limiting case of the model, allowing the accuracy of the numerical solution to be tested. The analytic solution was manipulated to reproduce most of the features of experimentally observed rate profiles. It could not however predict molecular weight behaviour. The sensitivity of product characteristics and autoclave behaviour to model parameters, initiator loadings and process conditions was demonstrated using both

the full numerical and the analytical solutions. Simple design rules for PVC autoclaves were developed.

Models of PVC particle aggregation, autoclave pressure and mass transfer were also used to analyse the effect of process conditions on the polymer properties.

The final model is thus able to describe the suspension polymerisation of vinyl chloride over the entire conversion range.

ACKNOWLEDGEMENTS

I would like to thank all those people who have helped me during the course of my research. There are some who have given special support for which I am particularly grateful.

Stephen Richardson, of Imperial College, Andrew Gilchrist (industrial supervisor), Peter Smallwood, Mike Allsop and Robin Burgess, all of ICI Plastics and Petrochemicals Division (ICIPPD) each gave encouragement, support and guidance at various stages of the project. Thomas Sippel-Dan, Mary Symons and Hillary Hughes helped to get the best from the Imperial College computer system. Peggy Browett and Caroline Fletcher tracked those elusive references. Oliver, Chris, Martin, Clive, George and Marcus were valued friends and fellow students.

The experimental staff in the PVC Research Section of ICIPPD were always prepared to assist and to discuss ideas with me, during my brief periods with them. Ron Hanson and Nigel Pinnock were especially helpful. However Martin, Adrian, Ray, Russ, Gordon and Derek all made me welcome there.

I was grateful for financial support from the SERC and ICI Plastics and Petrochemicals Division under the CASE Award scheme. I greatly appreciated the opportunity of interacting with the scientists, engineers and experimental officers mentioned above. I thank them for listening to my talks, and for supervising my reactor studies on the PVC Semitechnical Plant at Welwyn Garden City.

I met Matthew West almost by chance through Stephen Richardson. He studied the polymerisation of polystyrene using similar methods to those outlined in this thesis. The value of meeting someone who has had similar problems and overcome them, albeit in a slightly different way, is incalculable. I thank him for that valuable day's discussion.

In helping to produce this thesis, David Stroud did an excellent job with some of the diagrams in Chapter 6, while Jane Buss worked wonders in typing the manuscript. My employers, The Insurance Technical Bureau gave continual encouragement and support.

Geoff Maitland was a valuable supervisor. His comments were always pertinent and I believe our discussions together enlightened our understanding of polymerisation processes. I look forward to our continued friendship.

Finally, I would like to thank all my family and Sylvia, for their continued interest and unending support.

CONTENTS

LIST OF FIGURES

CHAPTER FOUR

CHAPTER FIVE

CHAPTER SIX

LIST OF TABLES

CHAPTER FIVE

CHAPTER SIX

CHAPTER ONE

INTRODUCTION

Poly vinyl chloride (PVC) is a long chain molecule composed of vinyl chloride (VC) monomer molecules ($CHCl = CH_2$). The chain is essentially linear with a small number of short branches off a main chain, whose length is typically about 1000 monomer units. The chlorine atoms on neighbouring monomer units show a slight tendency to alternate above and below the molecular plane as illustrated in Figure 1.1. This type of stereoregularity is known as syndioactivity and the degree of stereoregularity is reflected in the crystallinity of PVC, which is only 10 to 15%.

Figure 1.1

The PVC Molecule

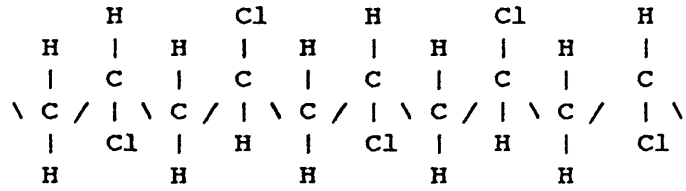

In its unprocessed form, PVC is a white powder which is relatively unstable when exposed to heat or light. Stabilisers are almost always used to prevent the initiation of the chlorine radicals responsible for decomposition. In addition, plasticisers, or molecular lubricants, such as dioctyl phthalate are used to ease processability.

Vinyl chloride is polymerised commercially at temperatures in the range 40°C to 80°C at pressures upto 16 atmospheres. The higher pressures ensure that the vinyl chloride remains as a liquid in the reactor; it normally boils at -14°C under atmospheric pressure. The polymerisation proceeds via a free radical mechanism: the free radicals being shortlived, reactive molecules, which have at least one lone electron available for the formation of a covalent bond. The free radicals add to VC molecules, opening up the double bond and

forming another, longer free radical. (Figure 1.2). Reactive chemicals, called initiators, such as organic peroxides, which undergo thermal decomposition are used as ready sources of nascent free radicals. Chain termination occurs when two growing radicals meet to produce a longer chain which cannot grow. As the polymerisation proceeds the 'dead' PVC chains are precipitated from the liquid VCM as solid 'globules', even at low conversions. The reaction is highly exothermic and the removal of heat is of vital importance to the success of the polymerisation.

Figure 1.2

Free Radical Polymerisation

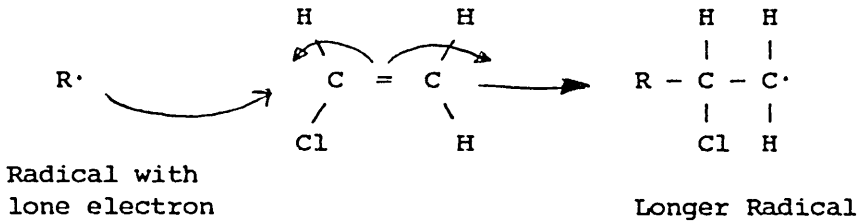

The most common method of polymerisation is suspension polymerisation. The vinyl chloride and initiator are agitated with water and a small amount of a protective surfactant such as polyvinyl alcohol to form droplets approximately 40μm in diameter. These droplets polymerise and are recognisable as subgrains within the final PVC grains, 150μm in diameter.

Emulsion polymerisation is very similar in operation to suspension polymerisation. Much higher concentrations of emulsifier are used to form colloids approximately 1μm in diameter. Polymerisation proceeds within the micelles of the colloid dispersion. Emulsion PVC is consequently much more impure than suspension PVC. However, as with the suspension process, the process water is vital for good heat transfer.

Bulk polymerisation makes the smallest contribution to overall PVC tonnage. It is a difficult process to control: there can be localised overheating problems due to the insulating properties of PVC and VC; water is not used as a dispersion medium. Bulk PVC not only has the advantage of low amounts of impurity (due to the presence of initiator decay products) but its method of manufacture achieves process economies with the need not to dry the product.

By whatever route it is produced PVC has a wide variety of applications, eg extruded films, cables, pipes and sheets, moulded bottles and coatings for papers and fabrics. The diversity of applications reflects the degree of control the manufacturer has over his process to produce a variety of grades of PVC. By altering process operating conditions, he can modify a wide range of physical properties including morphology and molecular weight enabling different stabilisers and plasticisers to be used to achieve the desired processability.

The value of a process mathematical model

The production scale for bulk polymers, including PVC, means that small improvements in process efficiency can have a significant effect on production costs. Since it is the difference between these costs and the price the manufacturer may ask for his product which determines the profitability of his process, there are large incentives to improve process efficiency. He can do this in a number of ways, eg by changing (a) his use of available manpower, (b) his process design, (c) his operating conditions and (d) his recipe, or any combination of these. The basis for making improvements in efficiency is, of course, a complete understanding of the physics, chemistry, engineering and management of the (polymerisation) process.

Although PVC, and its manufacture, have been extensively studied to this end for almost forty years, advances in analytical chemistry and computational techniques coupled with enormous reductions in the real cost of computing, make process mathematical models increasingly

viable aids for studying any process. In general, process mathematical models offer a number of benefits. They are:-

(a) Gaining a deeper understanding of the physical and chemical processes of polymerisation.

The act of writing a model down can clarify what is known and what must be deduced about a process.

(b) Screening a large number of available process options in, for example, the recipe or operating conditions.

These can be assessed prior to experimental studies of the most promising combinations of process operating conditions.

(c) Developing new, or improved, process control strategies for, or otherwise modifying, existing batch process.

Modifications can be assessed for their likely contributions to savings in the duration of the process cycle. (Further, for developing sophisticated feedforward controllers the existence of an accurate process model is essential for programming the controller).

and, finally,

(d) Developing new processes.

Continuous processes are generally more economic to operate than batch processes: they have to be satisfactorily developed for the manufacture of PVC.

Scope of this Thesis

Many theoretical models have been suggested for the polymerisation of vinyl chloride. However they all suffer from

deficiencies and are not generally applied to commercial processes. They are unsatisfactory for three main reasons:

(a) their treatment of heat and mass transfer; these effects are either assumed to be negligible or to happen so rapidly that an equilibrium is achieved: 'effective' kinetic parameters are thus generated;

(b) their neglect of morphology and its development;

(c) their use of kinetic rate constants.

True values of constants are rarely available, partly because of the approach adopted in (a), and partly because of the sparsity of appropriate, accurate experimental observations. Different workers tend to use different values for rate constants.

The principal aim of this thesis, therefore, is to develop a new process mathematical model for the polymerisation of vinyl chloride which addresses those deficiencies, and which is capable of predicting the effect of changes in process variables on the nature of the polymer produced in commercial reactors.

A rigorous approach has been adopted, with each stage of the model development having its basis in known physical and chemical kinetic processes of the polymerisation, including morphological development.

As a consequence of the approach adopted, the model can predict for a batch reactor, amongst other things:

* reaction rates
* molecular weight and its distribution
* porosity

as functions of time, or conversion, based on:

* initial recipe

* polymerisation temperature

and * a supplied primary particle flocculation rate.

Not only does the model have a predictive capability, but it correlates existing experience well. The model therefore has widespread application in studying existing process operation (eg reactor audit studies), process control and process design.

This has been an extensive study of the fundamental processes of vinyl chloride polymerisation. Model development has required the consideration of a large number of chemical and physical processes:

* chemical kinetics
  - initiation, propagation and termination reactions, together with various modes of chain transfer

* heat transfer
  - within the reactor and within polymerising particles

* mass transfer of various species
  - between phases in the reactor and within heterogeneous polymerising particles

* morphological development
  - considering simple models for nucleation, flocculation and coalescence of polymerising PVC particles.

The Structure of the Thesis

The structure of the thesis reflects the rigorous approach adopted in setting up and solving the model. Working from first principles, the narrative description of physical and chemical processes contributing to the overall polymerisation process preceeds the most general mathematical statement of the multicomponent, multiphase polymerisation model in Chapter 3. Subsequent chapters outline the solution methods and necessary approximations for satisfactory solution of this model. The final stages of the thesis

consider the response of the model to various parametric changes and the conclusions that can be made from observations of those responses.

The first part of Chapter 2 is therefore concerned with outlining both the technology and the underlying physical and chemical processes of vinyl chloride polymerisation. The final part of that chapter is a review of existing polymerisation models for vinyl chloride.

In Chapter 3 the phases taking part in the overall polymerisation are identified and a most general mathematical statement of mass conservation is made, both for the chemical kinetic terms and for the mass transfer terms linking the phases. A detailed description is derived for the chemical kinetics of each phase.

The model derived in Chapter 3 is ultimately a complex and difficult model to solve. In Chapter 4 the mathematical armoury required is explained, together with important observations about the 'conservation of mass' and 'stiffness' - two of the main problems in model solution. Some of the approximations necessary for satisfactory solution are outlined. The numerical solution relies upon integrating coupled ordinary differential equations for the moments of the molecular weight distribution, derived by transformation of the infinite number of mass conservation equations. However an important section of Chapter 4 deals with alternative solution methods suggested in the literature. These generally proved unsuccessful, but have been included because of their importance to future workers in this field.

In Chapter 5 an analytic solution is presented which agrees with and validates the numerical solution, under the constraints applicable to the analytic model. Chapter 5 also contains a collection of the models for other aspects of product polymer properties, together with values of rate constants used in the sensitivity analyses.

The results of the analytic model and the full numerical model

are presented in Chapter 6. Most of the parameters of the model are changed, over at least one order of magnitude to assess their influence on the predictions of the model. The changes are generally presented in graphical form.

Chapter 7 is the final chapter and is devoted to concluding remarks and recommendations for future work.

CHAPTER TWO

REVIEW OF VINYL CHLORIDE POLYMERISATION

Vinyl chloride is polymerised by three main routes:

(1) Suspension polymerisation accounting for about 83% of processes.
(2) Emulsion polymerisation accounting for 10% and
(3) Mass (or bulk) polymerisation, 7%.

Although polymerisation is undertaken in a variety of ways, downstream processing (such as monomer stripping, polymer isolation and drying) tends to vary only in the way it is performed rather than exploiting any alternative physical mechanism for the particular operation.

The influence of downstream processing is relatively minor: the overall philosophy is to minimise exposure to excessively high temperatures; poly(vinyl chloride) is particularly susceptible to thermal degradation. The reactor represents the crucial stage in manufacture, for it is there that the ultimate physical properties will principally be determined. Some of the most important properties include molecular weight and its distribution, bulk or apparent density, porosity, pore size distribution, melt flow index, plasticiser absorption characteristics, particle size and its distribution and the level of impurity in the polymer. By altering the process conditions, polymers with a diverse range of properties can be produced. A typical commercial range is shown in Table 2.1.

TABLE 2.1

The ICI "Corvic" Range of Vinyl Chloride Polymers

Suspension Homopolymers

Grade	Characteristics	Application
S71/102	General purpose High m.w. porous easily processed particles	Plasticised composition for film extrusion with few fish eyes; injection moulding
S68/173	Medium m.w. High packing density	Unplasticised compositions for extrusion of pipes etc at high rate
S67/111	Medium m.w. av. packing density similar to S71/102	Unplasticised compositions for pipes, sections etc. and plasticised compositions for films, sheeting and flooring
S67/113	Similar to S67/111 but with good electrical insulation characteristics	Plasticised compositions for cable covering
S62/109	Medium m.w. for products of excellent crystal clarity	Unplasticised compositions for extrusion of complex sections; highly plasticised for calendering of sheets, eg vinyl flooring
S57/116	Low m.w. good melt flow for products of excellent crystal clarity	Blow moulding of bottles, injection moulding of pipe fittings

In order to explain the polymerisation process, the study in this chapter will be divided into two broad sections. The first part will be devoted to a study of the suspension polymerisation process and the second part (Section 2.4 et seq) will be concerned with the physical and chemical mechanisms which form the basis of VCM polymerisation.

In Section 2.1 we will consider the basic concepts behind, and the operation of, a suspension PVC process. Section 2.2 will show how a process operator can influence the polymer product properties by altering the process operating conditions. The final section of this part (2.3) will compare the suspension process with bulk and emulsion polymerisation processes for vinyl chloride.

Section 2.5 will be concerned with the microscopic and macroscopic development of PVC morphology, and Section 2.6 will be devoted to a review of the major contributions to understanding the kinetic mechanism.

A number of review articles and books have appeared in the literature relating to PVC manufacture (1,2,3,4,5). The discussion of polymerisation processes will therefore aim to highlight those aspects which will be important in developing a process model.

2.1 SUSPENSION POLYMERISATION

2.1(A) Basic Concepts

In any free radical reaction the basic chemistry may be explained by the following mechanism.

(a) Initiator Decomposition

Nascent free radicals are formed by the symmetric decomposition of initiator molecules

(1) $$I \xrightarrow{k_D} 2R\cdot \qquad ; \qquad \frac{d[I]}{dt} = -k_D[I]$$

where [I], [R·] represent the concentrations of initiator and nascent free radical molecules respectively.

(b) Propagation

Monomer is able to add to free radicals to form (larger) growing chains.

$$R\cdot + M \xrightarrow{k_p} R_1\cdot$$

$$R_1\cdot + M \xrightarrow{k_p} R_2\cdot$$

$$R_x\cdot + M \xrightarrow{k_p} R_{x+1}\cdot \quad ; \quad \frac{d}{dt}[R_{x+1}\cdot] = k_p[R_x][M] \qquad (2)$$

where $[R_x]$,[M] represent the concentration of growing radicals of chain length x and monomer respectively.

(c) Termination

Radicals can lose activity in a number of ways

(i) Combination

$$R_x\cdot + R_y\cdot \xrightarrow{k_{tc}} P_{x+y} \quad ; \quad \frac{d}{dt}[P_{x+y}] = k_{tc}\,[R_x\cdot][R_y\cdot] \qquad (3)$$

where $[P_{x+y}]$ represents the concentration of dead (inactive) polymer of chain length (x+y).

(ii) Disproportionation

$$R_x\cdot + R_y\cdot \xrightarrow{k_{td}} P_x + P_y \quad ; \quad \frac{d}{dt}[P_x] = k_{td}\,[R_x\cdot][R_y\cdot] \qquad (4)$$

(iii) Chain Transfer

Radical activity is transferred to another species such as monomer, solvent or dead polymer.

$$S + R_x\cdot \xrightarrow{k_{trs}} P_x + S\cdot \quad ; \quad \frac{d}{dt}[P_x] = k_{trs}[R_x\cdot][S] \qquad (5)$$

The polymerisation of vinyl chloride however is further complicated by the interaction between PVC and VCM. The PVC formed as a result of the polymerisation is virtually insoluble in the VCM and precipitates from it at very low conversions as a denser phase swollen by VCM. The density of PVC at 50°C is 1400kgm^{-3}: for VCM it is 850kgm-^{3}.

Precipitation and phase separation in polymer solutions can be explained in terms of an equilibrium process. The Flory-Huggins theory (7) represents a fairly successful but approximate treatment. Using the theory, partial molar free energies may be obtained for solvent and polymer. The partial molar free energy is the free energy change per mole of component added, when an infinitesimal amount is added to a system with all other amounts of components remaining constant.

For solvent (VCM)

$$\Delta\bar{G}_1 = (\partial\Delta G/\partial n_1)_{n_2} = RT\{\ln\phi_1 + \phi_2(1 - 1/m) + \chi\,\phi_2^2\} \qquad (6)$$

and for polymer (PVC)

$$\Delta\bar{G}_2 = (\partial\Delta G/\partial n_2)_{n_1} = RT\{\ln\phi_2 + \phi_1(1 - m) + \chi m\phi_1^2\} \qquad (7)$$

where ΔG is the free energy

R, T have their conventional meanings

ϕ_1, ϕ_2 is the volume fraction of solvent (VCM) and polymer in the system respectively ($\phi_1 + \phi_2 = 1$).

m is the degree of polymerisation (average chain length) of the polymer

χ is the Flory interaction parameter.

At equilibrium the free energy of the system is at a minimum. The transfer of an infinitesimal amount of any component from one phase to another will produce no change in free energy: the chemical potential of each component is equal in both phases.

The precipitation of PVC from VC implies a large value of χ (~1.0); the two phases are nearly pure solvent (VCM) and slightly swollen polymer. The volume fractions of VCM in the polymer and polymer in the VCM can be obtained (approximately) by putting the corresponding expressions for $\Delta\bar{G}$ equal to that of the pure component, which is zero. The volume fraction of VCM in the polymer phase is given by $\phi_1 \simeq e^{-(\chi+1)}$ (setting $\Delta\bar{G}_1 = 0$) and the volume fraction of PVC in the VCM phase is given by $\phi_2 \simeq e^{-m(\chi-1)}$ (setting $\Delta\bar{G}_2 = 0$). Moreover, the change partial molar free energy when a pure liquid A passes from the pure liquid state with vapour pressure p_{Ao} to a solution vapour pressure P_A is given by

$$(8) \qquad \Delta\bar{G}_A = (\partial\Delta G/\partial n_A)_{ni,i\neq A} = RT \ln \frac{P_A}{P_{AO}}$$

Equating with (6) gives the vapour pressure above a polymer solution:-

$$(9) \qquad \ln \frac{P_1}{P_{1o}} = \{\ln\phi_1 + \phi_2(1 - 1/m) + \chi \phi^2{}_2\}$$

where P_{1o} is the saturated vapour pressure of the solvent, VCM.

2.1(B) A Typical Suspension Process

There are several ways of performing the polymerisation: suspension polymerisation is the most important method for PVC manufacture. A typical process flowsheet is shown in Figure 2.1. (2)

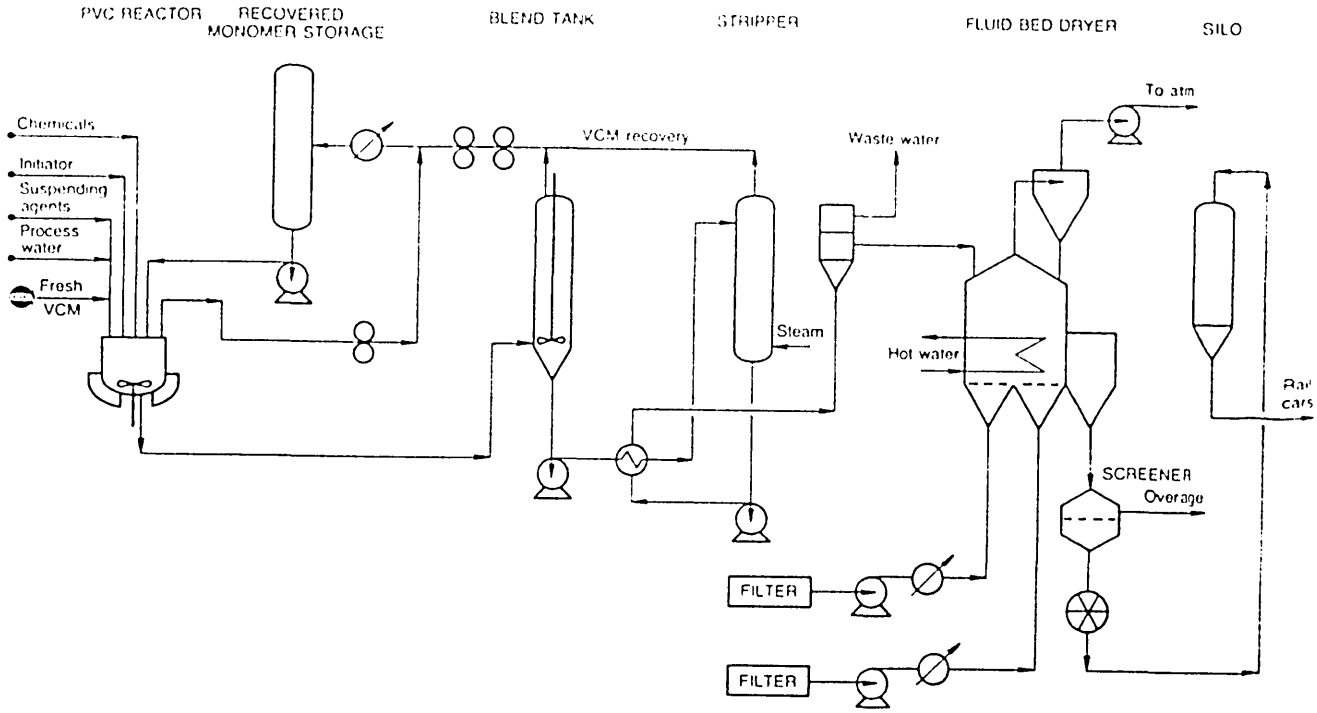

Figure 2.1 A Typical Suspension PVC Process

In the suspension process, VCM droplets stabilised by the action of adsorbed surfactants are suspended in water by the action of an agitator within an autoclave. The water acts as a heat transfer medium, with polymerisation proceeding within each drop as if it were a micro-bulk reactor.

The process is operated batch wise, so that when polymerisation is completed within the reactor, the slurry which has formed is forced downstream (by the application of pressure in the reactor) to a stripper. Within the stripping section, any VCM remaining as monomer swelling the slurry is released by steam sparging the slurry. VCM is subsequently recovered from the steam before being reused in a future batch.

The 'VCM free' slurry is centrifuged and dried in hot air dryers before being screened (sieved) and packed for shipping to the customer.

2.1(C) Operation of the Suspension Reactor

For a typical polymerisation in a $10m^3$ autoclave, the charge is (1):-

Water	5000kg
Stabilising Surfactant	3.5kg
Buffer	0.7kg
Initiator	1.5kg
Vinyl Chloride	3500kg

Components are carefully metered into the autoclave according to an operating schedule which ensures batch-to-batch reproducibility.

Process water, stabilising surfactant and initiator are mixed by agitation. The reactor is purged with nitrogen and evacuated to remove oxygen which inhibits polymerisation. VCM is added and agitation continued until the VCM is adequately dispersed. After sufficient agitation the autoclave is heated up to the desired polymerisation temperature. One way of heating up is by the injection of steam into water circulating in the autoclave jacket. (Alternatively, steam may be supplied directly to the autoclave jacket or electrical heaters). Initially any heat of reaction (ΔH_p = -1540kJ/kg VCM) is used to aid the heating up of autoclave contents. However as the desired polymerisation temperature is approached, the heat of reaction must be removed from the reactor. Cooling water supply replaces the steam supply to the jacket. The continued autoacceleration of the polymerisation requires increasing amounts of cooling water to be supplied to the jacket, forcing the jacket temperature to continually drop. When the reaction approaches high conversions the rate maximises and begins to fall: the requirement for cooling water is diminished and the jacket temperature rises (Figure 2.2). If the maximum rate of reaction and, therefore, maximum rate of heat evolution exceeds the capacity of the cooling system, 'runaway' conditions will exist in the reactor and the temperature of the autoclave will rise uncontrollably.

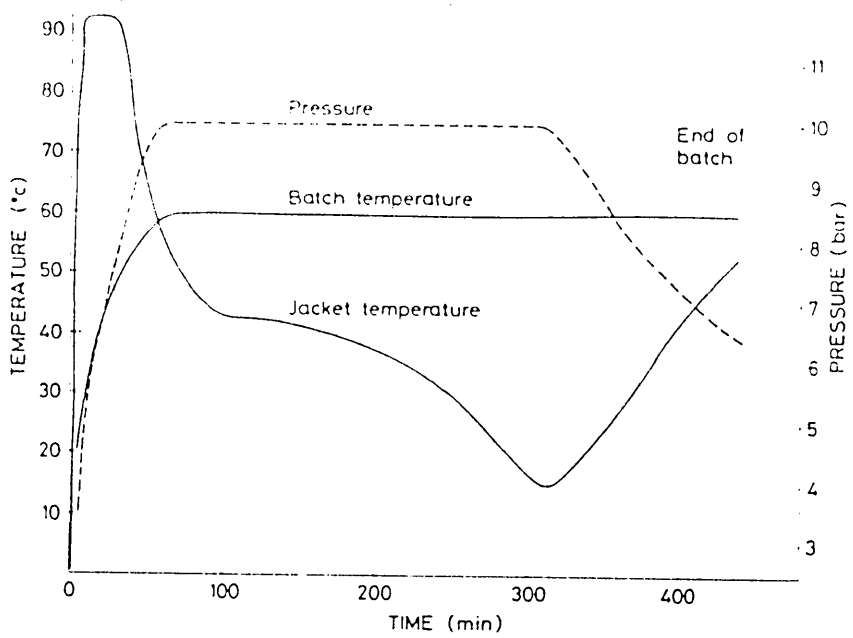

Figure 2.2 A Typical Suspension Polymerisation Reaction (1)

The pressure within the reactor remains at the saturated vapour pressure of vinyl chloride at the reaction temperature until the later stages of polymerisation (c.a. 75% conversion) when it starts to fall, as the VCM moves by mass transfer from the vapour phase through the water to the suspended polymerising VCM/PVC. All the liquid monomer in contact with the precipitated PVC/VCM gel has disappeared, with subsequent polymerisation taking place at the expense of the monomer swelling the polymer, which can only be replaced from the vapour phase. Providing that the mass transfer of monomer between phases is effectively instantaneous the variation of vapour pressure with conversion is given to a good approximation by the Flory-Huggins theory (Section 2.1A).

The degree of pressure drop gives a crude indication of conversion and when conversion is c.a. 90% (corresponding to a 40% decrease in pressure) the reaction is usually stopped by venting monomer. At high conversions the rate of reaction is uneconomically low.

During the course of the reaction the initial oily dispersion has become a wet slurry, which must be stripped of VCM and dried. These operations are usually carried out downstream of the reactor, though some stripping may be performed within the reactor. (1)

Before the reactor can be used again any polymer fouling it must be removed; the continued presence of polymer would expose it to the risk of thermal degradation. The occcurrence of degradation products in future batches of PVC would reduce the commerical value of the polymer. Automatic high pressure water spraying systems are used to clean the internal surfaces of the reactor. The amount of fouling by polymer can be controlled by chemical agents (suppresants) which are sprayed onto the internal surfaces.

2.1(D) Stripping Monomer from Polymer

During the course of the mid-sixties and early seventies, it became apparent that vinyl chloride was a highly toxic material. It was linked to two rare diseases, acro-osteolysis (a bone deficiency disease) and angiosarcoma (a form of liver cancer). The impact on the industry was enormous with pressing needs to change working practice, to reduce VCM emissions, monitor atmoshperic VCM levels and to minimise operator exposure to risks. Burgess (1) discusses these aspects at considerable length.

Residual concentrations of VCM in the final polymer had to be reduced by improved stripping of VCM. Much research effort was devoted by manufacturers to developing more porous grades with enhanced stripping performance. Porous grades were also more suitable for applications where plasticiser (a processing agent) had to be added.

Stripping is achieved by sparging the polymer resin with steam, either (a) in the reactor, with the released monomer and saturated steam passing to de-entrainment equipment and to a monomer recovery section of the plant, or, (b) in a packed (or trayed) column by counter-current contacting of slurry and steam.

2.1(E) Drying

Suspending water, which wets both the surface of the PVC and the internal pores of the PVC grain, is removed in two stages. Centrifuging reduces moisture content to about 20%, while secondary drying in purpose designed driers reduces moisture content to 0.5%. Virtually any option is open to the manufacturer depending on his requirements. Lovelock (1) considers in detail the various isolation processes, and the following table summarises his findings.

TABLE 2.2

Advantages and Disadvantages of Principal Drier Types

Drier Type	*Advantages*	*Disadvantages*
1. *Rotary Driers* (a) Indirect heat	Economical to operate. Can dry all grades of PVC.	Large rotating assembly. Difficult to clean. Prone to corrosion of the heating tubes. Difficult to control
(b) Direct heat	Easy to operate and to clean. Can dry all grades of PVC.	Large rotating assembly. Tendency to polymer build-up round inlet air ports and through end seals. Less economical than (a).
2. *Flash Driers* (a) Pneumatic conveying	Easy to operate and to clean. Very simple construction.	Can only dry porous PVC grades. High air temperatures cause danger of degrading some PVC.
(b) Spray	Very high evaporative capacity. Useful when not required for emulsion polymer drying.	Can only dry porous PVC grades. Very large installations with complex atomisation of wet-cake. High air temperatures cause danger or degrading some PVC.

3. *Fluidised Bed Driers* (a) Direct heat	Occupy a small space. Easy to operate and to clean.	Can dry all grades of PVC but has to be fed with a partially dry product. Degradation on fluidising plate is possible.
(b) Indirect heat	Occupy a small space. Can dry all grades of PVC. Economical to operate and maintain.	Corrosion of heating tubes requires special attention. Time consuming to clean. Tendency to overdry product.
4. *Combined Flash/Long Residence Time Driers* (a) 2(a) or (b) plus 1(b) or 3(a)	Very flexible in operation. Can dry all grades of PVC economically.	Has disadvantages of each component.

2.2 FACTORS AFFECTING ULTIMATE POLYMER PROPERTIES

The key stage in the manufacture of PVC is the reactor, where most of the ultimate polymer properties are determined. A large number of factors are significant in the development of the PVC resin (3), among them:-

(a) temperature and its control

(b) initiator, type and concentration

(c) agitation, including effects due to agitation speed, type and operation design of reactor, baffles and cooling system

(d) nature of the agitated medium, which is affected by
water to monomer ratio
water quality
and suspending agent and surfactants.

Amplification of some of these points will demonstrate much of the design and operating philosophy of suspension processes. While each is discussed separately, there is a complex interaction between all the factors, so that small changes in procedure markedly affect the type of polymer produced.

2.2(A) Temperature and its Control

The molecular weight is principally determined by the temperature of polymerisation; it is a function of all the chemical rate processes which are temperature dependant. Billmeyer (7) shows that the molecular chain length for free radical polymerisation, with chain transfer to monomer, is given by,

$$\frac{1}{x_n} = \frac{k_t}{k_p}\left[\frac{f\,k_D\,[I]}{kt}\right]^{1/2}\frac{1}{[M]} + C_m$$

where x_n = the degree of polymerisation

$C_m = k_{trm}/k_p$ and all other symbols are as previously defined.

and its variation with temperature is given by,

$$\frac{d\ln x_n}{dt} = \frac{E_p - E_{trm}}{RT^2}$$

where E_p, E_{trm} are the activation energies associated with polymerisation and transfer to monomer reactions respectively.

Since the molecular weight determines the processability of the polymer, with higher molecular weight polymers being more difficult to deform and extrude, the control of temperature is vital.

Control is achieved both by internal and external means. Internally, the higher heat capacity of water coupled with its higher thermal conductivity compared to both vinyl chloride and polyvinyl chloride, is used in a capacitative manner to moderate internal temperature changes and in a conductive manner to enhance heat transfer to the internal surfaces of cooling elements or jackets.

Externally, heat transfer and control is commonly effected by a recirculating water system with a dual range controller capable of allowing injection of steam, for heating up to polymerisation temperature, or injection of cooling water to remove heat of polymerisation (8).

Recirculating water systems are characterised by high flowrates to achieve a maximum jacket side heat transfer coefficient. Internal cooling surfaces are avoided because of the possibility of fouling and the difficulty in cleaning complex internal geometry.

The autoacclerating nature of the polymerisation means that any failure in temperature control is likely to lead to increased autoclave temperatures, and decreased molecular weight. Failures may arise because of reduction in the internal heat transfer coefficients due to poor agitation, or because the cooling system cannot remove all the heat of reaction at high rates of reaction.

2.2(B) Initiator - Type and Concentration

Vinyl chloride polymerises slowly without the use of initiators which decompose to form nascent free radicals. Initiation is the rate determining step in the polymerisation with the general mechanism for decomposition being:-

$$I \xrightarrow{k_D} 2R$$

with $\frac{d[I]}{dt} = -k_D[I]$ and $\frac{d[R\cdot]}{dt} = 2fk_D[I]$

The factor, f, represents the efficiency of nascent radicals in opening up the double bond of vinyl chloride. AZO-compounds, which decompose with the elimination of a centrally held nitrogen molecule, tend to be less energetic (efficient at initiating radicals) than peroxides which decompose with the splitting of a central O-O bond (1).

As can be seen from the following table, initiators which may be suitable for polymerisations at 50°C would deplete too quickly at 70°C, eg Di(2-ethylhexyl) peroxydicarbonate. Temperature of polymerisation is a vital factor in initiator choice.

TABLE 2.2

Half-lives of Initiators used in VCM Suspension Polymerisation (1)

Initiator	Half-life (min)		
	50°C	60°C	70°C
Azodi-isobutyronitrile	4200	1080	300
Azobis(2,4-dimethylvaleronitrile)	420	120	35
t-Butyl perpivalate	1300	360	100
Dibutyl peroxydicarbonate	300	70	18
Di(2-ethylhexyl) peroxydicarbonate	250	60	15
Di(*t*-butylcyclohexyl) peroxydicarbonate	250	60	15
Lauroyl peroxide	3000	800	200
Benzoyl peroxide	-	3000	800
Acetyl cyclohexylsulphonyl perioxide	80	18	4

The final consideration is how much initiator to use. With too little initiator, the initiator will deplete before all the monomer is consumed. When too much is used the high rates may exceed those which the cooling system may adequately cope with: 'runaway' conditions will occur.

By combining fast and slow decomposing initiators better use may be made of the cooling system. The fast decomposing initiator will give rise to very high initial rates, while the slow one will give rise to higher rates as the fast one depletes. By maintaining high rates throughout the course of polymerisation, the cycle time of batches may be considerably reduced, with maximum use being made of the cooling water system throughout the reaction (Figure 2.2).

2.2(C) Agitation

Agitation has important roles to play both in determining the heat transfer in the autoclave and in dispersing VCM. The action of the agitator is continually to break up vinyl chloride drops to smaller ones. A dispersion of vinyl chloride in water is created

with the monomer droplets having diameters in the range 50–150μm. Unless stabilised by the action of a stabilising surfactant such as hydrolysed PVA or methyl cellulose, these droplets would rapidly coalesce to large monomer droplets. A dynamic equilibrium between the dispersive action in the shear region around the agitator, and the coalescence in quiescent zones away from the agitator is achieved which has been represented diagramatically by Winslow and Matreyek (6).

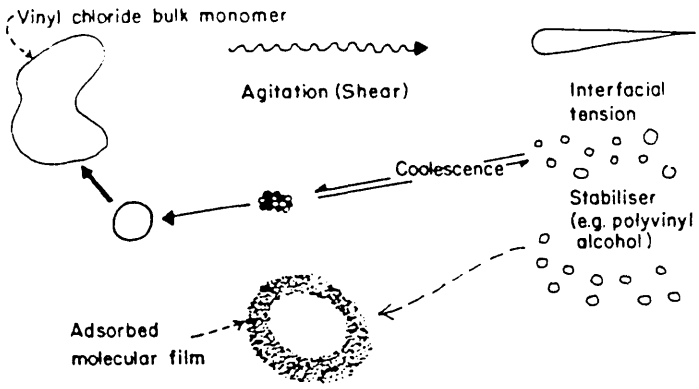

FIGURE 2.3 The Influence of Agitation on Initial Droplet Dispersion

As polymerisation proceeds the effectiveness of adsorbed surfactant alters and there may be a degree of floculation of initially stable drops as the final polymer grains are formed. The balance of dispersion and coalescence will determine to an extent the porosity of the final polymer product.

Agitator Design

Considerable attention has been paid to agitator and reactor design: the development of large reactors (9,10) has required scale-up rules so that large vessels are as well agitated as small ones, both for heat transfer considerations and to aid the development of morphology. A variety of agitators is available, possibly coupled with baffles, to enhance agitation and recirculation within the autoclave, allowing control over relative times spent by monomer droplets in high shear (breakup) regions near the agitator and quiescent (coalescence) zones away from the agitator. Each system will have its advantages and disadvantages which manufacturers must take into account when choosing their system.

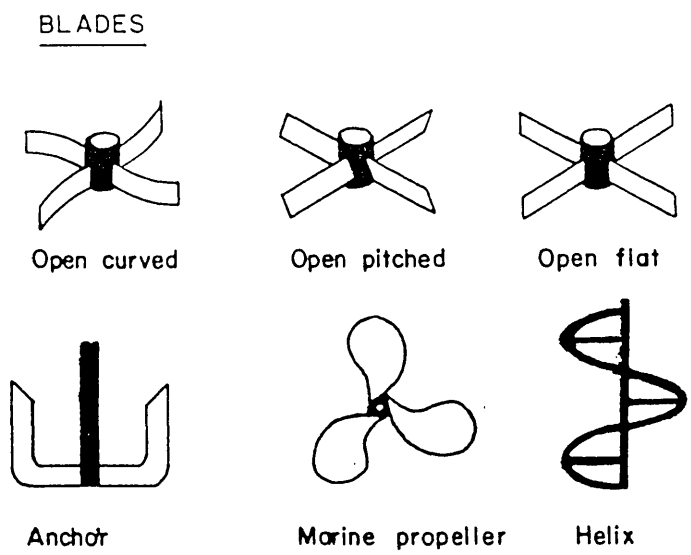

FIGURE 2.4 Agitators for Polymerisation Reactors

2.2(D) The Nature of the Agitated Medium

(i) Water

The polymerising suspension VCM system is one of changing viscosity as dispersed VCM changes to denser PVC. Water plays a vital role in temperature control and in the determination of slurry viscosity. The water/monomer charge ratio is adjusted so that the final slurry viscosities will not exceed those which can be agitated. If the final slurry viscosity is too high, the power required to agitate the slurry at constant speed will exceed that which the stirrer motor can supply. In order to prevent overloading the motor, it would be stopped automatically ('tripped') when this happens. More water would be added to allow further processing. In general the larger the water/monomer ratio, the more porous is the polymer (3).

The quality of the water must also be controlled. Buffers are used to ensure that the pH of the suspending water does not become too low because of the HCl produced by side reactions during the polymerisation. Acidic water affects the abililty of the stabilising surfactants to stabilise droplets.

(ii) Stablising Surfactant

A variety of these chemicals has been tried, among them polyvinyl alcohol (PVA) and methyl cellulose derivatives. All are water soluble polymers with oleophilic substituted groups which adsorb at the vinyl chloride/water interface and offer the vinyl chloride droplet steric stability. The precise degree of stability is determined by the concentrations used. Considerable control over porosity is achieved allowing a variety of grades to meet stripping and plasticiser requirements. Johnston (3) considers the properties of some commercial surfactant systems.

2.3 ALTERNATIVE POLYMERISATION PROCESSES

Although suspension polymerisation is predominant, mass and emulsion processes make up a considerable share of worldwide capacity (c.a. 20%). With reference to suspension polymerisation, both processes can be constrasted.

2.3(A) Bulk Polymerisation

This method has been widely applied to polymerisations where polymer is soluble in its own monomer, such as for manufacture of polystyrene or polymethylmethacrylate. Despite considerable rises in viscosity, reactor temperature control is generally achieved.

However with PVC, where polymer precipitates as 0.1μm primary particles are low conversions (<1%), particularly high viscosity changes are obtained. Further growth and aggregation of primary particles magnifies the control problems of (a) achieving a required particle size distribution, (b) avoiding fouling and (c) overheating.

Rhone-Poulenc (11,1) developed a two stage polymerisation process which overcomes many of the problems. The first stage reactor is used to grow seed polymer from a liquid phase up to 10% conversion. The second stage reactor is used to grow the polymer to a powdery grain, with overall conversions being in the range 70–85%. Cooling is enhanced by using reflux condensers. Process savings are made because the polymer does not have to be dried.

Bulk polymerised PVC has two main advantages over its suspension counterpart:

(1) lower levels of impurity - surfactants are not used.
(2) improved heat stability and dry blending characteristics - there is no skin on the grain.

2.3(B) Emulsion Polymerisation

The process principles for stripping and drying are similar for both emulsion and suspension polymerisation. There are drastic differences in reactor operating conditions. Principally:

(1) High concentrations of soap emulsifiers such as sodium dodecyl sulphate (up to 3% based on VC) are used compared to surfactant concentrations in suspension polymerisation of c.a. 0.1%.

(2) Water soluble initiators and initiator systems are used (eg ammonium persulphate/sodium persulphate and copper sulphate) to allow lower temperature polymerisations than suspension polymerisations, which are usually in the range 50–70°C.

These changes give rise to latex particles with narrow particle size distributions centering on 1μm, compared with suspension grains in the region 50 to 150μm. The emulsion polymers are highly impure because of the amount of emulsifier used.

The classical theories of emulsion polymerisation are due to Harkins (12) and Smith and Ewart (13). In the case of vinyl chloride they have been considerably extended by Ugelstad in a series of papers (14,15,16,17,18).

2.4 BACKGROUND TO PROCESS MATHEMATICAL MODEL

The first part of the chapter has concentrated on the process for the polymerisation of vinyl chloride and looked at the degree of control a manufacturer has over the process. In this work it is aimed to derive a mathematical model which can be used predictively, rather than correlating what has been done before; extrapolating correlations (for example, trying a new polymerisation recipe) is unsatisfactory because the bounds on correlation are not generally precise.

The key to a successful predictive model of any process is writing down the physics and chemistry we believe to be important in an unambiguous manner. All the parameters of the model must have basis in the physics of the process, though ultimately there may be considerable difficulty in their experimental determination. (The models can be used to determine over what range experimental measurements must be done to determine the parameter).

Having developed a mathematical model, we may be unable to solve it in its entirety. Experimental observations may be lacking to provide parameters for the model. More likely, the complexity of the proposed mathematical scheme may prove intractable. A complete solution may require more computational resource than is available.

The intitial mathematical description should however allow sufficient approximation to make the model viable yet still retain the essential features of the process physics.

The understanding of vinyl chloride polymerisation has developed along two main routes. Firstly researchers have looked at morphology and its development during polymerisation, and secondly, effort has

focussed on elucidating the kinetic mechanisms. Both aspects will be considered before the mathematical model is proposed in Chapter 3.

2.5 DEVELOPMENT OF MORPHOLOGY

The development of the morphology of PVC occurs on two difference length scales: macroscopically, the evolution of the initial droplet size distribution can be followed and microscopically the evolution of growing polymer is observed. A variety of terms have been used in the literature to describe all the observed entities. In order to rationalise the nomenclature, Geil (33) proposed that the definitions in Table 2.3 are adopted. Wherever possible these definitions are used in this work.

TABLE 2.3 - PVC Morphology

Term	Approx size in typical PVC	Origin or Description	Former Names
Grain	100μm	Free flowing powder at room temperature	Granule Cellular Grain
Subgrain	40μm	Original monomer droplet	Subgranule Unicell
Agglomerate	10μm	Formed during polymerisation by merging primary particles	Aggregate Cluster Macroglobule
Primary Particle	1μm	Formed from single polymerisation site at conversions 10-50%	Microgranule Primary Particle Granule Microglobule
Domain	100nm	Not clearly proven to exist, formed by mechanical working within or from primary particles	Primary Nucleus Granule
Microdomain	10nm	Crystallite or nodule	Basic Particle

2.5(A) Macroscopic Scale Development of Morphology

The vigorous agitation of an immiscible mixture of water and vinyl chloride (approximately 40% VCM by volume) coupled with the action of stabilising surfactants such as PVA serves to disperse the vinyl chloride as a suspension of droplets of diameter c.a. 40μm. Polymerisation proceeds within the droplet leading to the formation of a contiguous porous network of precipitated polyvinyl chloride. The droplets develop a pericellular membrane (19) which is thought to be a graft copolymer of the stabilising surfactant and the VCM (32). Under certain agitation/stabilising surfactant conditions the polymerising droplet is destabilised; stabilising surfactant is removed by the graft polymerisation causing a change in the nature of the droplet surface (i.e. interfacial tension/modulus) with polymerisation. The polymerising droplets aggregate to form a grain of diameter c.a. 100-150μm.

Johnson (20) has shown a strong correlation (Figure 2.5) between the particle size and its distribution with a modified Weber number, defined by

$$W_e = \frac{\rho N^2 D^3 W}{\sigma \Theta B_w}$$

where ρ is the two phase density
N is the agitator speed
D is the agitator diameter
W is the agitator blade width
σ is the interfacial tension
Θ is the agitator blade angle
and B_w is the baffle width

Physically the Weber number expresses the balance between inertial and surface forces.

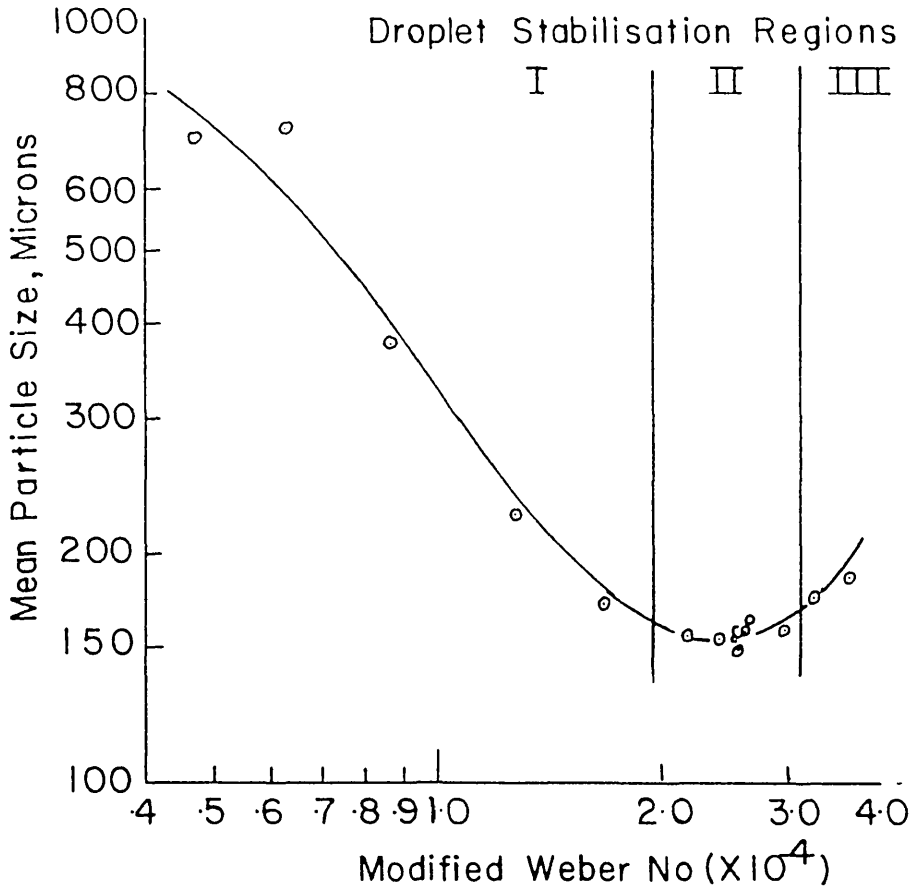

FIGURE 2.5 - Particle Size vs Modified Weber Number

Allsop (1,21) defines three degrees of VCM droplet stability.

(a) Monomer droplets are extremely well protected. Very little coalescence occurs, giving rise to spherical subgrains of low porosity. These effects are associated with region I on the Weber number plot where increasing stirrer speed leads to smaller stabilised droplets.

(b) Intermediate protection of droplets is achieved. The droplets undergo some coalescence, producing an irregular shaped grain of higher porosity. This level of protection corresponds to region II on the Weber number plot where the surface concentration of stabilising agent is at the minimum level affording protection.

(c) Inadequate protection is afforded. The monomer droplets coalesce from low conversions, giving rise to dense, low porosity polymers. This corresponds to region III on the Weber plot where because of high stirrer speed the droplets are too small for complete coverage by surfactant.

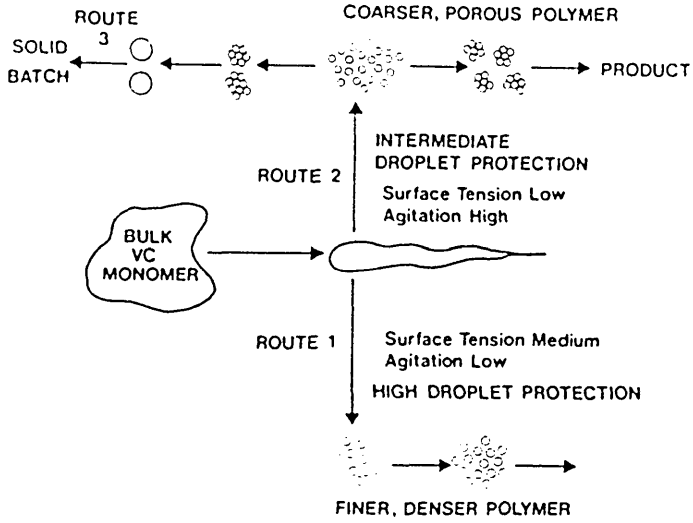

FIGURE 2.6 - Schematic diagram of the effect of VCM droplet stability on the macro-mechanism of polymerisation (1,21)

2.5(B) Microscopic Scale

There is considerable debate about the microphase nature of PVC (see for example 22,23). Some points appear to be well established:

(1) PVC is essentially insoluble in its monomer with the interaction parameter of the Flory-Huggins Equation, χ, of the order 0.9 (24,25).

(2) PVC is much denser than VCM ($\rho_{PVC} \simeq 1400 kgm^{-3}$; $\rho_{VCM} \simeq 850 kgm^{-3}$)

(3) PVC exhibits a small amount of crystallinity (typically 14% (23)).

These observations explain in part why the polymerisation follows a precipitation course within a suspended droplet. They do not explain the development of morphology within the polymerising droplet where a particulate agglomerate structure develops.

The direct experimental observation of the polymer phase as it polymerises has proved difficult, though attempts to use photon correction spectroscopy (26) have proved successful up to ~10^{-2} conversion. Turbidimetry (27) and spinning drop techniques (28) have looked at events in the conversion range 10-30%. The other important technique, of course, is direct observation of samples extracted from polymerising systems, using scanning electron microscopy (SEM). Although this technique offers the possibility of direct observation, its main disadvantage is that in order to obtain samples for SEM analysis polymer structures may be severely disrupted as monomer is vented to release pressure, before samples are transferred from the autoclave to the electron microscope. This disruption is particularly likely at low conversions where polymer structures may not be sufficiently developed to withstand the harsh conditions created in sampling. Nevertheless the technique has been extensively applied by Bort (29,30,31), Davidson and Witenhafer (32) and Tregan and Bonnemayre (19).

The generally agreed growth mechanism within monomer droplets follows a growth and flocculation process.

Growing chain radicals become insoluble at relatively short chain lengths (~10 monomer units) and continue to grow as precipitated coiled macro radicals. The growing chains then aggregate in groups of 50 or so producing small particles know as 'microdomains' with diameters in the region of 200Å. The microdomains then in turn flocculate to form domains (or primary nuclei) of radius 0.1-2μm. This is the first observable event using PCS and occurs up to conversions of 1%.

Any more macroradicals or microdomains formed after the formation of domains will be absorbed by the domains as they grow in size while their total number remains constant up to 3% conversion. The primary

particles eventually destabilise and flocculate as agglomerates with diameters of about 1μm from about 5% conversion upwards.

Further growth of the agglomerates will largely determine grain porosity and apparent density. They continue to grow up to 10μm by surface deposition and internal growth until the polymerisation is terminated at about 95% conversion. The sequence of events is summarised in Figure 2.7.

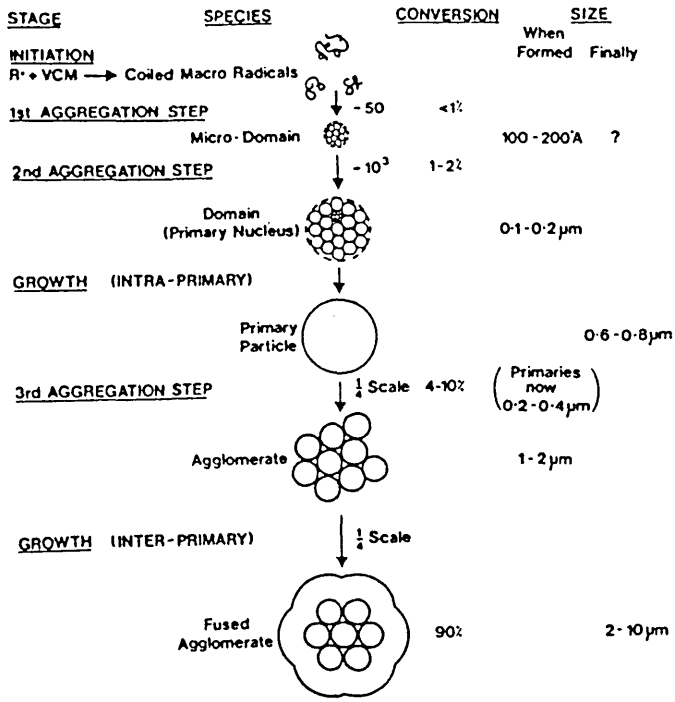

FIGURE 2.7 - Schematic Representation of the Mechanism of VCM Polymerisation (21)

2.5(C) Porosity

Porosity describes the nature of the space between neighbouring precipitated species. It may be applied at two levels. Firstly by describing the interstitial space between the sub-grains or secondly,

and more commonly, by describing the interstitial space between the primary particles and agglomerates within a sub-grain.

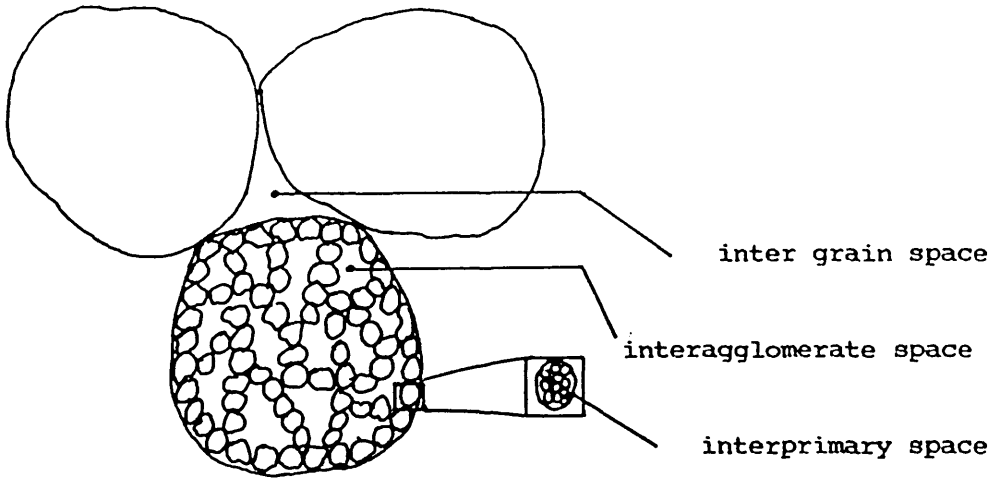

FIGURE 2.8 - Inter and Intra Sub-Grain Pores

Porosity is the cumulative measure of the pore size distribution, measureable by mercury porisimetry. It can be predicted from a complete understanding of the kinetic and aggregative processes occurring within the polymerising system. Even at low conversions (<3%) when no skin has formed round the sub-grains, it exists because of the interstices between primary particles. If polymerisation was terminated with only primary particles present (~1.0% conversion), and the monomer was stripped from the system, the porosity would represent the intersticial space between primary particles. Normally at low conversions any intersticies in the sub-grains would be occupied by free monomer.

The development of porosity implies, too, that the sub-grains have become rigid with the pericellular membrane or "skin" around them structurally prevented from collapsing as polymerisation proceeds. If this were not the case, the denser aggregates, (which are growing at the expense of the available monomer) would cause a volume contraction of the polymerising droplet without the development of interstices (pores). Since the polymeric species, such as the primary particles and agglomerates, grow and flocculate

with each other, they form a skeletal structure which grows outwards as the monomer/polymer droplet contracts on polymerisation. When the contiguous structure is 'locked' together by flocculation and subsequent bridging polymerisation, the droplet (sub-grain) can no longer contract to accommodate density differences between VCM and PVC. Further polymerisation leads to the development of pores filled with vapour within the sub-grains.

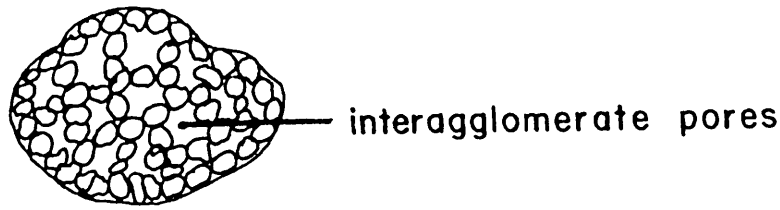

FIGURE 2.9 - Structure of a Porous Subgrain

If the 'locking' mechanism could be encouraged at very low conversions, particles of very high porosity would be obtained. Increasing the number of agglomerates and primary particles near the sub-grain surface would increase the possibility of 'locking' as volume shrinkage would force the precipitated particles together in a close packing arrangement.

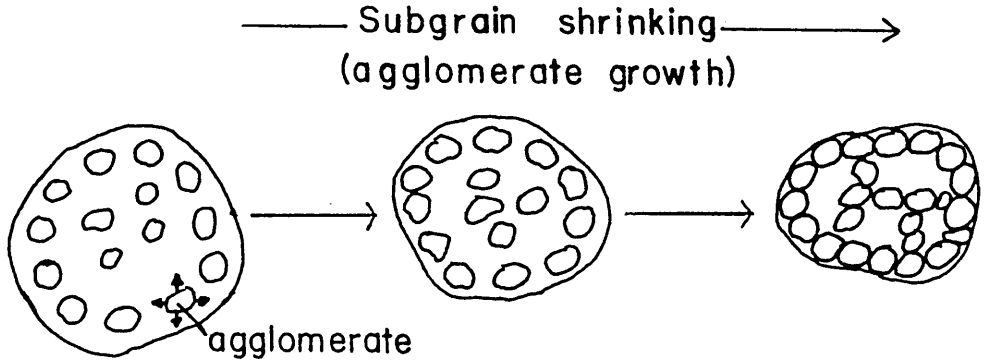

FIGURE 2.10 - 'Locking' of Sub-grains

2.5(D) Primary Particle Stabilisation

The primary particles survive as recognisable entitites throughout the polymerisation from the lowest conversions (~1%): they must be quite stable. The source of the stability has been ascribed to negative electric charge (demonstrated by electrophoresis) possibly arising from either:-

(i) Ionised hydrogen chloride formed by the decomposition of vinyl chloride peroxides (34,35,36)

or

(ii) Chloride ions produced by some unknown dehydrochlorination reactions with hydrogen as the counter ion (32).

Their destabilisation to form agglomerates appears to be due to the effects of agitation. Boissel and Fischer (27) noted that the primary particles aggregated at conversions ~10% to agglomerates. Since the essential difference between their studies and others by Mickley (40), Cotman (43) and Bort (45) (who had not observed agglomerates) was the agitation of the reactor, they deduced this was the cause. The other workers using unagitated systems had found that primary particles grew uniformly.

A more sophisticated view was presented by Davidson and Witenhafer (32) who proposed that the charge retention was due to a pericellular membrane around the polymerising droplets. Under varying conditions of agitation the fate of stabilised agglomerates will alter. In quiescent polymerisation they remain stable and act as growth centres, until shrinkage forces the particles into a compact mass. With 'mild' agitation coagulation within the polymer drop occurs at between 2% and 4% conversion. Violent agitation causes the pericelluar membrane to coagulate (Figure 2.11). The agitation was postulated to aid the migration of charge from the surface of the agglomerates through the pericellular membrane to be discharged by H^+ ions in the water.

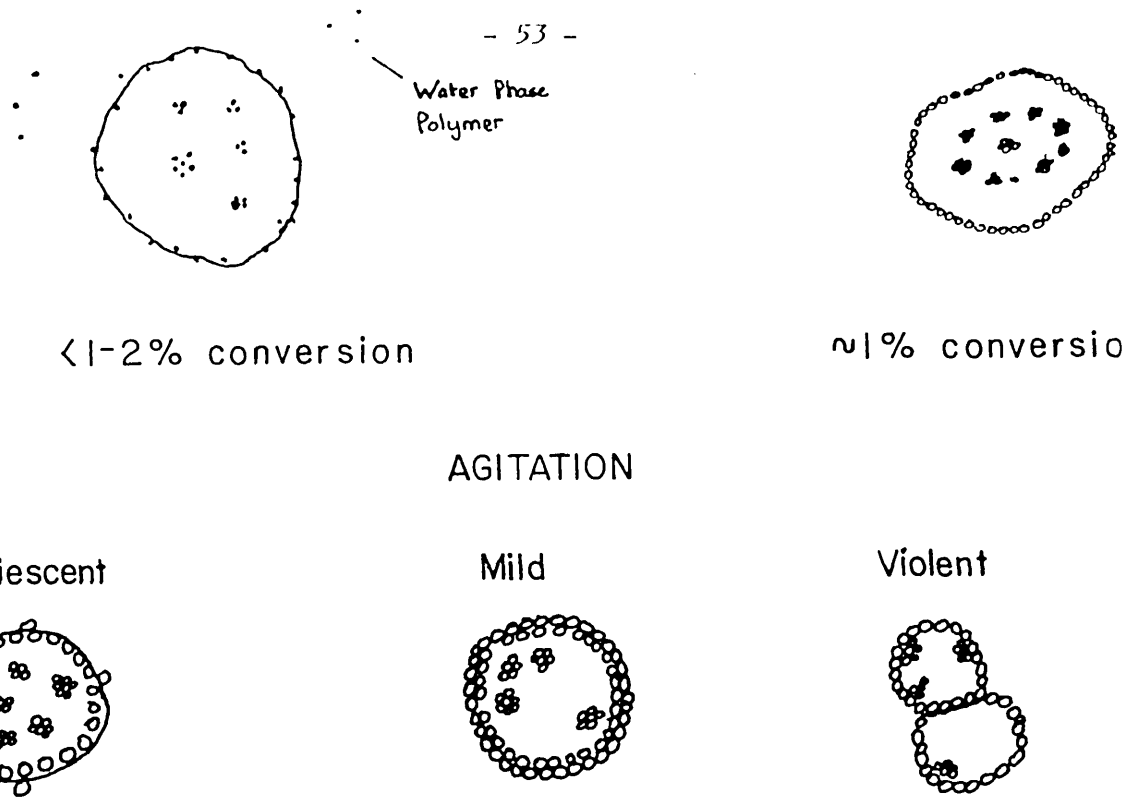

FIGURE 2.11 - Influence of Agitation on Morphology

Clearly whatever the precise mechanism of destabilisation the polymerising system is subject to conditions where a delicate balance exists between electrostatic repulsion forces between agglomerates and the inertial forces felt by them due to agitation. Too vigourous agitation tips the balance in favour of the inertial forces.

2.6 KINETIC MECHANISMS

The morphological development of PVC is determined by the rate of polymerisation and the nature of the intermolecular forces around the precipitated polymer species. Even the earliest kinetic models recognised the contribution made to rate by a second (polymer) phase. Despite this no published model satisfactorily assesses the influence of changing morphology on polymerisation kinetics: it is an important element of this study. This section reviews the increased understanding of the polymerisation mechanism (especially the chemical kinetics) which has arisen from the application of increasingly sophisticated experimental techniques and the interpretation of the experimental observations.

Bengough and Norrish (37) undertook the first major study of vinyl chloride polymerisation using benzoyl peroxide as an initiator and polymerisation temperatures between 33 and 75°C. The rate of polymerisation gradually accelerated over the first 30 to 40% conversion: at low conversions (<20%) the order of reaction with respect to initiator was 0.5 (c.f. homogeneous polymerisation where the rate of polymerisation, V_p, is given by

$$V_p = k_p \left[f \frac{k_d}{k_t} [I] \right]^{1/2} [M] \qquad (2.6.1)$$

where k_p,k_d and k_t are rate constants
f is the initiator efficiency
[I] and [M] are initiator and monomer concentrations).

The autoacceleration was shown not to be due to the removal of inhibitors from the vinyl chloride. It was ascribed to the precipitated 'dead' polymer behaving as a catalyst pellet allowing radical transfer at its surface (unlikely in view of the limited number of chain defects in PVC (56)!). The locus of polymerisation was postulated to be in the monomer phase at the surface of the precipitated polymer. They obtained a satisfactory fit to their experimental data with the relationship:

$$-\frac{dM}{dt} = K(M + K'' P^{2/3}) \left[\frac{I}{M}\right]^{1/2} \qquad (2.6.2)$$

where M,P,I are the mass of monomer, polymer and initiator respectively
K,K'' are constants

They also correctly identified, too, the mechanism of chain transfer to monomer which determines the molecular weight and its distribution for PVC.

A number of deficiencies are apparent in the approach of Bengough and Norrish:-

(i) No chemical reactions are considered within the precipitated polymer phase

(ii) no interphase transport of molecular species takes place

(iii) there is no consideration to the development of PVC morphology, nor the effects of agitation on this.

Bengough and Norrish noted the similarity between the autoacceleration in the rate of vinyl chloride polymerisation and the Trommsdorf or gel effect in homogeneous polymerisation, where the increasing viscosity of a polymerising solution leads to a decrease in the rate of termination and an increase in the overall rate of polymerisation. Whereas they saw the precipitated polymer phase as a significant factor in the description of autoaccelerating rate, Magat (38) thought that the failure to describe autoacceleration was due to a deficiency in the mathematical solution of the conservation equations for homogeneous free radical polymerisation (see 7).

In such polymerisations mass conservation equations for initiator, monomer and free radicals are generally solved by assuming that the population of free radicals is small and changing slowly compared to the populations of initiator and monomer molecules: the time derivative of the free radical population is set equal to zero. Algebraic manipulation of the conservation equations for monomer and initiator yields the rate of polymerisation as,

$$V_p = \left[\frac{2f\,k_d}{k_t}\,[I]\right]^{1/2}[M] \qquad (2.6.3)$$

Magat sought to describe vinyl chloride polymerisation by retaining the one phase nature of homogeneous polymerisation kinetics without making a quasi steady state approximation (QSSA) on the radical populations. He considered two cases of the solutions to the material balance equations:-

(i) with constant initiator concentrations

$$\frac{M_o - M}{M_o} = \frac{k_p}{k_t}\,\ln\{\cosh(k_d k_t\, I_o)^{1/2}\, t\} \qquad (2.6.4)$$

(ii) with first order decay of initiator

$$-\frac{dM}{dt} = k_p[M]\left[\frac{k_d I_o}{kt}\right]^{1/2} \frac{D K_1(\epsilon) - I_1(\epsilon)}{D K_o(\epsilon) + I_o \epsilon} e^{-1/2 k_{ot}}$$

$$\text{where} \quad \epsilon = 2\left[\frac{I_o k_t}{kd}\right]^{1/2} e^{-kd} \qquad (2.6.5)$$

$$\text{and} \quad D = \frac{I_1\left[2\left[\frac{I_o k_t}{k_d}\right]^{1/2}\right]}{K_1\left[2\left[\frac{I_o k_t}{k_d}\right]^{1/2}\right]}$$

and I and K are Bessel functions of the first and second kind.

The first case is of course highly idealised and unlikely to be observed in practice: the expression could only be used to fit experimental data up to 20% conversion. The second (more realistic) case was not tested by Magat; he had no computer to perform the integration. Although such an integration is now straight forward, Magat's model is not fundamentally different from the conventional homogeneous kinetic scheme: it does not describe the physical processes known to take place.

While Magat had attempted to explain the autoacceleration mathematically, Breitenbach and Shindler (39,39a) had recognised the importance of the precipitated polymer phase and the role of monomer in swelling that phase. Thus they confirmed the views of Bengough and Norrish and extended them by producing a model which allowed initiation, growth and termination in the precipitated phase. The main features of their model were:

(1) Precipitated polymer particles swollen by monomer
(2) Growing radicals present in both liquid phase and precipitated phase (by initiation and transport from the liquid phase).
(3) Autoacceleration explained by a reduction in the termination rates

$$(K_t)_{overall} = K_t/(1 + ax)$$

where a is a constant and x is conversion.

(4) Propagation rate constants equal in both phases.

(5) Chain transfer to monomer constants equal in both phases.

The overall rate expression is of the form:

$$\frac{x}{t} = a + bt \quad \text{where a,b are constants.}$$

It was found to be successful in representing experimental data for conversions of up to 20%.

Mickley, Micheals and More (40) considerably extended the two phase concept developed by Bengough and Norrish and Breitenbach and Schindler. They produced a model which was functionally similar to that of Bengough and Norrish: it differs in its derivation.

Bengough and Norrish thought that radicals could only be deactivated by transfer to polymer (this is not so; there are relatively few chain defects in PVC (56)). Mickley et al however realised that growing chains could aggregate (terminate) readily in a precipitating medium. Furthermore they argued that radical activity penetrated precipitated polymer particles because of transport into the polymer phase (c.f. Breitenbach and Schindler). They thought that radical propagation rate in the polymer phase might be reduced by the diffusional resistance to monomer with lower effective monomer concentrations at these polymerisation sites compared to the liquid phase. As shall be seen in this study, this effect is unlikely.

Mickley et al also recognised the contribution of primary particles make to the rate of reaction; their number concentration determines the interfacial transport areas. From Schmolukowski's theory of aggregation they deduced that because the lifetime of a growing chain is much shorter than the overall polymerisation time, every precipitated radical is absorbed as soon as it is formed into the (constant number of) primary particles.

The rate expression derived Mickley et al is:

Rate of polymerisation

$$R_p = k_p[M]\left[\frac{f\,k_D\,[I]}{k_t}\right]^{1/2} + \frac{D_L'\,k_p\,k_{trp}\,[P^*]}{D_L\,k_{trm}\,a}\,v\left[\frac{f\,k_D\,[I]}{k_t}\right]^{1/2} \qquad (2.6.6)$$

where D_L', D_L are diffusion coefficients representing absorption and desorption of radicals

$[P^*]$ represents the polymer concentration in the active zone of the precipitated phase

a is the ratio of the solubilities of monomer in the diluent and precipitated phases

V is the volume of the active zone

$V = N_p v_p$ at low conversions where the polymerisation proceeds throughout the precipitated phase (gives $Rp \alpha x$)

$= N_p S_p$ at high conversions where the polymerisation proceeds within a thin shell at the surface of a primary particle (gives $R_p \alpha x^{2/3}$)

N_p is the number of primary particles

v_p is the volume of each primary particle

δ is the thickness of the surface polymerising shell

and S_p is the area of the surface shell

The important features of the Mickley model are summarized viz:

(1) normal liquid phase kinetics
(2) radical occulsion by aggregation
(3) shallow penetration of radical activity into the primary particles
(4) negligible mutual termination in primary particles
(5) escape of trapped radicals by transfer to monomer
and (6) the limitation of radical escape by propagation and transfer to monomer.

The model due to Mickley et al represented a considerable advance in understanding of the polymerisation mechanism. However Talamini

(41) appreciating the heterogeneity of the polymerising VC/PVC system set down a simple model which lacked the sophistication of Mickley et al. It completely ignored the nature of development of the precipitated phase yet was able to fit experimental data well, up to 30% conversion.

Talamini assumed that the polymerising system phase separates to form a diluent phase and a precipitated one (with polymer volume fractions of <0.001 and ≥ 0.6 respectively); the interaction parameter χ in the Flory-Huggins theory is of order 0.88. The precipitated phase by virtue of its increased viscosity has a reduced rate of termination and increased overall polymerisation rate (equation 2.6.3). Therefore

$$R_p = Q R_M \quad (Q>1) \tag{2.6.7}$$

where R_p, R_M are the rates of polymerisation in polymer phase and monomer phase respectively.

As the conversion, x, increases, the fraction of reaction in the dilute phase will decrease: Talamini postulated that change to be proportional to conversion (from a consideration of the densities of PVC and VC and change in total volume with conversion). Therefore

$$\frac{dx}{dt} = R_M(1 - ax) + R_p\, ax \tag{2.6.8}$$

Substituting (2.6.7) and $q = Qa - a$ and integrating subject to the initial condition $t = 0$, $x = 0$

$$x = \frac{1}{q}\left\{\exp(q R_M t) - 1\right\} \tag{2.6.9}$$

The rate in the diluent phase is given by

$$R_M = k [I]^{1/2} \tag{2.6.10}$$

whence

$$x = \frac{1}{q}\left\{\exp(q\,k\,[I]^{1/2}t) - 1\right\} \qquad (2.6.11)$$

Hence although Talamini avoids the complexity of the kinetic mechanism, it is a useful tool for experimental studies: it is simple to apply. q and k must be fitted by comparison with experiment for a given initiator system and recipe. By expanding the exponential this expression also explains the higher orders of reaction with respect to initiator concentration observed experimentally.

Crosato-Arnaldi et al (42) used the Talamini equation (2.6.11) to interpret experimental observations for different initiator systems. (Their results were very close to those of Breitenbach and Schindler and of Farber and Koral). By fitting q for a number of polymerisation systems and recipes they were able to confirm the kinetic equivalence of bulk and suspension polymerisation for vinyl chloride.

The Talamini model however has a number of weaknesses:

(1) Q (and q) is not constant throughout the reaction.
(2) Radical transport between phases is ignored.
(3) Morphogenesis of the polymer is essentially ignored.

Despite all these, Abdel-Alim and Hamielec extended the treatment of Talamini to account for changes in initiator concentration caused by volume reduction as polymerisation takes place. The initiator concentration was postulated as uniform throughout the precipitated and diluent phases. The important extension to previous models made in this study was an attempt to characterise the molecular weight and its distribution. This they did by assuming the form of the molecular weight distribution (MWD) in the diluent and precipitated phases, summing them, and calculating the instantaneous values for number average chain length and weight average chain length. The principal mode of chain termination in polymerising vinyl chloride is by transfer to monomer. Under these conditions in a homogeneous polymerising solution the weight fraction of molecules of chain

length r is given by

$$W_r = \tau^2 r \exp(-\tau r). \qquad (2.6.12)$$

where $\tau = C_M + \frac{(f k_D k_t)^{1/2}}{k_p} \quad \frac{I^{1/2}}{[M]}$

The instantaneous MWD of the total mixture was postulated as

$$W_r = M_1 W_{r1} + M_2 W_{r2} \qquad (2:6.13)$$

where M_i are the mass fractions of polymer produced in phase i. Further analysis yielded the number average chain length,

$$P_n = \frac{1}{M_1 \tau_1 + M_2 \tau_2} \qquad (2.6.14)$$

and the weight average chain length,

$$P_w = \frac{2M_1}{\tau} + \frac{2M_2}{\tau_2} \qquad (2.6.15)$$

There polydispersity is given by

$$Z_p = r_w/r_n \qquad (2.6.16)$$

The principal disadvantage of this approach is that it assumes a MWD rather than generating one from a consideration fo the chemical kinetic scheme: just how this can be done is shown in Chapter Three.

So far all the models have ignored any effect the changing particle morphology may have on the rate of polymerisation. An early attempt to investigate this was made by Cotman et al (43).

Their study attempted to ascertain the role of precipitated particle properties in determining rates of polymerisation and involved both kinetic measurements and electron micrograph examination of the formed polymer. Using chain transfer agents to produce short chain PVC, they estimated the soluble chain lengths to be of order 25 to 30 monomer units long.

The free radicals were thought to precipitate on or within aggregates of partially swollen dead polymer. Accretion in this manner on an observed constant number of nuclei (~5 x $10^{11}cm^{-3}$) led to a uniform particle size which increased with conversion. The autoacceleration was ascribed to progressive reduction of termination rate (c.f. Breitenbach and Schindler (39)). The reason for the deminuation of termination rate was thought to be due to a reduction in the probability of chain transfer to monomer being able to produce mobile radicals to terminate occluded (stuck) free radicals in the precipitated polymer. Their experimental studies revealed a discontinuity in the rate curve at low conversions (~.005) which was thought to be due to an agglomeration of precipitated nuclei and a consequential loss of surface area. The model they propose however is similar in its functional form to that of Mickley et al.

Kuchanov and Bort (45) developed a model which extended and attempted to unify earlier experimental studies of the kinetics and morphology of PVC growth (29,30,31). Like Cotman et al, they had realised that morphological development might be significant in the determination of the rate of reaction, though they placed more emphasis on the transport of radicals between phases.

The precepts of their model are:-

(i) Polymerisation occurs in two phases: the first is a continuum of monomer with a very small concentration of dissolved polymer and the second is a dispersion of a constant number of 'microglobules' or primary particles of a dense precipitated polymer.

(ii) The rate of polymerisation is faster in the precipitated polymer phase than in the monomer phase because of the decreased rate of termination.

(iii) Free radicals can diffuse between polymer and monomer phases.

(iv) Initiator has different solubilities in each of the phases:

the ratio of the initiator solubilities in the polymer and monomer phases is γ (= $[I_2]/[I_1]$) the Nernst Distribution coefficient for initiator.

(v) There are different initiator efficiences in each phase. Initiator dissolved in the polymer phase is likely to be surrounded by a polymer matrix which restricts access of monomer and radicals to a nascent initiator radical. Such nascent radicals are less likely to propagate than similar radicals in the monomer phase which are surrounded by a sea of monomer.

Material balances were considered for monomer, initiator and radicals in each phase. The flux of radicals between the monomer and polymer phase was given by:

$$\bar{J}_{12} = 4\pi D_1 \, r \, N \, [R_1]$$

where D_1 is a radical diffusion coefficient in the primary particles (number, N)

r is the radius of the primary particles

and $[R_1]$ is the concentration of primary particles in the monomer phase.

Making a steady-state approximation on the number of radicals in the polymerisation system, they deduced the following rate expression after complex algebraic manipulations.

$$\phi(x,y) = \frac{w}{w_o} = \left[\frac{y}{1-x(1-\gamma)}\right]^{1/2} \left\{\frac{(1-x)F}{1+\sqrt{1+F^2}} + .29B\left[x\left[\lambda\gamma x + \frac{2(1-x)}{1+\sqrt{1+F^2}}\right]\right]^{1/2}\right\}$$

where y represents the proportion of initiator remaining

x is a dimensionless conversion (P/α_2)

α_1, α_2 are the mol fractions of polymer in the monomer and polymer phases respectively

F is a ratio of diffusion times of radicals to the initiation time

$$\left[F = \frac{A(1-x)y^{1/2}}{x^{1/3}[1-x(1-y)]^{1/2}} = \frac{(w_i^{\,i}\, k_{ti})^{1/2}\, V_i}{2\pi D_i\, r\, N}\right.$$

where $$\left. A = \frac{.27(2f\, k_i[I_i]\, k_{ti})^{1/2}}{D_i\, [N]^{2/3}} \right]$$

$B = \left[\frac{k_{t2}}{k_{t1}}\right]^{1/2}$, the ratio of the square root of the rate of termination in polymer and monomer phases.

$\lambda = \frac{f_2\, k_{D2}}{f_1\, k_{D1}}$, the ratio of the rates of initiation in the polymer and monomer phases.

$w_o^{\,i} = 2f_1\, k_{D1}\, [I_1]$, the rate of initiator in the monomer phase

$$w_o = k_p \left[\frac{w_o^{\,i}}{k_{t1}}\right]^{1/2} \qquad w = \alpha_2 \frac{dx}{dt}$$

The model describes the process well up to 20 to 30% conversion. Beyond this conversion, the extent of autoacceleration is underestimated by their theory. Kuchanov and Bort suggest therefore that poor heat removal from the polymerising droplets of PVC/VCM leads to increased temperatures and the development of 'hot spot kinetics', ie, higher rate of reaction, at the locii of polymerisation. They do not test this hypothesis (see Section 3.5).

The models of Kuchanov and Bort (45) and Abdel Alim and Hamielec (44) are compared in Figure 2.9. With low diffusion coefficients ($D < 1.2 \times 10^{-13} M^2 s^{-1}$) there is good agreement between the two models; the model of Abdel Alim is the limiting case of Kuchanov's model with no diffusion of radicals. Increasing the diffusional flux of radicals causes the initial rate to increase, with decreasing autoacceleration at higher conversions: this is not observed experimentally.

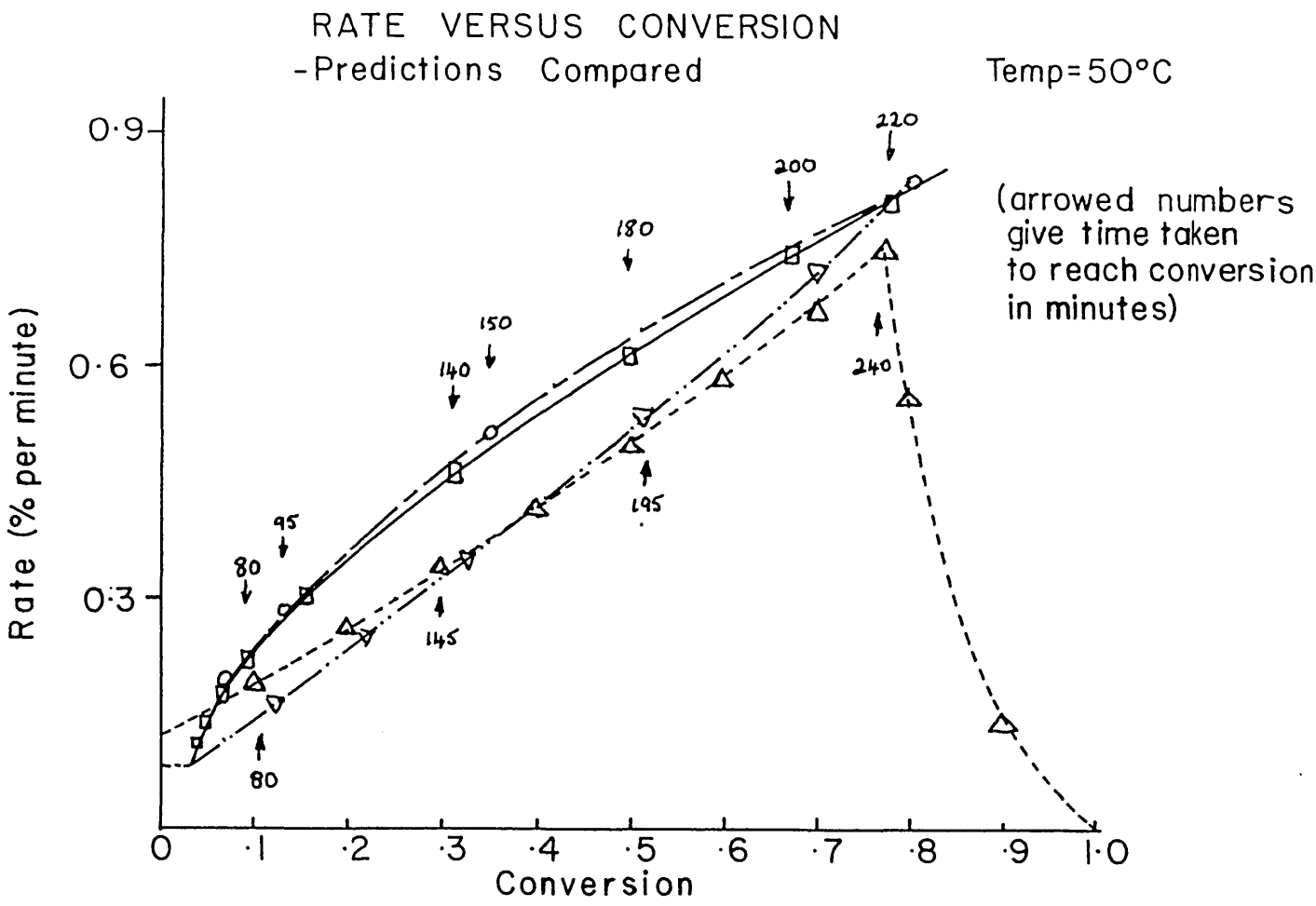

FIGURE 2.12

KEY

Temperature 50°C

Kuchanov and Bort

□ $D = 1.2 \times 10^{-11} m^2 s^{-1}$

Dynamic Solution of Mass Balance ODES

o $D = 1.2 \times 10^{-11} m^2 s^{-1}$

QSSA on radicals

▽ $D < 1.2 \times 10^{-13} m^2 s^{-1}$

△ Abdel Alim et al

Other conditions as Table 2.4

TABLE 2.4 - Parameters for Figure 2.12 For the Model Kuchanov and Bort

	Monomer Phase (1)	Polymer Phase (2)
Polymer Mass Fraction	$\alpha_1 = .03$	$\alpha_2 = .77$
Density Ratio (monomer:polymer)	$\nu_1 = .6071$	$\nu_2 = .6071$
Inititator Decomposition Rate Constant (s^{-1})	$k_{d1} = .2039 \times 10^{-5}$	$k_{d2} = .2039 \times 10^{-5}$
Termination Rate Constant ($m^3mol^{-1}s^{-1}$)	$k_{t1} = .18259 \times 10^{7}$	$k_{t2} = .19582 \times 10^{4}$
Initiator Efficiencies	$f_1 = .7$	$f_2 = .5$
Propagation Rate Constant	$1.69654 m^3mol^{-1}s^{-1}$	
Initiator Distribution Cofficient	$\gamma = [I_2]/[I_1] = .65$	
Initial Volume of Monomer	$1.0 m^3$	
Initial Rate of Initiation (w_o^i)	$0.12318 \times 10^{-3} mol\ s^{-1}$	
Concentration of Primary Particles ([N])	$5 \times 10^{17} m^{-3}$	
Initial Initiator Concentration (CIO)	$.4315 \times 10^{2} m^{-3}$	
Temperature	50°C	

For the model of Abdel Alim and Hamielec

Temperature	50°C
x_f	.77
Q	5.5
Combined rate constant eq 2.6.10) k_1	$1.25\ hr^{-1}(mol\ fract)^{-1/2}$
Rate enhancement in polymer phase P	22.7

Olaj (46,47,48) and Ugelstad (15,50,51) also considered the interphase transport of radicals to be significant in determining the rate of polymerisation of vinyl chloride.

Olaj (46,47,48) hypothesised that termination took place principally within the precipitated polymer phase. He presented a model of the form

$$\frac{dx}{dt} = a + b\, x^{1/2}$$

which modelled the conversion-time behaviour well, up to 10% conversion. Interphase radical transfer was considered important: with radicals initiated in the monomer phase terminating in the polymer phase. Auto-acceleration was ascribed to reduction in the gel phase termination constant, while an initial drop in rate (at conversions <1%) was due to a rapid reduction, by flocculation, of the number of precipitated primary particles. Olaj showed his model to be of the same form as Ugelstad's (47) and both were claimed superior in fitting experimental data up to 20% when compared with the models of Talamini (41), Bengough and Norrish (37) and Schindler and Breitenbach (39a). Olaj (48) used his model in determining the ratio $k_p(f/k_t)^{1/2}$ up to 10% conversion for polymerisations undertaken at different temperatures.

Ugelstad suggested a model where the interchange of radicals is important at low conversion (15,50,51). Using the steady state approximation for radicals, in the liquid phase:

$$2f\, k_D[I]_L - ka[R^\cdot]_L + ka_{-1}[R^\cdot]_p - 2k_{tl}[R^\cdot]_L^2\, V_L = 0 \qquad (2.6.19)$$

and in the polymer phase:

$$2f\, k_D[I]_p + ka[R.]_L\, ka_{-1}[R^\cdot]_p - 2k_{tl}[R^\cdot]^2\, V_p = 0 \qquad (2.6.20)$$

where ka, ka_{-1} represent adsorption and desorption coefficients for radicals onto and from the polymer phase.

If adsorption and desorption dominate, then

$$ka[R\cdot]_L = ka_{-1}[R_o]_p \qquad (2.6.21)$$

and

$$[R_o]_p/[R_o]_L = ka/ka_{-1} = Q$$

whence

$$[R\cdot]_L = [k_i\ I/(V_L\ k_{tL} + Q^2\ V_p\ k_{tp})]^{1/2} \qquad (2.6.22)$$

$$[R\cdot] = [k_i\ I/(V_L\ k_{tL} + Q^2\ V_p\ k_{tp})]^{1/2}\ Q \qquad (2.6.23)$$

The conservation equation for monomer becomes

$$\frac{-dM}{dt} = \left[k_i\ I/(V_L\ k_{t1} + Q^2\ V_p\ k_{tp})\right]^{1/2} k_p\left[M_L + QM_p\right] \qquad (2.6.24)$$

or in terms of conversion, c,

$$\frac{dc}{dt} = \left[\frac{k_i\ I}{(V_L k_{tL} + Q^2\ V_p\ k_{tp}}\right]^{1/2} k_p\left[1 - c - ac + qac\right] \qquad (2.6.25)$$

where $a = \rho_m/\rho_p$.

Q must be fitted to experimental data. This model is, despite consideration of interphase transfer of radicals, functionally similar to that of Talamini's (41). The principal drawback to the models of Olaj and Ugelstad is the assumption that interphase radical transport is instantaneous: it is therefore unimportant how the precipitated phase is formed: how much is formed is crucial.

Although Cotman et al (43) and Kuchanov and Bort (45) had incorporated the concept of a constant number of uniformly shaped primarly particles in their descriptions of the chemical kinetics and could thus calculate the amount of interphase radical transport, primary particles were known from studies of electron micrographs to have a particle size distribution and to agglomerate as aggregates.

Ray and Jain (49) considered the development of a particle size distribution with a conservation equation of the form:

$$\underset{(A)}{\frac{\partial F}{\partial t}(V,t)} + \underset{(B)}{\frac{\partial(\bar{c}\,F(V,t))}{\partial V}} = \underset{(C)}{\int_o^V k_c(V-v,v)F(V-v,t)F(v,t)dV} - \underset{(D)}{F(V,t)\int_o^\infty k_c(V,v)F(v,t)dV} + \underset{(E)}{\delta(V-v_c)r_{prec}(V_c)} \qquad (2.6.26)$$

where $F(V,t)dV$ is the concentration of particles having volume V to V + dV at time t.

Term (B) represents the rate at which particles enter the range V + dV by polymerisation growth (this term was assumed negligible).

Term (C) represents flocculation with particles of size V–v with those of size v to create particles of size V.

Term (D) represents flocculation of all particles of size V to remove them from the population.

Term (E) represents the precipitation of primary nuclei from the monomer phase.

$k_c(V,V)$ is a kinetic flocculation parameter of the form $\alpha(Vv)^{-1/3}$, α being a variable constant.

Total populations of primary particles given by

$$N_T(t) = \int_o^\infty F(V,t)dV$$

were found to agree well with experiment (43,31) though this entailed fitting α to experimental data: Ray and Jain suggest correlation with agitation conditions, viscosity, etc.

Ray and Jain assumed that the rate of precipitation of primary particles (term E) was proportional to the rate of polymerisation

which was assumed to be constant, facilitating the solution of (2.6.26). Hence, although the model avoids describing the chemical kinetic processes accurately, it offers the potential description of the particle size distribution (and possibly pore size distributions).

Two further models are worthy of consideration. The first is due to Thiele et al (52) and offers an extensive transport treatment of the kinetics, extending the interphase transport of radicals to monomer and initiator. The other model is due to Suresh and Chanda (53): it extends the treatment of Talamini (41) and Abdel Alim (44) who think that interphase transport of radicals is negligible.

The model due to Thiele (52) is a two-phase model with a liquid monomer phase and a monomer swollen disperse polymer phase. The conservation equations are:

For the liquid,

$$\frac{dn_j^l}{dt} = V^l \sum_{x=1}^{m} \nu_{xj}^l \, r_x^l - \beta A \Delta C_j \qquad (2.6.27)$$

and for polymer phase,

$$\frac{dn_j^s}{dt} = V^s \sum_{x=1}^{m} \nu_{xj}^s \, r_x^s + \beta A \Delta C_j \qquad (2.6.28)$$

where n_j represents the molar masses of component j (initiator, monomer, radicals or polymer) and β is a mass transfer coefficient. Mass transfer is non-selective and monomer acts as the carrying medium. The Bodenstein quasi-steady state approximation is applied to radicals and a least squares method is used to optimise kinetic parameters. Good agreement with experiment is achieved to high conversion. It is very disturbing however to see that the rate constants predicted by the optimisation study completely disagree with those published elsewhere (e.g. 45). See Table 2.5. The quantitative results of this study must be subject to doubt.

The model due to Suresh and Chanda (53) extends the Talamini/Abdel-Alim approach by assuming that rapidly growing polymer

TABLE 2.5 Comparison of Rate Constants

(1) from Thiele et al (52)

(2) from Kuchanov et al (45)

	Frequency Factor (M^3 $kmol^{-1}$ min^{-1})		Activation Energy $Jmol^{-1}$	
	(1)	(2)	(1)	(2)
Liquid Phase				
Propagation, K_{wo}^{l}	6.43×10^3	3×10^9	5.01×10^3	27.63×1
Termination by k_{uo}^{l} transfer to monomer	6.62	3.255×10^{11}	4.08×10^3	58.62×10^3
Termination k_{ao}^{l}	5.41×10^5	7.8×10^{13}	4.65×10^2	17.58×10^3
Polymer Phase				
Propagation, k_{wo}^{s}	2.02×10^3	3×10^9	O(?)	27.63×10^3
Termination by, k_{uo}^{s} transfer to monomer	4.83	3.255×10^{11}	4.00×10^3	58.62×10^3
Termination k_{ao}^{s}	9.58×10^3	4.2×10^3	4.9×10^2	34.358×10^3

(The most serious discrepancy appears to be the activation energy for termination. All the other results of Thiele could stem from this)

chains have considerably greater solubility than preformed polymer molecules of the same size: they can remain in solution under thermodynamically unfavourable conditions. This concept they call kinetic solubility and it is a function of chain length. How it differs from supersaturation is not clearly explained. The kinetic solubility curve (kinetic chain solubility versus chain length) is a priori unknown, and so an operating solubility curve is further defined in such a way that the kinetic solubility is removed from the rate expression. Although the authors assert that the operating solubility can be recovered from experimental rate data, how this can be done is not explained. Nor is it clear on what thermodynamic basis the operating solubility curve can possibly exist.

SUMMARY

There have been a considerable number of models to describe the polymerisation: most are reasonably accurate in describing low conversion behaviour. Most of those reviewed in this chapter agreed that the polymerisation proceeds in two phases: a monomer phase with a small amount of PVC dissolved in it and a polymer phase swollen by monomer. The models of Talamini and of Abdel Alim and Hamielec assumed that radicals grew so fast that they precipitated and terminated where they were initiated. Interphase transport of free radicals was negligible. Ugelstad and Olaj on the other hand assumed that mass transfer of radicals occurred instantaneously. For either of these limiting cases of a general mass transfer model, the structure of the precipitated phase is unimportant. Only the amount of the precipitated phase must be known.

Cotman et al, Mickley et al and Kuchanov and Bort recognised the significance of the structure of the precipitated polymer. They assumed that a constant number of primary particles grew uniformly and that the external surface formed an interface through which radicals could diffuse. Thiele et al adopted a similar approach: they additionally allowed non-selective mass transfer of initiator and monomer across the interface with the flux of these components being proportional to the flux of radicals. (All the other models

mentioned in this summary assumed that monomer and initiator could transfer freely between phases independently of the rate of radical mass transfer).

Only one model considered the particle size distribution of the precipitated primary particles. The model of Ray and Jain however neglected the rate of polymerisation by assuming it to be constant: this is a significant simplification; it autoaccelerates (Figure 2.2).

The other important characteristic which models predicted was molecular weight and its distribution. Thiele et al considered the number average molecular weight only. Abdel Alim and Hamielec, because of the dominance of chain transfer to monomer in VC polymerisation, used a known molecular weight distribution for homogeneous polymerisation with this mode of termination and calculated an average molecular weight over the precipitated and diluent phases.

Although most of the models can describe low conversion behaviour well (low conversion experiments can be performed with dilatometers) they are unable to reproduce the sharply peaked rate profiles seen in commercial process at c.a. 77% conversion (Figure 2.2) just before the autoclave pressure begins to fall as free monomer disappears from the system. The models outlined in this Chapter are not consistent with all the facts we now have about the kinetics, morphology and the physical properties of PVC.

The aim of this study therefore is to develop a detailed model of the PVC suspension process. A rigorous approach will be adopted in an attempt to unify the existing theories about the polymerisation process in an effort to produce a model which is capable of a complete description of all aspects of the polymerisation.

Such a model must consider the chemical kinetics occurring in the diluent and precipitated phases together with any transport of species between the phases whether it be monomer, initiator or radicals.

It should be capable of describing the development of the polymer

product structure. The precipitated primary particles must grow, flocculate and pack together within the grains. Ideally, particle size distributions of primary particles, agglomerates and subgrains should be predicted. Furthermore since these properties are affected by agitation, the model should consider the role of agitation and especially how it determines the initial grain size distribution.

The remaining polymer properties which should be modelled are the porosity, which arises because of the development of a "rigid" structure (skin) around a contiguous network of primary aggregates coupled with volume contraction with polymerisation, the packing density, the bulk density and the molecular weight and its distribution (which is related to the chemical kinetics).

Finally the model should describe the process conditions of pressure and temperature within an autoclave.

CHAPTER THREE

DEVELOPMENT OF THE MATHEMATICAL MODEL

From the study of the morphogenesis of PVC described in Chapter Two, a number of distinct phases participating in the polymerisation may be identified. In Section 3.1 the loci of polymerisation are described. The development of a complete set of conservation equations to describe the entire system follows. A number of simplifying assumptions for particular phases are introduced. The kinetic contributions to the model equations are covered in Section 3.3A and the mass transfer terms are described in the following section. The reduction of the infinite set of coupled differential equations for the mass of each species so developed to a tractable limited set for the moments of the overall polymer distributions is accomplished using a generating function (Section 3.4). Finally heat transfer within droplets and between them and the continuous phase is analysed using dimensionless groups. The chapter ends with a summary of the final formal equations of the model.

3.1 LOCI OF POLYMERISATION

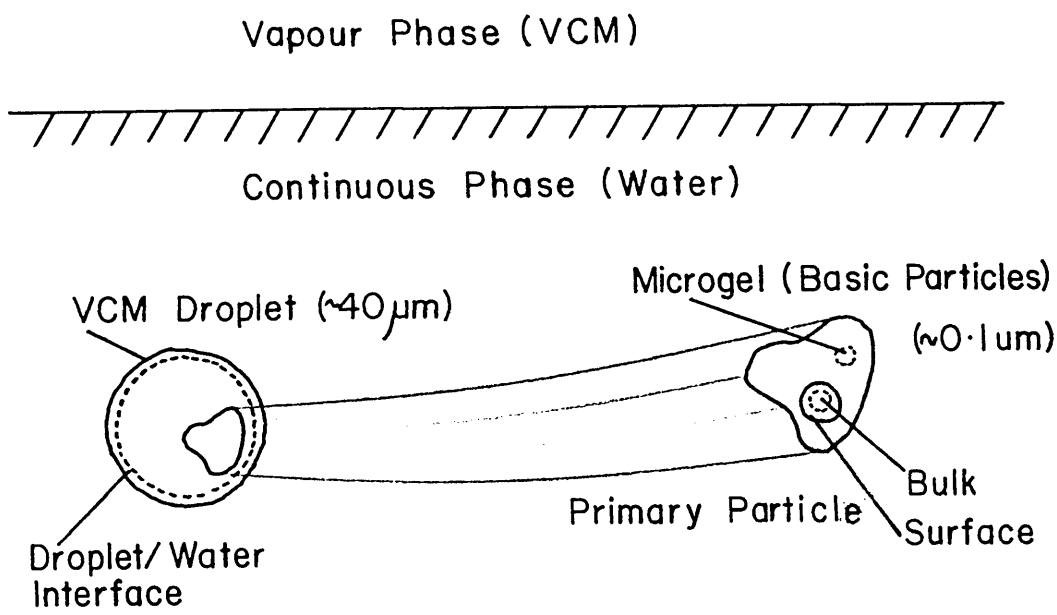

FIGURE 3.1 – Phases in an autoclave of polymerising vinyl chloride

The following loci may be identified for polymerisation:-

1. The Vapour Phase

In an autoclave 80% filled with a 1.5:1 water:monomer v/v charge, the fraction of monomer existing as vapour (assuming the vapour is principally composed of monomer) at 50°C is of the order 1.5%. Although the vapour phase has been cited as a reservoir of monomer after pressure drop (51), its contribution to the overall rate of polymerisation must be small because of the small concentrations of monomer and the insolubility of the initiator there. At 50°C the molar concentration of VCM is c.a. 300 mols m^{-3} (from the perfect gas law) compared to a concentration of 13600 mols m^{-3} in the monomer phase to be described. However this phase has an important role in terms of mass transfer because 1) reflux condensers may be used to cool the polymerisation by removing the latent heat of vapourisation of monomer, and because 2) the rate of pressure drop will be determined by the rate at which this small amount of vinyl chloride can transfer through the continuous phase.

2. Aqueous (Continuous) Phase

The major role for this phase is as a heat sink for the heat of polymerisation to pass from the monomer droplets to the reactor wall. The solubilities of vinyl chloride and initiator are usually small (solubility of v.c. at 50°C is .07g/100g H_2O ~ 11.29 mols m^{-3} (ICI data)). Despite this, the phase has an important role to play in mass transfer as a potentially undesirable resistance to monomer passage between vapour phase and suspended droplets.

3. VCM Droplet Surface

Electron microscopy studies (19,32) reveal that monomer droplets polymerising to subgrains develop a surface region which differs significantly in nature from the bulk of the subgrain. The number

density of primary particles is higher here, and the chemical nature of the polymer is different here because the adsorbed surfactant forms a graft copolymer with poly(vinyl chloride). Initiator, too, may migrate to the interface. All of these factors may contribute to this region attaining a coherent close packed structure much earlier in the polymerisation than in the bulk of the subgrain, as it forms a strong pericellular membrane. Further polymerisation within the droplets leads to the development of space inside the droplet because the polymer is much denser than the monomer. Liquid monomer vapourises to fill the spaces and to maintain equilibrium. Porosity is thus developed. For these reasons, the rate of polymerisation in this zone may be modified, to allow for the number concentration of primary particles, and so that initiator concentrations differ from the rest of the droplet.

Despite identifying this zone (which in a 40μm subgrain may occupy a depth of 1μm or 16% of the polymer volume) it is unlikely that its kinetic behaviour during polymerisation (as distinct from subsequent observation with an electron microscope) can be distinguished experimentally from the major loci of polymerisation which will now be described.

4. Continuous Monomer Phase (Subgrain Bulk)

This phase is essentially pure monomer; the mole fraction equilibrium solubility of PVC in vinyl chloride is of the order $\sim 10^{-3}$. At lower conversions than this, the monomer phase represents the sole polymerisation site. Beyond conversions of ~.77, when there is insufficient monomer to swell the polymer forming, this phase will disappear and the autoclave pressure will fall. Under well agitated conditions there are unlikely to be mass transfer limitations between the vapour and the monomer or polymer phases. The vapour pressure in the reactor will be described by a theory quantifying the behaviour of a concentrated polymer solution (PVC in VCM); in this work it will be assumed that the Flory Huggins theory, though by no means exact, is a sufficiently good approximation for our purposes (Figure 3.2).

Initiators are chosen to be highly soluble in this phase, and although radicals may grow here, they are likely to precipitate when only a few units long. Growing radicals, suspended in the monomerphase, are still referred to as monomer phase radicals since they are free to terminate with either dissolved or suspended radicals in this phase. Upon adsorption by the primary particles suspended in this phase, "monomer phase radicals" become polymer phase radicals.

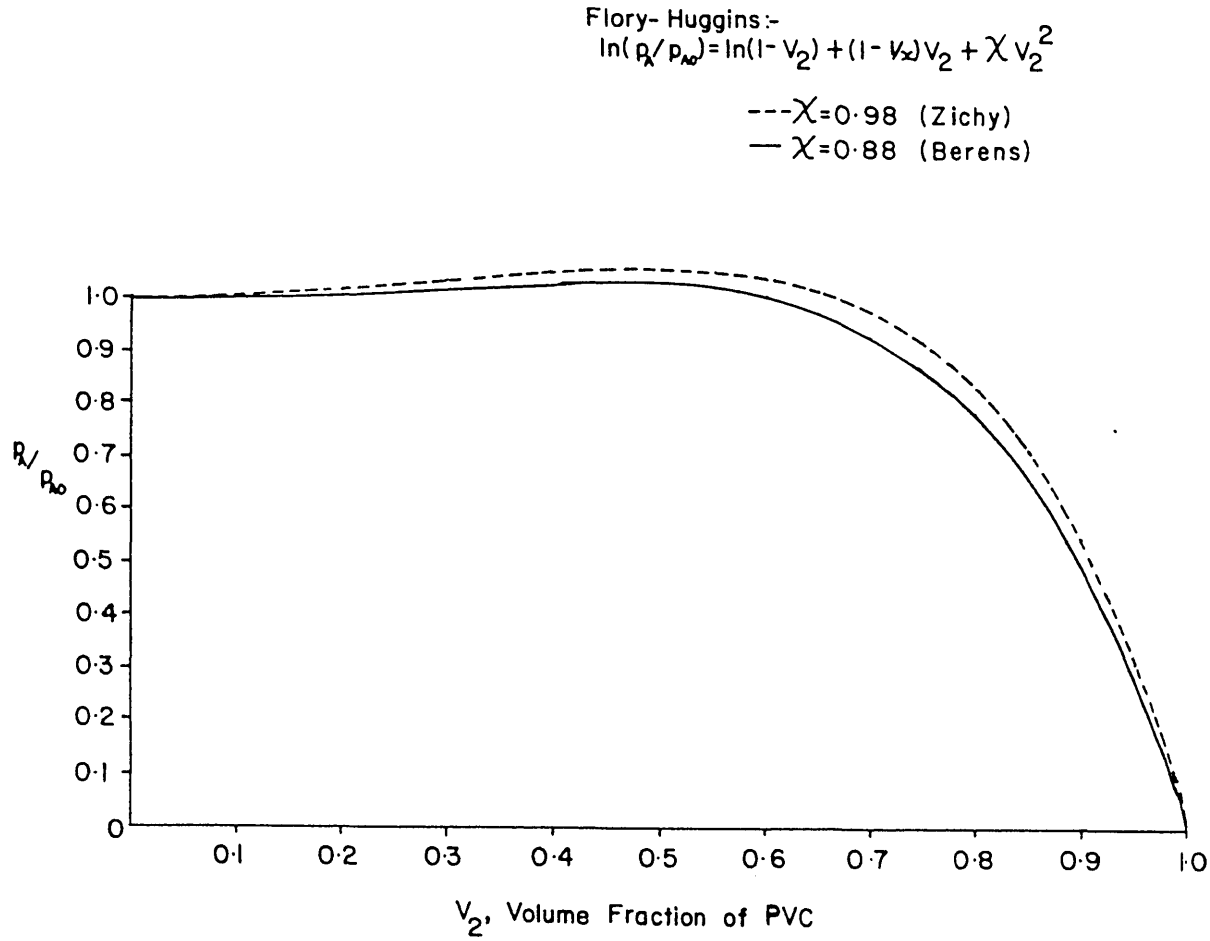

FIGURE 3.2 - Variation of Vapour Pressure Above Polymer System, PVC in VCM

Polymer Rich Phases

The precipitated polymer rich ('gel') phase has a composition of ~.77 polymer and ~.23 monomer by mass, and exists as the highly

deformable primary particles, whose history has been followed in the previous chapter. The high density of chains in this phase significantly reduces the chain-end segmental diffusion rate, and hence reduces the rate at which radicals can couple and terminate. This process is usually modelled by reducing the effective rate constant for termination.

Initiators may be soluble here, but not necessarily to the extent as in the monomer-rich phase. The precipitating dead polymer from the monomer phase is likely to carry monomer and initiator with it to the polymer rich phase. Polymerisation in this phase will therefore arise from radicals which have

(a) migrated from the monomer phase prior to termination or transfer

or (b) been initiated here.

It is convenient to differentiate further between three distinct sub-phases in the polymer rich phase.

5. The Micro-gel (Basic Particle) Phase

At very low conversions when polymer particles are first precipitated (as basic particles or primary nuclei, according to the previous description [Chapter 2]) the polymer chains are likely to be suspended in the monomer phase: the chains will be swollen with monomer. As this phase grows by polymerisation and flocculation the radii of the precipitated particles will increase and diffusionj of monomer (or initiator) to the centre of these precipitated particles may well be limited. At this stage, the microgel segregates into two phases:-

6. Primary Surface Phase, which is of a similar nature to the microgel phase because of its close proximity to the free monomer.

7. Primary Bulk Phase, where diffusion limitations may lead to deviations from the equilibrium swelling conditions.

This model represents a simplification of the real process, where continuous spatial variation of the concentrations of each species is to be expected throughout the precipitated particle. Although we can write down a model to incorporate the spatial variation (next section) the solution of such a model poses considerable difficulty; a large amount of (expensive) computer time would be required. Although such physical realism is to be appreciated, the physical model represents part of an overall process engineering model which may need to be frequently used. Therefore we choose to approach the ideal situation, with spatial variations in concentration, using the model outline above to allow for deviations from uniform concentrations within particles without incurring large computational overheads.

In the final computer model (Appendix 6.1) the microgel phase is allowed to grow until its radius exceeds an arbitrary multiple (five) of the root mean square end to end distance of a freely rotating PVC chain of molecular weight 60,000. This is 9.63nm (54). Thereafter, the growth of the primary bulk will depend entirely on the relative strengths of mass transfer and rates of chemical change in each of the phases.

3.2 CONSERVATION EQUATIONS

The continuity equation describes the conservation of mass for each component of the system in the autoclave. Within a fixed element of space, the rate of accumulation of mass of species i is given by the net flux of i out of the element plus the rate of generation of i by chemical reaction within the element. Vectorially, this is written

$$\frac{\partial \rho i}{\partial t} = -\underline{\nabla}.\underline{n}_i + r_i \qquad \text{all}_i \qquad (3.1)$$

where $\underline{n}_i$ is the mass flux of component i relative to stationary co-ordinates

ρ_i is the mass concentration (density) of i

r_i is the mass rate of generation of i

i is any species (initiator, monomer radicals or dead polymer)

$\nabla.$ is the divergence

However,

$$\underline{n}_i = \rho_i \underline{v}_i \tag{3.2}$$

where $\underline{v}_i$ is the velocity of i relative to stationary co-ordinates and the mass flux relative to the mass average velocity, v, is given by $\underline{j}_i$:

$$\underline{j}_i = \rho_i(\underline{v}_i - \underline{v}) \tag{3.3}$$

therefore

$$\underline{n}_i = \underline{j}_i + \rho_i \underline{v} \tag{3.4}$$

The continuity expression may be expressed by

$$\frac{\partial \rho_i}{\partial t} = \underset{(A)}{-\underline{\nabla}.(\rho_i \underline{V})} \underset{(B)}{+ \underline{j}_i} + r_i \tag{3.5}$$

[(A) represents the convection of a species into the control volume and (B) represents its diffusion into the element].

or

$$\frac{\partial \rho_i}{\partial t} = \underset{\text{TERM (1)}}{-\left(\underline{v}.\underline{\nabla}\rho_i\right.} \underset{\text{TERM (2)}}{+ \rho_i \underline{\nabla}.\underline{v}\left.\right)} \underset{\text{TERM (3)}}{- \underline{\nabla}.\underline{j}_i} \underset{\text{TERM (4)}}{+ r_i} \tag{3.6}$$

The mass flux $\underline{j}_i$ for a multicomponent system can be expressed as a sum of contributions; a contribution due to ordinary (concentration) diffusion $\underline{j}_i^{(x)}$; a contribution due to pressure effects, $\underline{j}_i^{(p)}$; and contributions due to forced diffusion $\underline{j}_i^{(g)}$ (eg due to electrostatic or gravitational fields) and thermal diffusion $\underline{j}_i^{(T)}$.

$$j_i = j_i^{(x)} + j_i^{(p)} + j_i^{(g)} + j_i^{(T)} \qquad (3.7)$$

For ordinary diffusion the mass flux is given by (p567, 55)

$$j_i^{(x)} = \frac{c^2}{\rho RT} \sum_{j=1}^{n} M_i M_j D_{ij} \left[x_j \sum_{\substack{k=1 \\ k\neq j}}^{n} \left[\frac{\partial G_j}{\partial x_k} \right]_{T,p,x_{s\neq j,k}} \nabla x_k \right] \qquad (3.8)$$

where M_i = molar mass of species i

C = total molar concentration

ρ = overall density

D_{ij} = multicomponent diffusion coefficients

G_j = partial molar free energy

If the interface between phases is denoted by S

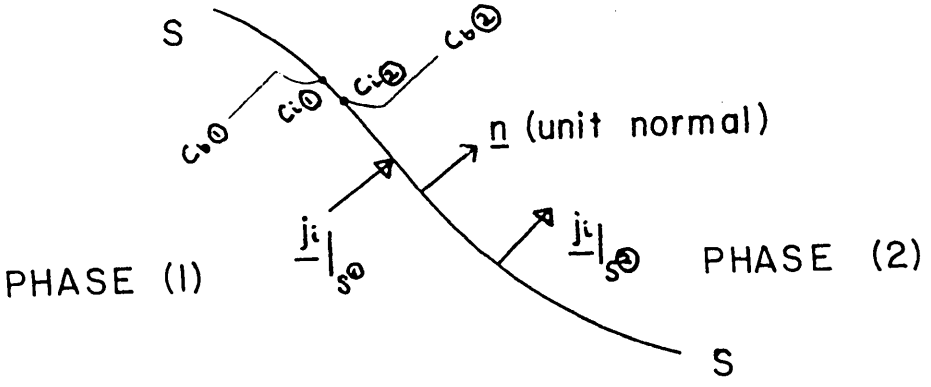

the equations of continuity (3.6) will be coupled by boundary conditions of the type

$$j_i.n|_{S(1)} = j_i.n|_{S(2)} = \beta \Delta C_{i(1)(2)} \qquad (3.9)$$

where $j_i|_{S(k)}$ represents the molar flux of i at the interface within phase (k), ΔC_i represents the concentration differences between the two phases at the interface, β is a mass transfer coefficient, and n is a unit vector normal to the interface.

Equations 3.6 and 3.9 can be used to write full continuity expressions for each of the phases outlined earlier. Before presenting this it is appropriate to make a number of simplifications

for some of these phases.

1. Vapour Phase

This phase is assumed to be well mixed and to be of constant density. These assumptions imply that the concentration of species i throughout the phase is uniform, $\underline{\nabla}x_i = \underline{0}$ and $\underline{\nabla}^2 x_i = 0$. In equation 3.6, terms (2), (3) and (4) drop out, whence

$$\frac{\partial \rho_i}{\partial t} = r_i \qquad \text{(vapour phase)} \qquad (3.10)$$

2. Aqueous (Continuous) Phase

The same assumptions as above apply, and therefore:

$$\frac{\partial \rho_i}{\partial t} = r_i \qquad \text{(aqueous phase)} \qquad (3.11)$$

3.-7. Other Phases

Although droplets are subject to considerable agitation and shear effects, they tend to move with the global fluid flow with little net movement relative to this flow. Since, also, as polymerisation proceeds a skin develops around the polymerising droplet, the fluid velocities (with respect to agitator tip speed) of monomer within droplets are likely to be small. Therefore we may take $\underline{V} = \underline{0}$.

One would expect the density of each of these phases, too, to remain reasonably constant (although the mass of the phase may change with time).

If either (or both) of these assumptions applies then the general conservation equation (3.6) reduces to:

$$\frac{\partial \rho_i}{\partial t} = -\underline{\nabla}.\underline{j}_i + r_i \qquad (3.12)$$

This is a partial differential equation in space and time, and while such equations can be solved easily for a small number of components (eg, diffusion of a gaseous species into a catalyst pellet), in multicomponent systems their solution rapidly becomes intractable. The multicomponent system under consideration here is one where the polymeric species (components) at any instant in time can vary in size from one monomer unit long to several thousand units long. It is therefore expedient to assume that spatial variation of concentrations within each of the monomeric and polymeric phases is neglible. This may represent the grossest approximation so far: the reasons for making it are threefold.

(a) The diffusion coefficients for each polymeric species, as defined by equation (3.8), cannot all be measured: empirical rules could be used to estimate each D_{ij}, for example by analogy with polymer molecules diffusing in solution.

(b) Experimental differentiation between diffusional resistance to mass transfer of species i through a particular phase and interphase resistance to transport as defined by Equation (3.9) is unlikely.

(c) Solution of the simple ordinary differential equation $\partial\rho_i/\partial t = r_i$ is anticipated to be sufficiently difficult that rigourous numerical treatment of equation (3.12) is too difficult for the current study.

Equation (3.12) reduces to:

$$\frac{\partial \rho_i}{\partial t} = r_i \qquad (3.13)$$

3.3 THE OVERALL MODEL

Now that these simplifying approximations have been considered, the overall equations for the model may be presented.

Vapour Phase

$$\frac{\partial \rho_{i1}}{\partial t} = r_{i1} - (\beta \Delta C_i)|_{12} \qquad t>0 \qquad (3.14)$$

Aqueous Phase

$$\frac{\partial \rho_{i2}}{\partial t} = r_{i2} + (\beta \Delta C_i)|_{12} - (\beta \Delta C_i)|_{23} \qquad t>0 \qquad (3.15)$$

VCM Droplet Surface

$$\frac{\partial \rho_{i3}}{\partial t} = r_{i3} + (\beta \Delta C_i)|_{23} - (\beta \Delta C_i)|_{34} \qquad t>0 \qquad (3.16)$$

Continuous Monomer Phase

$$\frac{\partial \rho_{i4}}{\partial t} = r_{i4} + (\beta \Delta C_i)|_{34} - \{H(t - t_5) - H(t - t_6)\} (\beta \Delta C_i)|_{45} - H(t - t_6)(\beta \Delta C_i)|_{46} \qquad (3.17)$$

Microgel Phase

$$\frac{\partial \rho_{i5}}{\partial t} = r_{i5} + (\beta \Delta C_i)|_{45} \qquad t_5<t<t_6 \qquad (3.18)$$

Primary Surface Phase

$$\frac{\partial \rho_{i6}}{\partial t} = r_{i6} + (\beta \Delta C_i)|_{46} - (\beta \Delta C_i)|_{67} \qquad t>t_6 \qquad (3.19)$$

Primary Bulk Phase

$$\frac{\partial \rho_{i}}{\partial t} = r_{i7} + (\beta \Delta C_i)|_{67} \qquad t>t_6 \qquad (3.20)$$

where H(t - a) is the unit step function

$$H(t - a) = \begin{cases} 1 & t \geq a \\ 0 & t < a \end{cases} \qquad (3.21)$$

t_s is the time when the microgel phase is first formed and t_6 is the time when the microgel phase segregates into primary surface and bulk phases.

The equations set down above could be applied to most multiphase multicomponent reacting systems. The specificity to polymerising vinyl chloride is determined by the form of the reactive "r_i" terms, which may be deduced from the chemical kinetics, and the form of the mass transfer $\beta\Delta C_i$ terms, which couple the phases together.

3.3(A) The "r_i" Terms

In any phase, the following reactions may be expected:

Initiation

$$I \xrightarrow{k_D} 2fR_o \qquad (3.22)$$

Propagation

$$\begin{aligned} R_o + M &\xrightarrow{kpo} R_1 \\ R_1 + M &\xrightarrow{kp_1} R_2 \\ R_n + M &\xrightarrow{k_{pn}} R_{n+1} \end{aligned} \qquad (3.23)$$

Termination by:

Disproportionation

$$R_n + R_m \xrightarrow{k_{tdn,m}} P_n + P_m \qquad (3.24)$$

Combination

$$R_n + R_m \xrightarrow{k_{tcn,m}} P_n + m$$

Transfer to Monomer

$$R_n + M \xrightarrow{k_{trmn}} P_n + R_1 \qquad (3.24)$$

Transfer to Polymer

$$R_n + P_j \xrightarrow{k_{trpn,j}} P_n + R_j$$

The overall reaction scheme is outlined in Table 3.2, which considers the conservation of all polymer chain length species.

Side reactions, which considerably affect the ultimate heat stability of vinyl chloride, are not considered in this overall scheme because of their relatively infrequent occurrence and the consequent lack of kinetic data (Table 3.1).

TABLE 3.1

Structural Defects of Poly(vinyl chloride) Chains per 1000 Monomer Units (a.m.u.) Ref (56)

Chloromethyl Branches	4 - 6
Chloroethyl Branches	.4 - 2.4
Butyl Branches	~.4 - 1.6
Long Branches	~.18 - 2.4
Head to Head Structure (Cl on neighbouring C)	~6 - 7
Total Double Bonds	1.4 - 3.0
(Internal Double Bonds)	(.07 - .27)
Labile Chlorine Atoms	.6 - 2.5
(Allylic Chlorine)	(.5 - 2.5)
(Ketochloroallylic Chlorine)	(.16 - 1.0)
(Chlorine on Tertiary Carbon)	(uncertain)

TABLE 3.2
Reactions

SPECIES	Initiation	Propagation	Transfer to:+ (i) Monomer	Transfer to:+ (ii) Polymer	Termination by:# (i) Combination	Termination by:# (ii) Disproportionation
Initiator	$\frac{dI}{dt} = -k_D I$					
Monomer		$\frac{dM}{dt} = -\left[\sum_{j=1}^{N} k_{pj} R_j\right] M$	$-\left[\sum_{j=0}^{N} k_{trmj} R_j\right] M$			
Nascent Radical	$\frac{dR_o}{dt} = 2fk_D I$	$- k_{po} R_o M$			$- 2k_{tco,o} R_o^2$	$- 2k_{tdo,o} R_o^2$
Growing Radicals		$\frac{dR_1}{dt} = (k_{po} R_o - k_{p1} R_1) M$	$+ \left[\sum_{j=0}^{N} k_{trmj} R_j\right] M$ $- k_{trm} R_1 M_1$			
		$\frac{dR_n}{dt} = (k_{pn-1} R_{n-1} - k_{pn} R_n) M$	$- k_{trmn} R_n M$ $- R_n\left[\sum_{j=0}^{N} K_{trpn,j} P_j\right]$ $+ k_{trpn,n} R_n P_n$	$- R_n\left[\sum_{j=0}^{N} k_{tcn,j} R_j\right]$ $- k_{tcn,n} R_n^2$	$- R_n\left[\sum_{j=0}^{N} k_{tdn,j} R_j\right]$ $- k_{tdn,n} R_n^2$
Growing Dead Polymer		$\frac{dP_1}{dt} =$	$+ k_{trm1} R_1 M$ $+ R_1\left[\sum_{j=0}^{N} k_{trp1,j} P_j\right]$ $- k_{trp1} R_1 P_1$		$- R_1\left[\sum_{j=0}^{N} k_{td1,j} R_j\right]$ $- k_{tdn,n} R_n^2$	
		$\frac{dP_n}{dt} =$	$+ k_{trm} R_n M$ $+ R_n\left[\sum_{j=0}^{N} k_{trpn,j} P_j\right]$ $- k_{trpn,n} R_n P_n$	$+ \frac{1}{2}\sum_{j=0}^{n-1} k_{tcj,n-j} R_j R_{n-j}$	$+ R_n\left[\sum_{j=0}^{N} k_{tdn,j} R_j\right]$ $+ k_{tdn,n} R_n^2$	

NOTES

#	in termination reactions when j=n, two radicals are consumed: the summation allows for one only.
+	in transfer reactions when j=n, radical activity swaps from radical to dead polymer without changing the concentration.
I, M, R_n, P_n	represent the concentrations of initiator, monomer, growing radicals and dead polymer.
	The convention of using brackets [] around species to denote concentrations has not been applied here.
N	represents the length of the longest molecule in terms of monomer units.

3.3(B) Mass Transfer Between Phases

The aim of this section is to provide a clearer interpretation of the "$\beta\Delta C$" terms of the general model. Each species in the system (monomer, initiator and polymeric chains (growing and terminated)) can be treated in the same way although each will have different equilibrium distributions between the phases and rates of attainment of this equilibrium state.

Previous workers (eg 44,45) consider the monomeric phase (x_p ~.001; x_m ~.999) at equilibrium with the polymeric phase (x_p ~ .77; x_m ~ .23). However the current treatment is a dynamic one, and deviations from equilibrium are to be expected on a sufficiently small scale. As more polymer phase is created, the mass transfer of monomer, initiator and growing polymer into this from the surrounding phases is treated explicity using conventional mass transfer theory.

The model for mass transfer may be represented by the following diagram.

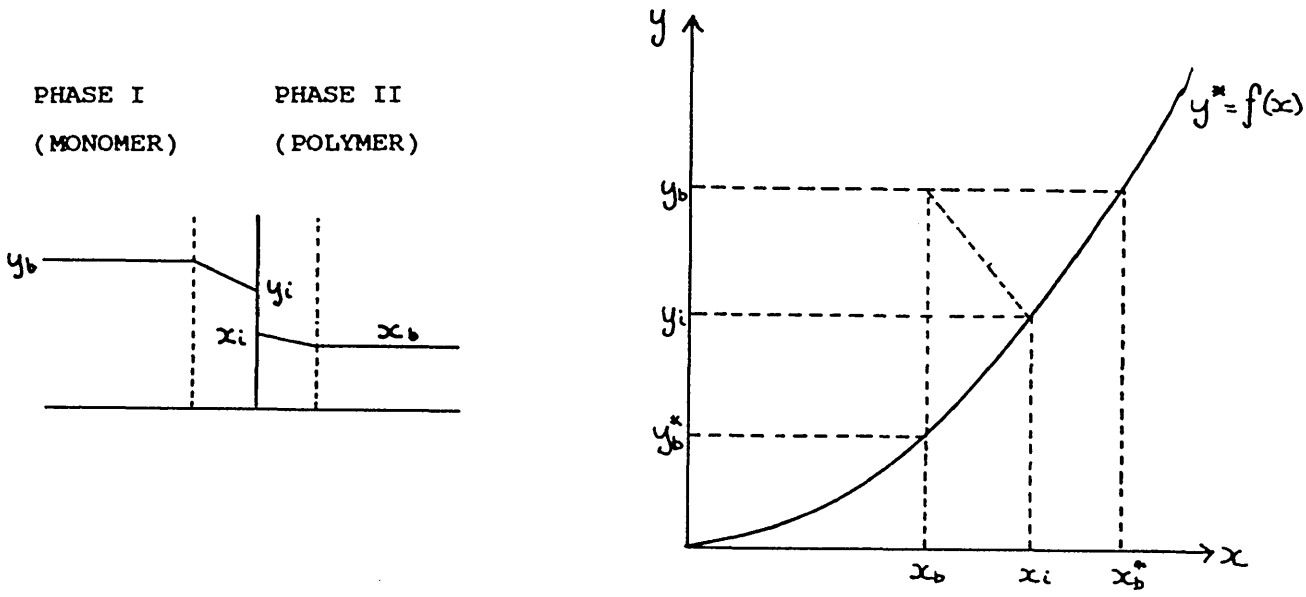

FIGURE 3.3 – Interphase Mass Transfer

where y is the concentration of j in phase I

x is the concentration of j in phase II

y_i, x_i are interfacial concentrations (assumed at equilibrium with one another)

y_b, x_b are bulk concentrations

y^* is the equilibrium relationship between phase I and phase II for j, ie y^* is the concentration of j in phase I at equilibrium with a concentration of x in phase II.

The flux through the interface for any species may be written as:

$$\underline{N}.\underline{n} = (k_I)_y(y_b - y_i) = (k_{II})_x(x_i - x_b) \qquad (3.25)$$

From phase I, the driving force towards equilibrium is given by $y_b - y_b^*$, where y_b^* represents the concentration of i in phase I which would be in equilibrium wiht the concentration x_b of j in phase II. An overall mass transfer coefficient is defined by

$$\underline{N}.\underline{n} = (K_{oI})_y(y_b - y_b^*) \qquad (3.26)$$

$$\text{whence } y_b - y_b^* = y_b - y_i + \frac{y_i - y_b^*}{x_i - x_b}(x_i - x_b) \qquad (3.27)$$

and

$$\frac{\underline{N}.\underline{n}}{(k_{oI})_y} = \frac{\underline{N}.\underline{n}}{(k_I)_y} + \gamma_{i,II}\frac{\underline{N}.\underline{n}}{(k_{II})_x} \qquad (3.28)$$

therefore, the overall mass transfer coefficient is:

$$\left[\frac{1}{K_{oI}}\right]_y = \frac{1}{(k_I)_y} + \frac{\gamma_{I,II}}{(k_{II})_x} \qquad (3.29)$$

$\gamma_{I,II}$ represents the local Nernst equilibrium constant, and $\underline{n}$ is the unit normal vector. The total mass transferred across the interface of a phase is given by:

$$\underline{j}.\underline{n} = A\,\underline{N}.\underline{n} = A(K_{oI})_I(y_b - \gamma_{I,II}\,x_b) \qquad (3.30)$$

where A is total interfacial area between phases. For the case of the primary particles (I≡4,II≡6) $A = N_p\, 4\pi r^2$ where N_p represents the number of precipitated polymeric particles and r is their average radius.

Clearly we can identify the terms "$\beta\Delta C$" in equations by:

$$\beta\Delta C|_{lm} \equiv A(K_{oI})_l\,(C_l - \gamma_{lm}\, C_m) \qquad (3.31)$$

and when $C_l = \gamma_{lm}\, C_m$, ie the concentration of a species in phase l is at equilibrium with that in phase m, the flux across the interface will be zero. The relationships for the Nernst distribution coefficients appropriate to monomeric and polymeric species are derived in Appendix 5.1.

3.4 A GENERATING FUNCTION METHOD OF SOLUTION

To solve the material balances generated in Table 3.2 in order to determine the molecular weight distribution of the polymer presents considerable difficulty, even if there were only one phase. Numerical integration, for example, would require the use of a vast amount of computer space: typically for each phase S^2 storage locations would be required to perform the integration where S represents the number of species (monomer, initiator, N radicals and N polymer). Since here N is large (~1000 for PVC) the storage needed would exceed that generally available on current computers.

Fortunately in the form of a generating function or its complement the Z transform there exists a discrete transform which makes solution of this large number of equations viable. Generating functions are a device for reducing the complexity of a large group of equations describing the relationship between a large distribution of variables. They can be defined for both radicals and dead polymer.

For radicals

$$G_R(S,t) = \sum_{n=0}^{\infty} S^n R_n(t) \qquad |S| \leq 1 \qquad (3.32)$$

and polymer

$$G_P(S,t) = \sum_{n=0}^{\infty} S^n P_n(t) \qquad |S| \leq 1 \qquad (3.33)$$

(The Z transform is achieved by putting $S = 1/Z$)

The individual (time varying) elements of the populations, $R_n(t)$ and $P_n(t)$, therefore become coefficients of a series expansion of the dummy variable S.

The conservation equations in one phase:

$$\frac{dI}{dt} = f_1(I) \qquad (3.34)$$

$$\frac{dM}{dt} = f_2(M,I,R,P) \qquad (3.35)$$

$$\frac{dR_n}{dt} = f_3(M,I,R_n,R_{n-1},R_{n-2},\ldots) \qquad (3.36)$$

$$\frac{dP_n}{dt} = f_4(M,I,R_n,R_{n-1},R_{n-2},\ldots,P_n,P_{n-1},\ldots) \qquad (3.37)$$

are multiplied throughout by S^n, and summed overall n for radicals and polymer, they reduce to

$$\frac{dI}{dt} = f^1{}_2(I) \qquad (3.38)$$

$$\frac{dM}{dt} = f^1{}_2(M,I,G_R,G_P) \qquad (3.39)$$

$$\frac{dG_{R(S)}}{dt} = f^1{}_3(M,I,G_R,G_P,S) \qquad (3.40)$$

$$\frac{dG_{P(S)}}{dt} = f^1{}_4(M,I,G_R,G_P,S) \qquad (3.41)$$

Table 3.3 shows the transform equations for the kinetic scheme in Table 3.2. The assumption that reaction rates are independent of chain length has been made. Whilst inversion of these equations would yield the molecular weight distributions of growing and dead polymer (R_n and P_n), the conventional and more convenient approach is to derive equations for moments of these population distributions. (A number of inversion techniques will be considered in the next Chapter).

The moments of the distributions are defined by:-

$$\sigma_k(E) = \sum_{n=1}^{\infty} n^k R_n(t) = \lim_{S \to 1} \frac{\partial^k G_R(s,t)}{\partial(\ln s)^k} \qquad (3.42)$$

$$\lambda_k(t) = \sum_{n=1}^{\infty} n^k P_n(t) = \lim_{S \to 1} \frac{\partial^k G_P(s,t)}{\partial(\ln s)^k} \qquad (3.43)$$

They are directly linked to the number and weight average chain lengths.

Repeated differentiation of the transform equations with respect to $\ln s (\equiv s\partial/\partial s)$ and setting $s = 1$ yields differential equations for the polymer moments dI/dt, dM/dt, $d\sigma_0/dt$, $d\sigma_1/dt$, $d\sigma_2/dt$, $d\lambda_0/dt$, $d\lambda_1/dt$, $d\lambda_2/dt$ (Table 3.3). Further moments could of course be generated by further differentation: recurrence relationships may be developed which express the algebraic relationship of high order moment to low order ones, simplifying the task enormously. The zeroth, first and second moments are however preferred; they relate to the important number average and weight average molecular chain lengths (or weights) of polymers. Since these quantities can be measured independently by experiment (7), they offer the possibility of experimental justification of any model.

$$\lambda_0(t) = \sum_{n=1}^{\infty} P_n(t) \qquad (3.44)$$

$$\lambda_1(t) = \sum_{n=1}^{\infty} n P_n(t) \qquad (3.45)$$

$$\lambda_2(t) = \sum_{n=1}^{\infty} n^2 P_n(t) \qquad (3.46)$$

whence,

Number average chain length, $\mu_n = \frac{\lambda_1}{\lambda_0}$

Number average molecular weight, $M_n = m\mu_n$

Weight average chain length, $\mu w = \frac{\lambda_2}{\lambda_1}$

Weight average molecular weight, $M_w = m\mu_w$

Polydispersity, $Zp = \frac{M_w}{M_n} = \frac{\mu_w}{\mu_n} = \frac{\lambda_0\lambda_2}{\lambda_1^2}$

TABLE 3.3

Transform and Moment Equations for Each Phase

<table>
<tr><td colspan="3">Concentration equations from Table 3.2 are transformed by the relationships
$G_R(s,t) = \sum_{n=1}^{\infty} s^n R_n(t) \qquad G_p(s,t) = \sum_{n=1}^{\infty} s^n P_n(t)$</td></tr>
<tr><td><u>Transform Equations</u></td><td colspan="2">$\frac{\partial I}{\partial t} = -k_D I$
$\frac{\partial M}{\partial t} = -k_p M\, G_R(1) - k_{trm}\, M\, G_R(1)$
$\frac{\partial G_R}{\partial t} = 2fk_D Is - k_{trm}\, M\, G_R(s) = k_{trm}\, M\, G_R(1)s - k_p\, M(1-s)G_R(s) - k_{trp}\, G_R(s)\, G_p(1) - (k_{tc} + k_{td})\, G_R(s)\, G_R(1)$
$\frac{\partial G_p}{\partial t} = k_{trm}\, M\, G_R(s) + k_{trp}\, G_R(s)\, G_p(1) + k_{td}\, G_R(s)\, G_R(1) + \frac{k_{tc}}{2} G_R^2(s)$</td></tr>
<tr><td><u>Moment Equations</u></td><td>$\sigma_k(t) = \sum_{n=1}^{\infty} n^k R_n(t)$</td><td>$\lambda_k(t) = \sum_{n=1}^{\infty} n^k P_n(t)$</td></tr>
</table>

Table 3.3 (cont)

	$\frac{\partial I}{\partial t} = -k_D\, I$
	$\frac{\partial M}{\partial t} = -(k_p M + k_{trm}\, M)\sigma_o$
	$\frac{\partial \sigma_o}{\partial t} = 2fk_D\, I - k_{trp}\, \sigma_o\, \lambda_o - (k_{tc} + k_{td})\sigma_o^2$
	$\frac{\partial \sigma_1}{\partial t} = 2fk_D\, I + k_{trm}\, M(\sigma_o - \sigma_1) + k_p\, M\, \sigma_o - k_{trp}\, \sigma_1\, \lambda_o - (k_{tc} + k_{td})\sigma_1\, \sigma_o$
	$\frac{\partial \sigma_2}{\partial t} = 2fk_D\, I + k_{trm}\, M(\sigma_o - \sigma_2) + k_p\, M(2\sigma_1 + \sigma_o) - k_{trp}\, \sigma_2\, \lambda_o - (k_{tc} + k_{td})\sigma_2\, \sigma_o$
	$\frac{\partial \lambda_o}{\partial t} = k_{trm}\, M\, \sigma_o + k_{trp}\, \sigma_o\lambda_o + k_{td}\, \sigma^2_o + \frac{k_{tc}}{2}\, \sigma_o^2$
	$\frac{\partial \lambda_1}{\partial t} = k_{trm}M\sigma_1 + k_{trp}\, \sigma_1\lambda_o + k_{td}\, \sigma_1\sigma_o + k_{tc}\, \sigma_o\sigma_1$
	$\frac{\partial \lambda_2}{\partial t} = k_{trm}M\sigma_2 + k_{trp}\, \sigma_2\, \lambda_o + k_{td}\, \sigma_2\sigma_o + k_{tc}(\sigma^2_1 + \sigma_o\, \sigma_2 + \sigma_o\, \sigma_1)$

(The convention of square brackets around species to denote their concentration has not been adopted in this Table.)

In a completely analogous manner, the coupling terms "$\beta\Delta C_{lm}$" can be treated using the generating function approach, to yield coupling terms for the moments of the molecular weight distributions:-

For radicals "$\beta\Delta C_{lm}$" - $A(K_{oI})_i\, (\sigma_{il} - \gamma^p_{lm}\, \sigma_{im})$ (3.52)

and for dead polymer "$\beta\Delta C_{lm}$" - $A(K_{oI})_i\, (\lambda_{il} - \gamma^p_{lm}.\lambda_{im})$ (3.53)

In Table 3.4 the partial differential equations become ordinary differential equations as the spatial variation in concentration throughout a phase is now being neglected as discussed on page 84.

TABLE 3.4

General Equations for Model with Mass Transfer Through Neighbouring Phases

	Phase j − 1	Phase j	Phase j + 1
$\frac{dn_I^j}{dt} = V^j \frac{dI^j}{dt} + A_{j-1j}(K_{oI})(I^{j-1} - \gamma^I_{j-1j} I^j) - A_{jj+1}(K_{oI})_j (I^j - \gamma^I_{jj+1} I^{j+1})$			
$\frac{dnm^j}{dt} = V^j \frac{dM^j}{dt} + A_{j-1j}(K_{oM})(M^{j-1} - \gamma^M_{j-1j} M^j) - A_{jj+1}(K_{oM})_j (M^j - \gamma^M_{jj+1}.M^{j+1})$			
$\frac{dn\,\sigma_i^j}{dt} = V^j \frac{d\sigma_i^j}{dt} + A_{j-1j}(K_{o\sigma i})(\sigma_i^{j-1} - \gamma^{\sigma i}_{j-1j}.\sigma_i^j) - A_{jj+1}(K_{o\sigma i})_j (\sigma_i^j - \gamma^{\sigma i}_{jj+1}\cdot\sigma_i^{j+1})$			
$\frac{dn\lambda_i^j}{dt} = V^j \frac{d\lambda_i^j}{dt} + A_{j-1j}(K_{o\lambda i})(\lambda_i^{j-1} - \gamma^{\lambda i}_{j-1j}.\lambda_i^j) - A_{jj+1}(K_{o\lambda i})_j (\lambda_i^j - \gamma^{\lambda i}_{jj+1}.\lambda_i^{j+1})$			

where n_i are the number of moles of species i

V is the phase volume

γ^i_{jj+1}, A, Koi are as previously defined

dI/dt, dM/dt, $d\sigma_i/dt$, $d\lambda_i/dt$ are previously defined (Table 3.3)

I, M, $\sigma_o, \sigma_1, \sigma_2, \lambda_o, \lambda_1, \lambda_2$ are the concentrations of intitiator and monomer and the moments of the concentrations for growing radicals and dead polymer.

3.5 TEMPERATURE EFFECTS OF POLYMERISATION

The need to develop polymers of specific molecular weight dictates that polymerisations are carried out under essentially isothermal conditions. Heat-ups are achieved in about 30 minutes for a 40m^3 autoclave, while the polymerisation may proceed for a further

six hours. Autoclave heat up, then, represents 8-10% of polymerisation time, or, in terms of conversion, less than ~4%. (For a 50°C polymerisation, the initial rate is of the order .13% per minute (results of this study). At temperatures lower than 50°C, the initial rate will be much lower and therefore, the cumulative conversion during heat-up much lower).

Having obtained the worst estimate for conversion achieved under non-isothermal conditions, the next point to consider is how isothermal the reactor is. Two questions may be posed:

(a) Is there any temperature gradient across a VCM/PVC droplet? Therefore do VCM/PVC droplet temperatures throughout the droplet match the measured autoclave temperatures?

(b) Are hot-spot kinetics likely to develop because of a breakdown in heat transfer between suspended droplets and the suspending water?

Clearly if the answer to (a) is yes, and the system is <u>adequately controlled</u> then the answer to (b) will be no.

In order to answer these questions, consider a model of an autoclave.

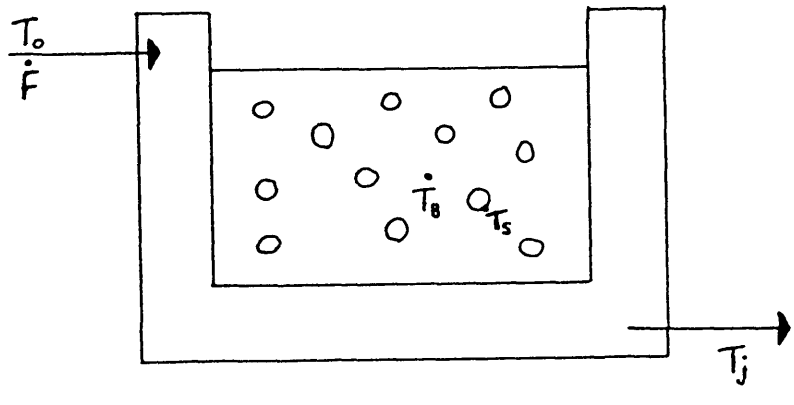

T_o, T_j are the jacket inlet and outlet temperatures

T_B, T_S are water and suspended droplet surface temperatures respectively

and F is the volumeric flow rate of water through jacket.

Subject to the following assumptions,

(i) no volume shrinkage of polymerisation

(ii) heat capacity of polymer and heat capacity of VCM are equal

(iii) reaction occurs uniformly throughout the droplet

(iv) film theory heat transfer is appropriate at the water/VCM interface

(v) dispersion and mass transfer effects are ignored within the droplet

(vi) the droplets are isothermal

Energy balances may be derived for the system.

For the jacket,

$$\dot{F}\, C_{pj}\rho_j(T_o - T_j) - (T_j - T_B)UA = V_j\rho_j cp_j \frac{dT_j}{dt} \qquad (3.54)$$

net heat to jacket — net heat from jacket to autoclave

for the water,

$$(T_j - T_B)UA + n(qS)|_R = (V\rho cp)|_{H_2O} \frac{dT_B}{dt} \qquad (3.55)$$

and for the drop

$$\frac{1}{r^2}\frac{\partial}{\partial r}\left\{r^2 \frac{\partial T}{\partial r}\right\} + \frac{r_v(-\Delta H_R)}{k_{vcm}} = \frac{\rho_m c_{pm}}{k_m}\frac{\partial T}{\partial r} \qquad (3.56)$$

(3.55) and (3.56) are coupled through the boundary conditions:-

$$-k_m \frac{\partial T}{\partial r}\bigg|_R = n(T_S - T_B) \quad ; \quad T|_R = T_S \qquad (3.57)$$

(where n is the number of suspended droplets,

$(qS)|_R$ heat flux x surface area of each droplet,

and $V, \rho, c_p, U, A, r_v, (-\Delta H_R)$ and k adopt their conventional meaning).

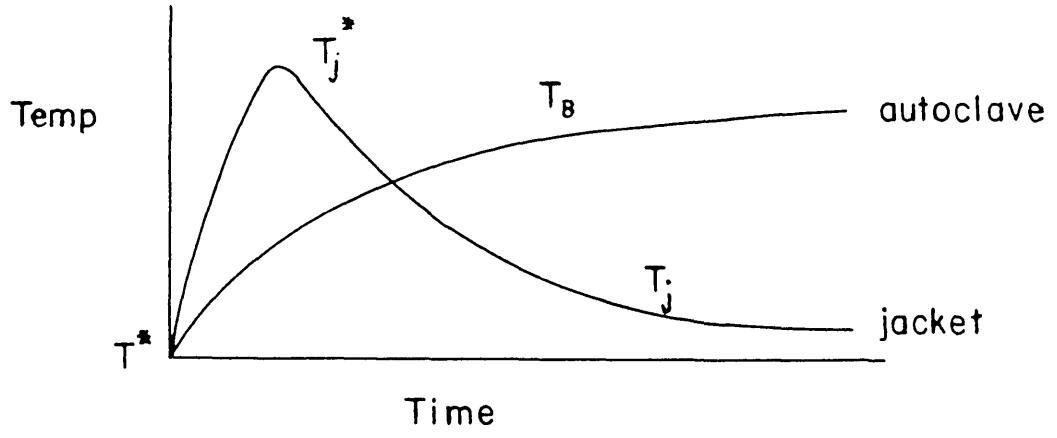

PIGURE 3.4 - Variation of Jacket and Autoclave Temperatures

Defining the dimensionless variables:-

$$\epsilon = \frac{r}{R} \qquad \theta_D = \frac{T - T^*}{T_j^* - T^*} \qquad \theta_F = \frac{T_B - T^*}{T_j^* - T^*}$$

$$\theta_j = \frac{T_j - T^*}{T_j^* - T^*} \qquad \theta_o = \frac{T_o - T^*}{T_j^* - T^*}$$

where T^* is the initial "cold" temperature

T_j^* is the maximum jacket temperature

and dimensionless parameters:

$$\alpha = \frac{UA}{Fc_{pj}\rho_j} \qquad \beta = \frac{nk_m\, 4\pi R}{Fc_{pj}\rho_j} \qquad \gamma = \frac{V_{H_2O}}{V_j}$$

$$\delta = \frac{\rho_m\, c_{pm}\, \dot{F}\, R^2}{k_m\, V_j} \qquad \phi = \frac{hR}{k^m} \qquad \eta = \frac{R^2\, r_v(-\Delta H_R)}{k_m(T_j^* - T^*)}$$

$$\tau = \frac{t\dot{F}}{V_j}$$

(3.54), (3.55), (3.56) and (3.57) transform to

$$(\theta_o - \theta_j) - (\theta_j - \theta_F)\alpha = \frac{\partial \theta_j}{\partial \tau} \qquad (3.59)$$

$$\alpha(\theta_j - \theta_F) - \beta \left.\frac{\partial \theta_D}{\partial \epsilon}\right|_{\epsilon=1} = \gamma \frac{\partial \theta_F}{\partial \tau} \qquad (3.60)$$

$$\frac{1}{\epsilon^2} \frac{\partial}{\partial \epsilon}\left[\epsilon^2 \frac{\partial \theta_D}{\partial \epsilon}\right] + \eta = \delta \frac{\partial \theta_D}{\partial \tau} \qquad (3.61)$$

$$\left.\frac{\partial \theta_D}{\partial \epsilon}\right|_{\epsilon=1} = -\phi(\theta_S - \theta_F) \quad ; \quad (\theta_D|_{\epsilon=1} = \theta_S) \qquad (3.62)$$

For a $40m^3$ autoclave, having the following dimensions L/D = 30, $V_j = 1.49m^3$, $A_j = 54.6m^2$, paddle diameter, P = 2m, operating at 80 rpm, the heat transfer coefficients have been determined in appendix 3.1. Using the thermodynamic data in appendix 3.1, values of the dimensionless parameters may be calculated (Table 3.5).

TABLE 3.5

Dimensionless Parameters

Dimensionless Parameters (T ~ 50°C)	Value	Order of Magnitude
α	1.446×10^{-1}	$10^{-1} - 10^{0}$
β	$2.87 \times 10^{4} \rightarrow 4.59 \times 10^{3}$ ($r \approx 40\mu m$) ($r \approx 100\mu m$)	$10^{3} - 10^{4}$
γ	12	10^{1}
δ	$2.189 \times 10^{-4} - 13.68 \times 10^{-4}$ ($r \approx 40\mu m$) ($r \approx 100\mu m$)	$10^{-4} - 10^{-3}$
ϕ	23.17 → 57.93	$10^{1} - 10^{2}$
η	$1.2 \times 10^{-6} \rightarrow 1.2 \times 10^{-5}$	$10^{-6} - 10^{-5}$
τ	0 → 1300	$10^{2} - 10^{3}$

Recasting equations (3.54) to (3.57) in dimensionless form allows easy comparison of terms on an order of magnitude basis. The largest order terms represent an important physical process and dominate the behavour of the system. Therefore in an equation containing a mixture of known and unknown terms of varying order, worst estimates of unknown order terms may be given by taking their order as equal to that of the largest order term known in the equation.

For equation (3.60), the known orders of magnitude are:

$$(10^{0} - 10^{0}) - 10^{+3}.O\left[\frac{\partial \theta_D}{\partial \epsilon}\bigg|_{\epsilon=1}\right] \equiv 10^{1}.10^{0}/10^{3} = 10^{2}$$

therefore

$$O\left[\frac{\partial \theta_D}{\partial \epsilon}\bigg|_{\epsilon=1}\right] \equiv 10^{-4} \quad : \quad O[\,] \text{ indicates order of magnitude of term.}$$

and from (3.62) $\theta_S - \theta_F$ is of order 10^{-5}.

ie, the difference between the droplet surfaces temperature and water

temperature is negligibly small.

From (3.61)

$$o\left[\frac{\partial \theta_D}{\partial \epsilon}\right] + 10^{-5} \equiv 10^{-3}\ 10^{o}/10^{3} = 10^{-6}$$

ie, the temperature gradient across the suspended droplet is also negligibly small, because $\partial \theta_D / \partial \epsilon$ is of order 10^{-6}.

It can be seen, too, that for this system the dynamics are governed by the ordinary differential equations (3.59 and 3.60) which determine autoclave and jacket temperatures (of order $\sim 10^{-3} - 10^{-2}$) rather than the partial differential equation (3.61) which governs droplet temperature (of order $\sim 10^{-6}$).

The important result of this analysis is that throughout the VCM/PVC droplet, temperature effectively equals the autoclave water temperature, and therefore given adequate control of the process water, hot-spot kinetics within the PVC system are unlikely to occur. Henceforward the model will assume that polymerisation proceeds isothermally.

SUMMARY

The overall model (Section 3.3) can be represented by the equations outlined in Table 3.4, a series of non-linear, coupled, first-order differential equations describing the conservation for initiator, monomer, radical and polymer moments in each of the phases present. Whereas these types of equation may be solved analytically for a small number of cases where single phases are involved (eg, anionic polymerisation without termination) in this case computer-based numerical integration is the only feasible method.

Order of magnitude arguments have been applied using a heat transfer model to justify isothermal treatment of the kinetics within the polymerising droplets and to show that the temperature is uniform throughout the suspending water and the dispersed VCM/PVC.

CHAPTER FOUR

SOLUTION METHODS

The model developed in Chapter 3 is composed of non-linear, coupled ordinary differential equations (ODE's). In this chapter the solution methods appropriate to this system will be discussed. Gear's method for the integration of ODE's will be introduced by considering Runge-Kutta methods and linear multistep methods of integration. The concept of stiffness and its impact on solution methods will be considered.

Further sections of this chapter will consider the relief of stiffness by (i) making use of the quasi-steady state approximation for radicals and (ii) rescaling the problem. The conservative nature of the equations developed in Chapter 3 will be analysed, with some restructuring of the model proving essential.

The final part of this chapter will consider alternative methods for the prediction of molecular weights and their distribution to the method proposed in Chapter 3, where the moments of the molecular weight distribution where derived form a generating function.

4.1(A) Runge-Kutta Methods and Linear Multistep Methods of Integration

'Stiff' integration problems are associated with systems which have widely different timescales. Polymerisation kinetics exhibit stiffness (67,68 and results of this work) because

(a) long chain radicals and dead polymer grow from nothing to molecules ≃1000 units long in a fraction of a second at the start of the polymerisation

and

(b) small changes in the low moments of the molecular weight distribution can cause very much larger changes in the

higher moments.

Integration step length must be limited to isolate the most rapidly changing components of the solution, and consequently computational effort may be considerable to produce solutions which are realistic and represent behaviour after long times. Special techniques have been developed to deal with this sort of problem (61,62,63). However the one which has won widest acceptance is due to Gear (64,65). Gear's DIFSUB routine has been implemented within the NAG Fortran Library (66).

Gear's method is a Backward Difference Formula (BDF) method, which through a sophisticated algorithm can change the order (defined in Appendix 4.1) and time step so that computational effort required to achieve a given local error tolerance (A4.1) is minimised. Hence although a complete description of Gear's method is inappropriate here, the concepts behind the method must be clearly understood.

Conventionally, the initial value problem

$$y' = f(x,y) \qquad y(a) = \eta \qquad (4.1)$$

may be solved numerically by an explicit Runge-Kutta method. A popular fourth order method (often loosely called <u>the</u> Runge-Kutta method) is (69):

$$y_{n+1} - y_n = \frac{h}{8}(k_1 + 3k_2 + 3k_3 + k_4) \qquad (4.2)$$

where $k_1 = f(x_n, y_n)$

$$k_2 = f(x_n + \frac{1}{3}h,\ y_n + \frac{1}{3}hk_1)$$

$$k_3 = f(x_n + \frac{2}{3}h,\ y_n - \frac{1}{3}hk_1 + hk_2)$$

$$k_4 = f(x_n + h,\ y_n + hk_1 - hk_2 + hk_3)$$

$y_n \simeq y(x_n)$

and $x_n = x_o + nh$, h being the steplength

The method is one-step and explicit: it requires no additional starting values and its steplength can easily be changed.

Linear multistep (LM) methods (which form the basis of Gears method) achieve higher order (accuracy) by casting aside the one step nature of the algorithm and retaining linearity with respect to y_{n+j} and f_{n+j}, $j=0(1)k$, where k is the stepnumber and f_n is $f(x_n,y_n)$. The general linear multistep method can be written

$$\sum_{j=0}^{k} \alpha_j y_{n+j} = h \sum_{j=0}^{k} \beta_j f_{n+j} \qquad (4.3)$$

where h is the (constant) steplength

α_j,β_j are constants of the method

The problem of LM methods is to find a sequence $\{y_n\}$ which satisfies the non-linear difference equation 4.3: it is non-linear because f_n is non-linear in y. An ancillary problem is to compute starting values y_j, $j=2(1)k-1$, ie $j=2,3,4...k-1$, for the method.

LM methods can be further distinguished into explicit methods, where $\beta_k=0$ and implicit methods where $\beta_k\neq 0$. For explicit methods 4.3 yields y_{n+k} directly in terms of y_{n+j}, f_{n+j} $j=0(1)k-1$ which have all been calculated previously. For implicit methods the equation becomes

$$y_{n+k} = h\,\beta_k\, f(x_{n+k}, y_{n+k}) + g \qquad (4.4)$$

where g is a function of previously calculated values y_{n+j}, f_{n+j}. For non-linearity with respect to y_n, there exists a unique solution for y_{n+k} which can be approached by the iteration

$$y_{n+k}^{[S+1]} = h\,\beta_k\, f(x_{n+k}, y_{n+k}^{[S]}) + g \quad ; \quad y_{n+k}^{[0]} \text{ arbitrary}$$

$$\text{if } h < 1/L[\beta_k] \qquad (4.5)$$

where L is the Lipschitz constant of f with respect to y.

The Lipschitz condition, Lipschitz constant, the definitions of order and error and the convergence of LM methods are all defined in Appendix 4.1.

Predictor-corrector algorithms (such as Gears) advance a solution using an explicit method (prediction) combined with an implicit method (correction) to converge with an implicit method (correction) to converge on an approximation of the true solution. Predictors are used to give a good initial guess y_{n+k} for the iteration (4.5) so that the number of function evaluations $f(x_{n+k}, y_{n+k})$ is minimised during the iteration.

The corrector can be applied until $y_{n+k} - y_{n+k} < \epsilon$, ie correcting to convergence where ϵ is a predetermined error tolerance related to round off or local truncation error, in which case the weak stability characteristics (which determines how errors propagate) are those of the corrector alone. The steplength must be chosen so that it lies within a range acceptable to the corrector. Should the number of applications of the corrector be limited to minimise function evaluations, the local truncation error and weak stability characteristics will depend on the overall method. Weak stability theory attempts to quantify the effect of stepsize on the accuracy of solution developed by the integration method, accuracy in this sense being how close the numerical solution is to the true solution.

In applying predictor-corrector methods, attention must be focussed on three problems:

(1) The choice of steplength (h).

This is closely associated with the accuracy of the numerical solution. Convergence only tells what happens in the limit $h \to 0$: it is no guarantee of an acceptable solution when h is small and finite.

As steplength is reduced the local truncation error is reduced, but at small steplengths, comparable with the last significant digits of the computer word length, roundoff

errors become significant and the method may become unstable.

(2) Solution of the implicit (non-linear) equation for y_{n+k} for the corrector (eg equation 4.5).

and (3) The generation of starting values.

If a k order method is to be used only $y_n(0)$, $f_n(0)$ are known: y_{n+k}, f_{n+k} k=1(1)k-1 must be supplied.

4.1(B) Systems of Ordinary Differential Equations

The general first order system may be written:

$$\underline{y}' = \underline{f}(x,\underline{y}) \qquad \underline{y}(a) = \underline{\eta} \tag{4.6}$$

Most of the operations derived for single equations can be applied directly to systems of ODE's with scalars being replaced by vectors and moduli of scalars replaced by suitable norms of vectors. The results of weak stability theory which govern stepsize for LM methods require some modification for systems.

For a single equation $\bar{h} = h\,\partial f/\partial y = h\lambda$ must lie within a certain range to ensure that errors do not grow. In systems λ, the estimate for $\partial f/\partial y$, must be replaced by λ_i, the eigenvalues of the Jacobian matrix J, where $J = \partial \underline{f}/\partial \underline{y}$. Any condition imposed on $\bar{h} = h\lambda$ for a single equation must be satisfied when λ is any eigenvalue of J.

4.1(C) Stiffness

In a system where one or more of the components in the solution may be changing rapidly (corresponding to large eigenvalues of the constant matrix A for $\underline{y}' = A\underline{y}$ or of the Jacobian $\partial \underline{f}/\partial \underline{y}$ for the non-linear system $\underline{y}' = \underline{f}(x,y)$) the stepsize of the method must be

limited, so that $h_i = h\lambda_i$ (all i) lies within the appropriate zone of stability. The fast changing component is not usually significant at large time, yet the steplength still must be limited for stability requirements. Stiff systems have large Lipschitz constants.

The general solution of the system

$$\underline{y}' = A\underline{y} + \underline{\phi}(x) \tag{4.7}$$

is

$$\underline{y}(x) = \sum_{i=1}^{M} k_i e^{\lambda_i x} \underline{c}_i + \underline{\psi}(x) \tag{4.8}$$

where λ_i are the distinct eigenvalues of A and $\underline{c}_i$ i=1(1)M are the corresponding eigenvectors.

If Re $\lambda_i < 0$ for all i, then $\sum_{i=1}^{M} k_i e^{\lambda_i x} \underline{c}_i \to 0$ as $x \to \infty$

The first term in the general solution represents the transient solution and $\underline{\psi}(x)$ represents the steady-state solution. In order to pursue the steady state solutions (4.7) must be integrated until the slowest decaying component is negligible ($e^{\lambda_v x} \to 0$), but the presence of components far out to the left in the complex plane ($|\lambda_\mu| >> 0$) ie, fast decaying species forces the use of excessively small steplengths where

$$|\text{Re } \lambda_\mu| \geq |\text{Re } \lambda_i| \geq |\text{Re } \lambda_v| \qquad i = 1(1)M$$

The following description of stiffness can be applied to linear systems ($\underline{y}' = A\underline{y} + \underline{\phi}(x)$):-

(i) $\text{Re } \lambda_i < 0 \qquad i = 1(1)M$ (4.9)

and

(ii) $\max_{i=1(1)M} |\text{Re } \lambda_i| >> \min_{i=1(1)m} |\text{Re } \lambda_i|$ (4.10)

As an indication of the state of stiffness a ratio is called the stiffness ratio is defined:

$$\left[\max_{i=1(1)M} |\text{Re } \lambda_i|\right] : \left[\min_{i=1(1)M} |\text{Re } \lambda_i|\right] \tag{4.11}$$

For non-linear systems, $\underline{y}' = \underline{f}(x,\underline{y})$, stiffness is exhibited if the eigenvalues of the Jacobian, $J = \partial\underline{f}/\partial\underline{y}$, which depends on x, behave in a similar way:

$\underline{y}' = \underline{f}(x,\underline{y})$ is stiff in an interval I of x, if for $x \in I$ the eigenvalues $\lambda_i(x)$ of $\partial\underline{f}/\partial\underline{y}$ satisfy (i) and (ii) above.

4.1(D) Stiff Systems - Solution Methods

Because explicit LM methods have such restrictive ranges of stability, implicit methods with suitable predictors are used of necessity for stiff systems. Each integration step requires simultaneous solution of the non-linear equations,

$$\underline{y}_{n+k} = h\,\beta_k\,\underline{f}(x_{n+k},\,\underline{y}_{n+k}) + \underline{g} \qquad (\underline{g} \text{ known}) \qquad (4.12)$$

The vector form of Newton's method can be applied

$$\left[\underline{y}^{[s+1]} = \underline{y}^{[s]} - J^{-1}(\underline{y}^{[s]}).\underline{F}(\underline{y}^{[s]});\ s=0,1 \text{ where } J(\underline{y}) = \partial\underline{F}(\underline{y})/\partial\underline{y})\right]$$

and 4.12 becomes

$$\underline{y}_{n+k}^{[s+1]} = \underline{y}_{n+k}^{[s]} - \left[I - h\beta_k\,\partial\underline{f}(x_{n+k},\,\underline{y}_{n+k})/\partial\underline{y}\right]^{-1} \cdot \left[\underline{y}_{n+k}^{[s]} - h\beta_k\,\underline{f}(x_{n+k},\,\underline{y}_{n+k}^{[s]}) - \underline{g}\right] \qquad (4.13)$$

Newton's method gives convergence with a much larger steplength than is allowed by stability requirements, providing an initial guess ($\underline{y}_{n+k}^{[o]}$) close to the expected solution is available. This strategy requires re-evaluation of the Jacobian $\partial\underline{f}/\partial\underline{y}$ and matrix inversion of $[I - h\beta_k\,\partial\underline{f}/\partial\underline{y}]$ at each step. Since this is a costly operation on a computer, $\partial\underline{f}/\partial\underline{y}$ is held constant for consecutive iterations. If covergence seems likely (after three steps say) the method will then iterate to convergence; otherwise the Jacobian is re-evaluated when the order or timestep are changed. Where $\partial\underline{f}/\partial\underline{y}$ changes slowly it may be kept constant for a number of integration steps.

Gear's Backward Difference Formula Method

Gear's Method belongs to a class of methods known as Backward Difference (BDF) Methods.

$$\sum_{j=0}^{k} \alpha_j \, y_{n+j} = h\beta_k \, f_{n+k} \qquad (4.14)$$

The coefficients of the method are given in Table 5.1 for k stepnumber and k order.

k	β_k	α_6	α_5	α_4	α_3	α_2	α_1	α_0
1							1	-1
2	$\frac{2}{3}$					1	$-\frac{4}{3}$	$\frac{1}{3}$
3	$\frac{6}{11}$				1	$-\frac{18}{11}$	$\frac{9}{11}$	$-\frac{2}{11}$
4	$\frac{12}{25}$			1	$-\frac{48}{25}$	$\frac{36}{25}$	$\frac{16}{25}$	$\frac{3}{25}$
5	$\frac{60}{137}$		1	$-\frac{300}{137}$	$\frac{300}{137}$	$-\frac{200}{137}$	$\frac{75}{137}$	$-\frac{12}{137}$
6	$\frac{60}{147}$	1	$-\frac{360}{147}$	$\frac{450}{147}$	$-\frac{400}{147}$	$\frac{225}{147}$	$-\frac{72}{147}$	$\frac{10}{147}$

TABLE 4.1

Coefficients of Gear's Method (6.9)

By a sophisticated algorithm, the order of the method and the length of timestep can be adjusted to minimise the local error tolerance and to minimise the amount of computational work performed.

4.2 REDUCTION OF COMPUTATIONAL EFFORT REQUIRED FOR SOLUTION OF THE MODEL

Early studies of the model developed in Chapter Three showed that a great deal of computer time was required to solve the model. (Table 3.4). Typical integrations using Gear's BDF method (NAG routine D02QBF) on a CDC Cyber 174/720 at Imperial College Computer Centre took 1200 cp sections to advance only 168 seconds into the polymerisation. Some of the relevant statistics relating to these runs were:-

Modelled time between interruptions for output of information	6s
Maximum stepsize	5.276×10^{-2}s
Minimum stepsize	1.341×10^{-4}s
Number of integration steps between interruptions	268
Number of Jacobian Evaluations between interruptions	31

This is an unacceptable amount of computation; a typical polymerisation lasts six hours not 168 seconds.

There are two problems which have to be overcome:

(i) The complexity of the model

Some of the phases (eg vapour and water phases) only contribute a small amount to the overall rate of polymerisation. However they demand just as much computational effort as those phases which are contributing significantly; the BDF scheme works with every component in every phase at each timestep.

(ii) The stiffness of the model equations

Analysis of those phases which are contributing significantly to overall rate of polymerisation showed them to be exhibiting very stiff behaviour (Section 4.1(C)). Two approaches were examined in an attempt to reduce the computer time without reducing the generality of the model. Firstly a quasi-steady state approximation (QSSA) was

introduced to overcome the restrictions imposed on steplength by the transient components of the solution. Secondly, the variables used in the model were rescaled.

To ease the discussion in the next sections it is convenient to recast the model of Table 3.4 in vector terms:

$$\dot{\underline{n}} = \underline{f}(t,\underline{n}) \qquad \underline{n}(0) = \underline{n}_0 \qquad (4.15)$$

where $\underline{n}$ represents the mass variables of all the components in the system

$\dot{\underline{n}} = \partial(\underline{n})/\partial t$

$\underline{n}$ may be decomposed to represent the species in each phase

$$\underline{n} = \sum_{j=1}^{7} \underline{n}_j \qquad (4.16)$$

where j represents the subscript appropriate to phase j (Section 3.1) and

$$\underline{n}_j = [n_{Ij},\ n_{Mj},\ n_{\sigma oj},\ n_{\sigma 1j},\ n_{\sigma 2j},\ n_{\lambda oj},\ n_{\lambda 1j},\ n_{\lambda 2j}]^T$$

4.2(A) Reducing the Complexity of the Model

Some simplification of the model can be performed by discarding the vapour(1), continuous(2) and monomer droplet surface(3) phases from the overall kinetic scheme. The BDF integration would be performed on the reduced vector

$$\underline{n}^r = \sum_{j=4}^{1} \underline{n}_j \qquad (4.17)$$

ie polymerisation is only considered important in the monomer(4), microgel(5), primary surface(6) and primary bulk phases(7).

The vapour phase(1) and continuous phase(2) were cast aside because of their contribution to the overall rate of polymerisation is negligible. The ratio of the rates of reaction are given to first order by the ratio of monomer concentrations in the different phases. At 50°C the vapour phase concentration of monomer is 300 mols m^{-3}: in the water phase, it is 11 mols m^{-3} and in the monomer phase it is 13,600 mols m^{-3}. Therefore, the rate of polymerisation in the

monomer phase:the rate in continuous phase:the rate in vapour phase is given by

$$[M]|_4 : [M]|_2 : [M]|_1$$

ie $1 : 8.1 \times 10^{-4} : 2.2 \times 10^{-2}$

Despite their removal from the kinetic scheme, these phases (vapour and continuous) have an important role to play in the consideration of mass transfer (Appendix 5.1).

The droplet surface phase (3) was discarded because of the difficulty in distinguishing, by experimental kinetic measurements, effects due to this phase and effects due to microgel and primary particle phases.

The simplifications discussed in this section have been made for mathematical reasons: the basis for making them has been the observed physics. In later studies it is anticipated that these simplifications will be relaxed.

4.2(B) Reducing the Stiffness of the Model

The simplification carried out in the previous section led to an approximate 50% reduction in the computer time required to model the first 170 seconds. Despite this saving the overall computer time required by the model is still too high. In order to understand the origins of the stiffness causing the excessively long computational times ($\simeq$ 5 cp seconds to model each second of the polymerisation) a simpler model was considered, in which polymerisation was taking place in the monomer phase with no precipitated species present. For this case, the model 4.15 becomes

$$\dot{\underline{n}}_4 = \underline{f}(t, \underline{n}_4) \qquad \underline{n}_4(0) = \underline{n}_{4o} \qquad (4.18)$$

The derivatives $n_4(0)$ were found to be:

$$\dot{n}_I \simeq 10^{-5} \text{ mols } s^{-1}$$

$$\dot{n}_m \simeq 10^{-1} \text{ mols } s^{-1}$$

$$\dot{n}_{\sigma o} \simeq 10^{-6} \text{ mols } s^{-1}$$

$$\dot{n}_{\sigma 1} \simeq 10^{-3} \text{ mols } s^{-1}$$

$$\dot{n}_{\sigma 2} \simeq 10^{0} \text{ mols } s^{-1} \qquad (4.19)$$

$$\dot{n}_{\lambda o} \simeq 10^{-4} \text{ mols } s^{-1}$$

$$\dot{n}_{\lambda 1} \simeq 10^{-2} \text{ mols } s^{-1}$$

$$\dot{n}_{\lambda 2} \simeq 10^{2} \text{ mols } s^{-1}$$

The Jacobian ($J = \partial \underline{f}/\partial \underline{n}_4$) was calculated by differencing, and its eigenvalues were calculated using NAG routine F02AFF.

After one second of polymerisation, the stiffness ratio given by the ratio of the largest to smallest eigenvalues was calculated to be $\simeq 10^{34}$, ie exceptionally high. For this simple model over the first 20s of polymerisation the ratio of computer time to model time was 1.3:1.

4.2(B)(i) The Quasi Steady State Approximation (QSSA)

The above analysis showed that the derivatives of the moments of the growing radical population are approximately two orders of magnitude less than the equivalent derivatives for dead polymer, ie $dn_{\sigma i}/dt / dn_{\lambda i}/dt$ is c.a. 10^{-2}. This suggests making a steady state approximation,

$$\frac{dn_{\sigma i}}{dt} = 0 \qquad (4.20)$$

may be a reasonable assumption. This yields from Table 3.3 algebraic relationships for growing radical populations as follows:

$$[\sigma_o] = \frac{-k_{trp}[\lambda_o] + \sqrt{(k_{trp}[\lambda_o])^2 + 8\, f\, k_D[I]\,(k_{tc} + k_{td})}}{2(k_{tc} + k_{td})}$$

$$[\sigma_1] = \frac{2f\, k_D[I] + k_{trm}[M][\sigma_o] + k_p[M][\sigma_o]}{k_{trm}[M] + k_{trp}[\lambda_o] + (k_{tc} + k_{td})[\sigma_o]} \qquad (4.21)$$

$$[\sigma_2] = \frac{2f\, k_D[I] + k_{trm}[M][\sigma_o] + 2k_p[M][\sigma_1] + k_p[M][\sigma_o]}{k_{trm}[M] + k_{trp}[\lambda_o] + (k_{tc} + k_{td})[\sigma_o]}$$

which may be solved concurrently with the remaining equations for the derivatives:

$$\frac{d[I]}{dt} = -k_D[I]$$

$$\frac{d[M]}{dt} = -(k_p + k_{trm})[M][\sigma_o] \qquad (4.22)$$

$$\frac{d[\lambda_o]}{dt} = k_{trm}[M][\sigma_o] + k_{trp}[\sigma_o][\lambda_o] + k_{td}[\sigma_o]^2 + \frac{k_{tc}}{2}[\sigma_o]^2$$

$$\frac{d[\lambda_1]}{dt} = k_{trm}[M][\sigma_1] + k_{trp}[\sigma_1][\lambda_o] + k_{td}[\sigma_1][\sigma_o] + k_{tc}[\sigma_o][\sigma_1]$$

$$\frac{d[\lambda_2]}{dt} = k_{trm}[M][\sigma_2] + k_{trp}[\sigma_2] + k_{trp}[\sigma_2][\lambda_o] + k_{td}[\sigma_2][\sigma_o]$$
$$+ k_{tc}([\sigma]^2 + [\sigma_o][\sigma_2] + [\sigma_o][\sigma_1])$$

Integrating this scheme yielded considerable improvement with the stiffness ratio, one second into the polymerisation being reduced to c.a. 10^{24}. This represents an improvement of 10^{10} over the earlier attempt. Computational effort was reduced to 0.2 cp seconds per second of polymerisation modelled. Values of the dead moments produced by this method were within 0.3-0.4% of the non-QSSA values.

4.2(B)(ii) Rescaling the variables of the model

When only one phase is present, algebraic manipulations which accompany use of the QSSA to obtain moments for the growing radical population are straightforward. If two or more phases are coupled by the boundary conditions, the possibility of making algebraic errors in similar manipulations is enhanced. Hence although the QSSA offers positive savings in computer time it is cumbersome to use. A more convenient method for reducing the stiffness of the problem is to rescale the variables.

It can be seen from (4.19) that the highest order moments of any population, eg radicals (σ_i) or dead polymer (λ_i) are the most rapidly changing at any instant. This means that over a time step the highest order moments for a population will have changed most. Any stiffness due to the behaviour of transients, eg the growth of the radical population from nothing will be exacerbated because of the rapid change in the high order moments. However this is a problem of length scale and much of the stiffness can be alleviated by considering the variation of the derivatives of a component (4.19) with respect to the absolute value of the component, ie $1/n_i.dn_i/dt$ (all i). Since $1/n_i.dn_i/dt$ is equivalent to the derivative $d/dt(\log_e n_i)$, integration is performed in terms of a natural logarithm of the variable. This indeed turns out to have considerable impact on the observed stiffness. For a similar set of conditions considered in Section 4.2B the scaled derivatives vary in the following manner:

$$
\begin{aligned}
(\log_e \dot{n}_I) &\simeq 10^{-5} \\
(\log_e \dot{n}_M) &\simeq 10^{-6} \\
(\log_e \dot{n}_{\sigma o}) &\simeq 10^{o} \\
(\log_e \dot{n}_{\sigma 1}) &\simeq 10^{o} \\
(\log_e \dot{n}_{\sigma 2}) &\simeq 10^{-1} \\
(\log_e \dot{n}_{\lambda o}) &\simeq 10^{o} \\
(\log_e \dot{n}_{\lambda 1}) &\simeq 10^{o} \\
(\log_e \dot{n}_{\lambda 2}) &\simeq 10^{o}
\end{aligned}
\qquad (4.23)
$$

There is now no a priori reason for making the QSSA on the radical population moments. Indeed any QSSA is more likely justified for the initiator and monomer derivatives. However the stiffness ratio of the Jacobian $\underline{J} = \partial(1/n\ f(t,\underline{n}))/\partial(\underline{\log_e n})$ is reduced to c.a. 10^{12} (i.e. 10^{12} less than for the QSSA) and the computational time is considerably reduced to 0.02 cp seconds per second modelled.

Scaling was therefore implemented in the final model as a necessary condition for the numerical integration to be performed in a reasonable time. The only note of caution related to the initial conditions, many of which are zero, and therefore have no logorithm. The model, as represented by equation (4.15):

$$\dot{\underline{n}} = f(t,\underline{n}) \qquad \underline{n}(0) = \underline{no}$$

must be integrated in the normal plane (as opposed to the logorithmic plane) using the BDF method for a small interval of time. This creates an ancillary set of initial conditions

$$\underline{n}(\Delta t) = \underline{n}_{\Delta t} \qquad (4.24)$$

whose logarithms exist.

4.3 CONSERVATIVE NATURE OF THE MODEL EQUATIONS

In attempting to model the polymerisation of vinyl chloride considerable attention must be paid to the conservative nature of the equations developed. The precipitated polymeric phase is growing at the expense of depleting monomer phase. At an early stage in the integration it is necessary to know the volume of each phase accurately in order to determine the interfacial areas for the mass transfer terms and the concentration of each species in the kinetic terms

Early attempts at estimating phase volumes were made by integrating the set of equations $d(\underline{c}_j)/dt$ (Table 3.3) holding phase volume, V_j, constant. Updates in phase volume were performed outside the Gear integrator DOZQBF. Because the phase volume is determined by the relationship

$$V_j = \sum_i (c_{ij}\, V_j)\, \bar{v}i_j \qquad (4.25)$$

where $c_{ij}, \bar{v}^i{}_j$ are the concentration of component i in j and its specific molar volume respectively. One "predictor" for V_j might be

$$\left.\frac{dV_j}{dt}\right|_{t+\Delta t} = \sum_i \left[V_j\Big|_t \left.\frac{dc_i}{dt}\right|_{t+\Delta t} + c_i\Big|_{t+\Delta t} \left.\frac{dV_j}{dt}\right| \right] \bar{v}_j{}^i \qquad (4.26)$$

where t is the time when updating was last performed

Δt is the time elapsed since t

$t+\Delta t$ is the current time

The new phase volume would be given by

$$V_j\Big|_{t+\Delta t} = V_j\Big|_t + \left.\frac{dV_j}{dt}\right|_{t+\Delta t}^{\Delta t} \qquad (4.27)$$

(A wide range of differencing schemes could be conceived incorporated in more sophisticated predictor mechanisms, eg Nordsieck (69)).

Prediction of $V_j|_{t+\Delta t}$ would be performed when

$$\left| \frac{\sum_i c_{ij}|_{t+\Delta t} \; V_j|_t}{\sum_i c_{ij}|_t \; V_j|_t} \right| > \epsilon_j \qquad (4.28)$$

This is a potentially costly operation involving the storage of the initial conditions, forward integration over Δt, and progressive reduction in Δt until the forward integration was bounded by (4.28). Even so conservation is only guaranteed in the limit $\Delta t \to 0$ when the numerical approximations 4.26 and 4.27 become analytic expressions. However keeping Δt small to maintain a conservative scheme will either jeopardise the stability of the method as roundoff errors will become significant (Section 4.1(A)) or increase the time taken to reach a solution.

For numerical integration the model equations developed in Chapter 3 (Table 3.4) were therefore recast so that mass rather than concentration is the variable updated and conserved at each time step. This is readily done by using the simple transformations.

$$I|_j = V[I]|_j \qquad M|_j = V[M]|_j$$

$$\sigma_o|_j = V[\sigma_o]|_j \quad \sigma_1|_j = V[\sigma_1]|_j \quad \sigma_2|_j = V[\sigma_2]|_j \qquad (4.29)$$

and $$\lambda_o|_j = V[\lambda_o]|_j \quad \lambda_1|_j = V[\lambda_1]|_j \quad \lambda_2|_j = V[\lambda_2]|_j$$

where [] denotes the molar concentration of the variable.

The problem of updating phase volume is now circumvented. The phase volume is given by:

$$V_j = \bar{v}_j^P(\lambda_1|_j + \sigma_1|_j) + \bar{v}_j^m M|_j \qquad (4.30a)$$

where v_j^P, v_j^m are the specific partial molar volumes of polymer and monomer in phase j. In differential form 4.30a becomes

$$\frac{dV_j}{dt} = v_j^P \left[\frac{d\lambda_1|_j}{dt} + \frac{d\sigma_1|_j}{dt} \right] + \bar{v}_j^m \left. \frac{dM}{dt} \right|_j \qquad (4.30b)$$

The phase volume can therefore be updated at the same time as the mass derivatives within the BDF derivative scheme (Table 4.2).

The degree of mass conservation can be calculated according to the relationship:

$$\frac{M(t)}{M_o} = \frac{\sum_j (M_j(t) + \sigma_{1j}(t) + \lambda_{1j}(t)}{M_o}$$

M_o is the initial molar charge of monomer
$M_j(t)$ is the molar mass of monomer in phase j at time t
and $\sigma_{1j}(t)$, $\lambda_{1j}(t)$ represent the number of mols of monomer converted to radicals and dead polymer respectively.

For all the polymerisation cases modelled the ratio $M(t)/M_o$ was greater than 99.9% (an arbitrarily chosen error criterion to check the degree of conservation of the model).

TABLE 4.2

Model Equations in Conservative Form

Kinetic Terms

$$\left.\frac{dI}{dt}\right|_j = - k_D I|_j$$

$$\left.\frac{dM}{dt}\right|_j = - (k_p M + k_{trm} M)\, \sigma_o|_j/V_{ji}$$

$$\left.\frac{d\sigma_o}{dt}\right|_j = 2f\, k_D\, I|_j - k_{trp}\, \sigma_o\, \lambda_o|_j/V_j - (k_{tc} + k_{td})\, \sigma_o{}^2|_j/V_j$$

$$\left.\frac{d\sigma_1}{dt}\right|_j = 2f\, k_D\, I|_j + k_{trm}\, M(\sigma_o - \sigma_1)|_j/V_j + k_p\, M\, \sigma_o|_j/V_j - k_{trp}\, \sigma_1\, \lambda_o|_j/V_j - (k_{tc} + k_{td})\, \sigma_1\, \sigma_o|_j/V_j$$

$$\left.\frac{d\sigma_2}{dt}\right|_j = 2f\, k_D\, I|_j + k_{trm}\, M(\sigma_o - \sigma_2)|_j/V_j + k_p\, M(\sigma_o + 2\sigma_1)|_j/V_j - k_{trp}\, \sigma_2\, \lambda_o|_j/V_j - (k_{tc} + k_{td})\, \sigma_2\, \sigma_o|_j/V_j$$

$$\left.\frac{d\lambda_o}{dt}\right|_j = k_{trm}\, M\, \sigma_o|_j/V_j + k_{trp}\, \sigma_o\, \lambda_o|_j/V_j + k_{td}\, \sigma_o{}^2|_j/V_j + \frac{k_{tc}}{2}\, \sigma_o{}^2|_j/V_j$$

$$\left.\frac{d\lambda_1}{dt}\right|_j = k_{trm}\, M\, \sigma_{o|j}/V_j + k_{trp}\, \sigma_1\, \lambda_{o|j}/V_j + k_{td}\, \sigma_1\, \sigma_{o|j}/V_j + k_{tc}\, \sigma_o\, \sigma_{1|j}/V_j$$

$$\left.\frac{d\lambda_2}{dt}\right|_j = k_{trm}\, M\, \sigma_{2|j}/V_j + k_{trp}\, \sigma_2\, \lambda_{o|j}/V_j + k_{td}\, \sigma_2\, \sigma_{o|j}/V_j + k_t(\sigma^2_1 + \sigma_o\sigma_1\ \sigma_o\sigma_2)|j/V_j$$

Kinetic Terms Plus Mass Transfer Fluxes.

$$\frac{dn_{Ij}}{dt} = \left.\frac{dI}{dt}\right|_j + A_{j-1,j}\,(K_{oI})_{j-1}\,[I_{j-1}/V_{j-1} - \gamma^I_{j-1,j}\, I_j/V_j] - A_{j,j+1}\,(K_{oI})_j\,[I_j/V_j - \gamma^I_{j,j+1}\, I_{j+1}/V_{j+1}]$$

$$\frac{dn_{mj}}{dt} = \left.\frac{dM_i}{dt}\right|_j + A_{j-1,j}\,(K_{oM})_{j-1}\,[M_{j-1}/V_{j-1}\ \gamma^M_{j-1,j}\, M_j/V_j] - A_{j,j+1}\,(K_{oM})_j\,[M_j/V_j - M\gamma_{j,j+1}\, M_{j+1}/V_{j+1}]$$

$$\frac{dn_{\sigma ij}}{dt} = \left.\frac{d\sigma_i}{dt}\right|_j + A_{j-1,j}\,(K_{o\sigma_i})_{j-1}\,[\sigma_{ij-1}/V_{j-1} - \gamma^{\sigma_i}_{j-1j}\, \sigma_j/V_j] - A_{j,j+1}\,(K_{o\sigma_i})_j\,[\sigma_{ij}/V_j - \gamma^{\sigma_i}_{jj+1}\, \sigma_{j+1}/V_{j+1}]$$

$$\frac{dn_{\lambda ij}}{dt} = \left.\frac{d\lambda_i}{dt}\right|_j + A_{j-1,j}\,(K_{o\lambda i})_{j-1}\,[\lambda_{ij-1}/V_{j-1} - \gamma^{\lambda_i}_{j-1j}\, \lambda_{ij}/V_j] - A_{j,j+1}\,(K_{o\lambda i})_j\,[\lambda_{ij}/V_j - \gamma^{\lambda_i}_{ij+1}\, \lambda_{ij+1}/V_{j+1}]$$

$$\frac{dV_i}{dt} = \bar{v}^P_j \left[\frac{dn_{\lambda ij}}{dt} + \frac{dn_{\sigma ij}}{dt}\right] + \bar{v}^M_j \left[\frac{dn_{mi}}{dt}\right]$$

where n_{ij} represents the number of moles of species i in phase j through chemical reaction and mass transfer and A_{jj+1} represents the interfacial area between phase j and j+1.

NB This set of equations can be represented

$$\underline{\dot{n}}_j{}^T = \frac{d}{dt}(\underline{n}_j) \quad \underline{n}_j = [n_{Ij},\ n_{Mj},\ n_{\sigma oj},\ n_{\sigma 1j},\ n_{\sigma 2j},\ n_{\lambda oj},\ n_{\lambda 1j},\ n_{\lambda 2j},$$

and in order to reduce stiffness the set integrated is:

$$\frac{1}{n_{ij}} \frac{dn_{ij}}{dt}$$

4.4 ALTERNATIVE SOLUTION METHODS

In Chapter 3 a generating function was used to reduce the large number of differential equations describing the polymerisation system, viz:

$$\left.\begin{array}{lll} \text{initiator} & \dfrac{dI}{dt} = f_1(I) & \\ \text{monomer} & \dfrac{dM}{dt} = f_2(M,R_i) & \text{All } i \\ \text{growing radicals} & \dfrac{dR_i}{dt} = f_3(I,M,R_i,P_i) & \text{All } i,j \\ \text{formed polymer} & \dfrac{dP_i}{dt} = f_4(I,M,R_i,P_i) & \text{All } i,j \end{array}\right\} \quad (4.31)$$

to a smaller number of transform equations:

$$\left.\begin{array}{ll} \text{initiator} & \dfrac{dI}{dt} = f_1'(I) \\ \text{monomer} & \dfrac{dM}{dt} = f_2'(M,G_R(1) \\ \text{radicals} & \dfrac{dG_R(s)}{dt} = f_3'(I,M,G_R(s),G_p(s),s) \\ \text{polymer} & \dfrac{dG_p(s)}{dt} = f_4'(I,M,G_R(s),G_p(s),s) \end{array}\right\} \quad (4.32)$$

where $G_R(S) = \sum_{n=1}^{\infty} s^n R_n$ $\qquad$ $G_p(S) = \sum_{n=1}^{\infty} s^n P_n$

In a limited number of cases (72,73) it is possible to manipulate the transformation variables and invert them, by series expansion to extract the molecular weight distribution. The main analytic results for cases where this is possible are summarised in the table below.

TABLE 4.3

Molecular Weight Distributions for Ideal Polymerisation Mechanisms

Polymerisation Type (all homogeneous)	Generating Functions	MWD
Anionic Chain in Batch Reactor	$G(s,t) = e^{(s-1)t_s P_{1o}}$	$P_n(t) = P_{1o} e^{-t} \frac{t^{n-1}}{(n-1)!}$
Anionic Chain in CSTR	$G(s) = \frac{I_o}{1+k_p M\theta} \frac{s}{1-\left[\frac{k_p M\theta_1}{1+k_p M\theta}\right]s}$ ($\theta \equiv$ residence time)	$P_j = ab^{j-1}$ Most probable or Flory Distribution
Free Radical in Batch Reactor	$G_R(s) = \frac{as}{1-bs}$ $a = \frac{2f k_i I}{k_p M + (2f k_i k_t I)^{1/2}}$ $b = \frac{k_p M}{k_p M + (2f k_i k_t I)^{1/2}}$ $\frac{dG_p(s)}{dt} = \frac{k_t}{2} \left[\frac{as}{1-bs}\right]^2$	Growing Chains $R_j = ab^{j-1}$ $\frac{dP_n}{dt} = \frac{k_t}{2} a^2 b^{n-2}(n-1)$

Because of the complexity of the model developed in Chapter 3 such an analytic treatment to give the full MWD is intractable in this case. Consequently equations describing only the moments of the molecular weight distribution were derived. It would be of great benefit if a solution for (4.31) could be advanced in the (s,t) plane, at suitable values of s, and, after specific periods of time invert the transform equations numerically to obtain the molecular weight distribution directly. This would give invaluable evidence for direct comparison with g.p.c. results, rather than using the moments of the distribution to fit particular polynomial functions, such as Laguerre Polynomials (67, 67a) or Pearson Functions (67). Numerical inversion of the Z-transform ($Z \equiv 1/s$) has been suggested before (74,75). Indeed it is often tacitly assumed that such an inversion may be performed (eg 68), yet no-one appears to have tried this. It was therefore decided to investigate the feasibility of numerical inversion of polymerisation generating functions with a

view to applying such techniques to complex polymerisation mechanisms such as the one involved in the present PVC model.

4.4(A) Numerical Inversion of Generating Function, $G(s)=\sum_{n=1}^{\infty} s^n P_n$

Motivated by the existence of numerical inversion techniques for Laplace transforms (eg 76,77,78,79) and the similarity of the generating function and Laplace transform (80) one method of inversion may be through transformation of the generating function equations into the Laplace transform domain and subsequent inversion of the 'psuedo' Laplace transform.

The similarity of Laplace transform and the generating function can be demonstrated by considering two functions D(n) and C(n), the (discrete) MWD of a sample polymer and its continuous approximation respectively. The MWD is discrete because polymer chains consist of integral numbers of monomer units, and the approximation of the MWD as continuous arises because the interval between sampling points (monomer units) is small in comparison with ultimate chain lengths.

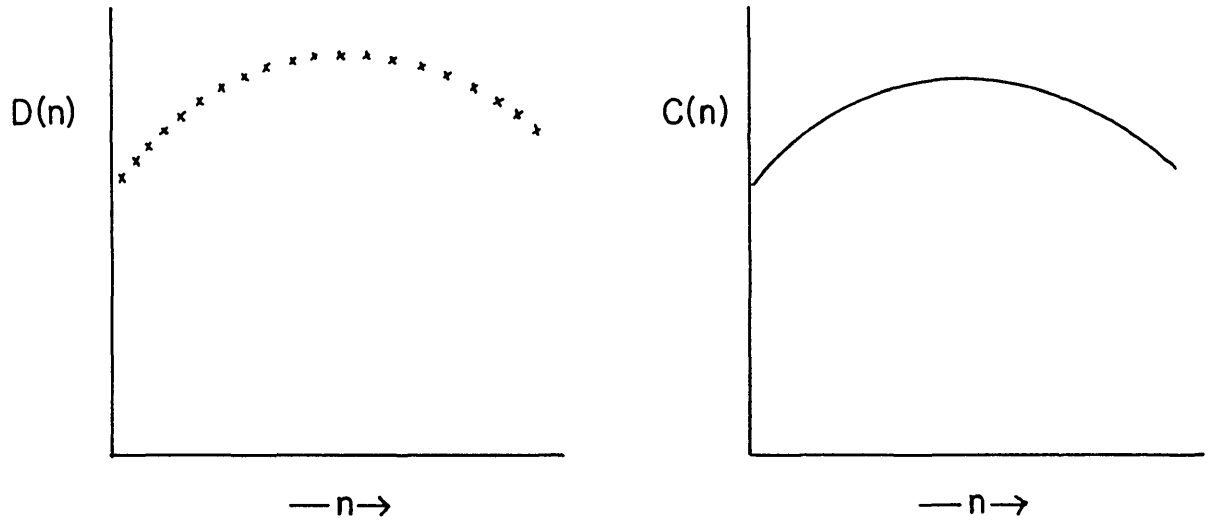

FIGURE 4.1 - Discrete and Continuous MWD

The approximate transforms are given in Table 4.4.

TABLE 4.4

Transformations Appropriate to Discrete and Continuous Functions

Function	D(n)	C(n)
Transform	$G(s) = \sum_{n=1}^{\infty} D(n)s^n$ Generating Function	$F(p) = L\{C(n)\}$ $= \int_0^{\infty} C(n)e^{-pn}\,dn$ Laplace Transform
Inversion Integral	$D(n) = 0_{\Gamma} \frac{1}{s^{n+1}} G(s)\,ds$ Γ is the unit circle	$C(n) = \frac{1}{2\pi i} \int_{c-i\infty}^{c+i\infty} F(p)e^{pn}dp$ C is to the right of all poles of F(p)

Jury (80) makes use of the sampling property of the Dirac delta function,

$$\delta(n) = \begin{cases} \infty & n=0 \\ 0 & n\neq 0 \end{cases} \quad ; \quad \int_{-\infty}^{\infty} \delta(n)\,dn = 1 \qquad (4.33)$$

to derive the relationship between the Z-transform amd the Laplace transform.

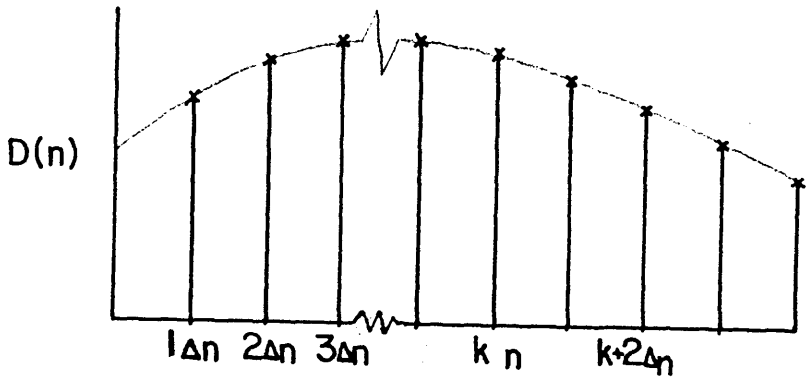

FIGURE 4.2

Taking the Laplace transform of the impulsed function,

$$D^*(n) = C(n) \sum_{k=0}^{\infty} \delta(n - k\Delta n) = \sum_{k=0}^{\infty} C(k\Delta n)\delta(n - k\Delta n)$$

where Δn represents the sampling interval of the discrete function, and putting $e^{-p\Delta n} = s$ yields

$$F^*(p) = L[D^*(n)] = \int_0^\infty D^*(n)\, e^{-pn}\, dn = G(s)|_{s=e^{-p\Delta n}}$$

If a rectangular box of width Δn and height $D^*(n)$ is constructed around each spike of the impulsed function $D^*(n)$, an approximation to the continuous function $C(n)$ is achieved

$$C(n) \cong \Delta n\, D^*(n)$$

Hence, a pseudo Laplace transform is given by

$$L\{C(n)\} \cong \left\{\Delta n\, G(s)|_{s=e^{-p\Delta n}}\right\}_{T\to 0} \qquad (4.34)$$

Points in the s and p phases can be mapped into one another by the relationship

$$s = e^{-p\Delta n}$$

($\Delta n = 1$ for polymer systems)

(The validity of the result (4.34) may be tested on the sample functions appearing in Grabbe (81) where functions are given, with their Laplace transforms and Z transforms.

For example,

e^{-an} has Laplace transform $\frac{1}{p+a}$ and Z transform $z/(z - e^{-a\Delta n})$

Setting $s = 1/z$, $(z/z - e^{-a\Delta n}) \to 1/(1 - Se^{-a\Delta n})$
Writing $s = e^{-p\Delta n}$ and multiplying by Δn

$1/(1 - Se^{-a\Delta n}) \to \Delta n/(1 - e^{-(p+a)\Delta n}) \to \frac{1}{p+a}$ if expanded and $\Delta n \to 0$.

4.4(A)(i) Numerical Inversion of Laplace Transform

While several methods exist to do this (eg 76-79) that due to Bellman et al demonstrates the general principle of replacing the

indefinite integral of the Laplace transform by the finite quadrature:

$$F(p) = \int_0^\infty e^{-pn}\, C(n)\, dn \qquad (4.35)$$

Writing $x = e^{-n}$

$$F(p) = \int_0^1 x^{p-1}\, C(-\log x)\, dx \qquad (4.36)$$

and with $g(x) = C(-\log x)$ (4.37)

$$F(p) = \int_0^1 x^{p-1}\, g(x)\, dx \qquad (4.38)$$

which approximates to

$$\sum_{i=1}^{N} W_i\, x_i^{p-1}\, g(x_i) = F(p) \qquad (4.39)$$

where x_i, W_i are roots and weights associated with the N-order shifted Legendre polynomial. Letting p assume N values yield a system of N unknowns:

$$\sum_{i=1}^{N} W_i\, x_i^{k}\, g(x_i) = F(k+1) \qquad k = 0(1)N-1 \qquad (4.40)$$

which may be solved by matrix inversion for $g(x_i \upsilon)$ and hence $C(-\log x)$ or $C(n)$.

4.4(B) Application of Inversion Technique to Polymer Systems

The pseudo Laplace transform relationship was used to convert generating function transforms of simple function (eg e^{-an} or n) to the Laplace transform domain. Bellman's method was used to invert the functions. Difficulties were experienced with the inversion: these were associated with the ill conditioning of the matrix inversion at equation 4.40 and were reduced by using longer computer word lengths (ie double precision on a CDC computer with a 60 bit word). Agreement was within 10% of the expected solution.

With known polymeric distribution test functions (Table 4.3) the

method failed completely, with highly oscillatory inverse functions being obtained (positive and negative MWD!) instead of the known smooth solutions. This was initially thought to be due to the failure of the numerical inversion procedure. However, further analysis shows this not to be the case.

The existence theorem for inverse Laplace transforms (82) states that the order of F(p) with respect to p must be less than -1 for the inverse of a Laplace transform to exist.

If we consider the case of anionic polymerisation which has a generating function (Table 4.3):

$$G(s,t) = e^{(s-1)t}\ s\ P_{10} \qquad (4.41)$$

The Laplace transform of this (from equation 4.34) is given by

$$F(p) = \Delta n\ P_{10} \exp\ [(\exp(-p\Delta n) - 1)t]\ \exp(-p\Delta n) \qquad (4.42)$$

Expanding this in terms of P shows it to be of order p and higher, ie no inverse Laplace transform exists. Similar results hold for all the test functions in Table 4.3.

It may be concluded therefore that since inversion of the transform equations fails for these particular polymerisation cases, it is an unsatisfactory method for general use and in particular for the PVC case. All further work was confined to moment analyses of the MWD.

4.4(C) Numerical Derivation of Moment Equations

Another approach worthy of consideration is the numerical differentiation of the transform equations G(s,t) (4.32) with respect to s. The model would be solved numerically for G(s,t) for different values of s near s=1 as time was increasing. Numerical differentiation of G(s,t) with respect to s would yield the moments, without analytic differentiation. This would be a very useful step

in developing a model of wide ranging application for more complex polymerisation kinetic schemes. A computer program would only integrate the transform equations in the (s,t) plane and then derive the moments of the distribution when required. The need for integrating all the differential equations for the moments would be obviated.

The k'th moment of a polymer population is defined by

$$\lambda_k(t) = \sum_{j=1}^{\infty} j^k \, P_j(t) \qquad (4.43)$$

and since $G_p(s,t) = \sum_{n=1}^{\infty} s^n \, P_n(t)$ (4.44)

$$\lambda_k(t) = \frac{\partial k}{\partial (\ln s)^k} \, G_p(s,t)\Big|_{s\to 1} = \left[s \frac{\partial}{\partial s}\right]^k G_p(s,t)\Big|_{s\to 1} \qquad (4.45)$$

Therefore (by continuous differentiation of the operator)

$$\left[s \frac{\partial}{\partial s}\right]^k \Bigg]$$

$\underline{\lambda} = \underline{\underline{Q}} \cdot \underline{G_p}^s$ where

$$\underline{\lambda}(t) = [\lambda_o(t), \lambda_1(t), \lambda_2(t), \lambda_3(t) \ldots .]^T \qquad (4.46)$$

$$\underline{G_p}^s(t) = [G_p{}^o(1,t), G_p{}^1(1,t), G_p{}^{11}(1,t), G_p{}^{111}(1,t) \ldots .]^T$$

$$G_p{}^i(1,t) = \frac{\partial i}{\partial s^i} \, G_p(1,t)$$

and $\underline{\underline{Q}}$ is the matrix

$$\begin{bmatrix}
1 & & & & & & \\
1 & 1 & & & & & \\
1 & 3 & 1 & & & & \\
1 & 7 & 6 & 1 & & & \\
1 & 15 & 25 & 10 & 1 & & \\
1 & 31 & 90 & 65 & 15 & 1 & \\
\cdots & \cdots & \cdots & \cdots & \cdots & \cdots & \cdots
\end{bmatrix}$$

Method:-

Solution of the transform equations is advanced in the (s,t) plane at suitably chosen values of s (eg, zeroes of shifted Chebyshev polynomial of order N,

$$S_i = \{1 - \cos[(2i - 1)\pi/2N]\}/2 \quad ; \quad i = 1,N$$

The derivatives of the transforms with respect to S are evaluated at s = 1 and finally the moments are derived from (4.46).

Derivatives are calculated by approximating the generating function in s(0,1) by a truncated Taylor series

$$G(1 - s) = \sum_{j=1}^{N} \frac{(-s)^{j-1}}{(j-1)!} \; G_p^{j-1}(1,t) + O(s^n) \qquad (4.47)$$

Applying this approximation at each zero of the shifted polynomial, a set of equations

$$\underline{T}\; \underline{G_p^S}(t) = \underline{G}(1 - S) \qquad (4.48)$$

is generated, where $\underline{T}$ is matrix containing all the coefficient of the expansion

$$\frac{(-s_i)^{j-1}}{(j - 1)^1}$$

The solution for $\underline{G_p^S}(t)$,

$$\underline{G_p^S}(t) = \underline{T}^{-1} \; . \; \underline{G}(1 - s) \qquad (4.49)$$

is achieved by Crout's Factorisation method (NAG routine F04 AEF)

The method was tested with the test function

$$G(s,t) = se^{(s-1)t} P_{10} \qquad \text{(Table 4.3)}$$

with t = 5, P_{10} = 10.0 which has moments λ_0 = 10, λ_1 = 60.0, λ_2 = 410, λ_3 = 3110 and λ_4 = 25760.

Values of G(s,t) were calculated at the zeroes of shifted Chebyshev polynomials of order N (of which there are N in the interval (0,1). A secondary polynomial was fitted through these points using a least squares method in orthogonal polynomials (83). This was done so that G(1-s) could be calculated without recourse to the test function, which under normal circumstances would not be available. For orders greater than three the matrix $\underline{\underline{T}}$ had determinants $<10^{-7}$ and the inversion Δ was deemed ill conditioned. More than 20 zero positions for function evaluation of G(s,t) were required before the fitted polynomial (subroutine FIT, appendix 4.2) matched the test function over the whole interval, such that

$$\frac{G(s,t) \mid \text{approx}}{G(s,t) \mid \text{real}} < 10^{-6} \quad (s = 0,1)$$

With fewer than 20 points the fitted polynomial showed poor agreement, with negative approximate values being obtained. When more than 50 zeroes were evaluated, poor agreement was obtained in calculated moments

$\lambda_0 = 13.00993$ (cf 10.0)
$\lambda_1 = 112.7420$ (cf 60.0)
λ_2 not available.

Closest agreement with the test function was obtained with 24 points when

$\lambda_0 = 9.999914$ (relative error 8.6×10^{-4}%)
$\lambda_1 = 69.90688$ (relative error 16.5%)
$\lambda_2 = 515.9048$ (relative error 25.8%)

While numerical differentiation is accepted as a low accuracy method (83), these results seem unacceptably poor. If the behaviour of the test function is analysed in s(0,1), it can be seen (Figure 4.3) that for $t > 100$, say, the function has become essentially a step function at $s = 1$. Such functions display precisely the wrong sort of behaviour (ie, rapidly changing slopes) for reasonable numerical differentiation.

It was therefore concluded that this method too is unacceptable for implementation with transform equations: it required a considerable number of points in the s plane to yield low accuracy estimates of the second order moment of the molecular weight distribution. For such low order moments analytic differentiation of the transform equations (Chapter 3) offers no difficulty.

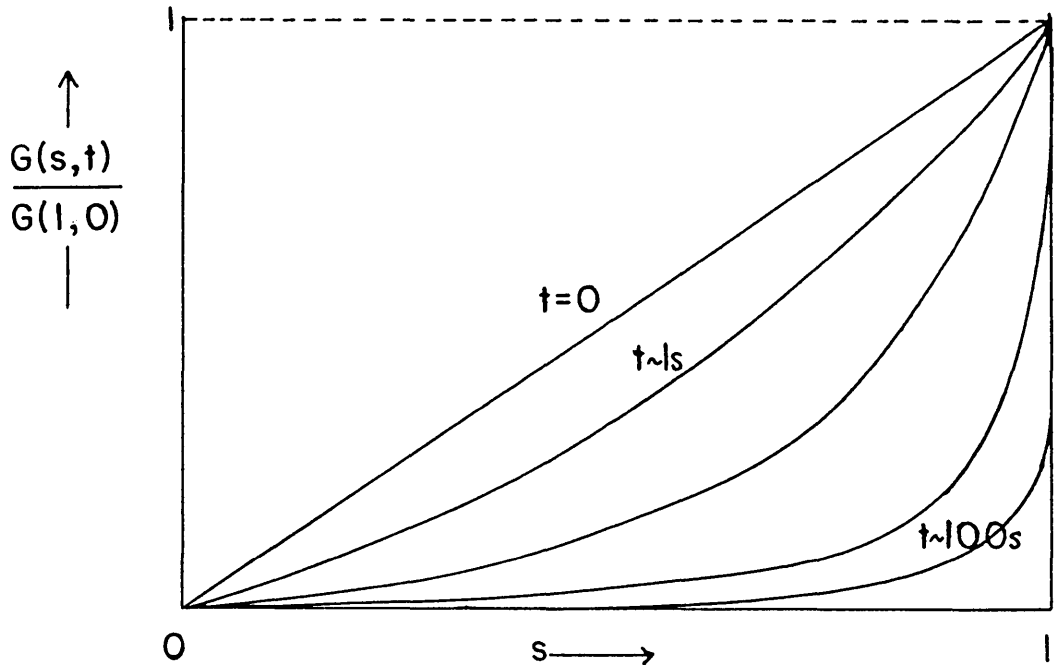

FIGURE 4.3 - Schematic Representation of Behaviour of $G(s,t)/G(1,0) = e^{(s-1)t_s}$

CHAPTER FIVE

USING THE PROCESS MODEL

In previous chapters we have considered the background to the physical model of the polymerisation of vinyl chloride (Chapter 2), developed this into a mathematical model to explain the process (Chapter 3) and looked at the methods appropriate to the solution of the model equations (Chapter 4). The present chapter covers a number of topics concerning the details of the practical implementation of the model:

a) Section 5.1 concentrates on how various product and process characterisitcs have been incorporated into the model.
b) Section 5.2 contains an analytic solution for a limiting case of the model outlined in Chapter 3. Amongst other things this allows the numerical techniques used in the solution of the full model to be checked (see Section 5.4).

5.1 MODELLING OF THE PRODUCT AND PROCESS CHARACTERISTICS (98)

5.1(i) Primary Particle Aggregation

On the macroscopic scale, grains (polymerising monomer droplets) will aggregate if the steric stabilisation offered by surfactants in the autoclave becomes inadequate. This will reduce the surface area available for mass transfer of VCM from the vapour phase to the suspended droplets. The effect of the loss of surface area on the rate of polymerisation will be negligible; the vapour space is only a small reservoir of VCM (Section 3.1.1). However inside the droplets any loss of surface area between the liquid monomer and the precipitated polymer particles is potentially much more significant, especially if the rates of reaction within the precipitated polymer phase are exhibiting any degree of diffusion controlled behaviour. It is important therefore to have a quantitative model for the aggregation processes involved.

In Section 2.5(D) the stability of primary particles was discussed qualitatively. Early studies of electron micrographs of PVC produced in bulk polymerisation had found that the number concentration of primary particles was constant at c.a. $5 \times 10^{11} cm^{-3}$. (40,43,45). Such observations are consistent with many of the models for nucleation modified for oligomer capture which are discussed in some depth by Barrett (84) and summarised below in Figure 5.1 and Table 5.1. All these models predict that the number of precipitated particles monotonically increases with time and asymptotes to a final fixed number, N_o (shown schematically in Figure 5.2(i)).

More recent evidence (26,27,32) indicates that the number of precipitated particles is decreasing with conversion because primary particles are agglomerating (Figure 5.2(ii)). The overall nucleation of basic particles and agglomeration of primary particles is illustrated schematically in Figure 5.2(iii) which shows the variation in the total number of precipitated particles with time. During the period when agglomeration of the primary particles is occurring, we have chosen to model the number of precipitated particles according to the empirical relationship

$$\frac{N - N_\infty}{N_o - N_\infty} = e^{-\epsilon_{agg} x} \qquad (5.1a)$$

$$\epsilon_{agg} = A_{agg}\ e^{(-\epsilon_{agg}/RT)} \qquad (5.1b)$$

where N_∞ is the limiting number of agglomerates of primary particles at high conversions which has been found to be essentially constant and equivalent to $5 \times 10^{17} m^{-3}$ (31).

N_o is the number of primary particles created during the initial burst of nucleation which is a function of the initiation rate (α $2f k_D[I]_4$) and therefore determined by temperature and the nature of the initiator.

x is the conversion

ϵ_{agg} is a rate coefficient for the agglomeration process which is postulated as showing Arrhenius behaviour with an activation energy E_{agg}.

The motivation for using this relationship comes from some interesting experimental data of Smallwood (86). He performed experiments where samples of suspension PVC were withdrawn from an autoclave at different conversions. The samples were investigated by using scanning electron microscopy and image analysis techniques, to determine the mean primary particle diameter as a function of conversion at several different temperatures.

The number of primary particles and their concentration per unit volume can be calculated as a function of conversion (Appendix 5.1 III). [It has been assumed that in taking samples of PVC and subsequently stripping the monomer which swells the polymer, the polymer matrix does not collapse: ie the micrographs of PVC show primary particles which are fully swollen]. When Smallwood's data are treated in this way the curves in Figure 5.3 are obtained. The results are fitted by equations 5.1 when

$$A_{agg} = 1.337 \times 10^{6}$$

$$E_{agg} = 33.55 kJmol^{-1} \qquad (5.2)$$

The initial nucleation period (upto t_o in Figure 5.2iii) occurs over a range of conversion to 10^{-3} (26). Because:

(a) greater than 99.9% of the rate of polymerisation is due to the diluent (monomer) phase over this range
(b) the surface area of the precipitated phase is growing rapidly
(c) in view of (a) and (b) diffusion limitation is not expected to be significant at such early conversions
(d) the range ($0 - 10^{-3}$) represents the conversion range modelled in the first few time steps (typically 10 timesteps out of 1500)

The nucleation burst was therefore not modelled accurately upto t_o because of the overhead in computing time this would have incurred. Any of the models in Figure 5.1 and Table 5.1 could have been used to provide an initial value for N_o and included in the overall derivative scheme. However, in this study N_o was estimated from experimental data and the overall number of precipitated particles described by equation 5.1.

FIGURE 5.1 - Mechanisms of Oligomer Capture

<table>
<tr>
<td>DIFFUSION CAPTURE

Primary Particle

 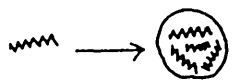 </td>
<td>An oligomer diffuses towards and existing particle and is irreversibly caught.
Condition:
time for diffusion <
time for self nucleation</td>
</tr>
<tr>
<td>EQUILIBRIUM CAPTURE

 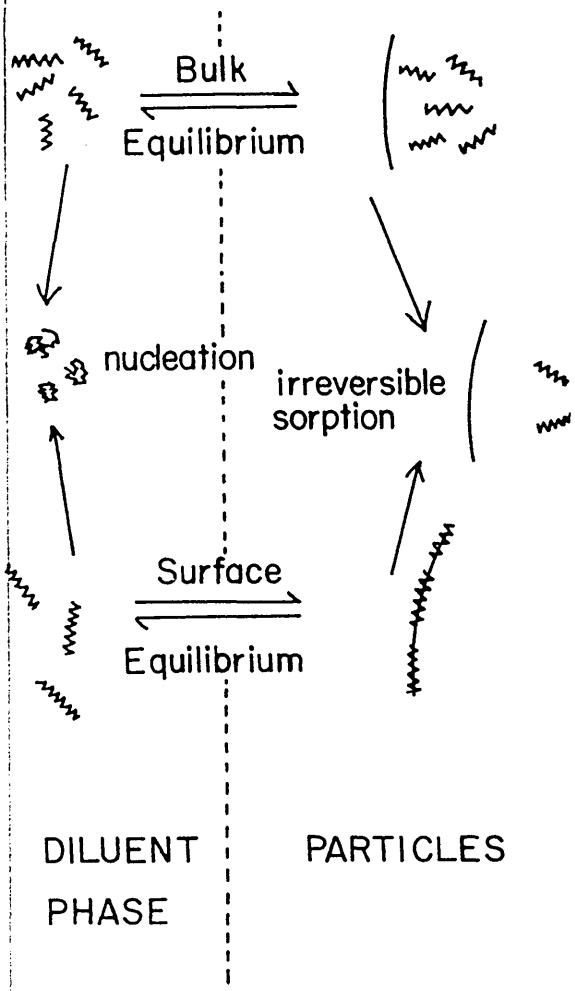
</td>
<td>Oligomers which are soluble in the diluent phase are at equilibrium with
(1) oligomers in the surface of the precipitated particles or with (2) oligomers in the bulk of the precipitated particles.
POINTS
(a) The proportion of oligomers undergoing nucleation or capture is determined by an equilibrium constant.
(b) Nucleation or irreversible sorption occurs when oligomers have grown longer than a threshold molecular chain length.</td>
</tr>
</table>

TABLE 5.1

Models for Nucleation Modified for Oligomer Capture

Model	$\frac{dN}{dt}$ =	where Z =
Equilibrium Capture (with bulk)	$\frac{R_i}{Q} \frac{1}{1 + \pi r^3 NZ}$	$\frac{4}{3} S_p^{-1} = \frac{4}{3} e^{P(\chi-1)}$
Equilibrium Capture (with surface)	$\frac{R_i}{Q} \left[\frac{1}{1 + \pi r^2 NZ}\right]$	$4 K_p^{-1} = 4j^{-1} e^{aP}$
Diffusion Capture (thy of Fitch and Tsai (85))	$\frac{R_i}{Q} \left[1 - \pi r^2 NZ\right]$	$(2PD/k_p[M])^{1/2}$
Diffusion Capture (Fick's Law)	$\frac{R_i}{Q} \left[1 + \pi r NZ\right]^{1-P}$	$4D/k_p[M]$

where R_i is the rate of generation of oligomers which can be predicted from the chemical kinetics

*Q is the number of oligomers per particle

πr^2 is the surface area of the particle

*S_p is the degree of supersaturation of monomer with polymer

*χ is the Flory interaction parameter

*P is the threshold degree of polymerisation for nucleation

*D is the diffusion coefficient for radicals

*K_p is an adsorption coefficient given by

$$K_p = \frac{\text{[concentration of n-mers in diluent]}}{\text{[concentration of n-mers in surface/bulk]}} = je^{-aP}$$

j,a are arbitrary constants

* quantities which have not been measured accurately by experiments

Eg, Equilibrium capture (with surface) predicts a limiting value of N_o, $N_{o(t\to\infty)} \propto R_i^{2/5} Q^{-4/5} j^{3/5} e^{-3aP/5}$.

FIGURE 5.2 - Nucleation and Agglomeration of Primary Particles

(i) Nucleation of primary particles

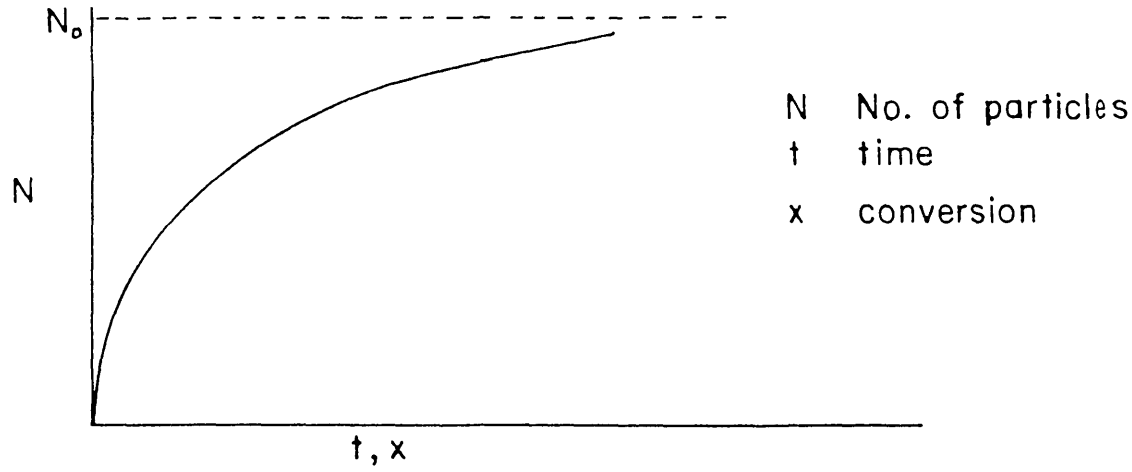

(ii) Agglomeration of primary particles

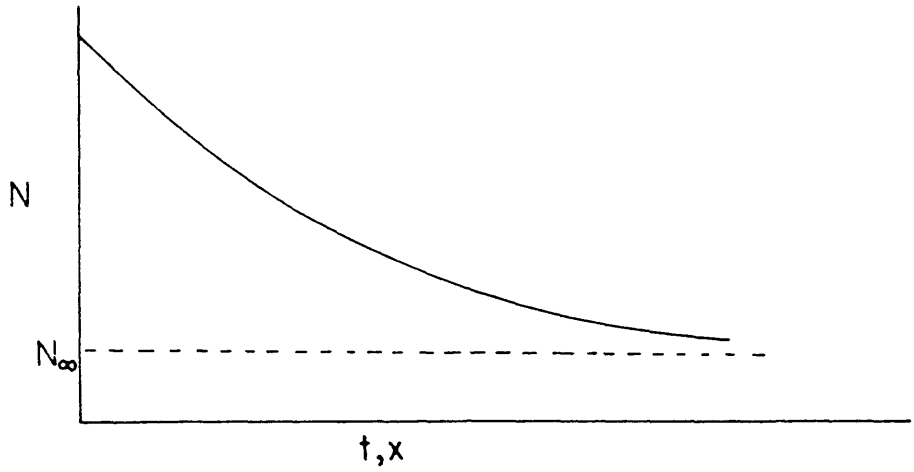

(iii) Nucleation and Agglomeration

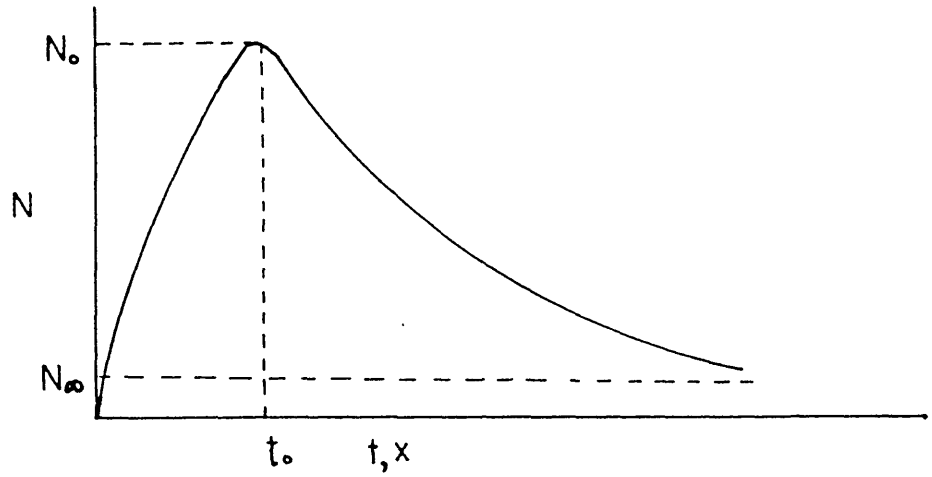

FIGURE 5.3(i)

Number of Primary Particles as a function of Conversion
(assuming that number is independent of particle radius)
Micrographs(86) analysed using results of appendix 5.1

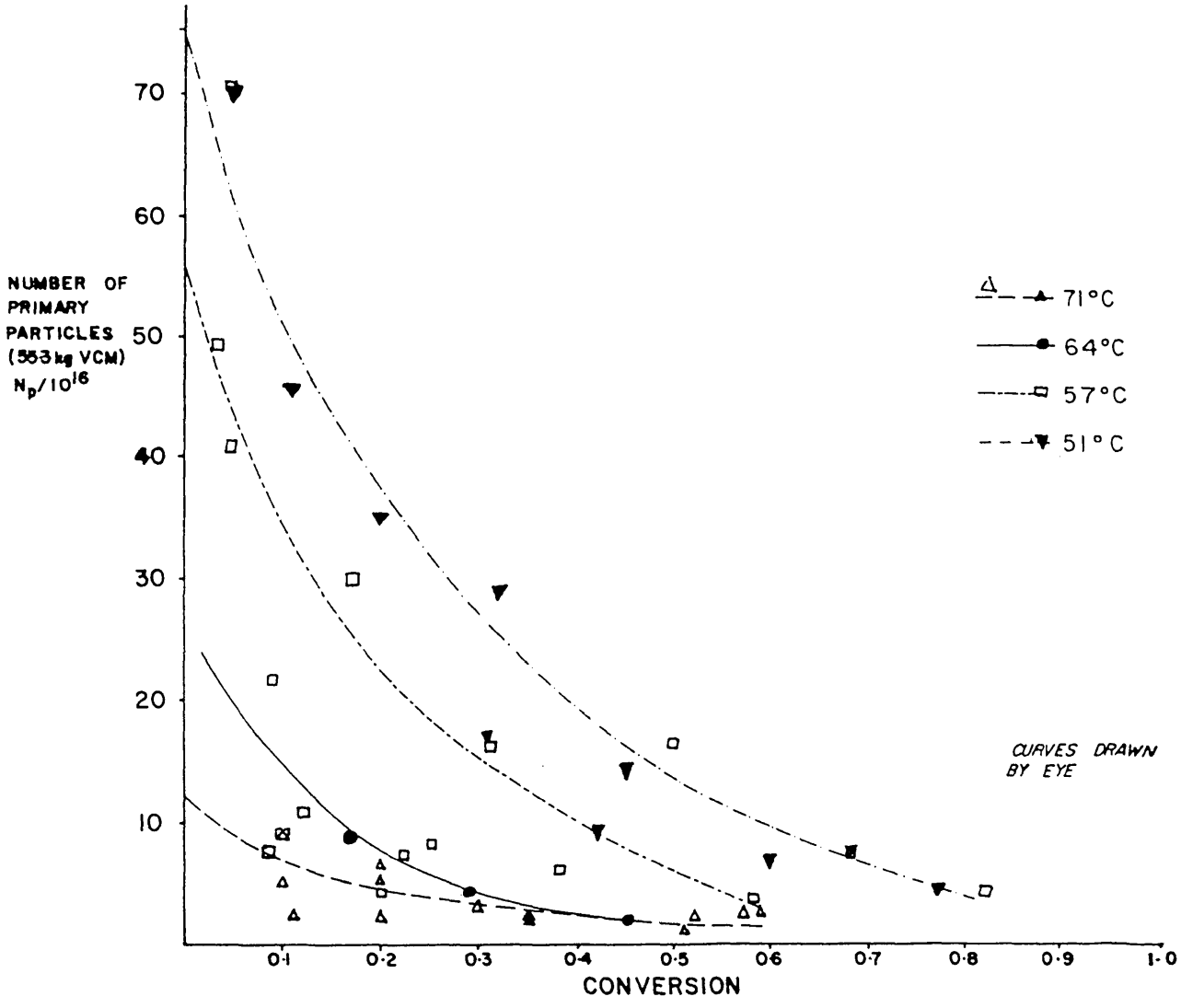

FIGURE 5.3(ii)

Number Concentration of Primary Particles as a function of Conversion,
(assuming that number is independent of particle radius)
Micrographs(86) analysed using results of appendix 5.1

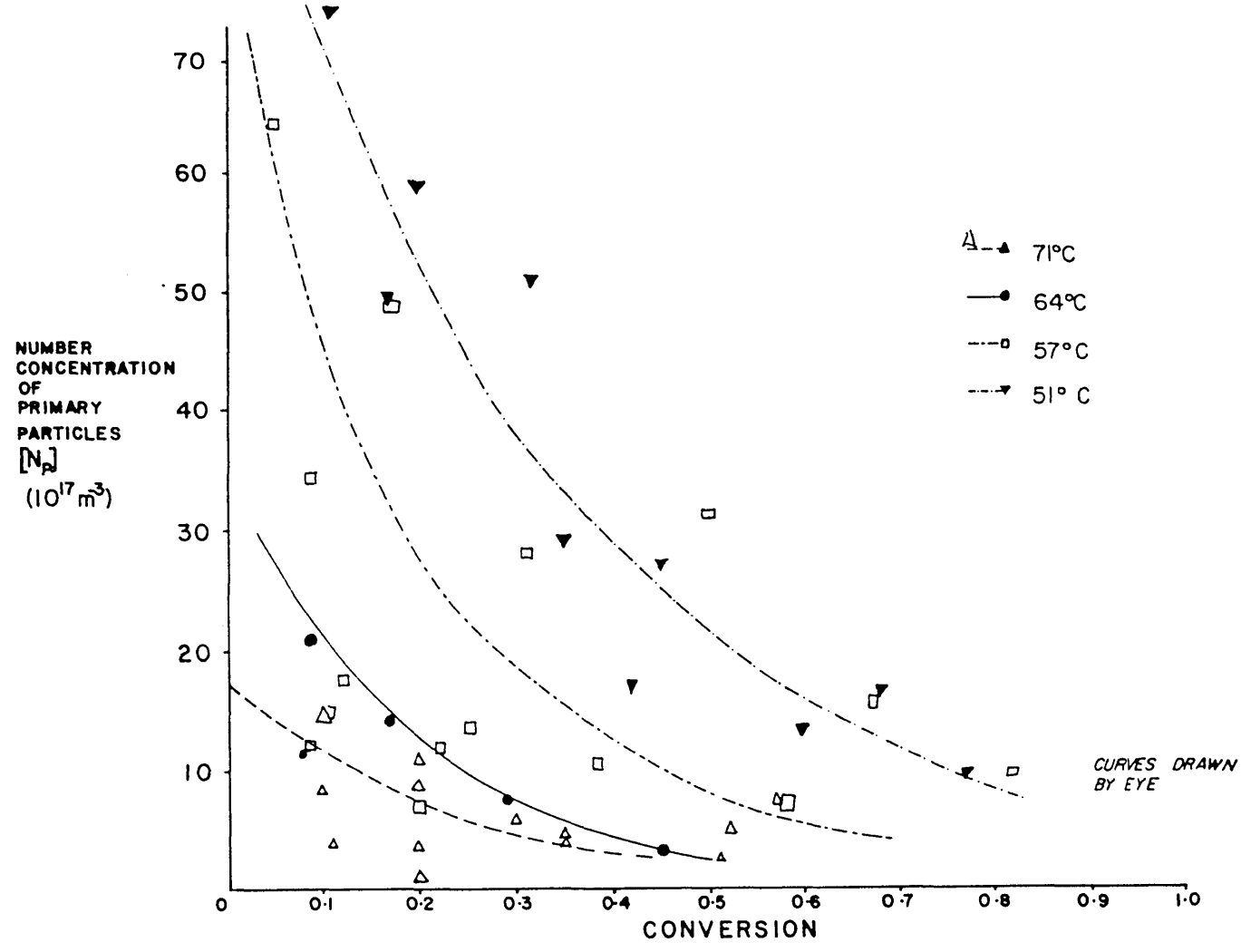

5.1(ii) Particle Size Distributions

The model for the aggregation of primary particles (equation 5.1) considered all the primary particles to be equal in size. In practise we might expect the particle sizes to be distributed around a mean particle size. Indeed any particulate species whether it be polymerising monomer droplets or primary particles will have a particle size distribution. For the purposes of this study it is assumed that all particular species will have the mean particle size for the species.

(a) For Primary Particles

The mean radius of a primary particle at conversion, x is given by

$$r = \left[\frac{3}{4\pi} \frac{\text{total volume of polymer + swelling monomer at conversion } x}{N}\right]^{1/3} \qquad (5.3)$$

where N is the number of primary particles given by equation 5.1.

(b) For Suspended Monomer Droplets (grains and subgrains)

In Section 2.5(A) the development of grain and subgrain morphology from polymerising monomer droplets was discussed. The change in mean grain size was plotted against a modified Weber number in Figure 2.5. As the inertial forces increased relative to the surface tension forces (as the agititation speed increased) the mean particle size decreased to a minimum (d_{min}) and then increased as the surface concentration of surfactant became too small to stabilise the suspended droplets which were beginning to coalesce. The characterisation of this behaviour is important for two reasons. Firstly, the subgrain and grain sizes and their distribution are among the important product properties by which PVC is marketed. Secondly, the interfacial areas of the suspended droplets are required for calculating the mass of VCM transferred from vapour into the suspended droplets, when autoclave pressure is falling.

There have been a considerable number of investigations of the effect of agitation conditions on the particle size distribution in polymerising and non-polymerising liquid-liquid dispersions (eg, 20, 87-92,94). Results of such studies yield a wide range of empirical and semi-empirical correlations for the initial droplet formation which vary greatly (20,93) in suspension polymerisation where the agitation behaviour is further complicated by the changing nature of the surfactant and the coalescence of the droplets, no fundamental treatment of the overall behaviour is available. Therefore, for the purposes of this model, to see whether such processes are likely to affect polymerisation rates a semi-empirical approach was adopted based on the observation that the diameter of the grains depends on Weber number as shown in Figure 2.5 (20,94).

<u>At low stirrer speeds</u> ($N_S < N_S^{agg}$)

(N_S^{agg} represents the stirrer speed at which the minimum droplet diameter is achieved).

Relatively large droplets are formed protected by stabiliser. The mean droplet size can be represented by a modified Calderbank equation (92,97):-

$$\bar{d}_{32} = .224\ We^{-0.6} \left[\frac{V_O}{D^3}\right]^{0.4} P_O^{-0.4}\ H^{0.5} \left[\frac{\mu_{VCM}}{\mu_{H_2O}}\right]^{.25} D \qquad (5.4)$$

where the subscripts 3,2 denote the interface between droplet and continuous phase (Chapter 3)

D is the agitator diameter

We is the Weber number $=(N_S^2\ D^3\ \rho_{H_2O}/\sigma_{H_2O})$

N_S is stirrer speed

σ_{H_2O} is the surface tension of water (Nm^{-1})

H is the volume fraction of VCM droplets in the system

P_O is the power number $= P/(N_S^3\ D^5\ \rho_{H_2O})$

$\cong 0.4$ at high Reynolds numbers ($>10^5$) (57,93)

V_O is the liquid volume in the reactor

(The modification to the Calderbank Equation (92) is simply that the constant .224 is a factor of 10 smaller than Calderbank's original value; the expression over estimated particle diameter (97)). At the high Reynolds numbers equation 5.4 predicts $d_{32} \propto N_S^{-1.2}$.

At intermediate stirrer speeds (N_S - N_S^{agg})

When $d_{32} = d_{min}$ the surface concentration of surfactant is at the minimum level required to prevent coalescence.

$$d_{min} = \frac{6\ V_2}{S_{max}} = \frac{6\ m\ V_2}{W} \qquad (5.5(a))$$

where V_2 is the total volume of dispersed phase

S_{max} is the maximum stable surface area of dispersal phase

W is the charge of stabilising surfactant

M is the minimum mass of surfactant per m^2 required to stablise the droplets

Once $N_S > N_S^{agg}$ the droplets formed by the agitator will have a diameter $d_{32} < d_{min}$ and therefore coalesce. A dynamic equilibrium will exist between breakup in the turbulent extensional flows near the agitator and agglomeration in the quiescent regions of the autoclave such that $d_{32} \simeq d_{min}$. The detailed behaviour of d_{32} will depend on the amount of time spent away from the agitator.

At high stirrer speeds ($N_S > N_S^{agg}$)

The dynamic equilibrium achieved above begins to breakdown when the circulation time is so short that the droplet cannot reagglomerate between successive visits to the agitator zone. The aggregates are continually broken up so that $d_{32} << d_{min}$: the surface area of the droplets is largely unprotected which leads to rapid, unstable coalescence above stirrer speeds N_S^{crit} (equivalent to We^{crit}). The grain size rises rapidly with increasing stirrer speeds, and can be represented by the approximation (98);

$$\bar{d}_{32} = d_{min} \frac{We}{(We)_{crit}} \qquad (5.5(b))$$

FIGURE 5.4 - Schematic Variation of Droplet Diameter, d_{32}, with Agitator Speed N_S

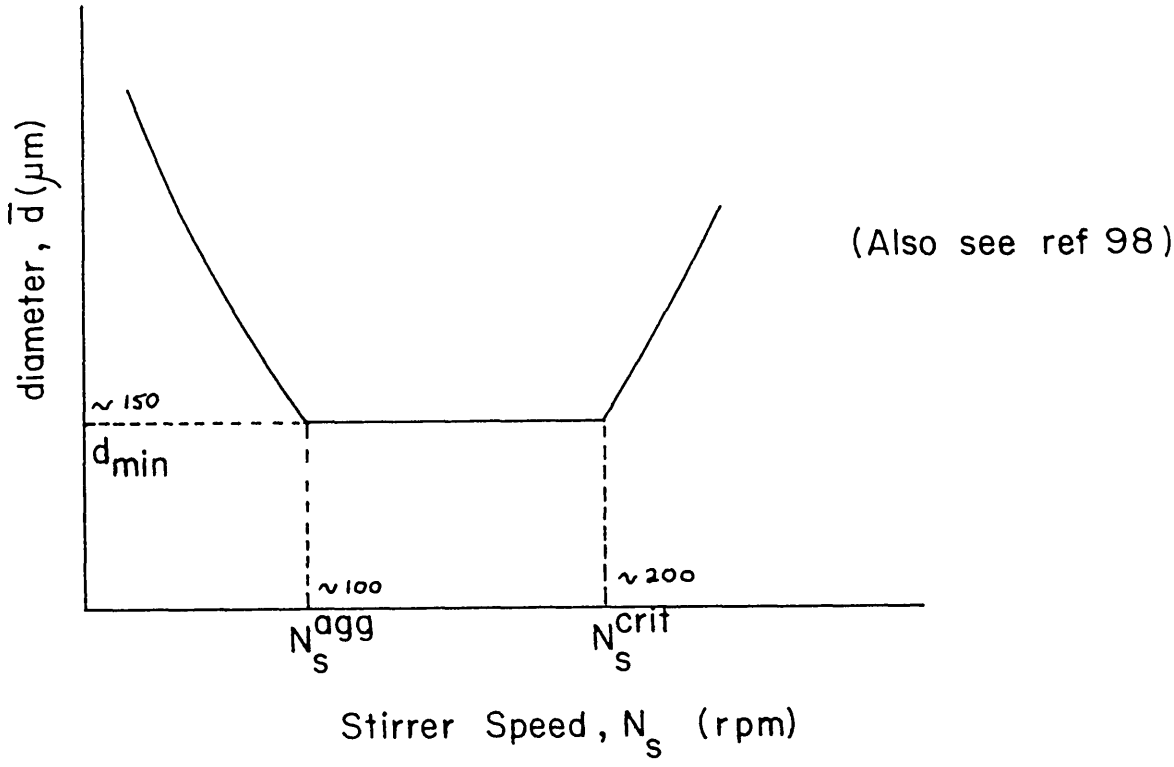

5.1(iii) Porosity

While the particle size and distribution of the polymerised monomer droplets determines much of the appearance of the resin product, its porosity is essentially determined by that of the subgrains which make up the final grains: it is a measure of the cumulative pore size distribution arising from interstitial spaces between and within agglomerates of primary particles. The subgrains originate as monomer droplets which, if uniform volume contraction proceeded as conversion increased, would ultimately produce non-porpous entities of density ρ_p. The porous nature of the polymer arises because at some critical intermediate conversion, x_{set}, the subgrains become sufficiently rigid to prevent any further inward contraction of the droplet 'skin'. There is therefore no further reduction in overall sub-grain volume: further polymerisation produces voids within the loosely packed primary particle structure. The earlier volume contraction ceases (ie the lower x_{set}) the higher

the resulting voidage or porosity, ϕ. The porosity at intermediate conversions ($x_{set} < x < x_{end}$) is given by

$$\phi(x) = \left[\sum_{j=4}^{7} V_j(x_{set}) - \sum_{j=5}^{7} V_j(x)\right] / \sum_{j=4}^{7} V_j(x_{set}) \qquad (5.6)$$

$$x > x_{set}$$

where the subscripts 4-7 refer to the monomer, basic, primary particle surface and primary particle bulk phase.

If during the calculations of the model the ratio,

$$\sum_{j=5}^{7} V_j(x) / \sum_{j=4}^{7} V_j(x_{set}) \qquad (5.7)$$

exceeds a value APV corresponding to a close packing fraction the precipitated polymer particles will impinge on one another. At this stage the interfacial area between the precipitated phases and the monomer phase is at a maximum for a constant number of precipitated particles. Further polymerisation will cause radial growth of all the polymer particles: the initial points of contact become areas of contact (Figure 5.5). This loss of interfacial area must be corrected for in the mass transfer calculations.

FIGURE 5.5 - Impinged Primary Particles

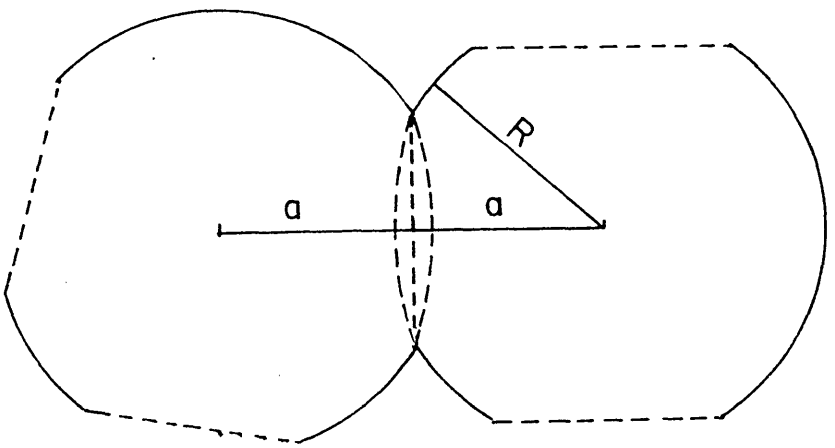

a is the radius when close packing is achieved

R is the radius after close packing and further polymerisation

The value of the primary particle radius R after impingement is given by the root of the equation,

$$\sum_{j=s}^{l} V_j(x) = N\left[\frac{4\pi R^3}{3} - N_c\left\{\frac{2\pi R^3}{3}\left[1 - \frac{a}{R}\right] - \frac{1}{3}\pi(R^2 - a^2)a\right\}\right] \quad (5.8)$$

where N is the number of primary particles

N_c is the co-ordination number of the primaries in the agglomerates

The area available for interphase transfer per primary particle is given by

$$\frac{A_{46}}{N} = 4\pi R^2 - N_c.2\pi R^2\left[1 - \frac{a}{R}\right] \quad (5.9)$$

(Equations 5.8 and 5.9 have been deduced from volume integrals for the segments and excluded volumes of intersecting spheres).

5.1(iv) Apparent Density

Once the porosity of the product is known, the apparent density of resin can be calculated.

The density of a grain is given by

$$\rho_g = \rho_p(1 - \phi) \quad (5.10)$$

If the packing fraction of the grains in the final powder is ψ, the density the powder appears to have is given by

$$\rho_A = \rho_g\,\psi \quad (5.11)$$

$\psi \simeq 0.5$ when irregular aggregates of similar size are packed together (57).

5.1(v) Molecular Weight Distributions

A polymer characteristic which, unlike the numbers or the sizes and their distribution of any of the particulate species, can be predicted directly from the chemical kinetics is the molecular weight

of the PVC. In section 3.4, the instantaneous number and weight average molecular chain lengths were defined as

$$\mu_n^j(t) = \frac{\lambda_1^j(t)}{\lambda_0^j(t)} \quad \text{and} \quad \mu_w^j(t) = \frac{\lambda_2^j(t)}{\lambda_1^j(t)} \quad \text{respectively}$$

where the superscript j denotes the phase they are measured in. However experimentally only the cumulative (time averaged) chain lengths can be measured. Therefore the instantaneous values appropriate to each phase were averaged over all the phases by the relationship:

$$\mu(t) = \sum_j m_j \mu^j(t) \qquad (5.12)$$

where m_j is the mass fraction of phase j given by

$$\left\{m_j = (\lambda_1^j + M^j)/\sum_j(\lambda_1^j + M^j)\right\}$$

and the cumulative chain lengths were calculated according to the relationship:

$$\bar{\mu}(t) = \frac{1}{t}\int_0^t \mu(t)\, dt \qquad (5.13)$$

In order that the integral 5.13 did not have to be completely re-evaluated after each time step, which would have required the storage of all previous values of $\mu(t)$, the new cumulative molecular weights at time $t + \Delta t$ were calculated from the previous cumulative molecular weight at time t according to the trapezium rule:

$$\bar{\mu}(t + \Delta t) = \frac{1}{t + \Delta t}\left\{\int_t^{t+\Delta t} \mu(t)\, dt + \bar{\mu}(t)\, t\right\} \qquad (5.14)$$

5.1(vi) Autoclave Pressure

The one major variable which has been largely ignored so far is the autoclave pressure. During most of the polymerisation the autoclave pressure is almost equal to the saturated vapour pressure of vinyl chloride: the presence of any inerts such as nitrogen or water vapour will modify the vapour pressure. (When the autoclave is charged initially it is evacuated to minimise the quantities of the

inerts).

The pressure begins to fall when all the free monomer has been consumed by polymerisation and further polymerisation is proceeding at the expense of the monomer which is swelling the polymer. To replace the monomer consumed by polymerisation, gas phase monomer transfers to the polymer gel. The reduction in vapour pressure when there are no mass transfer limitations is approximately given by the Flory-Huggins equation (Section 2.1A), equation 2.9 and Figure 3.2).

$$\ln \frac{P_1}{P_{10}} = \left\{ \ln \phi_1 + \phi_2 \left[1 - \frac{1}{m} \right] + \chi \phi_2^2 \right\} \qquad (2.9)$$

where all the symbols have been defined in Section 2.1A, ϕ with a subscript now represents a volume fraction rather than porosity.

Under normal operating conditions the rate of mass transfer is reduced because of the resistance to mass transfer offered by the water phase which separates the suspended droplets of PVC/VCM from vapour phase VCM. The pressure in the autoclave will not truly reflect the gel-phase composition of the polymer.

Consider an agitated reactor (Figure 5.6) where the effect of agitation is to create large eddies with bulk movement of the fluid round the reactor. Elements of the fluid (eg packets of water with suspended droplets) will come to the surface and spend varying amounts of time in contact with the vapour phase.

FIGURE 5.6 - An Agitated Autoclave

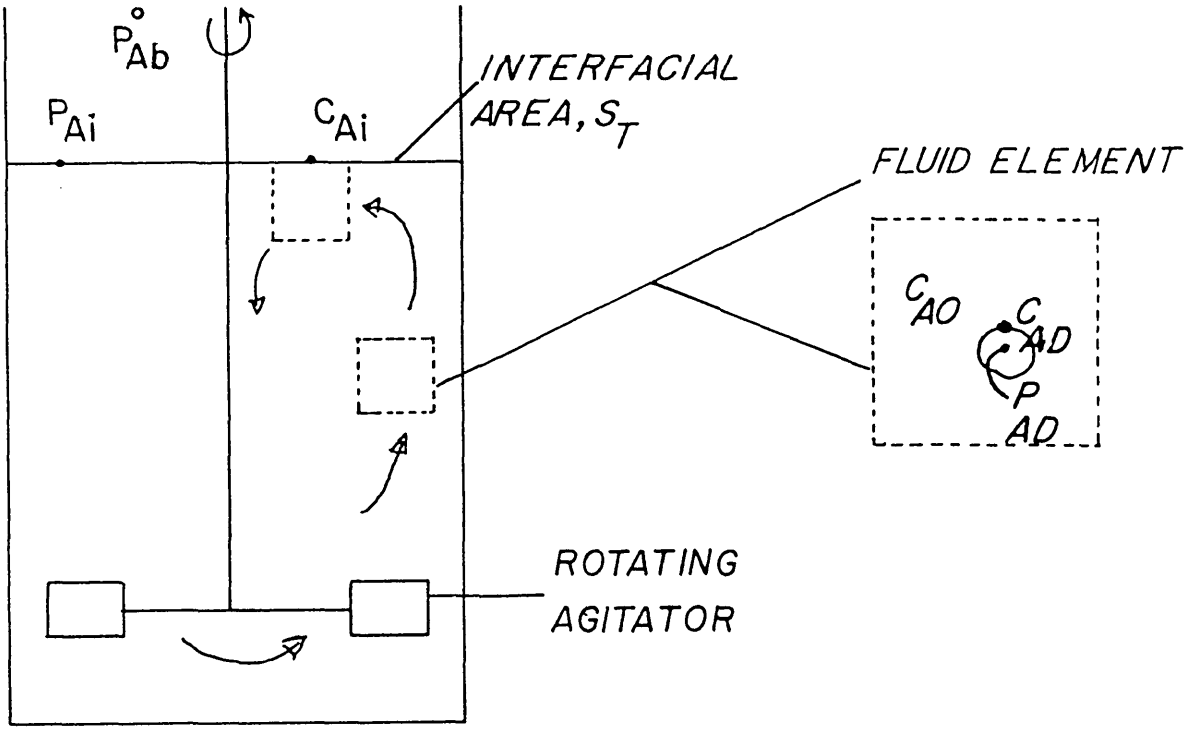

The mass transfer relationships for monomer are given by the equations:

From vapour to vapour/water interface,

$$n_m = S_T N_{Ai} = S_T K_G^{o}(P_{Ab}^{o} - HC_{Ai}) \qquad (5.15)$$

through the water phase from vapour/water to "bulk" water

$$n_m = S_T N_{Ai} = S_T K_L^{o}(C_{Ai} - C_{Ao}) \qquad (5.16)$$

and from bulk water into the PVC/VCM droplets

$$n_m = a V K_L^{D}\left[C_{Ao} - \frac{P_{AD}}{H_D}\right] \qquad (5.17)$$

whence $n_M = S_T N_{Ai} = S_T K_{OG}\left[P_{Ab}^{o} - \frac{H}{H_D} P_{AD}\right]$ (5.18)

where the overall mass transfer coefficient is given by

$$\frac{1}{K_{OG}} = \frac{1}{K_G^{o}} + \frac{H}{K_L^{o}} + \frac{S_T H}{aVK_L^{D}} \simeq \frac{1}{K_G^{o}} + \frac{H}{K_L^{o}}\left[1 + \frac{S_T}{aV}\right] \qquad (5.19)$$

and S_T is the area of the vapour/water interface [m^2]

N_{Ai} is the flux of monomer through this interface [mols/sm^2]

n_M is the mass of monomer passing through the interface [mols/s]

$K_G^{o}, K_L^{o}, K_L^{D}$ are gas-side and liquid-side mass transfer coefficients [mols/sN]

P_{Ab}^{o} is the pressure of the vapour [Nm^{-2}]

$P_{AD}(=P_{1o})$ is the pressure the VCM/PVC droplets would exert if free to do so (from the Flory-Huggins Theory) [Nm^{-2}]

C_{Ai}, C_{AO} are the water/vapour interfacial and bulk water monomer concentrations [mols m^{-3}]

a is the surface area per unit volume of the droplets [m^2/m^3]

V is the volume of liquid in the a/C [m^3]

H, H_D are Henry's Law constants [Nm/mol]

For much of the process, zero net flux conditions apply because

$$P_{Ab}^{o} = P_{AD} = P^{*} \qquad (5.20)$$

where P^{*} is the saturated vapour pressure of VCM

therefore $H/H_D = 1$ (5.21)

and (5.18) becomes

$$N_{Ai} = K_{OG} (P_{Ab}^{o} - P_{AD})$$

Since the pressure in the vapour space is principally determined by the vapour pressure of vinyl chloride and assuming that VCM behaves as a perfect gas, differentiation of the perfect gas equation of state with respect to time gives the temporal variation of pressure as molecules of VCM migrate from the vapour.

$$\frac{dP_{Ab}^{o}}{dt} = \frac{RT}{V} \frac{dn_m}{dt} \qquad (5.22)$$

with

$$\frac{dn_m}{dt} = - S_T N_{Ai} = - S_T K_{OG}(P_{Ab}^{o} - P_{AD}) \qquad (5.23)$$

Integrating, subject to the initial conditions

$$t = t_{pd} \qquad P_{Ab}^{o} = P^{*}$$

where t_{pd} is the time that pressure would begin to fall in the droplet free to, gives

$$P = P_{AD} + (P^{*} - P_{AD}) \exp\left\{- \frac{RT\ S_T\ K_{OG}}{V_1} (t - t_{pd})\right\} \qquad (5.24)$$

This expression gives qualitatively the results which are inuitively correct, viz

(i) as $K_{OG} \rightarrow \infty$ $P = P_{AD}$ ie the pressure in the autoclave matches the Flory-Huggins pressure given by equation 2.9.

(ii) as $K_{OG} \rightarrow 0$ $P = P^{*}$ ie the saturated vapour pressure of VCM

(iii) when mass transfer limited (intermediate K_{OG}) as $t \to \infty$ $P \to P_{AD}$

The Overall Mass Transfer Coefficient, K_{OG}

The overall mass transfer coefficient K_{OG} (5.19) reduces to $K_{OG} = K_L^o/H$ because (i) the mass transfer resistance in the gas phase ($1/K_G^o$) is negligible compared to that in the liquid phase in agitated vessels (93) and (ii) the ratio

$$S_T/aV = \frac{S_T\, dp}{6\, V_{vcm}} \ll 1$$

where dp is the diameter of the suspended droplets and

V_{vcm} is the volume of vinyl chloride charged.

The liquid phase mass transfer coefficient K_L^o can be estimated from correlations for gas absorption, eg (93).

$$Sh = 0.42\ Gr^{1/3}\ Sc^{1/2} \qquad (5.25)$$

where Gr is the Grashoff number ($d_p^3 g\ \rho_{H_2O}\ \Delta\rho/\mu_{H_2O}^2$)

Sh is the Sherwood number ($k_L^o\ d_p/D_f$)

Sc is the Schmidt number ($\mu_{H_2O}/\rho_{H_2O}\ D_f$)

D_f is the diffusion coefficient of VCM through H_2O

Alternatively it can be calculated from Danckwerts' model of mass transfer for gas adsorption in agitated systems where the penetration theory of mass transfer is coupled with random surface renewal (95)

$$k_L^o = [D_f\ \$]^{1/2} \qquad (5.26)$$

where \$ is the fractional rate of surface renewal. Both methods give estimates of mass transfer coefficients which are of the same order of magnitude, namely $10^{-4} ms^{-1}$.

5.1(vii) Autoclave Temperature

Most of the model calculations were performed isothermally. In some cases idealised temperature profiles were used to assess the model's response to temperature change. This strategy is to be preferred especially if new operating procedures for polymerisations are being investigated with the model. It has the advantage of avoiding the need to model exactly the temperature control system of an autoclave, which would make the model specific to a particular plant. (Operating companies may want to do this).

5.2 CHOICE OF RATE CONSTANTS

Kuchanov and Bort (45) carried out an extensive literature survey and used the following values for rate constants:

Polymerisation (Propagation) Rate Constant

$$k_p = 50 \times 10^3 \exp\left[\frac{-27627.6}{RT}\right] \ m^3mol^{-1}s^{-1}$$

(6 references cited by Kuchanov and Bort)

Ratio of Chain Transfer Rate Constant to Propagation Rate Constant

$$\frac{k_{trm}}{k_p} = 108.5 \exp\left[\frac{-30988}{RT}\right]$$

therefore

$$k_{trm} = 5.425 \times 10^6 \exp\left[\frac{-58615.6}{RT}\right] \ m^3mol^{-1}s^{-1}$$

(7 references cited by Kuchanov and Bort)

Termination Constants:

In monomer phase

$$k_{t_4} = 1.3 \times 10^9 \exp\left[\frac{-17588}{RT}\right] \ m^3mol^{-1}s^{-1}$$

(1 reference cited by Kuchanov and Bort)

In polymer phase

$$k_{ts} = 0.7 \times 10^{9} \exp\left[\frac{-34338}{RT}\right] \ m^3mol^{-1}s^{-1}$$

(Results of Kuchanov and Bort)

where R is the universal gas constant expressed in $Jmol^{-1}K^{-1}$.

The initiator decomposition rate constant was derived from temperature-half life data published by Akzo Ltd (96).

For Perkadox-16 (Bis(4-tert butylcyclhexyl)peroxydicarbonate)

$$k_D = 7.74703 \times 10^{15} \exp\left[\frac{-125040}{RT}\right] \ s^{-1}$$

Other initiator decomposition rate constants have been calculated by regression of the Akzo Data, and appear in Table 5.2(b).

The presence of double bonds in the polymer is due to transfer to polymer reactions (56) and also because of termination due to disproportionation. No rate constants are available for the transfer to polymer reactions in the literature, therefore because these defects occur approximately twice for every 1000 monomer units (Table 3.1) the transfer to polymer rate constant k_{trp} was chosen as

$$k_{trp} = k_p/500 \ \ m^3mol^{-1}s^{-1}$$

The contribution of termination by disproportionation can be assessed by modifying the amount of termination which proceeds by this mode using the factor p (Table 5.2(a)).

Table 5.2(a) also shows how the rate constants given above are used in each phase. Where polymer phase rates of reaction are available these are used, otherwise rates of reaction are independent of phase.

TABLE 5.2(a)

Modification of Rate Constants in Each Phase

Phase Reaction	Monomer Phase (subscript 4)	Basic Particle (subscript 5)	Primary Particle (subscript 6)	Primary Particle (subscript 7)
Polymerisation (propagation)	k_p	k_p	k_p	k_p
Transfer to Monomer	k_{trm}	k_{trm}	k_{trm}	k_{trm}
Termination by disproportionation	$p\ k_{t4}$	$p\ k_{t5}$	$p\ k_{t6}$ $k_{t6} = k_{t5}$	$p\ k_{t7}$ $k_{t7} = k_{t5}$
Termination by combination	$(1-P)\ k_{t4}$	$(1-P)\ k_{t5}$	$(1-P)\ k_{t6}$	$(1-P)\ k_{t7}$
Transfer to polymer	k_{trp}	k_{trp}	k_{trp}	k_{trp}
Initiator Decomposition Constant	k_D	k_D	k_D	k_D

Notes:-

k_p, k_{trm}, k_{t4}, k_{t5}, k_{trp}, k_D are defined in Section 5.3
p represents the proportion of termination due to disproportionation

TABLE 5.2(b)

Activation Energies and Pre-exponential Factors for Various Initiators

	Activation Energy^{+} Ea/kJ mol^{-1}	Pre-exponential Factor$^{\#}$ A/s^{-1}
Azo di-isobutyronitrile	121.5	1.246×10^{14}
Azo bis (2,4 dimethylvaleronitrile)	114.4	8.859×10^{13}
t-Butyl perpivalate	118.1	1.129×10^{14}
Dibutyl peroxydicarbonate	129.6	3.469×10^{16}
Bis (2 ethylhexyl) peroxydicarbonate	129.6	4.163×10^{16}
Di (t-butyl cyclohexyl) peroxydicarbonate	129.6	4.163×10^{16}
Lauroy Peroxide	124.7	5.694×10^{16}
Benzoyl Peroxide (in Benzene)	125.5	1.883×10^{14}
Acetyl cyclohexylsulphonyl peroxide	138.0	2.967×10^{18}

Rate Constant $k_D = A \exp(-Ea/RT)$

Evaluated from Table 2.2 and Ref 96 according to:-

Activation Energy^{+} $\quad Ea = R\left[\frac{\ln t_{1/2}|_1 - \ln t_{1/2}|_2}{T_2 - T_1}\right] T_2.T_1$

$t_{1/2}|_i$ is the initiator half life at T_i(K)

Pre-exponential Factor$^{\#}$ $\quad A = \frac{\ln 2}{t_{1/2}|_1} \exp\left[T_2\left\{\frac{\ln t_{1/2}|_1 - \ln t_{1/2}|_2}{T_2 - T_1}\right\}\right]$

5.3 ANALYTIC SOLUTION

It is essential when carrying out numerical work of the type described in this thesis to verify that the results produced by a model are meaningful: do the results of the numerical studies indicate potential experimental observations or are they purely consequences of the mathematical description and the formulation of the problem for the computer?

Verification is partly achieved by developing analytic solutions for limiting conditions of the more complex model. Comparing the numerical results when the complex model is run for the same limiting conditions with the analytical solution gives confidence in the numerical procedures used.

In order to test the complex model developed in this thesis (Chapter 3) such a simplified analytic solution has been developed. The solution retains some of the functional simplicity of the model due to Abdel-Alim and Hamielec (44), yet allows initiator to be distributed between the monomeric and polymeric phases. While this is an essential feature of the model due to Kuchanov and Bort (45), their model cannot be integrated analytically and is therefore unsuitable for test purposes. The analytic solution describes the conversion-time locus of the polymerisation: it ignores molecular weight considerations.

The first assumption made in simplifying the complex model is that the microgel phase (see Section 3.1) does not segregate into a surface layer and bulk layer and remains in equilibrium with the monomer from which it has precipitated.

The polymerisation can be characterised by three distinct zones:

(a) Upto conversion, X_{bppte} where any polymer formed is completely miscible with the monomer from which it is produced.

(b) Upto conversion, X_{pd} where a distinct polymer phase has precipitated from the monomer, and polymerisation is

occurring within both precipitated and diluent phase. This is the heterogeneous zone.

(c) Beyond conversion, X_{pd} where the monomer phase has disappeared and polymerisation proceeds within the polymeric phase consuming the monomer swelling the polymer.

From Tables 3.3 and 3.5, the following conversion equations apply

In the monomer phase:

$$\text{Initiator } \left.\frac{d[I]}{dt}\right|_4 = -k_D[I]\Big|_4 - \frac{A_{4s}K_{AI}^{4s}}{V_4}\left[[I_4] - \gamma_{4s}^{I}[I_s]\right] \tag{5.27}$$

$$\text{Monomer } \left.\frac{d[M]}{dt}\right|_4 = -(k_p + k_{trm})[M][\sigma_o]\Big|_4 - \frac{A_{4s}K_{AM}^{4s}}{V_4}\left[[M_4] - \gamma_{4s}^{M}[M_s]\right] \tag{5.28}$$

$$\text{Radicals } \left.\frac{d[\sigma_o]}{dt}\right|_4 = 2f\,k_D[I]\Big|_4 - k_{trp}[\sigma_o][\lambda_o]\Big|_4 - (k_{tc} + k_{td})[\sigma_o]^2\Big|_4 - \frac{A_{4s}K_{AP}^{4s}}{V_4}\left[[\sigma_{o4}] - \gamma_{4s}^{P}[\sigma_{os}]\right] \tag{5.29}$$

and for the polymer phase:

$$\text{Initiator } \left.\frac{d[I]}{dt}\right|_s = -k_D[I]\Big|_s + \frac{A_{4s}K_{AI}^{4s}}{V_s}\left[[I_4] - \gamma_{4s}^{I}[I_s]\right] \tag{5.30}$$

$$\text{Monomer } \left.\frac{d[M]}{dt}\right|_s = -(k_p + k_{trm})[M[[\sigma_o]\Big|_s + \frac{A_{4s}K_{AM}^{4s}}{V_s}\left[[M_4] - \gamma_{4s}^{M}[M_s]\right] \tag{5.40}$$

$$\text{Radicals } \left.\frac{d[\sigma_o]}{dt}\right|_s = 2f\,k_D[I]\Big|_s - k_{trp}[\sigma_o][\lambda_o]\Big|_s - (k_{tc} + k_{td})[\sigma_o]^2\Big|_s + \frac{A_{4s}K_{AP}^{4s}}{V_s}\left[[\sigma_{o4}] - \gamma_{4s}^{P}[\sigma_{os}]\right] \tag{5.41}$$

where [] have been used to denote concentrations and symbols are as previously defined.

If (a) the number of radicals in the system is small σ_{o4}/M_o, $\sigma_{os}/M_o << 1$ and (b) interphase transport of radicals is negligible then, ignoring transfer to polymer reactions, and assuming

$d[\sigma_o]/dt = 0$,

$$[\sigma_{o4}] = \left[\left[\frac{2f\,k_D}{k_{tc} + k_{td}}\right][I]\Big|_4\right]^{1/2} \quad \text{and} \quad [\sigma_{os}] = \left[\left[\frac{2f\,k_D}{k_{tc} + k_{td}}\right][I]\Big|_s\right]^{1/2} \tag{5.42}$$

The decomposition of initiator is given by:-

$$\frac{dI}{dt} = - k_D\, I \tag{5.43}$$

whence $I = I_o\, e^{-k_D t}$

where I_o represents the initial number of mols of initiator present.

Therefore, because,

$$[I_4]\, V_4 + [I_5]\, V_5 = I_o e^{-k_D t} \tag{5.44}$$

$$[I_4] = \frac{\gamma_{45} I}{V_4\, \gamma_{45} I + V_5}\, I_o e^{-k_D t} \tag{5.55}$$

$$\text{and } [I_5] = \frac{1}{V_4\, \gamma_{45} I + V_5}\, I_o e^{-k_D t} \tag{5.56}$$

($V_4\, \gamma_{45} I + V_5 = a - bx$, where a and b are defined below).

The conservation equation for monomer is given by (5.28, 5.40)

$$-\frac{M_o dx}{dt} = \frac{dM}{dt} = \left[\frac{dM_4}{dt} + \frac{dM_5}{dt}\right] = -\left\{(k_p + k_{trm})[\sigma_o]M\Big|_4 + (k_p + k_{trm})[\sigma_o]M\Big|_5\right\} \tag{5.57}$$

Using the results of 5.42, 5.55, 5.56 and Appendix 5.1 the rate of polymerisation is given by

$$\frac{dx}{dt} = C_4\left[e^{-k_D t}\right]^{1/2} \frac{\alpha_5 - x}{(a - bx)^{1/2}} + C_5\left[e^{-k_D t}\right]^{1/2} \frac{x - \alpha_4}{(a - bx)^{1/2}} \tag{5.58}$$

where

$$C_4 = (k_p + k_{trm}) \left[\frac{2f\,k_D}{k_{tc} + k_{td}}\right]^{1/2}\Big|_4 (\gamma_{45} I)^{1/2}\, I_o^{1/2} \left[\frac{1 - \alpha_4}{\alpha_5 - \alpha_4}\right]$$

$$C_5 = (k_p + k_{trm}) \left[\frac{2f\,k_D}{k_{tc} + k_{td}}\right]^{1/2}\Big|_5 I_o^{1/2} \left[\frac{1 - \alpha_5}{\alpha_5 - \alpha_4}\right]$$

$$a = \frac{V_o}{(\alpha_5 - \alpha_4)} \left\{ \frac{[(1-\alpha_4)\bar{V}_4^M + \alpha_4 \bar{V}_4^P]\gamma_{45} I\alpha_5}{\bar{V}_4^M} - \frac{[(1-\alpha_5)\bar{V}_5^M + \alpha_5 \bar{V}_5^P]\alpha_4}{\bar{V}_5^M} \right\}$$

$$b = \frac{V_o}{(\alpha_5 - \alpha_4)} \left\{ \frac{[(1-\alpha_4)\nabla_4^M + \alpha_4 \nabla_4^P]\gamma_{45} I}{\bar{V}_4^M} - \frac{[(1-\alpha_5)\nabla_5^M - \alpha_5 \nabla_5^P]}{\bar{V}_5^M} \right\}$$

The time-conversion locus can be derived by the change of variable, $u^2 = a - bx$, and by use of integral 61 in reference (71). This leads to

$$t = -\frac{2}{k_D} \ln \left\{ \exp\left[\frac{-k_D t_o}{2}\right] - \frac{k_D}{2} \text{Int} \right\} \quad t_o \leq t < t_{pd},\ x_{bppte} \leq x < x_{pd} \tag{5.59}$$

where

$$\text{Int} = \left[-\frac{2u}{C_4 - C_5} + \frac{K}{(C_4 - C_5)\sqrt{-(C_4 - C_5)K}} \ln \left[\frac{K + u\sqrt{-(C_4 - C_5)K}}{K - u\sqrt{-(C_4 - C_5)K}} \right] \right]_{u=(a-b\alpha_4)^{1/2}}^{u=(a-bx)^{1/2}}$$

$(C_4 - C_5)K < 0$

$K = C_4(\alpha_5 b - a) + C_5(a - b\alpha_4)$

t_o is the time when precipitation occurs, ie when $x = x_{bppte}$

The relationship (5.59) describes the time-conversion locus during the heterogeneous zone of polymerisation. By similar analysis, the time-conversion locus upto x_{bppte} (the first homogeneous zone) is given by

$$t = -\frac{2}{k_D} \ln\left\{1 - \frac{k_D}{2} \text{Int}'\right\} \qquad 0 \leq t < t_o,\ x < x_{bppte} \tag{5.60}$$

where

$$\text{Int}' = -\frac{2}{C_4'} \left[u + \frac{1}{2} \left[\frac{\bar{V}_4^P}{\bar{V}_4^P}\right]^{1/2} \ln\left[\frac{u - [\bar{V}_4^P/\bar{V}_4^M]^{1/2}}{u + [\bar{V}_4^P/\bar{V}_4^M]^{1/2}}\right] \right]_{u=1}^{u=\left[1-x\left[\frac{\bar{V}_4^M - \bar{V}_4^P}{\bar{V}_4^M}\right]\right]^{1/2}}$$

and $C_4' = (k_p + k_{trm}) \left[\frac{2f\, k_D}{k_{tc} + k_{td}}\right]^{1/2}\Big|_4 \left[\frac{I_o}{V_o}\right]^{1/2}$

and beyond x_{pd} by

$$t = -\frac{2}{k_D} \ln \left\{ \exp\left[-\frac{k_D\, t_{pd}}{2}\right] - \frac{k_D}{2} \text{Int}'' \right\} \quad t_{pd} \leq t, x_{pd} \leq x \tag{5.61}$$

where

$$Int'' = -\frac{2}{C_s'}\left[u + \frac{1}{2}\frac{\bar{V}_s^P}{\bar{V}_4^P}\ln\left[\frac{u - [\bar{V}_4^P/\bar{V}_4^M]^{1/2}}{u + [\bar{V}_4^P/\bar{V}_4^M]^{1/2}}\right]\right]_{u=\left[1-x\left[\frac{\bar{V}_4^M - \bar{V}_4^P}{\bar{V}_4^M}\right]\right]^{1/2}}^{u=\left[1-\alpha_4\left[\frac{\bar{V}_4^M - \bar{V}_4^P}{\bar{V}_4^M}\right]\right]^{1/2}}$$

$$C_s' = (k_p + k_{trm})\left[\frac{2f\,k_D}{k_{tc} + k_{td}}\right]^{1/2}\Big|_s\left[\frac{I_o}{\bar{V}_o}\right]^{1/2}$$

and t_{pd} is the time when $x = x_{pd}$

NB $\dfrac{\bar{V}_s^P}{\bar{V}_s^M} \approx \dfrac{V_4^P}{\bar{V}_4^M} \simeq \dfrac{\rho_m}{\rho_p}$

5.4(i) Comparison of Numerical and Analytic Solutions

The analytic solution of the model equation was compared with the results from a numerical integration of the model for identical process conditions: the numerical integration was performed with the same constraints used to develop the analytic solution, ie high mass transfer rates for the initiator and monomer and no mass transfer of radicals (they terminate in the same phase in which they are formed. The conditions used for the comparison are shown in Table 5.3.

When these conditions are used, the rate and conversion curves of the numerical and analytic solutions are virtually coincident (Figure 5.7). Furthermore as an indication of the proximity of the solutions, the times taken to reach 77% conversion (the onset of pressure drop) are

(i) for the analytic case

4.261 hours (255.66 minutes)

and

(ii) for the numerical case

4.272 hours (256.32 minutes)

An agreement of 40s in 4.261 hours (.26%).

TABLE 5.3

Process Condition Used to Compare Numerical and Analytic Solutions

Initiator Charge (Perkadox 16 MW 398.8)	30g
Monomer Charge	54.4kg
Temperature	50°C
Initiator Distribution Coefficient $\gamma = \frac{[I_{monomer}]}{[I_{polymer}]}$	1.54

Mass Transfer Coefficients for Numerical Integration

For	From Phase	To Phase	Symbol	Value ms^{-1}
Monomer	Monomer	Basic Particles	k_{AM}^{45}	10^{-3}
	Monomer	Primary Particle Surface	k_{AM}^{46}	10^{-3}
	Primary Particle Surface	Primary Particle Bulk	k_{AM}^{67}	10^{-3}
Initiator	Monomer	Basic Particles	k_{AI}^{45}	10^{-3}
	Monomer	Primary Particle Surface	k_{AI}^{46}	10^{-3}
	Primary Particle Surface	Primary Particle Bulk	k_{AI}^{67}	10^{-3}
Radicals	Monomer	Basic Particles	k_{AP}^{45}	0
	Monomer	Primary Particle Surface	k_{AP}^{46}	0
	Primary Particle Surface	Primary Particle Bulk	k_{AP}^{67}	0

Tolerance in Relative Local Error Test 10^{-6}

FIGURE 5.7

Comparison of the Analytical and Numerical Solutions of the Model for identical parameters

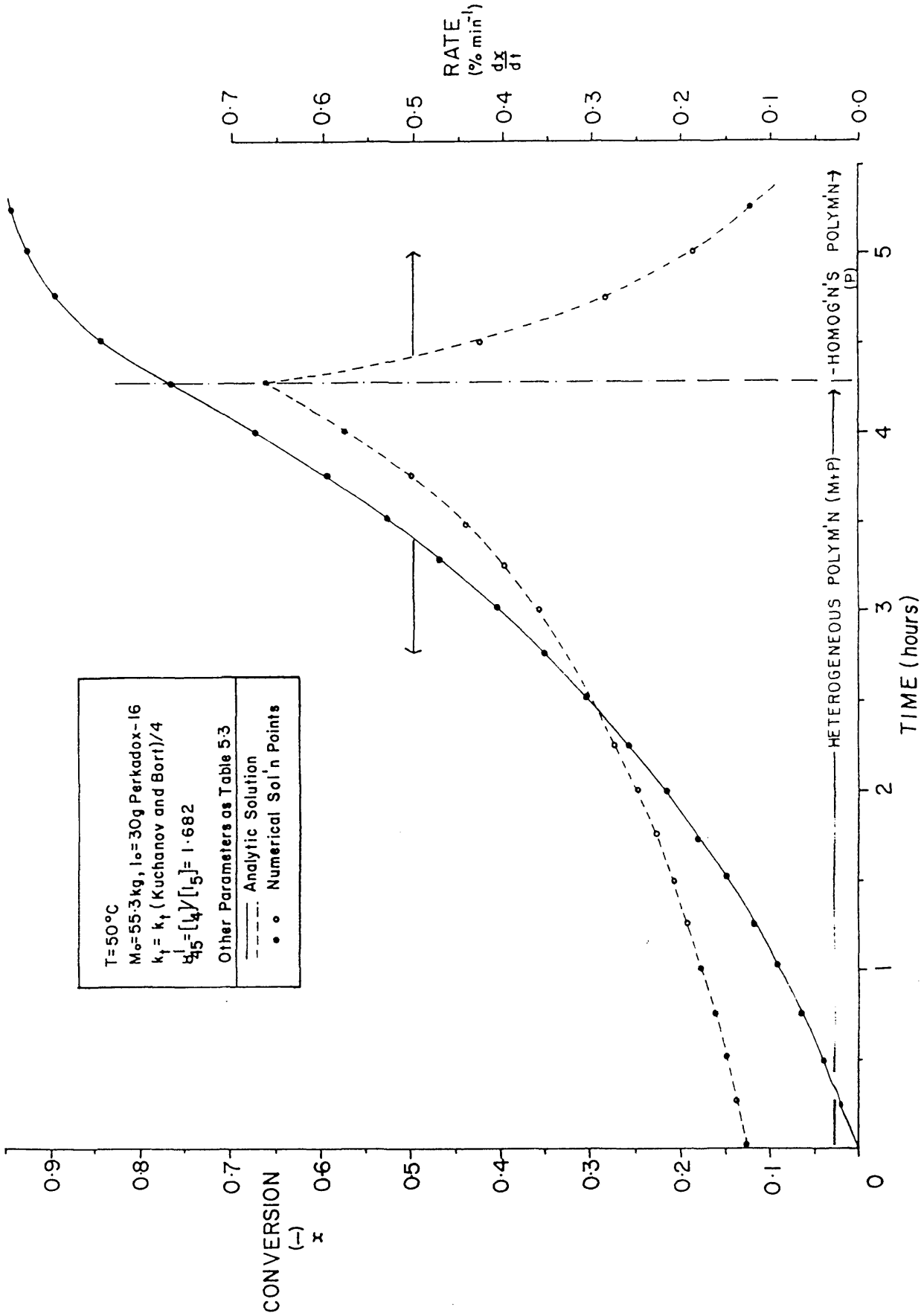

The close agreement of the two solutions gives confidence in the results of the numerical calculations, confirming the reliability of the numerical algorithms chosen. In Chapter 6 we shall be extending the numerical solutions to look at those cases for which the analytic solution does not apply. Combined with a sensitivity analysis of the parameters of the analytic model, this will help to form an entire description of the time-conversion behaviour of polymerising vinyl chloride. The numerical and analytic models will provide benchmark results (i) against which experimental evidence may be used to confirm aspects of the mechanism of polymerisation and (ii) to provide information allowing the parameters of the model to be optimised for more accurate future descriptions of specific processes and recipes.

5.4(ii) The Choice of Error Tolerance

The decision to use a relative error tolerance, RET, (66) of 10^{-6} for the numerical integrations described in Chapter 6, and in the comparison of the analytic and numerical models, was based on the numerical studies summarised in Table 5.4.

At tolerances greater than 10^{-5} the integrator failed to integrate the ODEs successfully, whereas at tolerances less than 10^{-6} the time taken for the integration was much larger without appreciable improvement in accuracy. A tolerance of 10^{-6} was judged to give the best compromise between accuracy and computer time.

Figure 5.8 shows what work the integrator is doing during the integration with a tolerance of 10^{-6}. The plots of the stiffness ratio for unscaled and scaled derivatives (Section 4.2B) show that stiffness is preserved throughout the calculation because high order moments are very sensitive to changes in the low order moments. The number of integration steps per call to the integrator shows how in the first minute (when the radical population is growing rapidly to its steady state value) the integrator does most work (158 steps/(minute modelled) compared with a normal value of ~6 steps/(minute modelled)). The plot of Jacobian

evaluations/(minute modelled) indicates how often the integrator is having to change the order of the method in order to achieve the local error tolerance.

TABLE 5.4

Effect of Change in Local Error Tolerance on Computer Time

TOLERANCE IN RELATIVE LOCAL ERROR TEST	NUMBER OF CALLS TO INTEGRATOR	MINUTES MODELLED PER CALL TO INTEGRATOR	CDC 7600* CPU TIME (SECONDS)	CPU TIME PER CALL TO INTEGRATOR SECONDS
10^{-2}	2	1	.232	.116^{+}
10^{-3}	300	1	35.725	.119^{+}
10^{-4}	300	1	39.299	.131^{+}
10^{-5}	300	1	45.246	.151^{o}
10^{-6}	300	1	61.360	.205^{o}
10^{-7}	300	1	73.248	.244^{o}
10^{-8}	257	1	116.277	.452$^{\#}$
10^{-9}	257	1	116.326	.453$^{\#}$
10^{-10}	257	1	116.279	.452$^{\#}$

NOTES

+ All these runs aborted

o 77% conversion reached between 225 and 260 runs
99.5% conversion reached after 300 minutes

All these runs hit computer time limits before 99.5% conversion reached. 77% conversion reached in 257th minute

* A CDC 7600 model was the fastest computer used in this study. The relative speeds of all the computers used is given below:-

APPROXIMATE SPEEDS OF COMPUTERS USED

	COMPUTER CENTRE	SPEED/ARBITARY UNITS
CDC CYBER 174	ICCC	1
CDC 6600	ICCC	2
CDC 7600	ULCC	6

ICCC Imperial College Computer Centre

ULCC University of London Computer Centre

FIGURE 5.8 Work done by the integrator during numerical solution :integration statistics

LEFT AXIS (number)

Integration steps per minute modelled ▽

Jacobian Evaluations ▼

RIGHT AXIS ($\log_e$(stiffness ratio))

scaled derivatives o

unscaled (normal) derivatives •

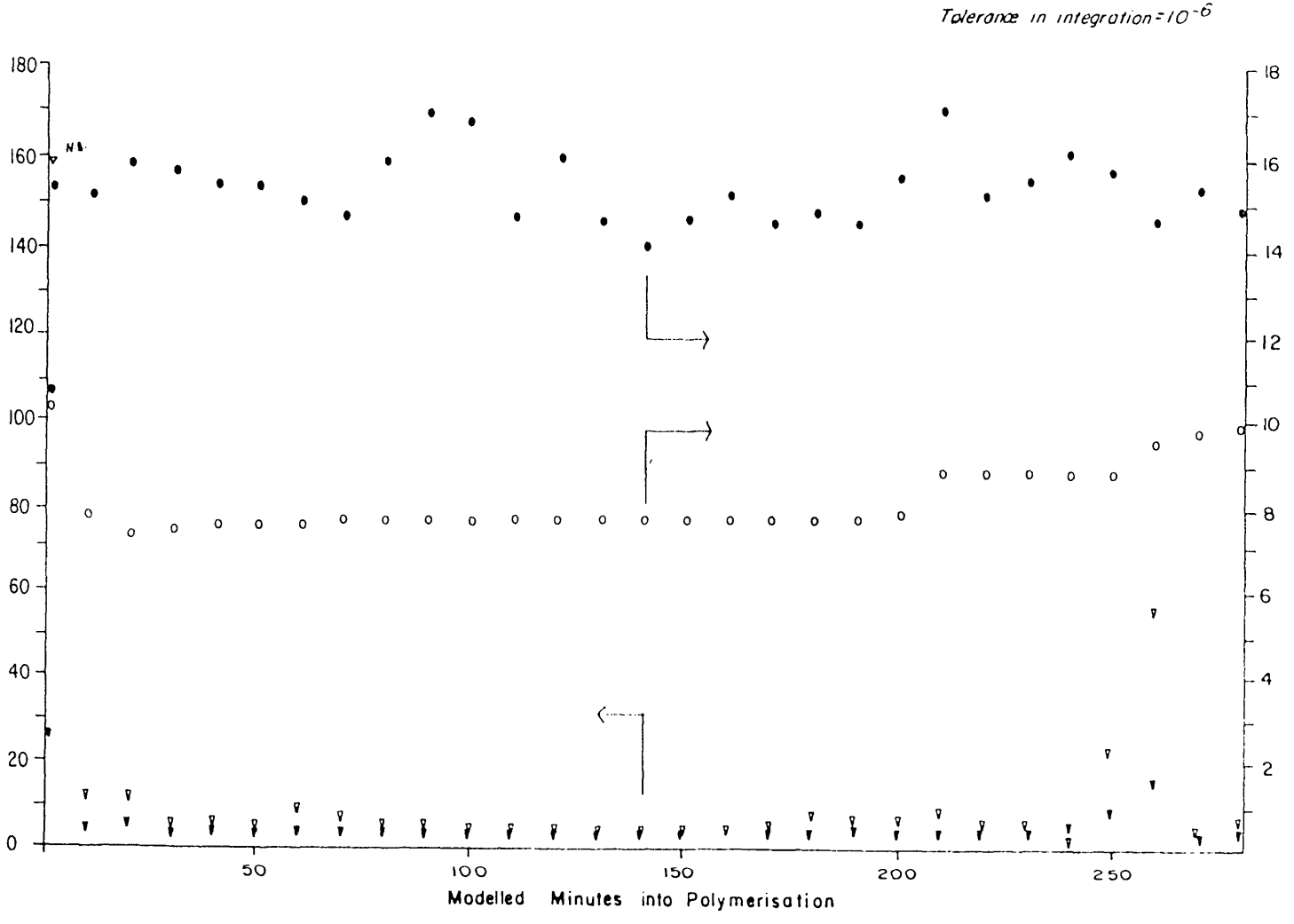

CHAPTER SIX

RESULTS AND DISCUSSION

In developing the computer model for vinyl chloride polymerisation considerable attention has been paid to the effectiveness of the numerical techniques. These ensure that the model is conservative, accurate with respect to the ideal (analytic) solutions and performs its calculations in the minimum possible time. It only remains to present the predictions of the model, showing how they compare with experimental observations and how they reproduce all the essential features of vinyl chloride polymerisation.

Although the results of the model compare favourably with experimental observation, the lack of sufficient accurate experimental data precludes numerical optimisation of all the model parameters (even if it were possible). The model has been used instead to perform benchmark calculations, to show the trends caused by changes in variables and process conditions and from this provide better estimates of the model parameters. By confirming the approximate time and length scales of model parameters, experiments may be better designed to measure those parameters to specified degrees of accuracy.

The results were generated by changing each of the parameters in turn. The relative importance of, for example, the rates of termination, the rate of chain transfer to monomer, the solubility of initiator or the flocculation of primary particles was judged by the effect on the rate and molecular weight curves.

Since a single experimental run can create numerical and graphical output for a wide range of dependent process variables, for example, the variations of rate, conversion, molecular weight, polydispersity, porosity and the concentrations of initiator, monomer and radicals with time or conversion it is essential to be selective in presenting the results. Hence, although the results of the numerical experiments are tabulated in Appendix 6.1, only graphs pertinent to a particular feature of the polymerisation are presented

in this chapter.

Most graphs show rate profiles; they are easily transformed to the temperature profiles observed in practice. The rate of reaction can easily be shown proportional to the temperature difference in between the jacket and autoclave when autoclaves are controlled to be isothermal:

$$r_m = \frac{UA(T_B - T_j)}{M_B(-\Delta H_R)} \qquad (6.1)$$

where r_m is the rate of reaction per unit mass

M_B is the mass of the autoclave and all the other symbols have been defined in Chapter 3.

Furthermore, rate-time profiles have an advantage over the sigmoidal conversion-time curves normally used to support previous models (38 to 45 and 50); they reveal more clearly the nature of the second derivative, the rate of change of rate d^2x/dt^2. This can change quite subtly with process conditions and mechanism. Figure 6.1 highlights the difference in shape of some typical rate and conversion curves predicted by the numerical model.

6.1 PREDICTIONS OF THE MODELS

6.1.1 The Analytic Model

The analytic model derived in Section 5.3 is a very powerful tool. It allows a very rapid analysis of the chemical kinetics of vinyl chloride polymerisation when the radicals terminate where they are initiated and where the total radical chain end population is small. It provides no information about molecular weight or its distribution.

In using the analytic model most credance was placed upon the k_p's and k_d's; they are well substantiated in the literature (45, 96). Initiator efficiences, the distribution of initiator, and the k_t's in the monomer and polymer phases were all varied independently.

FIGURE 6.1 The presentation of model predictions in graphical form : typical profiles.
($T=50^{\circ}C$, $\chi_{45}^{I}=1.538$, $[I_0]=1.1754$ molm^{-3} Perkadox-16)

(i) Conversion as a function of Time.

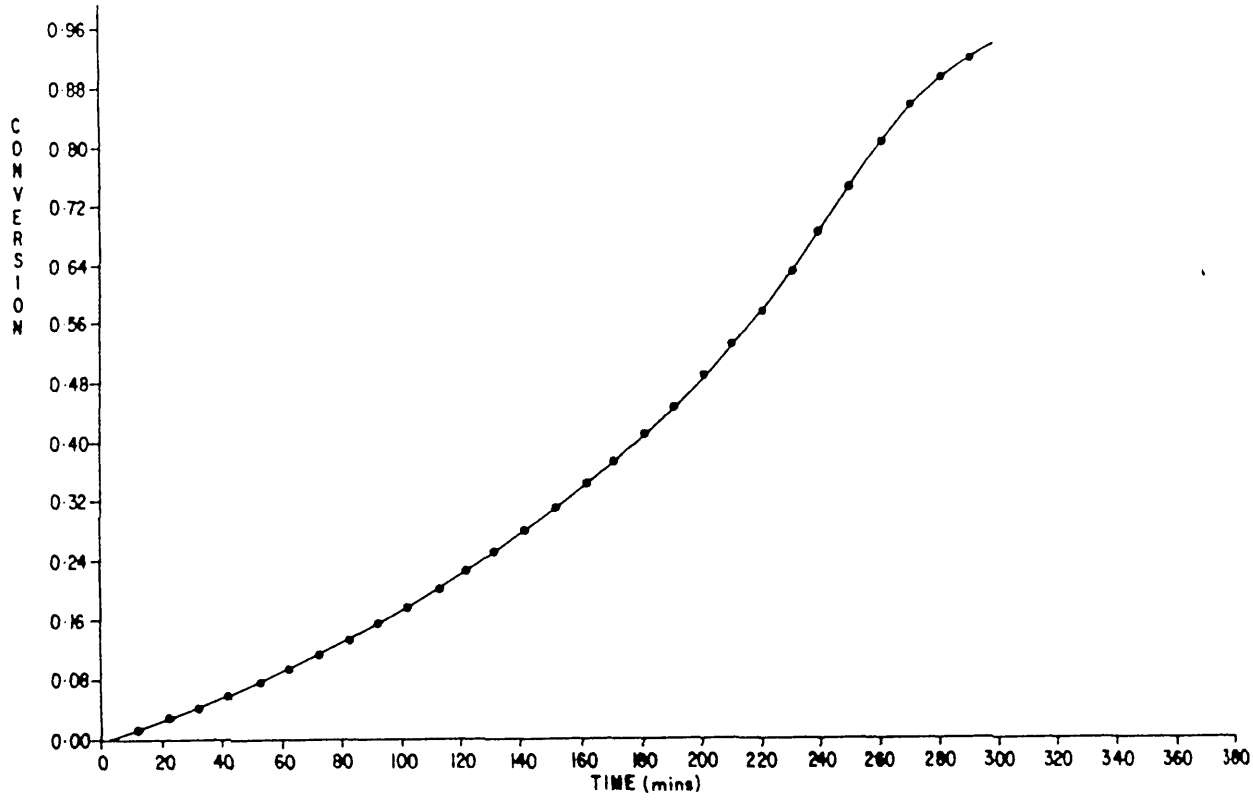

(ii) Rate as a function of Time.

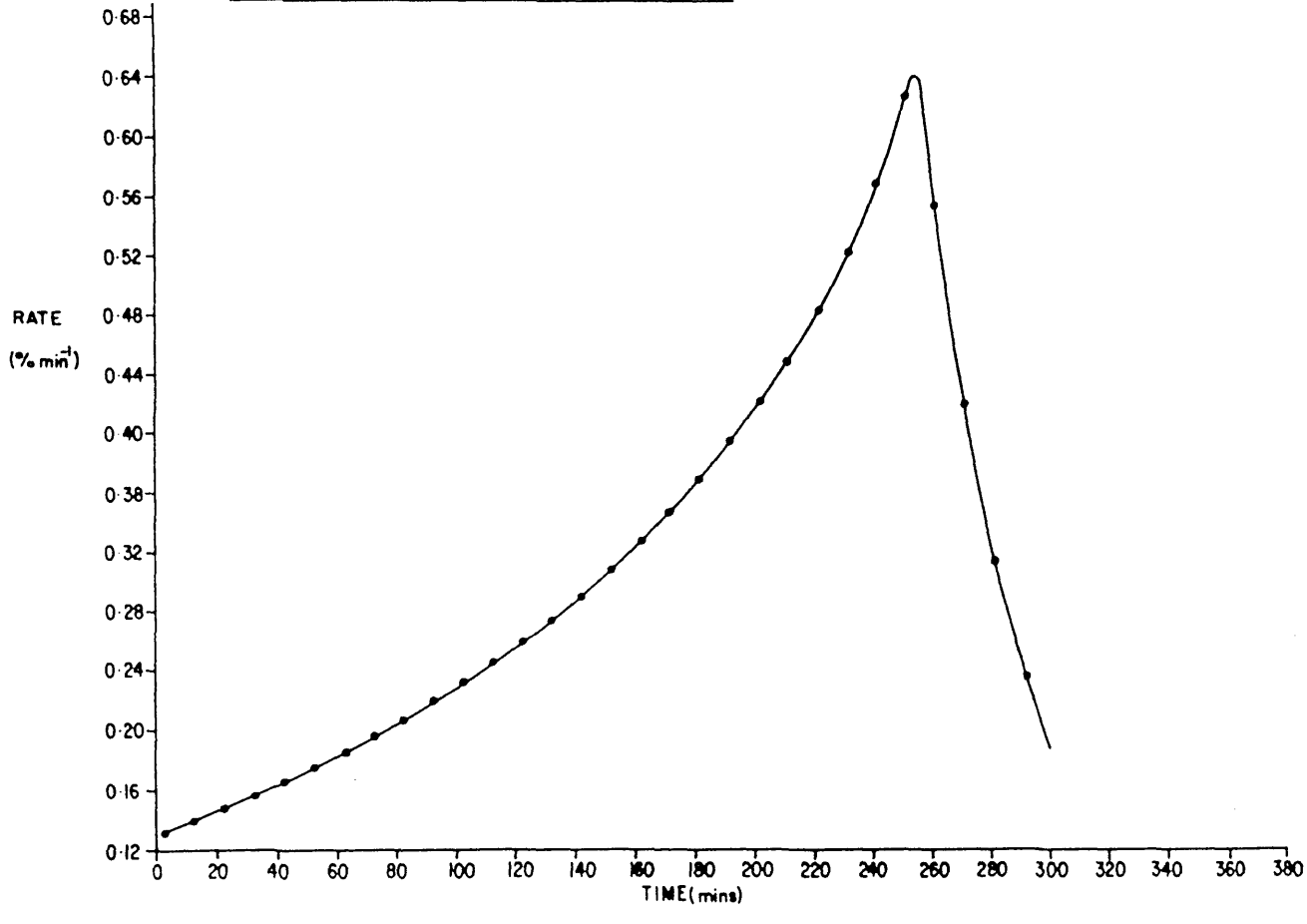

FIGURE 6.1 (cont)

(iii) Rate as a function of Conversion.

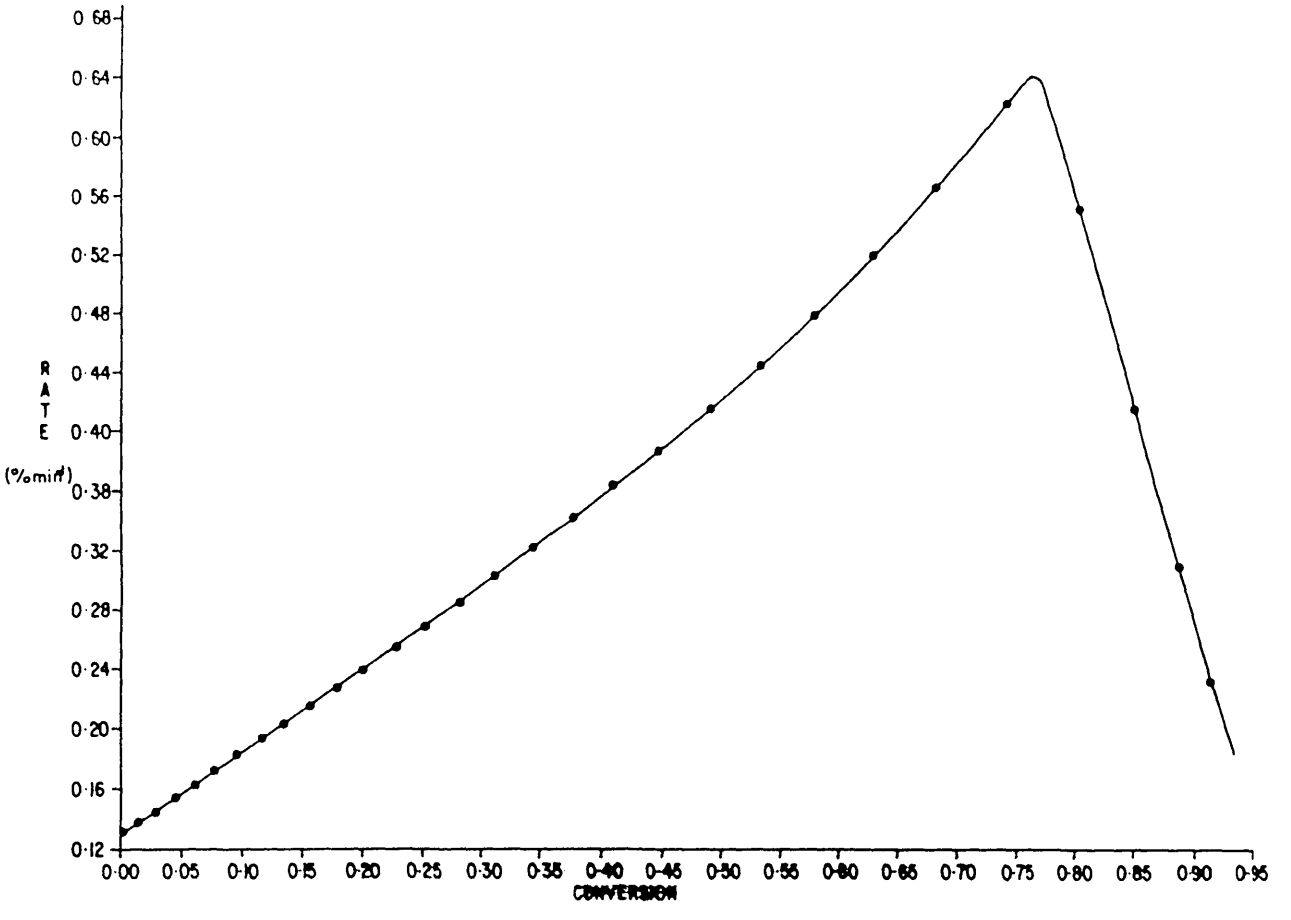

With the parameter set given in Tables 5.2 and 5.3, total polymerisation time was found to be that of the order 22 hours. Typical times in process plant for the same recipe show the polymerisation time to be about six hours for ultimate conversions of 93% at 55°C. (Appendix 6.2). Decreasing k_{t_4}, k_{t_5}, k_{t_6} and k_{t_7} (Section 5.2) by a factor of four doubled the overall rate of reaction (eq 5.58). More realistic polymerisation time scales of five hours are achieved. Figure 6.2 shows how changing the k_t's from their base values affects the polymerisation rate.

The fourfold decreased termination constants were used for much of the sensitivity analysis.

Modifying the overall rates by the variation of k_t's is preferred; it only has a small effect on molecular weight. It is the ratio k_p/k_{trm} which principally determines molecular weight, although the relative strengths of initiation to termination determine its conversion dependence. Molecular weights at high conversions are easily measured, thus defining the ratio k_p/k_{trm}. The k_t's therefore remain as the constants most easily changed without affecting other aspects of the model

Temperature Effects

In Figure 6.2 the effect of temperature on rate for a constant initial initiator charge is also seen.

At 'low temperatures' (less than 60°C in this case) the rate is seen to peak: the peak occurs at ~77% conversion when all the diluent monomer phase has been consumed and polymerisation is starting to proceed at the expense of the monomer swelling the polymer. The rate falls thereafter. Upto the peak, the rate increases linearly with conversion, as the proportion of the polymer phase, where growth is fastest, increases (equation 5.58). In the time domain, this appears as autoacceleration.

FIGURE 6.2 The effect on rate of reaction caused by changing rates of termination in the monomeric and polymeric phases.

Legend:

Initial Initiator Concentration, $[I_0]$ = 1.1754 $molm^{-3}$

Initiator Efficiencies:

Monomer Phase, f_4 = 0.7

Polymer Phase, f_5 = 0.5

Initiator Distribution Coefficient, γ^I_{45} = 1.538

CURVE	TEMP (°C)	RATE RATIO (polymer/ monomer)	REMARKS
a	50	6.851	k_t as Kuchanov et al, § 5.2 t_p - 22 hrs
b	50	3.425	monomer , k_t^4(@ a)/4
c	50	13.702	polymer , k_t^5(@ a)/4
d	50	6.851	k_t^4(@a)/4, k_t^5(@a)/4
e	55	6.538	" "
f	60	6.244	" "
g	65	5.971	" "
h	70	5.717	" "
i	55	6.538	k_t^4(@a)/2, k_t^5(@a)/2
j	50		k_t^4(@a)/40, k_t^5(@a)/40
k	55		" "
l	57		Experimental Observ'n ($[I_0]$=1.413 mol/m^3 Perkadox16)

FIGURE 6.2

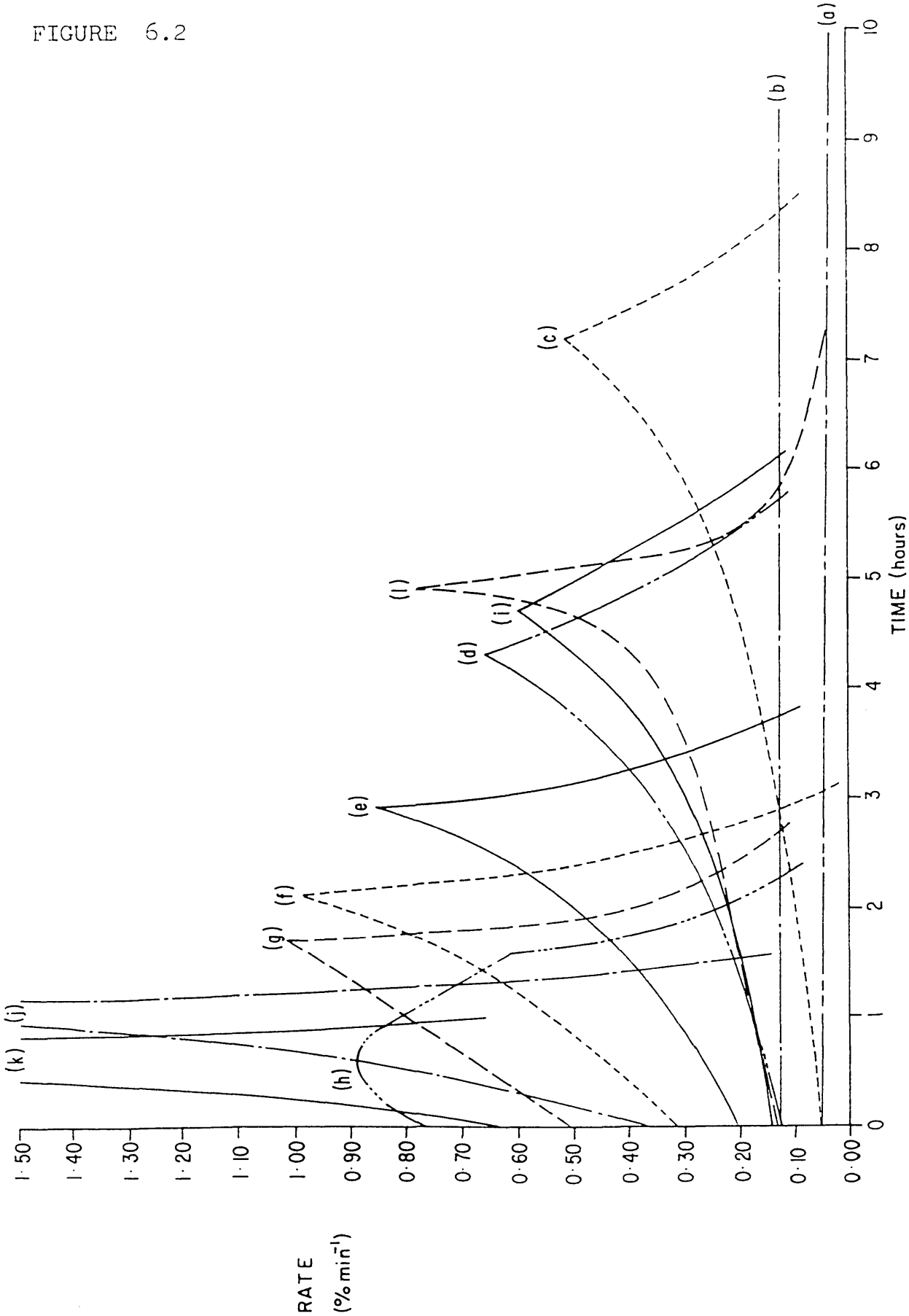
RATE
(% min⁻¹)
1·50
1·40
1·30
1·20
1·10
1·00
0·90
0·80
0·70
0·60
0·50
0·40
0·30
0·20
0·10
0·00
0
1
2
3
4
5
6
7
8
9
10
TIME (hours)
(a)
(b)
(c)
(d)
(e)
(f)
(g)
(h)
(i)
(j)
(k)
(l)

Initiator Effects

Figures 6.3(i) to (vi) reveal how important the location of the initiator is. As γ_{45}^{I} increases - initiator more soluble in the monomer phase - the rate curves increase less rapidly with time (or conversion) in the early stages and show an increasingly pronounced peak at 77% conversion. Insufficient initiator is present in the polymer phase in the early stages to generate the radicals necessary to support the dominant polymer phase growth necessary for autoacceleration. The peakiness in the rate profiles, seen for example in Figure 6.3(iii) when $\gamma = 7.5$, arises because eventually sufficient initiator is forced into the polymer phase by high concentrations in the monomer phase. Enough free radicals are then generated for a (belated) autoacceleration. Increasing γ_{45}^{I} not only suppresses the early rate, it decreases the ratio of peak rate to initial rate. The latter observation is a direct consequence of the low early rate; it increases the time taken to reach the 'pressure drop' conversion. Initiator, therefore, has more time to decay and its contribution to the magnitude of the peak rate at pressure drop is reduced. This can be seen in equation 5.58 when x is set to α_5: the rate peak is then proportional to the square root of the remaining initiator, $[\exp(-k_d\ t)]^{1/2}$.

6.1.2 Higher Temperatures

At higher temperatures, above 60°C for this initiator, although initial rates of polymerisation are higher, initiator depletion becomes significant. In Figure 6.3(v), where the polymerisation temperature is 65°C, the onset of depletion conditions is observed. For curve (a) ($\gamma_{45}^{I} = 1.5$) there is enough initiator in the polymer phase to support the dominant rate there. The rate continuously rises to a peak maximum at 77% conversion. With higher γ's, eg $\gamma_{45}^{I} = 7.5$ in curve (c), when more initiator remains in the monomer phase, with its lower intrinic rate, the rapidly decomposing initiator causes a reduction in the monomer phase rate. This is not quite matched by rising rate contribution in polymer phase over the first two hours. The rate falls from an early maximum to a

FIGURE 6.3 The effect of variations in the initiator distribution coefficient on the rate of polymerisation at different temperatures.

Initial initiator concentration, $[I_0] = 1.413$ mol m^{-3}
At each temperature:

Curve	$\gamma_{I_{45}}$
a	1.5
b	3.0
c	4.5
d	6.0
e	7.5

(i) Temperature= 45°C

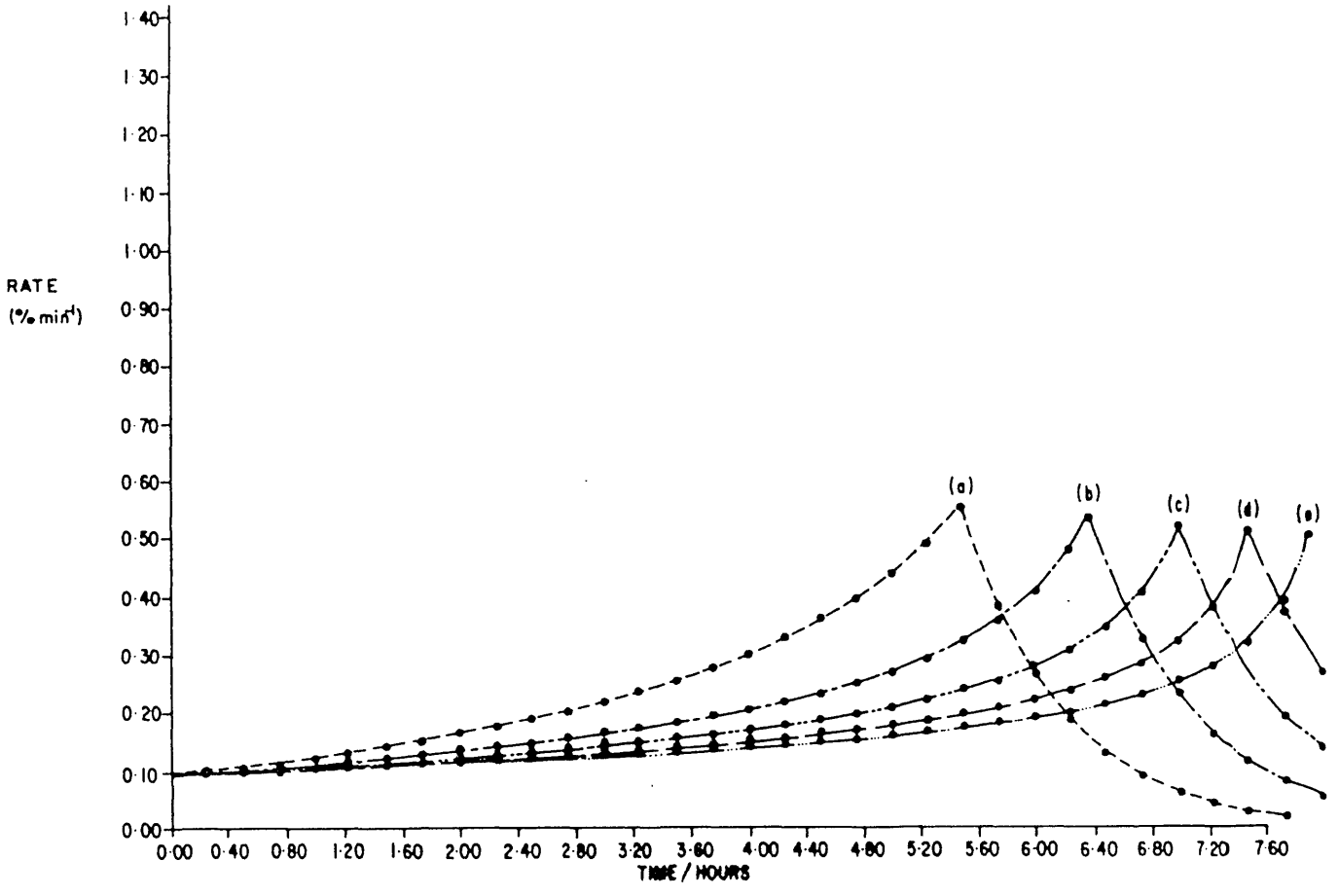

(ii) Temperature=50°C

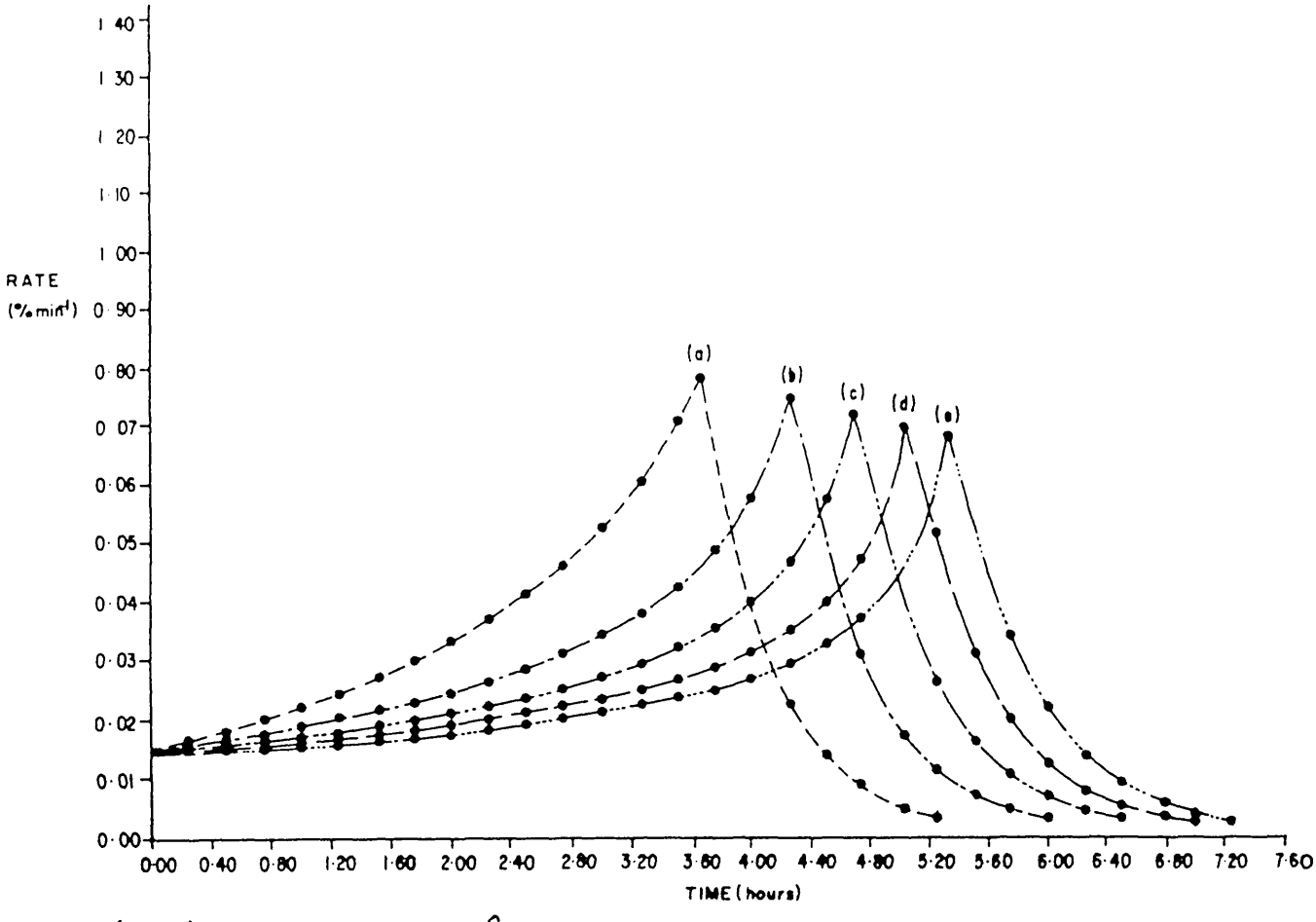

(iii) Temperature=55°C

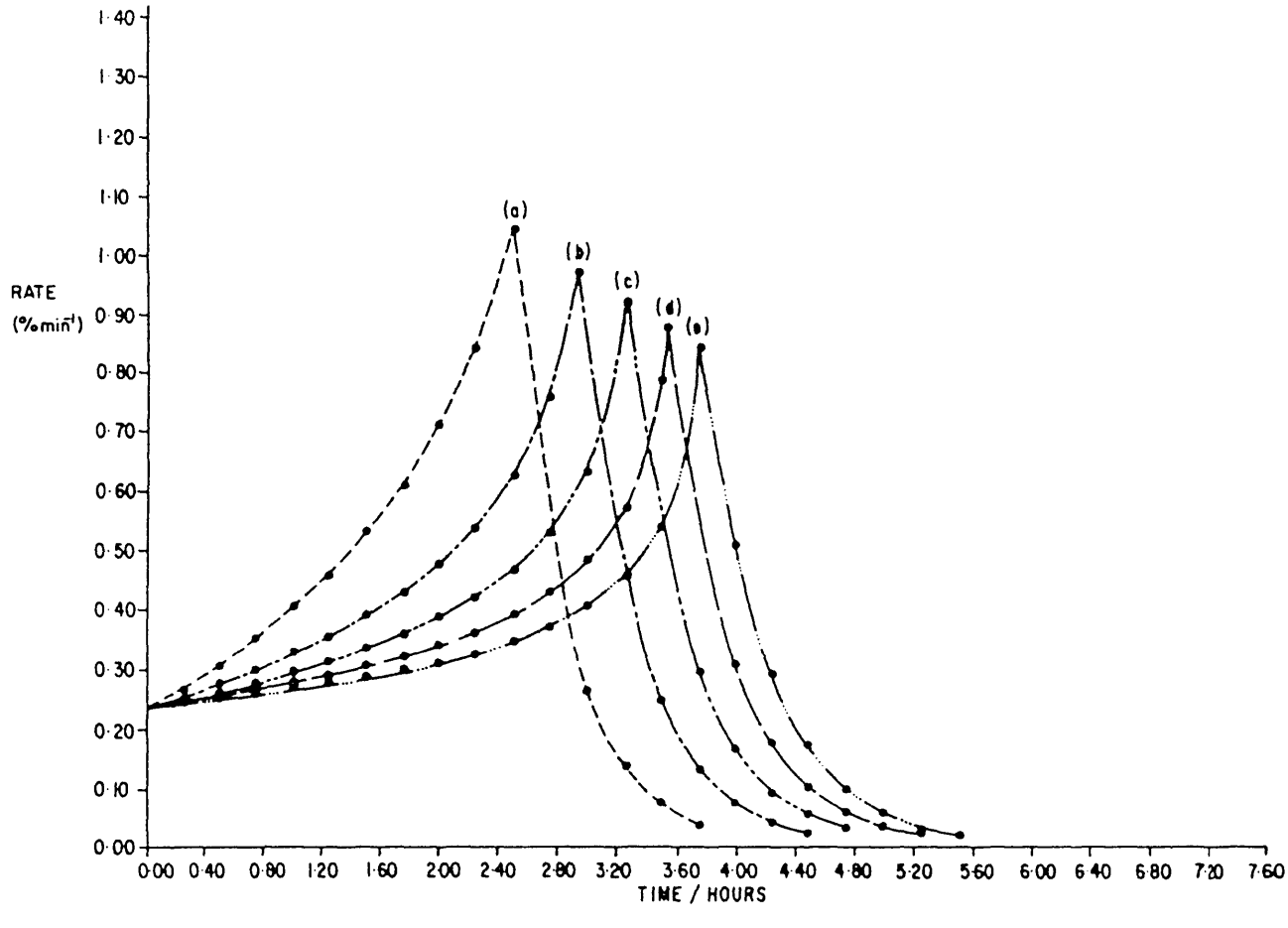

(iv) Temperature=60°C

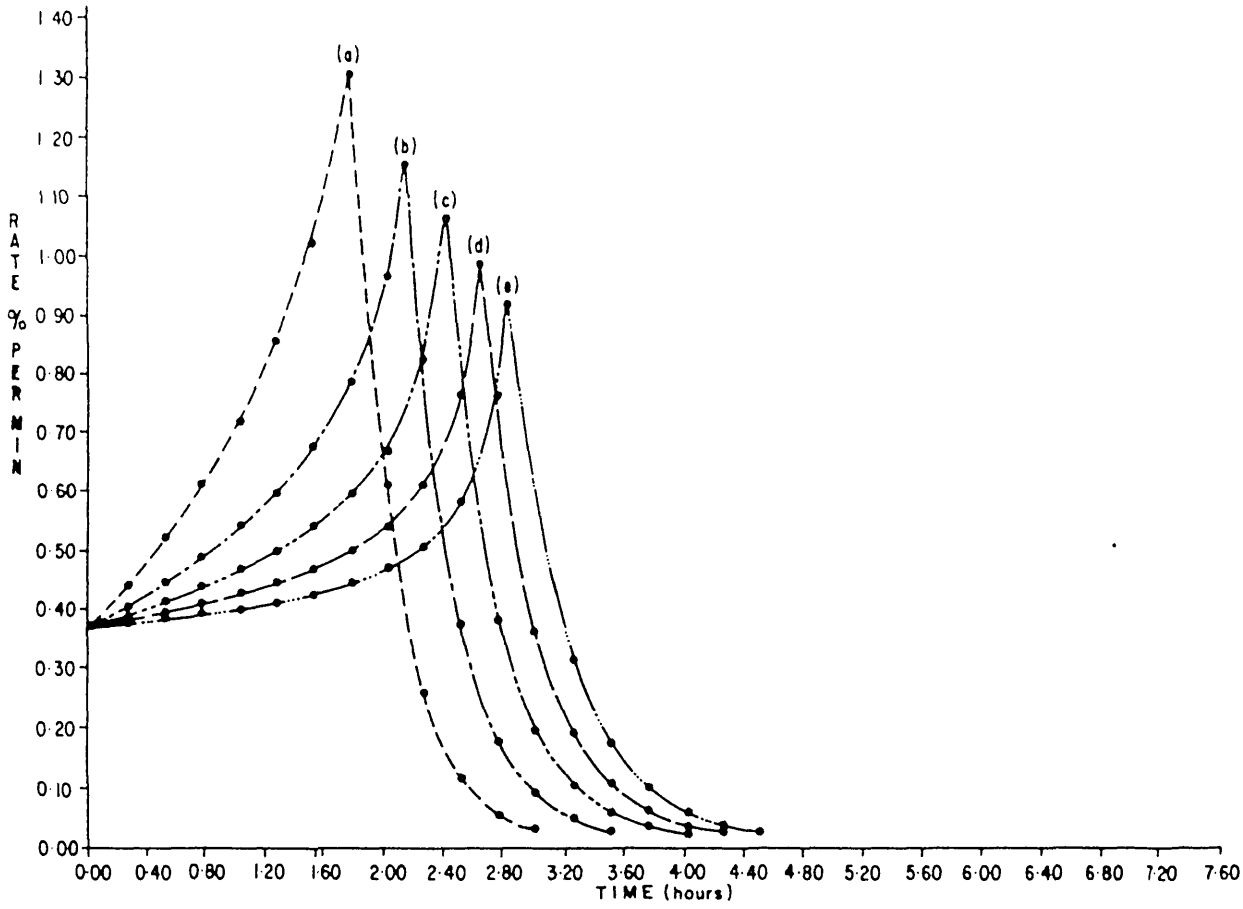

(v) Temperature=65°C

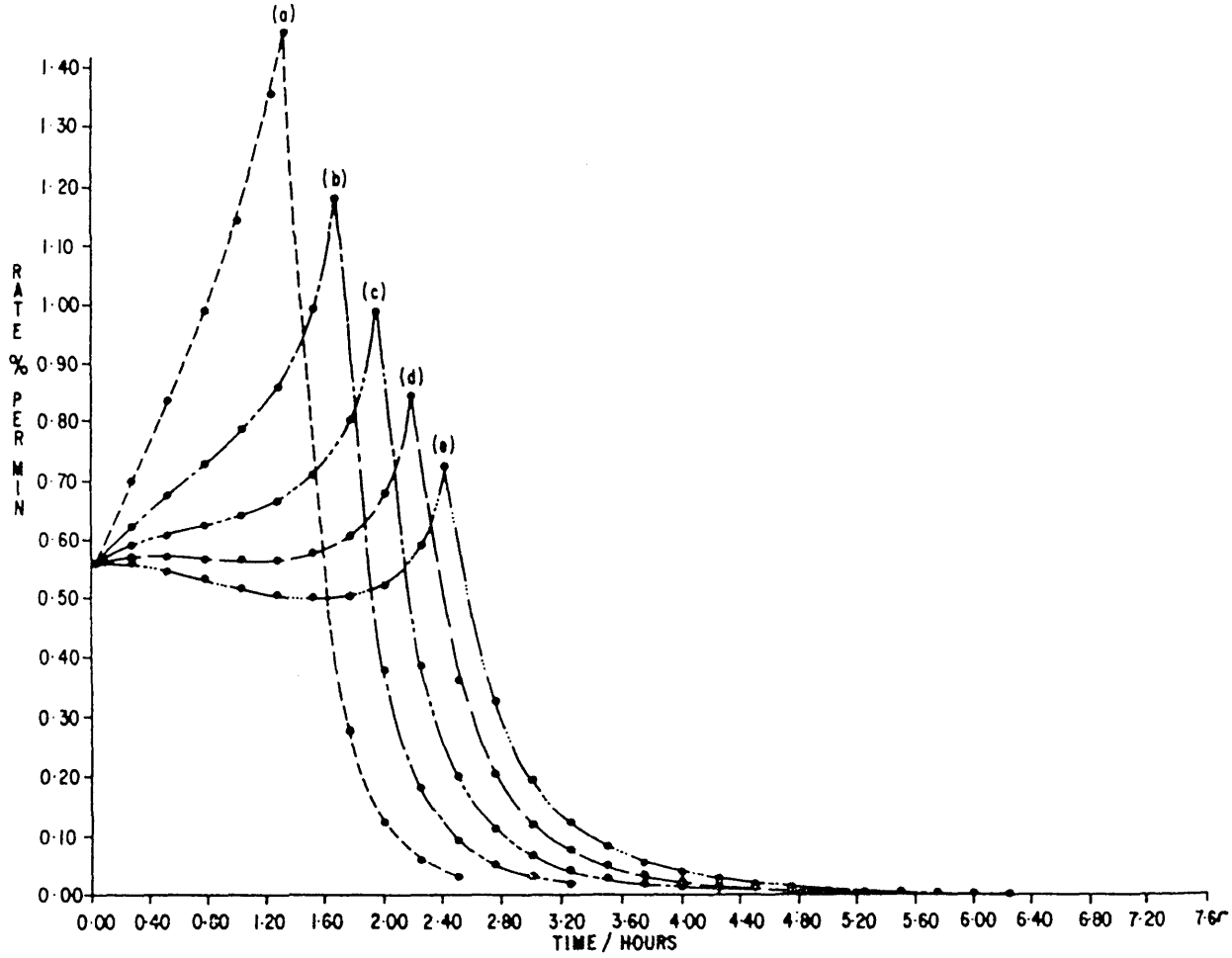

(vi) Temperature=70°C

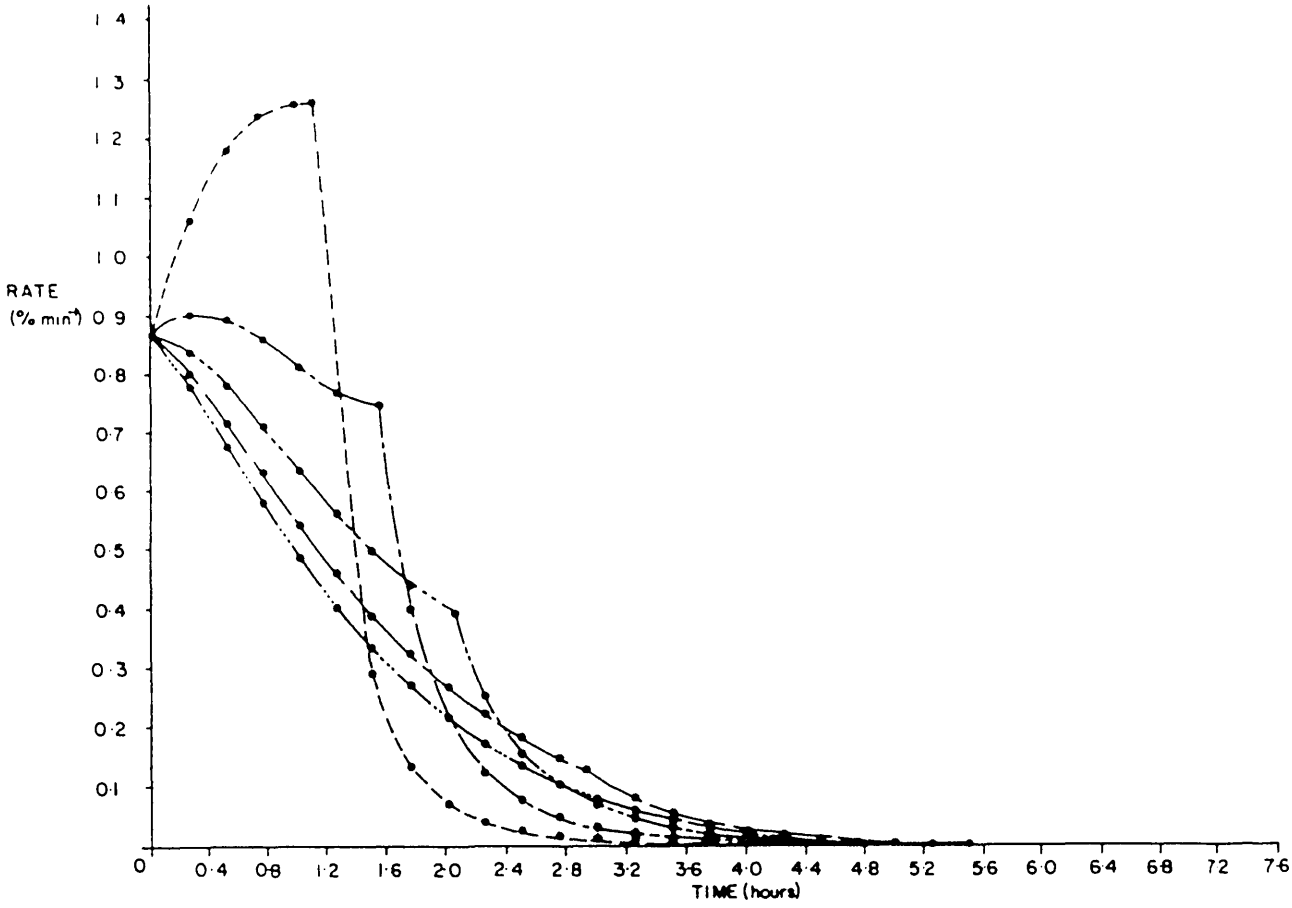

pre-pressure drop minimum. At this point polymer phase kinetics become dominant again and a rate peak is observed on the decreasing rate tail.

At still higher temperatures - in Figure 6.3(vi), T = 70°C - initiator depletion completely dominates the polymerisation, especially when γ^I is high. The maximum conversion reached is approximately 50%, depending on recipe and operating conditions: pressure drop conversion is not attained as the polymerisation proceeds under dead end conditions (99).

6.1.3 Initiator Efficiency

In Figure 6.4 the importance of initiator efficiency is highlighted. By considering the ratio:

$$\beta = \frac{\text{Initiator Efficiency in Polymer Phase}}{\text{Initiator Efficiency in Monomer Phase}} = \frac{f_5}{f_4} = \frac{f_6}{f_4} = \frac{f_7}{f_4}$$

it can be seen as β decreases from .866 to .01, the mean and peak rates are lowered, in a manner similar to that observed for higher temperature polymerisations. (The overall rate is of course much lower than in those cases) in curves (a) to (c), efficiency of initiation in the polymer phase is sufficiently high enough to ensure dominant polymer phase growth. In curve (d), the efficiency is only just high enough to support polymerisation in the precipitated phase: initiator depletion is becoming important after five hours and a maximum rate is observed significantly before pressure drop at approximately seven hours. With the lowest polymer phase initiator efficiencies, virtually all the polymerisation is occurring in the monomer phase at very small overall rates.

6.1.4 Interpreting the Observations

The studies so far indicate that the fourfold decrease in k_t's underestimates the time to pressure drop conversion by some two hours; it is usually about four hours at 55°C. Therefore in Figure 6.5, the k_t's have been reduced by a factor of two and the initiator

FIGURE 6.4 The effect of changing the polymer phase initiator efficiency, f_5, on the observed total rate.

Legend: Temp=50°C, $[I_0]$=1.177 molm^{-3} Perkadox-16, γ^I_{45}=1.538,

Monomer Phase Initiator Efficiency, f_4=0.75

Curve	f_5	Rate Ratio (polymer/ monomer)	$\beta = f_5/f_4$
a	0.866	25.101	1.155
b	0.750	23.363	1.000
c	0.562	20.224	0.749
d	0.316	15.165	0.421
e	0.100	8.531	0.133
f	0.010	2.698	0.013

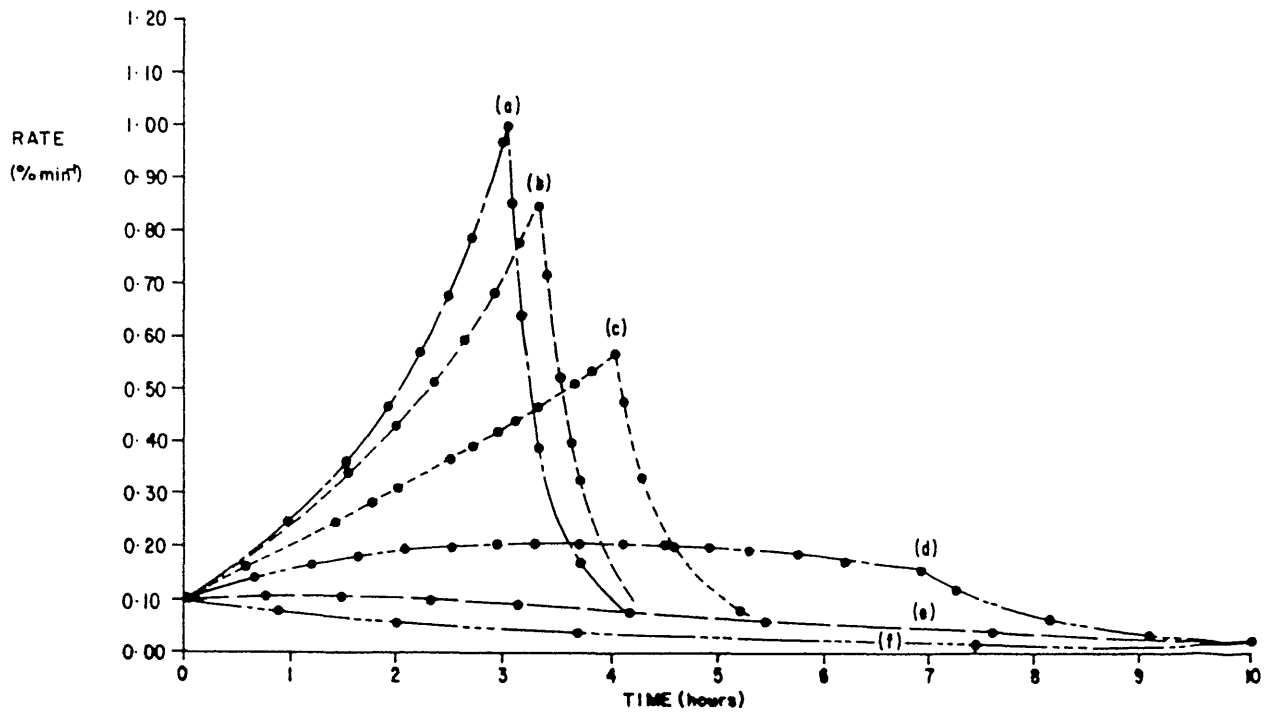

FIGURE 6.5 Realistic Rate Curves as functions of Time and Temperature.

γ^{I}_{45}=3.0, $[I_0]$=1.4105 molm^{-3} Perkadox-16, f_4=0.7, f_5=0.5,
k_t's=k_t's(Kuchanov and Bort)/2

TEMP (°C)	X_{max}
50	0.9261
55	0.9878
60	0.9786
65	0.8116
70	0.4802

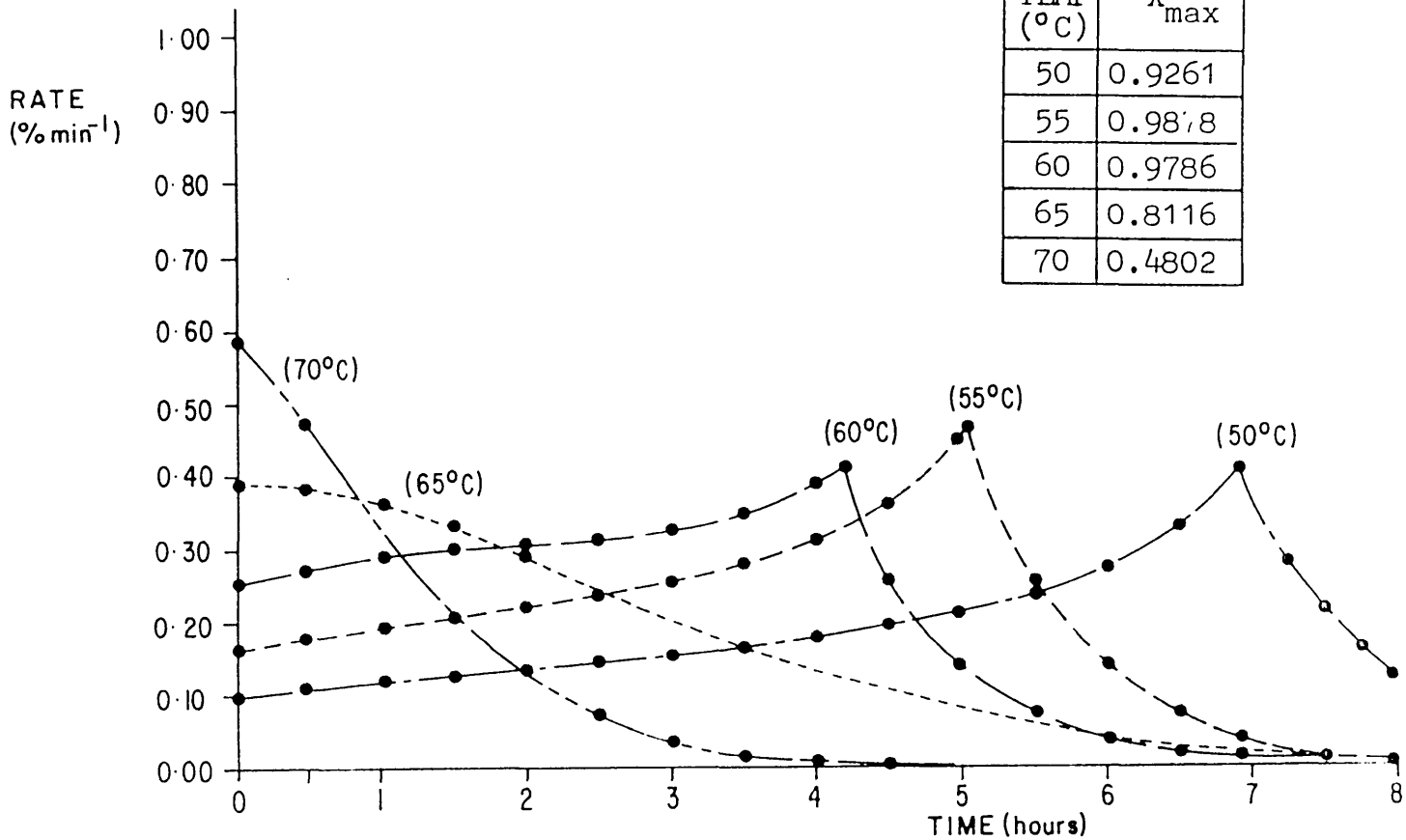

distribution coefficient, y_{45}^{I}, has been set to 3.0 to produce more realistic rate-time curves. Despite the change in k_t's the transition from high temperature polymerisation (with initiator depletion and dead end polymerisation dominating) to low temperature 'peaky' reactions is clearly shown.

At approximately 60°C, as is seen in Figure 6.5, the rate of initiator decay approximately matches the rate of growth of the polymeric phase with its enhanced rate: the rate profile is "square" or plateau shaped. "Square" shaped profiles are observed in practice at intermediate temperatures (70°C > T >50°C): they can represent ideal temperature profiles. If the rate of polymerisation is at the maximum permitted by the cooling system, the cycle time between successive batch charges is minimised, optimising the utilisation of the reactors.

The analytic model provides a ready means to interpret the results demonstrated in Figures 6.2 to 6.5. The quantity to study is the ratio of the rate at the onset of pressure drop (the 'peak rate') to the initial rate. All the initiator related effects can be explained by this ratio: the conditions for 'peaky', 'plateau' and 'initiator depletion' reactions can be determined.

From equation 5.58, the initial rate of polymerisation is given by:

$$\left.\frac{dx}{dt}\right|_o = (k_p + k_{trm})\left[\frac{2fk_D}{k_t}\right]^{1/2}_{\substack{\text{monomer}\\\text{phase}}}\left[\frac{I_o}{V_o}\right]^{1/2} \qquad (6.3)$$

and the rate of polymerisation at the onset of pressure drop is given by:

$$\left.\frac{dx}{dt}\right|_{pd} = (k_p + k_{trm})\left[\frac{2fk_D}{k_t}\right]^{1/2}_{\substack{\text{polymer}\\\text{phase}}}\left[\frac{I_{oe}^{-k_D t_{pd}}}{V_o\left\{\frac{(1-\alpha_5)\,\bar{v}_5^{m} + \alpha_5\,\bar{v}_5^{p}}{\bar{v}_5^{m}}\right\}}\right]^{1/2}(1-\alpha_5) \qquad (6.4)$$

The rate constants for propagation, chain transfer to monomer and initiator decomposition are idential in each phase, so

$$R = \frac{dx/dt|_{pd}}{dx/dt|_{o}} = \left[\frac{f_s\, k_{t4}}{f_4\, k_{ts}}\right]^{1/2} \frac{1 - \alpha_s}{\left\{\frac{(1-\alpha_s)\,\bar{v}_s{}^n + \alpha_s\,\bar{v}_s{}^p}{\bar{v}_s{}^n}\right\}^{1/2}} .e^{-k_D t/2} \qquad (6.5)$$

The ratio R lies within an exponential envelope whose magnitude is principally determined by

$$\left[\frac{f_s\, k_{t4}}{f_4\, k_{ts}}\right]^{1/2}$$

Its precise value depends on the amount of initiator depletion which has occurred when pressure drop starts; this modified $\exp(-k_D t)$.

Qualitatively (6.5) gives the correct picture. For example, when the efficiency of initiation was decreased in the gel phase in Figure 6.4, the maximum possible rate ratio is reduced and the time taken to reach the peak rate is increased: initiator depletion therefore gives a smaller value for $.e^{-k_D t_{pd}/2}$. A transition from peaky ((a) to (c)) to plateau (d) and finally initiator depletion polymerisations ((e) and (f)) is observed.

Equation 6.5 can be used to deduce the three basic types of polymerisation (Figure 6.6) and to develop a procedure for predicting the type of polymerisation produced by a particular initiator type and charge. Initiator selection becomes more systematic.

FIGURE 6.6

TYPES OF VC POLYMERISATION

Relationship	Type of Reaction	Temp Regime	Diagram
$R = \frac{dx/dt\|_{pd}}{dx/dt\|_{o}} > 1$	Peaky	Low	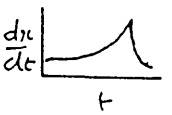
$R = 1$	Plateau	Intermediate	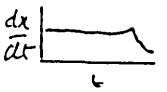
$R < 1$	Initiator Depletion (Dead End)	High	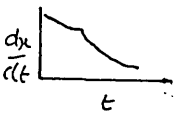

6.1.5 Predicting the Peak Nature of Polymerisation

If the type of polymerisation is to be predicted, a number of steps have to be followed:

a) Calculate the initial rate from equation 6.3.

b) Calculate the time taken at this rate to reach the pressure drop conversion, $t_{pd|r(o)}$.

c) Calculate the time required for the rate at pressure drop to equal its initial value, ie for R = 1, from equation 6.5, $t_{pd|R=1}$.

d) (i) If $t_{pd|r(o)} < t_{pd|R=1}$ the pressure drop conversion will be reached before the initiator depletion term $.e^{-k_D t_{pd}/2}$ dominates the behaviour of 6.5: the rate will show a maximum at pressure drop.

(ii) If $t_{pd|r(o)} = t_{pd|R=1}$, the pressure drop conversion is reached at precisely the moment the depletion term has reduced the maximum rate ratio to 1: the rate will show a plateau upto pressure drop.

(iii) If $t_{pd|r(o)} > t_{pd|R=1}$, the initiator depletion dominates equation 6.5. If the polymerisation proceeds at the initial

rate, the initiator will have depleted so much so that it cannot support a high rate at pressure drop.

The effectiveness of this procedure can be demonstrated with the polymerisation rates shown in Figure 6.5. Using the parameters given in Section 5.2, equation 6.5 becomes:-

$$R = 0.3172\ e^{(8375/RT - k_D t/2)} \qquad (6/6)$$

The transition from 'peaky' to 'initiator depletion' reactions is shown in Table 6.1 together with $t_{pd|r(o)}$ and $t_{pd|R=1}$. The conditions of step (d) above are clearly met.

TABLE 6.1

PREDICTING POLYMERISATION TYPE

Temperature (°C)	Time to reach pressure drop at initial rate $t_{pd\|r(o)}$ (hrs)	Time required for ratio of pressure drop rate to equal 1 $t_{pd\|R=1}$ (hrs)	Type of Polymerisation
50	12.65	23.55	Peaky
55	7.97	11.30	Peaky
60	5.09	5.54	Peaky/Plateau
65	3.29	2.77	Initiator Depletion
70	2.16	1.41	Initiator Depletion

This rule is of immediate application in choosing initiators to run at the ideal 'plateau' rate profile. The 'desired' pressure drop time is calculated from the maximum rate and the pressure drop conversion, vis:-

$$t_{pd|des} = x_{pd}/(dx/dt|_{max}) \qquad (6.7)$$

From 6.5 (or 6.6) the necessary k_D to achieve a plateau profile at a particular temperature is calculated: an initiator can be chosen and the necessary charge can calculated from equation 6.3.

This is a simple yet powerful application of the model. Indeed some of the previous models such as Hamielec's could have been used in the same manner. No-one appears to have noted this particularly practical application; it is clearly not so important in an academic study to predict when the maximum rate occurs or what its value will be.

In an industrial environment mixed initiator systems are used to circumvent the initiator depletion problem. A fast decomposing initiator is used to give a high initial rate. Mixed with it is a slow decomposing initiator which sustains polymerisation at high conversions when the fast initiator has all but disappeared.

Even under these circumstances the procedure can be used in a modified form, to estimate how much of each type of initiator is required. Equation 6.3 is used with value of I and k_D for the fast initiator, while 6.5 is used with values of k_D for the slow initiator. Now, since the reactor will be run with a "square" profile, back-calculation with equation 6.3 indicates how much slow initiator is required.

6.1.6 Predicting Principal Rate Curve Characteristics from Experimental Studies - Optimising Initiatior Utilisation

In commercial studies a significant amount of time and effort can be wasted in working our how much initiator to use. A series of experiments may be performed on pilot plants until the correct charge is determined. The analytic model provides a practical solution to this problem. Given the experimental rate curve for a given temperature and initiator charge, the principal characteristics of the rate curve for different initiator charges at the same temperature can be predicted, namely:

* initial rate
* rate at pressure drop
* time pressure drop occurs.

Using the methods outlined in the previous section, any change in the nature of the rate profile can also be predicted.

The known rate profile is recorded from a reactor jacket temperature profile such as shown in Appendix 6.2. When more or less initiator is added, the rate will change and the time taken to reach the pressure drop conversion will be affected. The amount by which it changes is easily predicted. The method relies on the functional form of the mathematical model and thereby avoids the need to know precise values for most of the model parameters.

The basis of the analytic model is equation 5.58 which is integrated by separating variables. It takes the form:

$$\frac{dx}{dt} = f(x)\, g(t) \qquad (6.8)$$

where x is the conversion

$f(x)$ is a function which represents the conversion dependent parameters

and $g(t)$ is a function which represents the time dependent decay of initiator

If the rate increases by a constant factor, a, over the entire conversion range:

$$\frac{dx}{dt} = a\, f(x)\, g(t) \qquad (6.9)$$

At constant temperature the terms representing the essential physics of the process, $f(x)$, and the initiator decay, $g(t)$, remain unaffected, therefore

$$\int_o^x \frac{dx}{f(x)} = \int_o^T g(t)dt = a\int_o^{T'} g(t)\, dt \qquad (6.10)$$

where T,T' represent the times for the 'standard' and the modified reactions to reach conversion x. Since,

$$G(T) = \int_o^T g(t)dt \equiv \frac{2}{k_D}\left[1 - e^{-k_d T/2}\right] \qquad (6.11)$$

T maps into T' by the relationship:

$$T' = \frac{-2}{k_d} \text{Ln}\left\{1 - \frac{1}{a}\left(1 - e^{-k_d T/2}\right)\right\} \qquad (6.12)$$

Since, for changed initiator charges, rate scales with $I^{1/2}$ (equation 5.58), the factor, a, is given by

$$a = \left[\frac{I}{I_o}\right]^{1/2} \qquad (6.13)$$

where I_o is the initiator charge for the know profile

I is the new charge

Thus from a known rate curve the principal characteristics of the new curve are predicted,

(i) For initial rate,

$$\left.\frac{dx}{dt}\right|_o' = a \left.\frac{dx}{dt}\right|_o \qquad (6.14)$$

(ii) For time to pressure drop, equation (6.12)

(iii) For ratio for 'peak', pressure drop rate to initial rate (using 6.10)

$$R' = \frac{e^{-k_D T'/2}}{e^{-k_D T/2}} \; R_o \qquad (6.15)$$

where ' indicates prediction from experimental observation $_o$.

This method of approximation is of immediate engineering application and demonstrates the wide ranging scope of the mathematical model. In the next part of the chapter the ability of

the numerical model to look at more detailed aspects of micro-mechanism will be seen.

6.2 THE NUMERICAL MODEL

The analytic model is of vital importance in understanding and quantifying the chemical kinetic effects of vinyl chloride polymerisation. The effects of mass transfer limitation are however beyond its scope. This is not the case for the numerical model, which has the capability for independent variation of all the mass transfer coefficients. Hence any limitations in the mass transfer of initiator, monomer or radicals, and their consequent effects on the polymerisation process, can be analysed.

An essential feature of the model is its ability to describe the continual variation of interfacial area between basic, or primary, particles and the monomer phase, as the precipitated species grow and flocculate. Its other main feature is the prediction, from the zeroth, first and second moments of the molecular weight distribution, of the number and weight average molecular weights.

No other model for vinyl chloride polymerisation so rigorously relates kinetic, mass transfer, molecular weight and particle formation effects within a single framework. The comparison of the model predictions with experimental observations, such as rate with time or molecular weight with conversion, will verify the model and the significant contributions to mechanism.

With the fine tuning which accrues from repeated model calculations, more realistic values for flocculation, mass transfer and kinetic parameters will be determined. In Table 6.2 the variables which the model requires as input are listed, with their default values. In this thesis many of those variables are modified over a large range, to determine their significance in the polymerisation process. Table 6.3 shows what 'experiments' were performed with the model and summarises how parameters were changed to observe particular effects.

TABLE 6.2

VARIABLES INPUT TO THE MODEL AND STANDARD VALUES

Section 1: Basic Thermodynamic Data for Each Phase

Line 1: Partial Molar Volumes for Initiator $\bar{v}_I^{(i)}$, i = 1,7

Line 2: Partial Molar Volumes for Monomer $\bar{v}_M^{(i)}$, i = 1,7

$\bar{v}_M^1 = .29762 \times 10^{-2}$ $m^3 mol^{-1}$

$\bar{v}_M^2 = .46507 \times 10^{-3}$ $m^3 mol^{-1}$

$\bar{v}_M^{3-7} = .725744 \times 10^{-4}$ $m^3 mol^{-1}$

Line 3: Partial Molar Voume for Polymer, per monomer unit in chain

$\bar{v}_P^i$, i = 1,7

$\bar{v}_P^{3-7} = .446429 \times 10^{-4}$ m^3(mol monomer units)$^{-1}$

Section 2: Variable Input Data

Line 4: Run Number (Identifier)

Line 5: Temperature of Polymerisation, 50°C

Line 6: Initiator Type, Perkadox-16

Line 7: Initiator Charge, 30g

Line 8: Molecular Weight of Initiator, 398.5kg/kmol

Line 9: Volume of Monomer Charge to Autoclave, 64×10^{-3} m^3

Line 10: Volume of Water Charged to Autoclave, 66.8×10^{-3} m^3

Line 11: Stirrer Speed, 200 rpm

Line 12: Autoclave Size, .16 m^3

Line 13: Autoclave Internal Radius, .2 m

Line 14: Default Radius of droplets, 40μm

Line 15: Default Conversion when primary particles Start to Precipitate, 3×10^{-5}

Line 16: Default Conversion when primary particles form surface and bulk phases, .05

Line 17: Default Conversion when subgrains stop contracting, .67

Line 18: Conversion when pressure drop commences, .77

Line 19: Packing Fraction of Primary Particles necessary for close packing to occur in subgrain, .74

Line 20: Co-ordination Number of Floccs of Primary Particles, 12

Line 21: Degree of Supersaturation before Primary Particles precipitate from monomer, 1.5

Section 3: Variable Mass Transfer Coefficients and Initiator Distribution

Line 22: Initiator m.t.c.'s, k_{AI}^{45}, k_{AI}^{46}, k_{AI}^{67}

Line 23: Monomer m.t.c.'s, k_{AM}^{45}, k_{AM}^{46}, k_{AM}^{67}

Line 24: Radical m.t.c.'s, $k_{a\sigma}^{45}$, $k_{a\sigma}^{46}$, $k_{a\sigma}^{67}$

Line 25: Fraction of Precipitated Primary Particle initially in phase 6, .85

Line 26: Initiator Distribution Coefficients, γ_I^{45}, γ_I^{46}, γ_I^{67} = 1

Section 4: Integrator Control Variables - see Nag Routine D02QBF

Line 27: TO , 0(S)

Line 28: TEND , 28800(S)

Line 29: (CIN(I),I=1,5) / 1.0 2.0 0.0 60.0 0.0

Line 30: TOL , 1.0×10^{-5}

Line 31: (COMM(I),I=1,5) / 0.0 0.0 0.0 1.0 60.0

Line 32: MAXITS , 20000

Section 5: Flocculation Model (equation 5.3) Parameters

Line 33: FLOCF, ϵ = 10

Line 34: CKFLOC,100 (No = CKFLOC * N_∞

TABLE 6.3

SUMMARY OF EXPERIMENTS PERFORMED WITH THE NUMERICAL MODEL

Series	Aim of Experiment and Means of Achievement
A	Assessing Initiator Mass Transfer Effects between Primary Surface and Primary Bulk. By:- starving primary particle bulk of initiator by lowering m.t.c. between primary surface and bulk ($10^{-7}ms^{-1}$ to $10^{-15}ms^{-1}$) with (i) Fast m.t. of monomer ($10^{-3}ms^{-1}$) (ii) No m.t. of radicals ($0ms^{-1}$)
B	Assessing Initiator M.T. Effects between Monomer and Basic/Primary Surface By:- Lowering m.t.c. between monomer and basic particle or primary particle surface ($10^{-7}ms^{-1}$ to $10^{-15}ms^{-1}$) with (i) Fast m.t. of monomer ($10^{-3}ms^{-1}$) (ii) No m.t. of radicals ($0ms^{-1}$)
C	Assessing monomer M.T. effects between monomer and basic/primary surface By:- Lowering m.t.c. between monomer and basic particle or primary particle surface ($10^{-7}ms^{-1}$ to $10^{-15}ms^{-1}$) with (i) Fast m.t. of initiator ($10^{-3}ms^{-1}$) (ii) No m.t. of radicals ($0ms^{-1}$)
D	B and C combined with (i) Fast m.t. of initiator and monomer from primary surface to bulk ($10^{-3}ms^{-1}$) (ii) No m.t. of radicals ($0ms^{-1}$)

Series	Aim of Experiment and Means of Achievement
F	Assessing Radical M.T. effects between monomer and basic/ primary surface by:- lowering m.t.c. between monomer and basic particule or primary particle surface ($10^{-3}ms^{-1}$to $10^{-13}ms^{-1}$) with (i) Fast m.t. of initiator and monomer ($10^{-3}ms^{-1}$) (ii) No m.t. of radicals from surface to bulk of primary.
H	Assessing influence of the mode of termination on molecular weight by increasing the proportion of termination due to combination. $k_t = k_{tc} + k_{td}$ (a) $k_{tc} = f\ k_t$ $f \leq 1$ (b) with (i) Fast m.t. of initiator and monomer ($10^{-3}ms^{-1}$) (ii) No m.t. of radicals (iii) Rate of chain transfer constant.
I	Assessing influence of change in rate of termination by chain transfer to monomer on molecular weight $k_{trm}^{j} = 10^{n}\ k_{trm}^{j}\|_{standard}$ (Section 5.2) with (i) Fast m.t. of initiator and monomer ($10^{-3}ms^{-1}$) (ii) No m.t. of radicals (iii) Rate of termination by combination and disproportionation constant.

Series	Aim of Experiment and Means of Achievement
K	Assessing influence of primary particle flocculation according to rule $N(x) = N_\infty + (N_O - N_\infty)e^{-\epsilon x}$ $N_O = F\ N_\infty$ with (i) Fast m.t. of initiator and monomer ($10^{-3}ms^{-1}$) (ii) Radical m.t.c. (monomer to basic particle or primary surface) $2 \times 10^{-7}ms^{-1}$ $n_\infty = 5 \times 10^{17}m^{-3}$ $F = 10,100$ $\epsilon = 0,1,10,30,50,70$
M	Effect of Variation in Initiator Distribution Coefficient (Monomer/basic particle or primary surface) coupled with initiator m.t.c. variation, with ($2 \times 10^{-7}ms^{-1}$) and without ($0ms^{-1}$) radical transfer, and with fast m.t. of monomer ($10^{-3}ms^{-1}$)

6.2.1 Mass Transfer Effects

In Chapter Three the formation of the various phases was discussed. Basic particles were postulated to grow upto critical sizes, arbitrarily chosen in the model to be ten molecular dimensions across, when they segregated into surface and bulk phases. Thereafter the relative strengths of mass transfer of species from monomer to surface, and from surface to bulk, determine what the proportions of surface and bulk will be.

For some values of k_{AI}, k_{AM} or $k_{A\sigma o}$ the polymerisations will exhibit kinetic control where mass transfer is unhindered. For other values they will be mass transfer limited. In between the extremes there will be a transition from kinetic to mass transfer control. Experimental evidence (eg 100 to 103) indicates that typical diffusion coefficients for molecules, such as VCM, diffusing through polymer (PVC) networks are of order $10^{-11}m^2s^{-1}$. Taking the mass transfer coefficient m.t.c. as $k_A = D/L$, where L is the diffusion pathlength, this value for D corresponds to a m.t.c. of $10^{-5}ms^{-1}$. (A diffusion pathlength of $10^{-6}m$ is chosen; this is the approximate size of a primary particle).

Mass transfer effects would therefore be most significant for values of k_A which were smaller than $10^{-3}ms^{-1}$.

Initiator Mass Transfer Limitations

In the series A experiments, when $k_{AI}{}^{67}$ decreased from $10^{-3}ms^{-1}$ to $10^{-15}ms^{-1}$, with $k_{AI}{}^{46}$ held constant at $10^{-3}ms^{-1}$, the time at which pressure drop conversion is reached increases only slightly from 257 to 262 minutes. However when $k_{AI}{}^{46}$ was decreased over the same range in series B, the time to pressure drop increased significantly from 257 minutes to in excess of 400 minutes. There is a clear transition from kinetically to diffusionally controlled polymerisation, with the transition occurring for m.t.c. in the range $10^{-9}ms^{-1}$ to $10^{-12}ms^{-1}$. Large decreases in autoacceleration are observed for m.t.c. smaller than $10^{-10}ms^{-1}$ (Figure 6.7). At low m.t.c.'s ($<10^{-10}ms^{-1}$) the upper

FIGURE 6.7 Initiator Mass Transfer Limitation : (i) Rate Profiles

Refer to appendix 6.1, series B.

Conditions for Fig 6.7: $[I_0]$ =1.413 molm^{-3} Perkadox-16, γ^{I}_{45}=1.538, T=50°C, $k_t=k_t$(Kuchanov)/4

Run no.	$k_{aI}^{4-5/6}$ (ms^{-1})
111	10^{-9}
112	10^{-10}
113	10^{-11}
114	10^{-12}

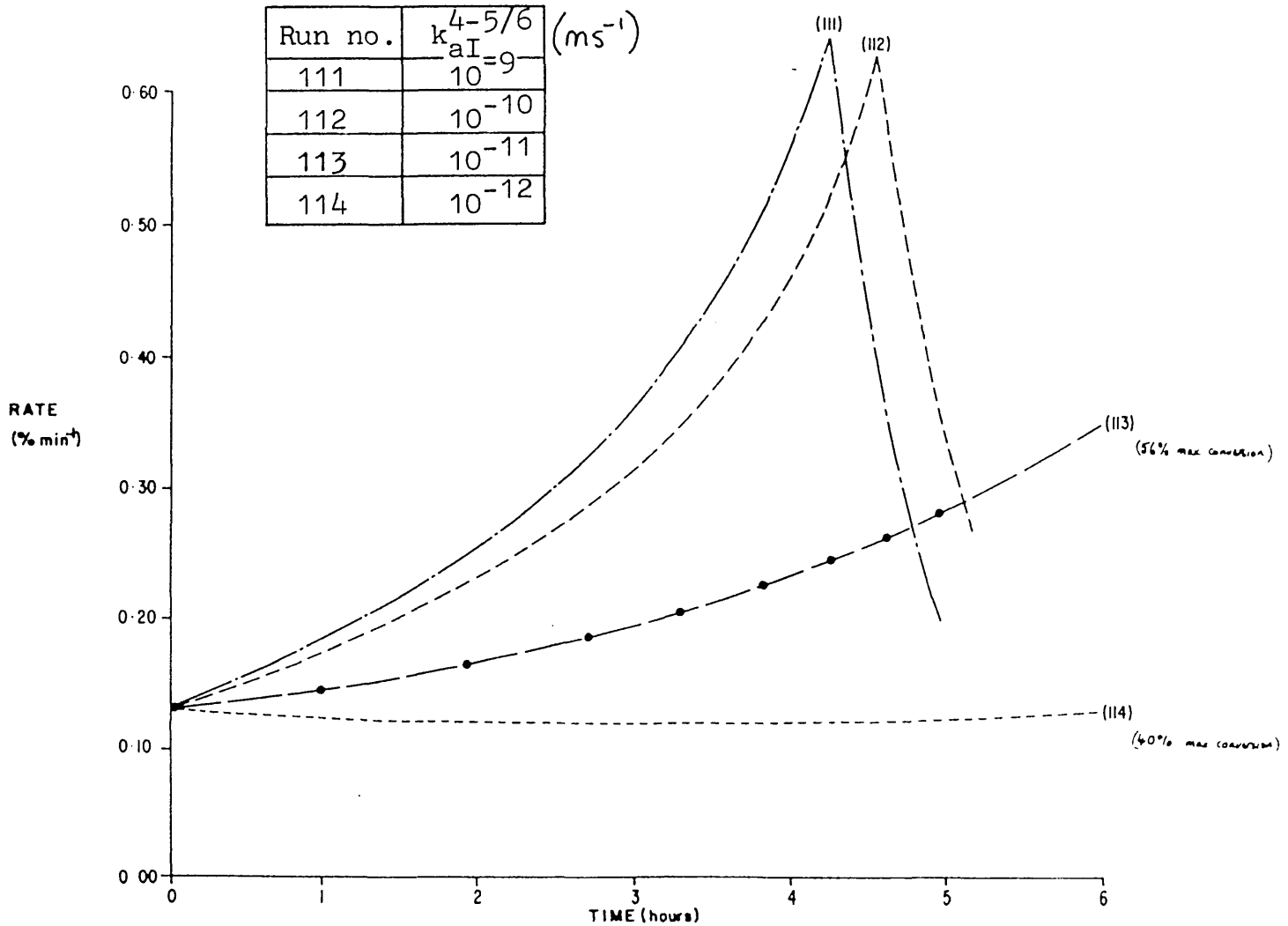

FIGURE 6.7 Initiator Mass Transfer Limitation : (ii) Concentration Profiles (Initiator)

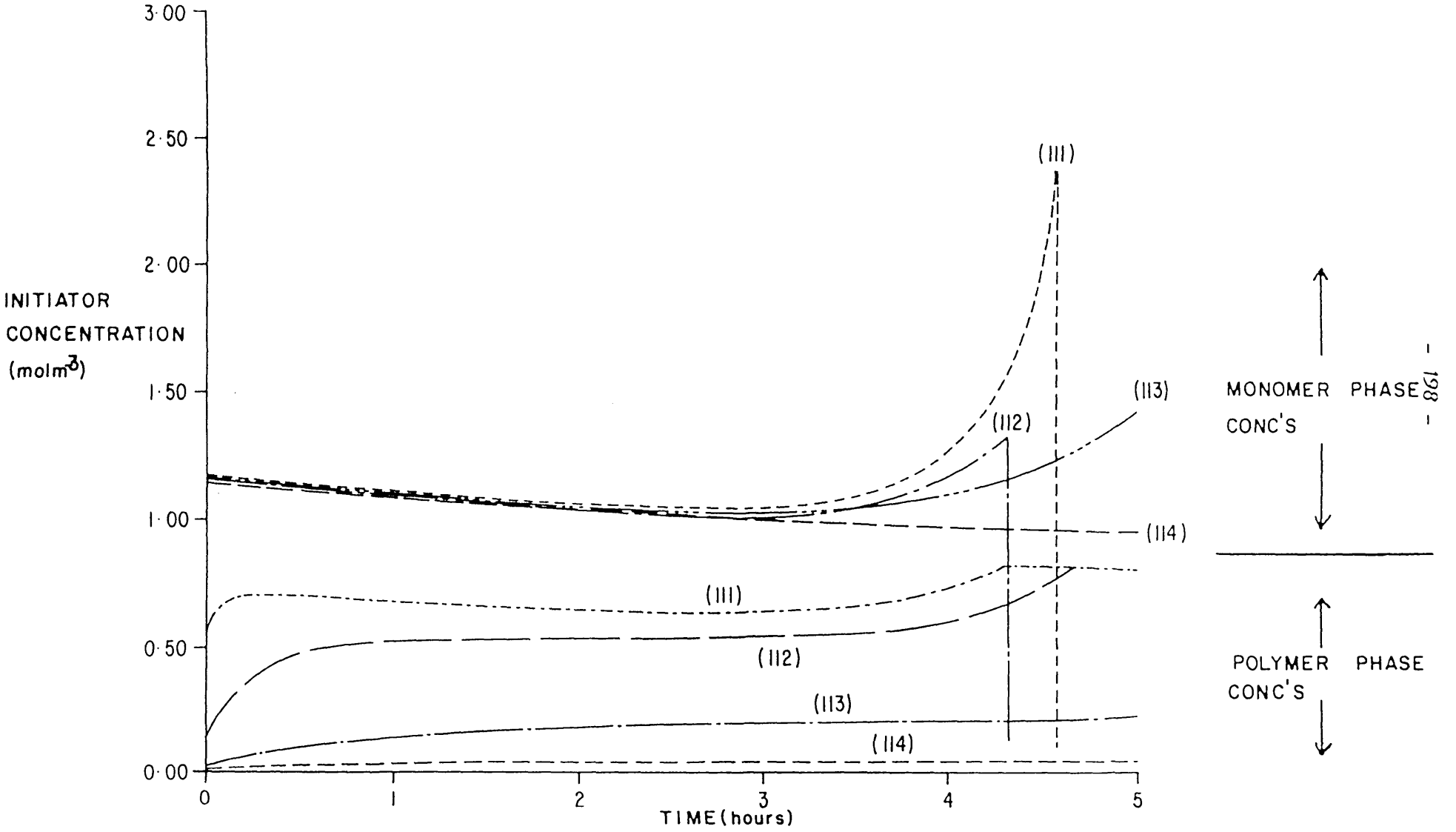

conversions were limited by imposed computer time limits: these curves typically took 600 cp seconds to compute.

In Figure 6.7(ii) it can be seen that changing $k_{AI}{}^{46}$ has a significant influence on both the time taken for the initiator to equilibrate and the level of equilibrium attained in the polymer phase. For curve 111, $k_{AI}{}^{46} = 10^{-9}ms^{-1}$, the reaction can be considered kinetically controlled, and the polymer phase equilibrates with the monomer phase after approximately ten minutes. With $k_{AI}{}^{46} = 10^{-10}ms^{-1}$, there is some mass transfer limitation and equilibration takes approximately an hour. The concentration of initiator in the polymer phase is now lower than its thermodynamics limit; the consumption rate of initiator in the polymer phase just exceeds its mass transfer rate from the monomer phase. With $k_{AI}{}^{46} = 10^{-11}$ or $10^{-12}ms^{-1}$ the rate of initiator mass transfer is so low that the polymer phase is effectively starved of initiator. Most of the polymerisation occurs in the monomer phase, and the exponential decay in initiator is seen in the concentration curve 114.

Diffusion limitation is thus demonstrated for initiator m.t.c.'s in the range $10^{-9}ms^{-1}$ to $10^{-12}ms^{-1}$, equivalent to maximum diffusion coefficients of $10^{-15}m^2s^{-1}$ to $10^{-18}m^2s^{-1}$. This corresponds to the maximum Thiele modulii ranging from ~0.79 to ~24.91 (the significance of this observation will be explained after diffusion limitations of monomer have been discussed).

Despite such a signficant effect on rate of polymerisation, diffusion limitation of initiator appears to have only a small effect on the ultimate molecular weight. Decreasing $k_{AI}{}^{46}$ from $10^{-9}ms^{-1}$ to $10^{-12}ms^{-1}$ decreases $\bar{\mu}_n$ from 875 to 850 (Appendix 6.1B). This is indicative of the strength of chain transfer; the ratio k_p/k_{trm} is 946.3 at 50°C. The topic of molecular weight is amplified in a later section (6.2.7).

6.2.2 Monomer Mass Transfer Limitation

The m.t.c.'s for monomer, $k_{AM}{}^{45}$ and $k_{AM}{}^{46}$ were similarly scanned over the range $10^{-3}ms^{-1}$ to $10^{-15}ms^{-1}$. As with initiator the transition from kinetic control to mass transfer controlled reaction occurred over the much more limited range $10^{-9}ms^{-1}$ to $10^{-12}ms^{-1}$ (Figure 6.8(i)). Taking $10^{-6}ms^{-1}$ as the maximum possible path length for diffusion in a primary particle, this range corresponds to maximum diffusion coefficients for $10^{-15}m^2s^{-1}$ to $10^{-18}m^2s^{-1}$.

In Figure 6.8(ii) for $k_{AM}{}^{46} = 10^{-9}ms^{-1}$ there is rapid equilibration for monomer to its thermodynamics limit, its solubility in the polymer gel phase, within ten minutes. As $k_{AM}{}^{46}$ decreases the time taken to equilibrate increases and the equilibrium concentration of monomer in the gel phase decreases from the thermodynamic limit. A 'dynamic' equilibrium exists with just sufficient monomer to maintain the polymerisation diffusing into the precipitated gel phase, but not enough to saturate the polymer phase. At very low $k_{AM}{}^{46}$ the precipitated phase is starved of monomer: polymerisation proceeds in the monomer phase and it eventually dies out (Figure 6.8(i)).

As with the reduction in $k_{AI}{}^{46}$, the reduction in $k_{AM}{}^{46}$ from $10^{-9}ms^{-1}$ to $10^{-12},s^{-1}$ has only a small effect on molecular weight; chain transfer to monomer principally determines molecular weight. There is a small decrease in $\bar{\mu}_n$ from 841.4 to 822.2 (Appendix 6.1C).

Initiator and Monomer Mass Transfer - The Thiele Modulus and Effectiveness Factor

The theoretical studies performed above indicate maximum credible diffusion coefficients for initiator and monomer mass transfer limitation of $10^{-15}m^2s^{-1}$: for larger diffusion coefficients than this, translational diffusion is not rate determining.

In the light of experimental evidence (100, 101, 102, 103) which shows typical values for diffusion coefficients for molecules moving

FIGURE 6.8 Monomer Mass Transfer Limitation : (i) Rate Profiles

Refer to appendix 6.1,series C.

Conditions for Fig 6.8: $[I_0]$ =1.413 molm^{-3} Perkadox-16, γ^{I}_{45}=1.538

T=50°C, k_t=k_t(Kuchanov)/4

Run no.	$k_{AM}^{4-5/6}$(ms^{-1})
120	10^{-9}
121	10^{-10}
122	10^{-11}
123	10^{-12}

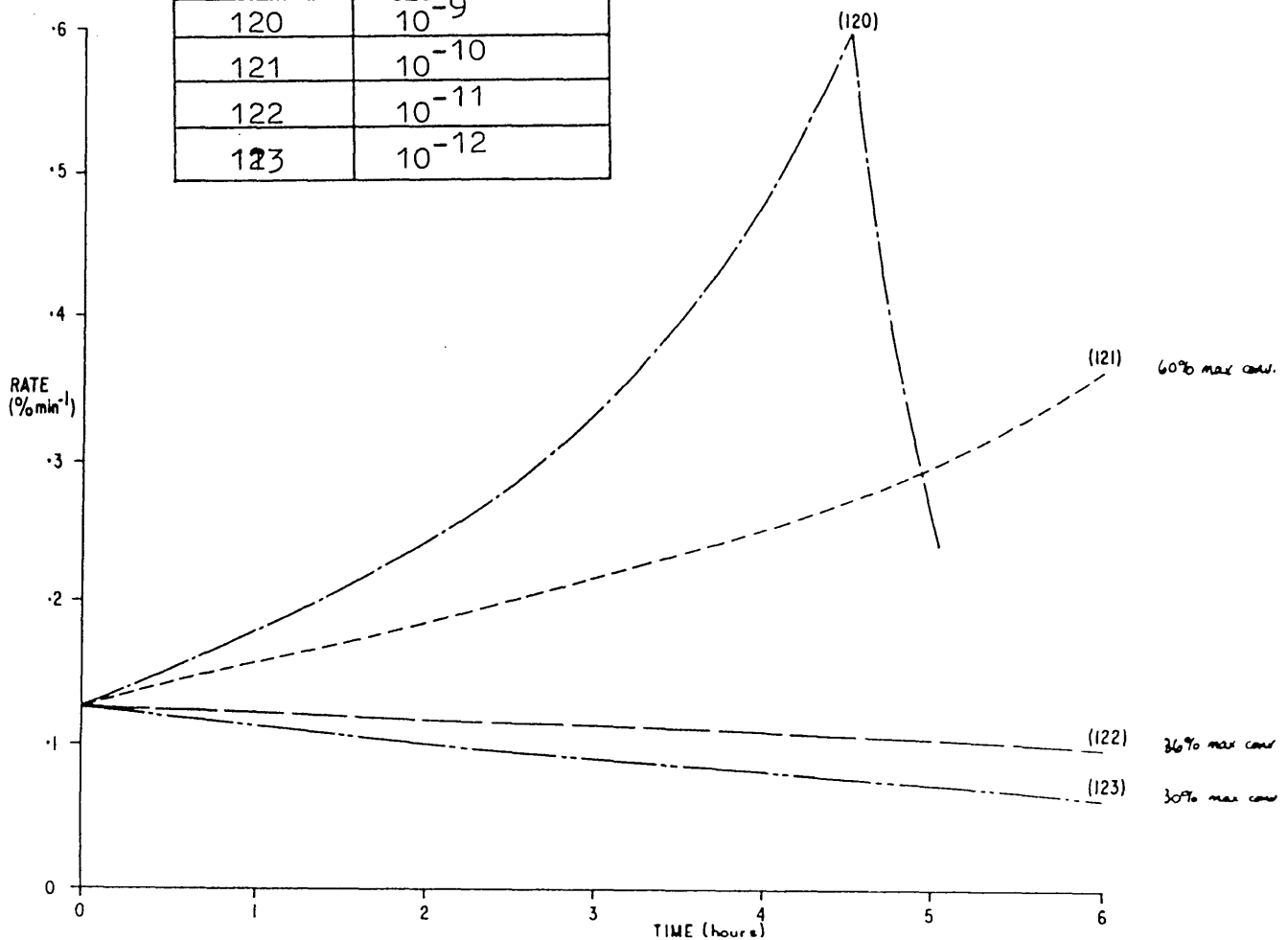

FIGURE 6.8 Monomer Mass Transfer Limitation : (ii) Concentration Profiles

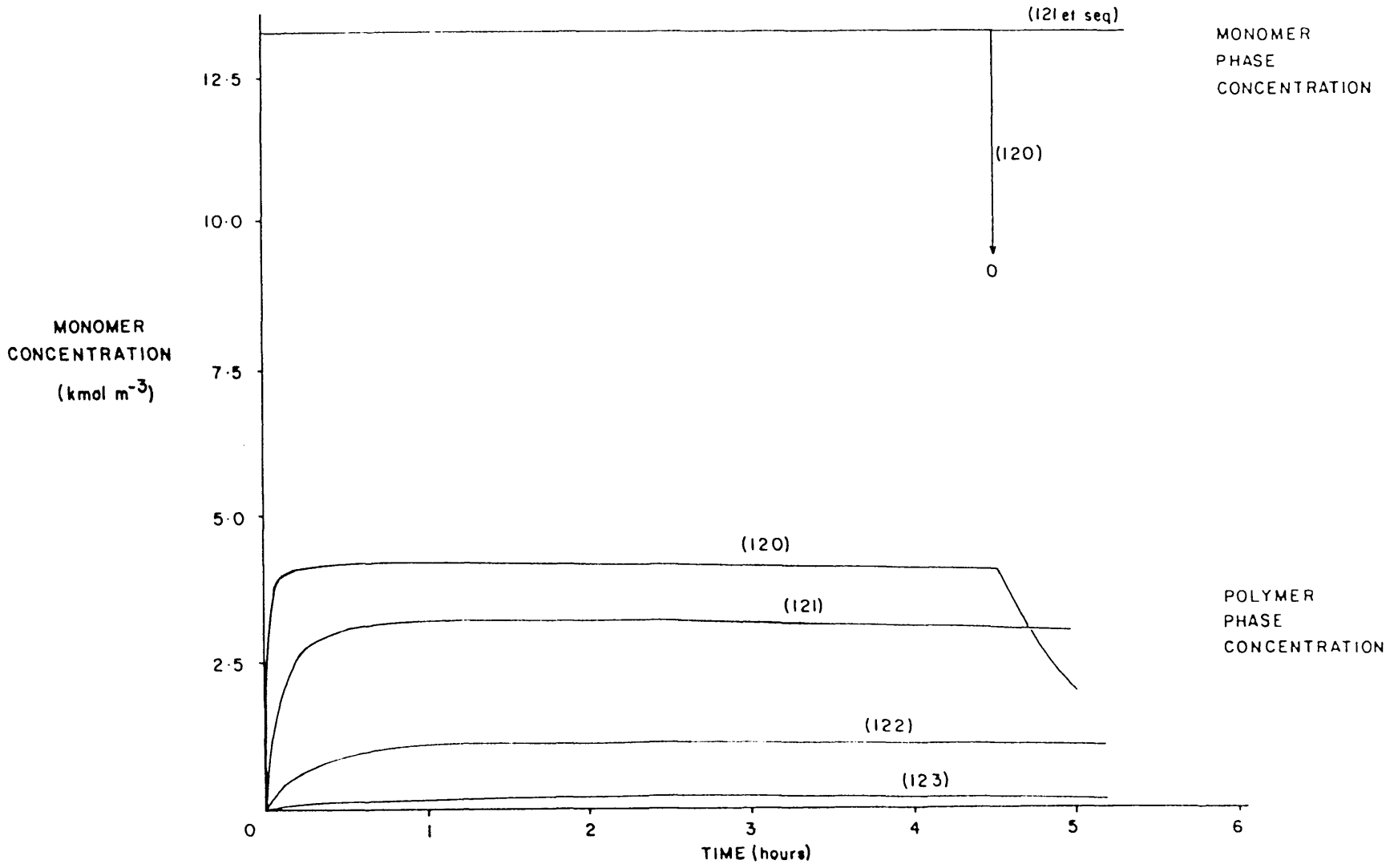

through polymer matrices, to be $\sim 10^{-11} m^2 s^{-1}$, it is highly unlikely that the rate of polymerisation will be limited by the mass transfer of initiator and monomer within the system.

The Thiele modulus and effectiveness factor for monomer support this conclusion. The effectiveness factor is used to characterise the reduction in the expected rate because of the diffusion resistance of a reactant. It is defined as:

$$\eta = \frac{\text{observed rate}}{\text{expected rate}} \qquad (6.16)$$

For a first order reaction ($A \xrightarrow{k} B$) with reactant, A, diffusing through a spherical particle, of radius R, to the locus of reaction, it can be shown (55) that:

$$\eta = \frac{1}{3\theta^2} (3\theta.\coth 3\theta - 1) \qquad (6.17)$$

where θ is the (dimensionless) Thiele modulus. The magnitude of the Thiele modulus indicates the relative strengths of the kinetic and diffusional processes:

$$\theta = \left[\frac{k}{D}\right]^{1/2} . R = \left[\frac{Rk}{k_A}\right]^{1/2} \qquad (6.18)$$

When θ is small (~ 0.3), $\eta \simeq 1.0$ and the reaction does not exhibit any diffusional limitation. For $\theta > \sim 3$, $\eta = 1/\theta$ and the reaction exhibits increasing diffusional limitation.

Based on the rate parameters used in this study and an experimental value for D, the mass transfer limitation of monomer seems unlikely. This can be shown, independently of the model calculations presented earlier, with the Thiele modulus.

In Chapter 3 the rate of polymerisation per unit volume was shown to be:

$$R_p = k_p [M] [\sigma_o] \qquad (6.19)$$

and in Section 5.3, for the analytic model,

$$[\sigma_o] = \left[\frac{2fk_D}{k_t}\right]^{1/2} [I]^{1/2} \qquad (6.20)$$

Thus, a pseudo first order reaction constant for monomer consumption can be defined as:-

$$k' = k_p \left[\frac{2fk_D}{k_t}\right]^{1/2} [I]^{1/2} \qquad (6.21)$$

Substituting k_p, $k_{ts/4}$, f and k_D from Section 5.2 yields

$$k' = 3.9362 \times 10^8 \exp\left[\frac{-72977.6}{RT}\right].[I]^{1/2} \qquad (6.22)$$

Since, in sorption experiments, Berens (104) obtained a diffusion coefficient for VCM diffusing through unswollen PVC of:

$$D = 4.0728 \exp\left[\frac{-71,000}{RT}\right] m^2s^{-1} \qquad (6.23)$$

The Thiele modulus for monomer with $R = 10^{-6}m$ is expected to be:

$$\theta_M = 9830 \times 10^{-3} [I]^{1/4} \exp(-988.8/RT) \qquad (6.24)$$

With the concentration of initiator being approximately 1 $molm^{-3}$ (Figure 6.7(ii)) θ takes the value $\sim 7.0 \times 10^{-3}$ over the range 50°C to 70°C. Hence the Thiele modulus for monomer is always less than 0.3: the rate of polymerisation will not be mass transfer limited for monomer.

If θ_M is defined as $(k'R/k_A)^{1/2}$, $k_{AM} = 10^{-9}ms^{-1}$ corresponds to a maximum θ_M of .79 while for $k_{AM} = 10^{-12}$, $\theta_M = 24.9$. The observed transition in rate behaviour is thus supported independently by the Thiele modulus. So although the values of k_{AM} are unrealistically small, the validity of the model in its treatment of mass transfer is confirmed.

In precisely the same way as θ_M was defined for monomer θ_I could be defined for initiator, however no values of D_I appear in the

literature. Based on the studies outlined above, qualitatively similar results would be expected for initiator, despite the probability that $D_I > D_M$ (initiator molecules usually have higher molecular weights and therefore lower mobilities than VCM molecules).

6.2.3 Initiator and Monomer Mass Transfer - Concluding Remarks

On the basis of the evidence produced by the model it appears that on the time scale of interest both these species will be freely mobile throughout the continuous monomer and the precipitated polymer phases. Their concentrations will be determined by the thermodynamic solubilities in the polymer.

Thus for the first time, this model rigorously justifies the starting assumption of many other models (15, 37, 39, 41, 43) that initiator and monomer can diffuse freely within the system.

After 'pressure drop' the assumption may need tightening up; when the gel phase becomes more and more solid like, the mobility, D, may indeed be decreased and mass transfer is consequently slightly limited. Qualitatively this effect is already observed because of the reduced rate of mass transfer due to the lower gel phase monomer concentrations. However a decrease in D over six orders of magnitude would be necessary to take θ form 7.0×10^{-3} to >3. This is highly improbable.

6.2.4 The Mass Transfer of Radicals

The analytic model assumed that radicals grew rapidly and terminated in the phase in which they were initiated; $k_{A\sigma i}{}^{45}$ and $k_{A\sigma i}{}^{46}$ were therefore taken to be zero. When mass transfer of radicals takes place, the rate profile is critically dependent on the values for $k_{A\sigma i}$.

In Figure 6.9(i) the rate profiles are shown for a range of values of $k_{A\sigma i}$ from $10^{-3}m^2s^{-1}$ to $10^{-9}m^2s^{-1}$ (corresponding to maximum

FIGURE 6.9 Radical Mass Transfer Limitation : (i) Rate Profiles

Refer to appendix 6.1, series F

T, $[I_0]$, γ^I_{45} as Fig. 6.8

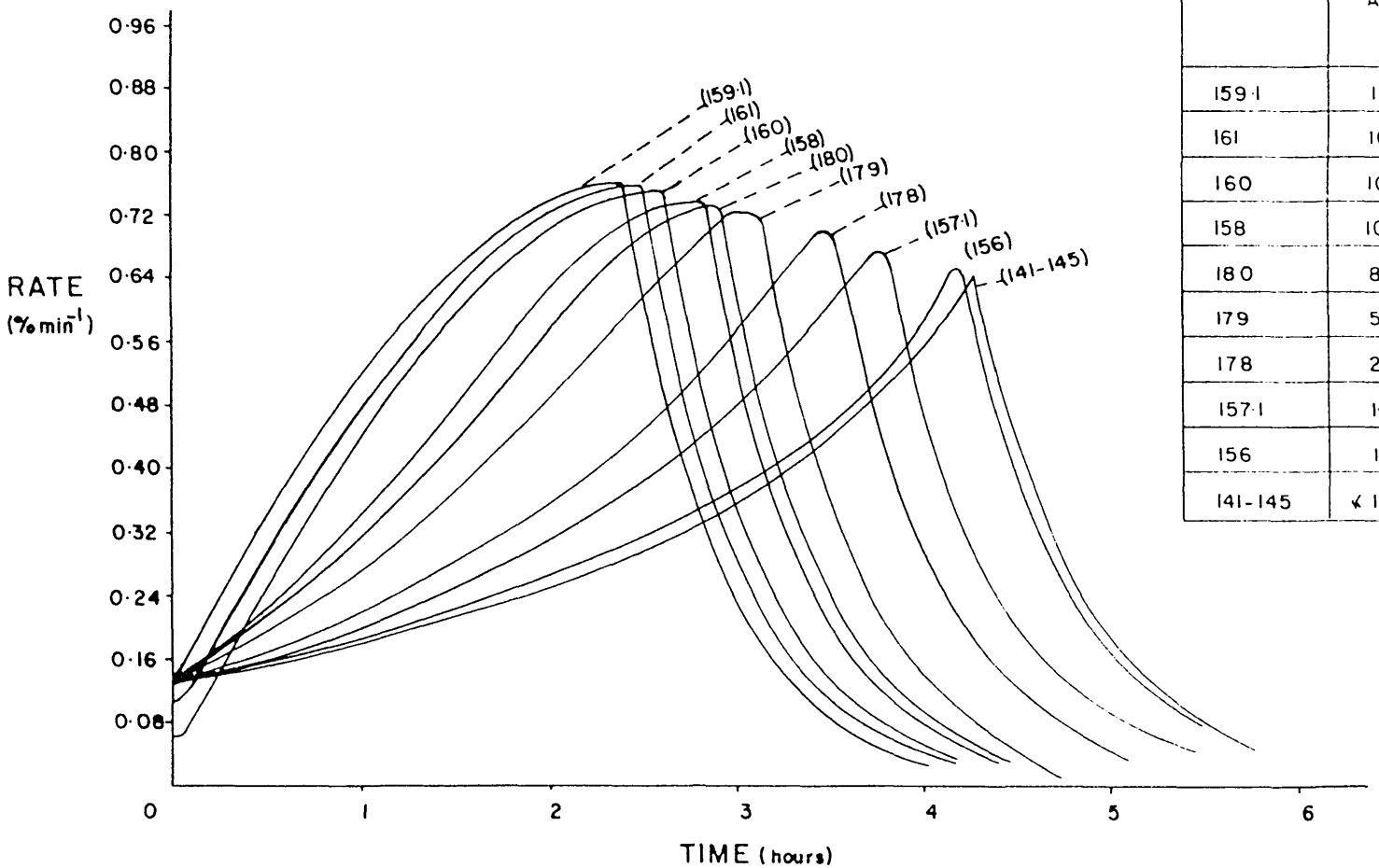

Run No.	$k^{45}_{Ao.}$, $k^{46}_{Ao.}$ (ms^{-1})
159·1	10^{-3}
161	10^{-4}
160	10^{-5}
158	10^{-6}
180	8×10^{-7}
179	5×10^{-7}
178	2×10^{-7}
157·1	10^{-7}
156	10^{-8}
141-145	$\leq 10^{-9}$

FIGURE 6.9 Radical Mass Transfer Limitation : (ii) Radical Concentration Profiles

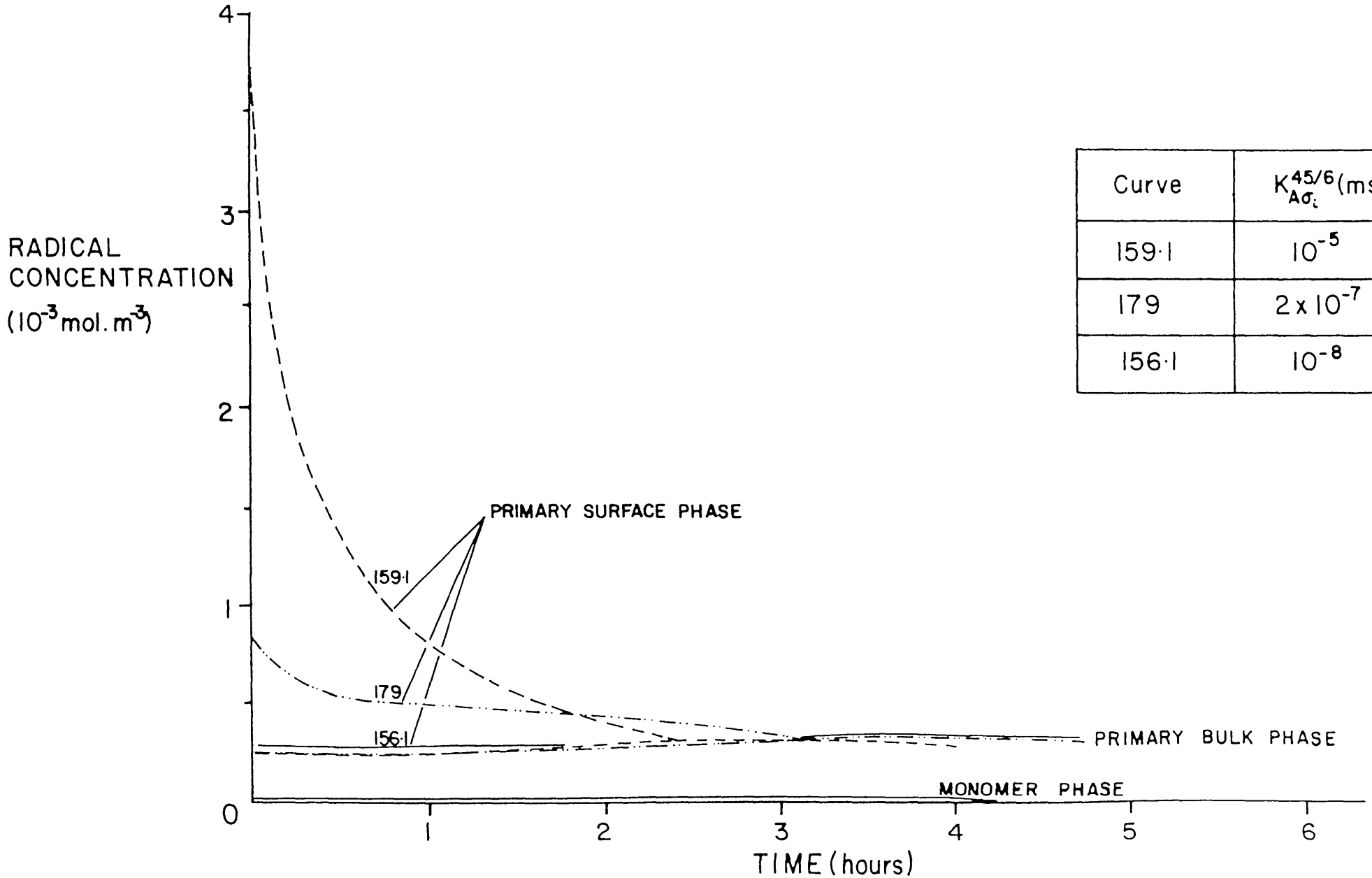

Curve	$K_{A\sigma_i}^{45/6}$ (ms^{-1})
159·1	10^{-5}
179	2×10^{-7}
156·1	10^{-8}

FIGURE 6.9 Radical Mass Transfer Limitation : (iii)Fractional Rate as a function of Time

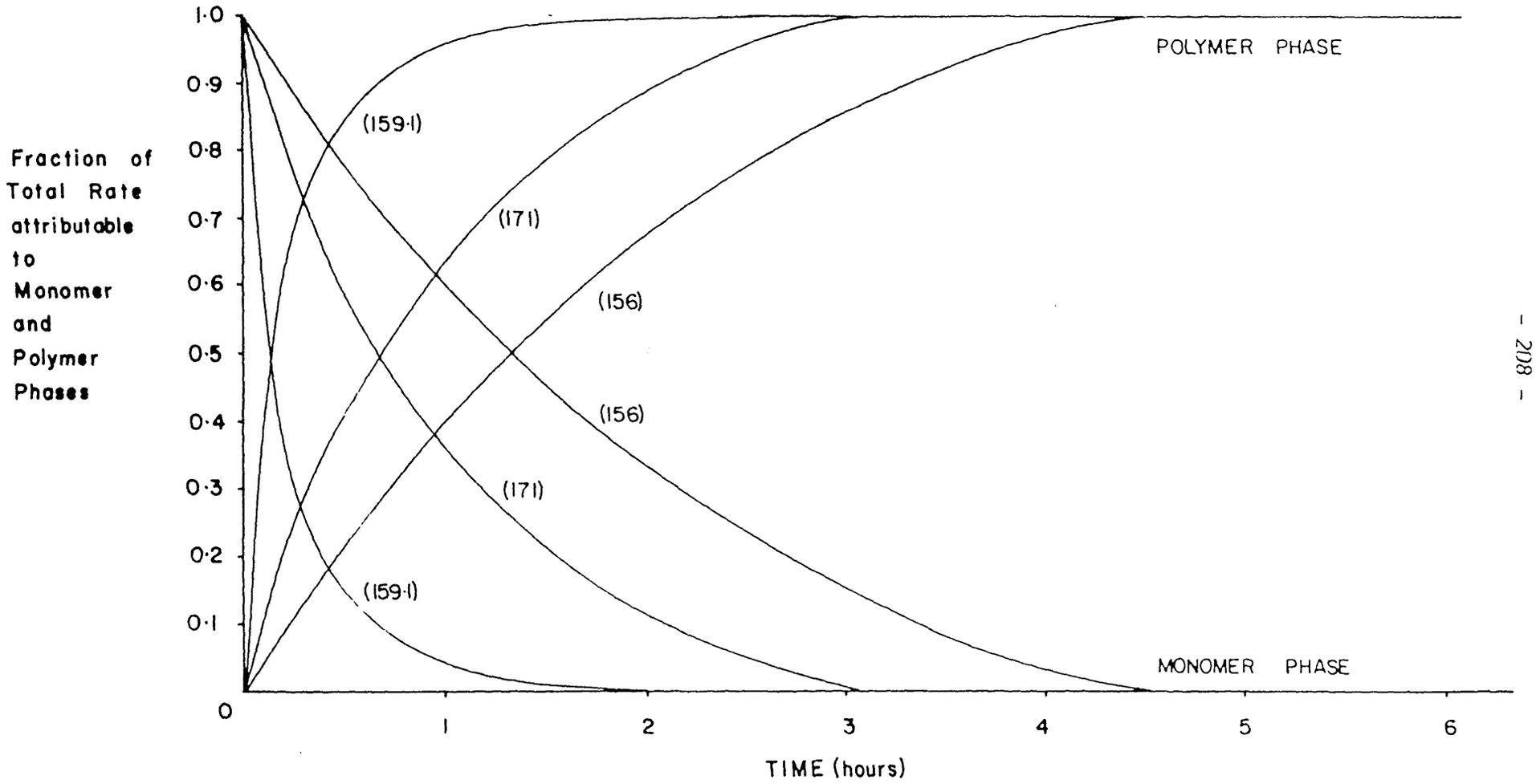

$D_{\sigma i}$ in a 1 micron particle of $10^{-9}m^2s^{-2}$ and $10^{-17}m^2s^{-2}$ respectively). With effectively no radical transfer, at $k_{A\sigma i} = 10^{-9}ms^{-1}$ and lower, the rate profiles are as predicted by the analytic model. Rate is proportional to conversion. γ_I, f_5/f_4, k_{t5}/k_{t4} all significantly affect the rate profile behaviour as predicted by equation 5.58. The rate profiles for $k_{A\sigma i} \simeq 0$ continuously accelerate to a maximum 'peak' rate.

Conversely at high radical mass transfer rates, $k_{A\sigma i} = 10^{-3}ms^{-1}$, the radicals initiated in the monomer phase are rapidly absorbed into the gel phase. As Figure 6.9(iii) shows most of the growth takes place in the gel phase from an early stage. Greater than 80% of the rate after 20 minutes is attributable to the gel phase, which also has a much higher surface phase concentration of radicals. In Figure 6.9(ii) the radical concentrations in the various phases can be seen for different values of $k_{A\sigma i}$. The first feature of note is that in comparison to initiator and monomer concentrations of ~1 $molm^{-3}$ and between 4500 and 13700 $molm^{-3}$ respectively, the values are small (on the whole must less than 4×10^{-3} $molm^{-3}$). This reflects their short lifetime. The second feature of note is that monomer phase radical concentrations are much lower, almost negligible, in comparison with gel phase concentrations. This is due to the lower termination rate in the gel phase and the consequent increased lifetime of radicals there. At high values of $k_{A\sigma i}$, although radicals are initiated in the monomer phase their rapid adsorption into the gel phase means that termination is in that phase. Because of the lower termination rates there, radical lifetimes are increased and therefore concentrations of radicals are much higher in the gel phase, as shown in Figure 6.3(ii). The change in the nature of the gel phase and its contribution to the polymerising system is reflected in the rate profiles, Figure 6.9(i). For $k_{A\sigma i} = 10^{-3}ms^{-1}$, the low initial rate rises sharply as the gel phase develops and levels out as the maximum attainable rate is achieved. Instead of d^2x/dt^2 continuously increasing to the peak rate, it now decreases on the final approach to the maximum rate.

In between the extremes in value of $k_{A\sigma i}$, there is a transition in the shape of the rate profiles from 'peaky' (for low $k_{A\sigma i}$) to

'rounded' (for high $k_{A\sigma i}$).

The benefit of a series of curves like those in Figure 6.9 is that it allows the instant comparison of experimental results in a qualitative manner. For example the first curve in Appendix 6.2 shows observed process variables for a pilot plant scale polymerisation of VC. It is clearly less 'peaky' than the second curve which shows the observed rate profile on a production scale autoclave. Although such differences may reflect the nature of the control system and small differences in the process recipe, the first profile seems indicative of a high value in $k_{A\sigma i}$.

Returning to model predictions, it is surprising to observe that the transition from kinetic to diffusion controlled reaction takes place for $k_{A\sigma i}$ in the range $10^{-3}ms^{-1}$ to $10^{-9}ms^{-1}$ ($10^{-9}m^2s^{-1} > D_{\sigma i}|_{max} > 10^{-17}m^2s^{-1}$). This is six orders of magnitude compared with the range of three orders needed for the same transition with monomer and initiator. From a consideration of the Thiele modulus, defined as $\theta_{\sigma i} = (k_p[M].R/k_{A\sigma i})^{1/2}$, the transition is expected for $k_{A\sigma i}|_{max}$ for $8.5 \times 10^{-2}ms^{-1}$ to $8.5 \times 10^{-4}ms^{-1}$ corresponding to $\theta_{\sigma i} = .3$ (kinetic control) and $\theta_{\sigma i} = 3$ (diffusion control). The sensitivity of the model to $k_{A\sigma i}$ reflects the contribution that the radical population makes to the kinetics. In Figure 6.9(ii) typical radical concentrations are $10^{-3}molm^{-3}$, which compares with concentrations for monomer and initiator of 10^3 to 10^4 and 10^0molm^{-3} respectively. Their reactive nature ensure their short lifetime and small instantaneous concentrations in the precipitated polymer phase. Any slight absolute change in the gel phase radical population with its intrinsically faster rate is bound to have an amplified effect on the rate profile. Since the $k_{A\sigma i}$ in the middle of the observed transition range corresponds to $D_{\sigma i}|_{max} \cong 10^{-12}m^2s^{-1}$ - the size of a realistic diffusion coefficient in a polymer gel - the likelihood of radical mass transfer limited reaction is indeed much much higher than it is for monomer and initiator.

This is an important conclusion based on the models predictions. Not only does it confirm the views of Bort, Cotman et al and Ugelstad et al who all believe in its contribution but it imposes doubt on the conclusions of Hamielec (107) who dismissed the contribution made

by the diffusion of radicals solely on an order of magnitude basis.

Indeed the whole question of radical (translational) diffusion is currently provoking widespread debate. At a recent conference (104) one of the main points of discussion was the role of radical diffusion and its contribution to polymerisation kinetics. As has been shown with this model for PVC, a theoretical basis can be demonstrated for its contribution in both styrene and methyl methacrylate polymerisation (104). The problem however is to design experiments which uniquely measure the translational diffusion coefficient for radicals. It would be the results of this experiment which conclusively proved the existence of radical translational diffusion.

6.2.5 Initiator Distribution and Radical Mass Transfer

Figure 6.10 shows the interaction between initiator distribution and radical mass transfer. The two groups of curves are for a range of $\gamma_{4s}{}^{I}$ with and without radical mass transfer. With some radical mass transfer the effects due to initiator (ie the different γ^{I}) are preserved in the manner discussed in Section 6.1.3, although the overall rate of reaction is slightly higher. The significant difference however is in the shape of the peak at the maximum rate: instead of the 'peaky' curve as would be predicted by the analytic model there is a gradual transition through the maximum rate as the polymerisation proceeds to its final homogeneous gel phase stage.

6.2.6 Influence of Morphological Development

For all the previous results primary particle numbers were kept constant at $5 \times 10^{17} m^{-3}$. When N is made to decrease with x according to the primary particle population equations 5.1 and 5.2 with $k_{A\sigma i}{}^{45} = 2 \times 10^{-7} ms^{-1}$ ($D_{\sigma i}|_{max} \cong 2 \times 10^{-13} m^2 s^{-2}$) there are some significant changes in observed rate behaviour, as shown in Figure 6.11. With no effective flocculation, $\epsilon = 0$, high surface areas are preserved throughout the reaction and the overall rate is higher. At high flocculation rates, corresponding to $\epsilon = 70$, the rapid loss of

FIGURE 6.10 The effect of changing initiator distribution coefficients and radical mass transfer coefficients on the polymerisation rate.

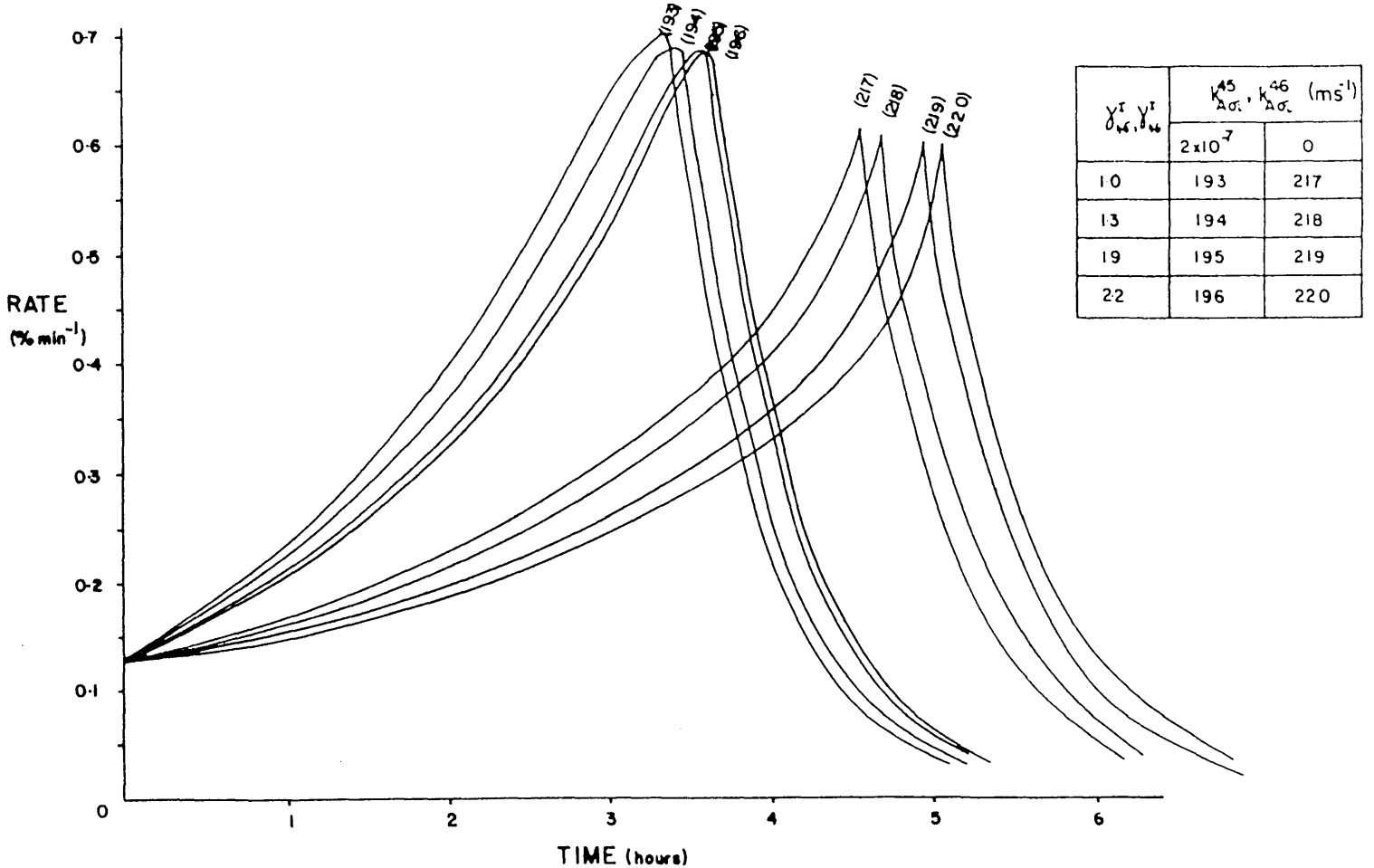

$\gamma^I_{45}, \gamma^I_{46}$	$k^{45}_{\Delta\sigma_c}, k^{46}_{\Delta\sigma_c}$ (ms⁻¹)	
	2×10^{-7}	0
10	193	217
13	194	218
19	195	219
22	196	220

FIGURE 6.11 The effect of changing primary particle flocculation rate on the rate of vinyl chloride polymerisation.
T, $[I_0]$, γ^{I}_{45} as Fig. 6.8

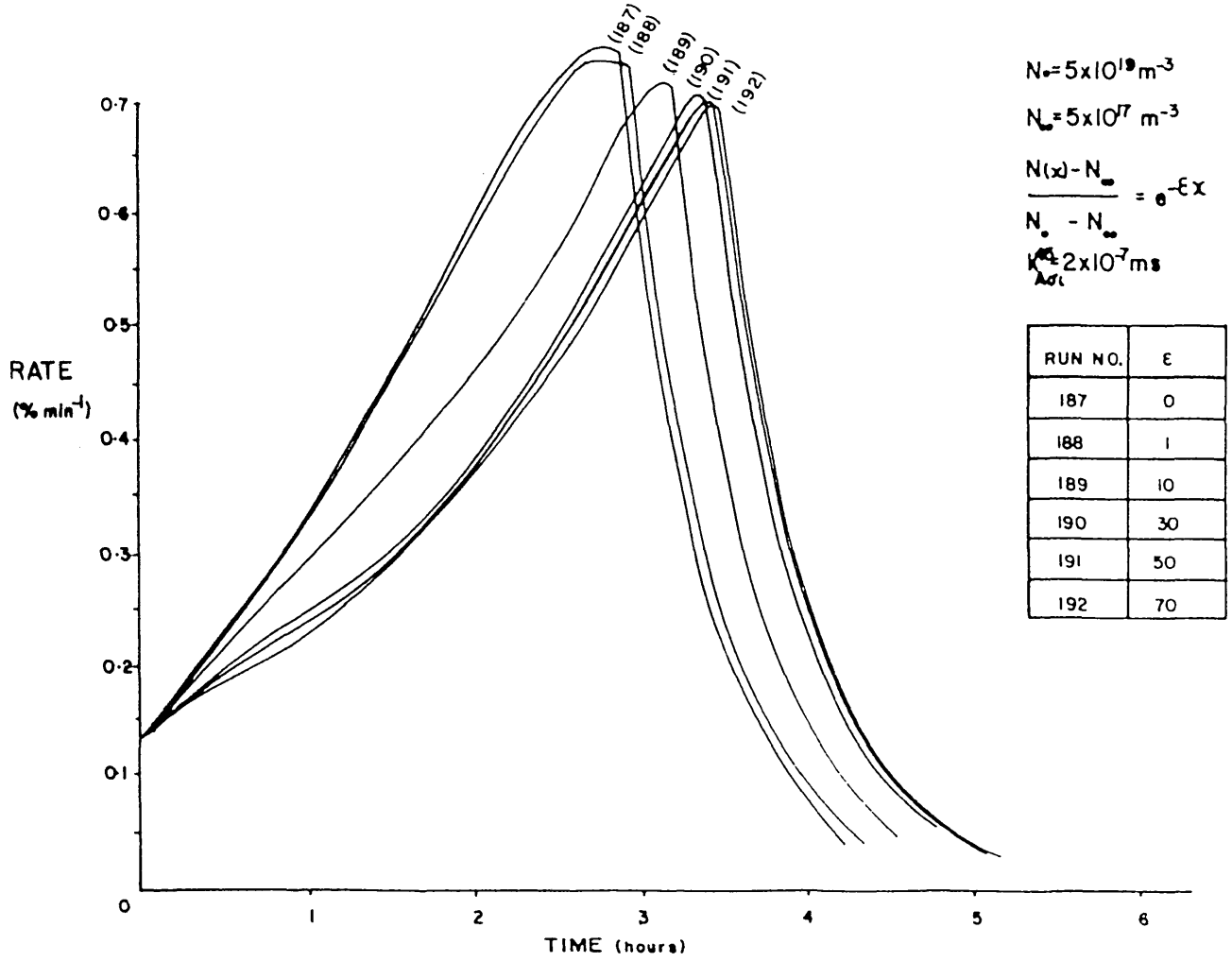

RUN NO.	ε
187	0
188	1
189	10
190	30
191	50
192	70

interphase area in the earliest stages of reaction gives rise to some diffusion limitation in reaction. This is manifested as a lower rate with a tendency to inflect towards a plateau in rate at lower conversions: a plateau is not achieved in practice. There is the expected transition between these extremes in behaviour. As can be seen from Table 6.4, the proportional change in rate for deviations away from values of ϵ, observed in practice, does not exceed ±10%.

TABLE 6.4

FLOCCULATION RATE: THE TIME TAKEN TO REACH PRESSURE DROP

(i) Observed Flocculation Rates

T/K	ϵ_{obs} (Eq5.2)
323	5.02
328	6.07
333	7.30
338	8.73
343	10.39

(ii) Time taken to reach pressure drop at 323K

(Appendix 6.1K)

ϵ_{theory}	t_{pd}/mins	Deviation from ϵ = 10/%*
0	174	- 9.38
1	176	- 8.33
10	192	0
30	206	+ 7.29
50	210	+ 9.38
70	211	+ 9.90

* ϵ = 10 is taken as an approximation to ϵ_{obs}.

The development of morphology clearly does not affect the chemical kinetics as strongly as the relative termination rates in the monomer and gel phase or the nature, distribution and amount of initiator do. It is however significant in influencing rate profile because of its effect on radical mass transfer rate.

6.2.7 Prediction of Molecular Weight

Although some of the predictions of molecular weight have been discussed briefly in Section 6.2.1 to 6.2.6, it is convenient to consolidate them in one section with the other results pertinent to the prediction of molecular weight.

When mass transfer of initiator, monomer and radicals was discussed in those sections, the number average chain length, μ_n, was found to be relatively insensitive to the value of k_A. Table 6.5 summarises how μ_n is affected by k_A.

TABLE 6.5

MOLECULAR WEIGHT AND MASS TRANSFER

T = 50°C

Experimental Series	Parameter Varied	From	To	Change in μ_n(x = 100%)		
				From	To	Proportion (%)
B	$k_{AI}^{45}, k_{AI}^{46}(ms^{-1})$	10^{-7}	10^{-15}	875	850	- 2.86
C	$k_{AM}^{45}, k_{AM}^{46}(ms^{-1})$	10^{-7}	10^{-15}	841.4	822.1	- 2.29
F	$k_{A\sigma i}^{45}, k_{A\sigma i}^{46}(ms^{-1})$	10^{-3}	10^{-13}	903.1	892.6	- 1.16
M	$\gamma_I^{45}, \gamma_I^{46}$	1.0	2.2	894.9	893.9	- 0.11

The insensitivity stems from the dominance of chain transfer to monomer as the terminating step. It is easily shown that for the values of k_p and k_{trm} given in Section 5.3, the ratio $1/C_M = k_p/k_{trm}$ takes the value 946.3 at 50°C. This is the maximum attainable chain length when chain transfer to monomer is the only terminating mechanism for radicals. Indeed, the dominance of chain transfer to monomer is further confirmed by the values of Z_p (Appendix 6.1) which remain remarkably close to 2.0 for all the cases summarised in Table 6.5. In series H and I experiments, the dominance of chain transfer is specifically tested.

In series H, the proportion of termination due to combination was altered from 0 to 100% while the proportion due disproportionation was correspondingly decreased from 100% to 0. k_{trm} was held constant for these runs. Despite such a significant change in the relative strengths of termination, μ_n only increases from 883 to 908, ie only a 2% difference.

In series I, the value of k_{trm} was changed. The effects on μ_n, μ_w and Z_p are shown in Figure 6.13. k_{trm} was reduced from ten times its base value (Section 5.3) to a one thousandth of its base value. Whereas there is little effect on the overall rate (t_{pd} remains at 257 to 258 minutes because k_p is much greater than k_{trm}) μ_n and μ_w are significantly altered. For the base case, μ_n and μ_w increase slightly with conversion, in qualitative but not quantitative agreement with experiment, and Z_p stays remarkably close to 2.0 - again in agreement with experiment. With k_{trm} much smaller than its base case not only are μ_n and μ_w increased, but their conversion dependence is also magnified. Z_p also increases above 2.0 to maximum values of 3.3 and 5.7 (for $k_{trm}/100$ and $k_{trm}/1000$ respectively) at 77% conversion when all the monomer phase has been consumed: thereafter it falls away as initiator and monomer are consumed in the polymer phase. Both the increasing breadth of the distribution and greater conversion dependence of average molecular weight indicate significant shifts away from chain transfer to monomer as the dominant mode of chain termination.

Although the conversion dependence of μ_n and μ_w are more clearly

FIGURE 6.12 The effect of reducing the rate of termination by chain transfer to monomer on the molecular chain length : Base Case.
Run no. 102, parameters as table 5.3, $k_t = k_t$(Kuchanov)/4

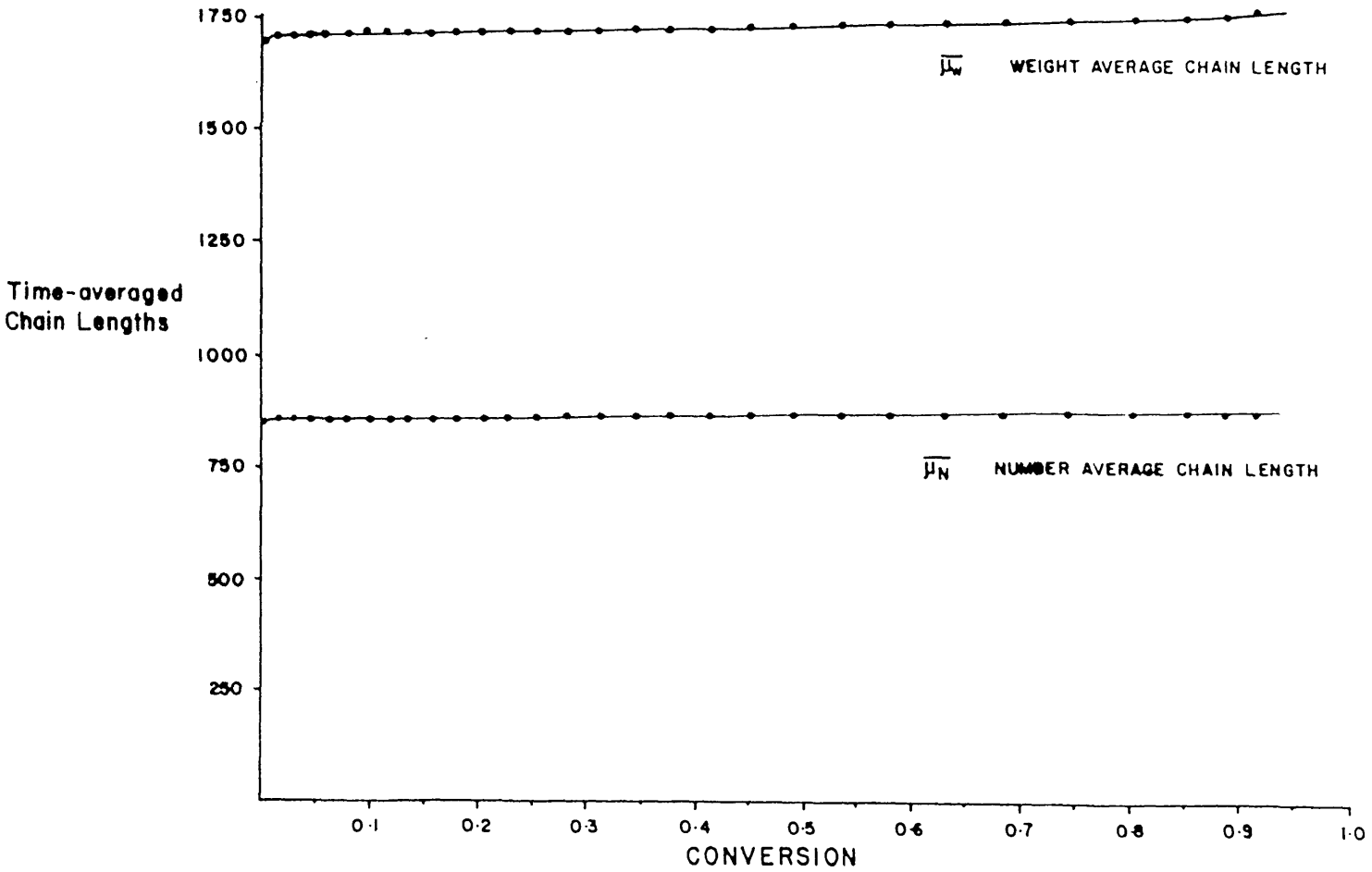

FIGURE 6.13 The effect of reducing the rate of termination by chain transfer to monomer on the molecular chain length.
(i) Time-averaged chain lengths.

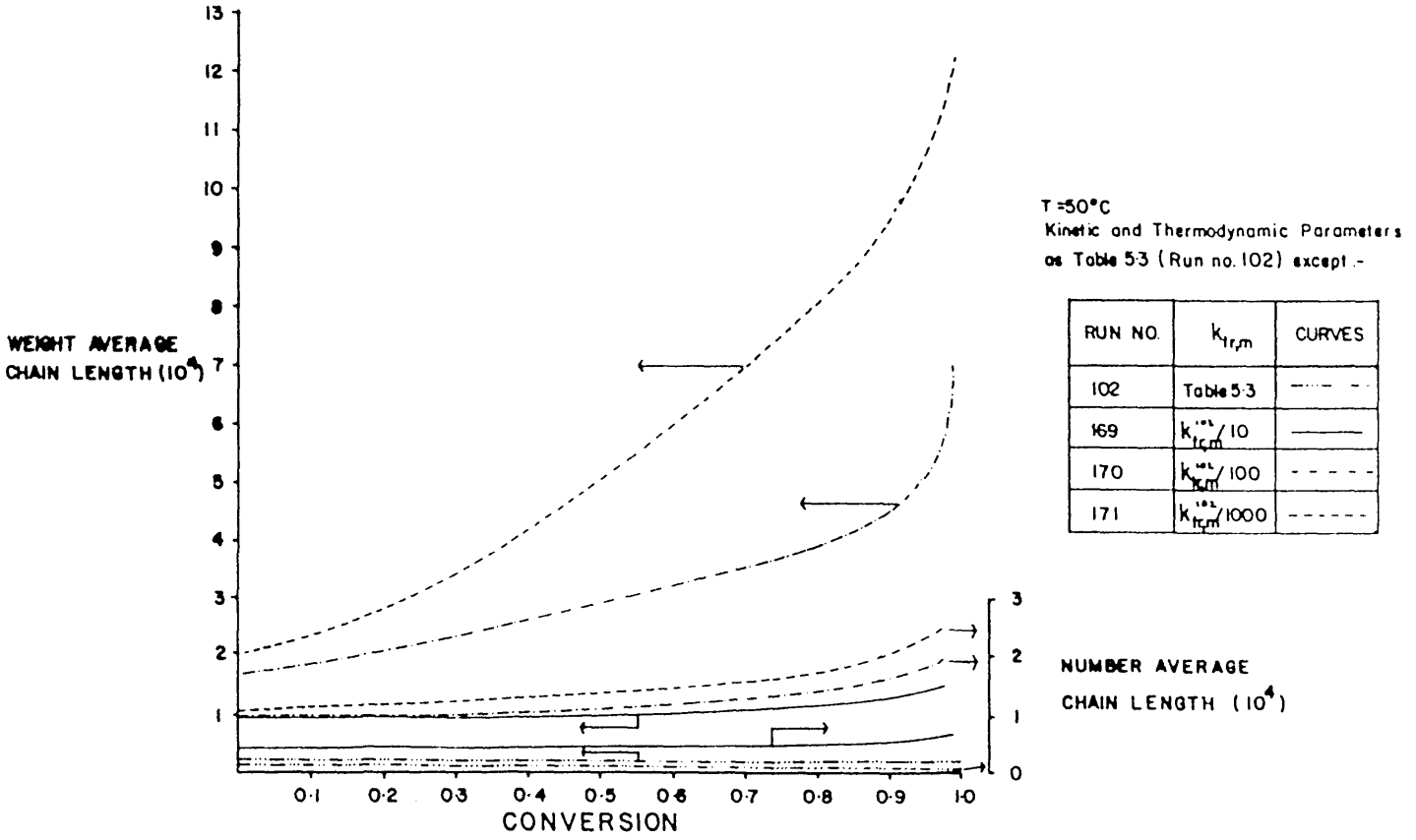

FIGURE 6.13 The effect of reducing the rate of termination by chain transfer to monomer on the molecular chain length.
(ii) Polydispersity

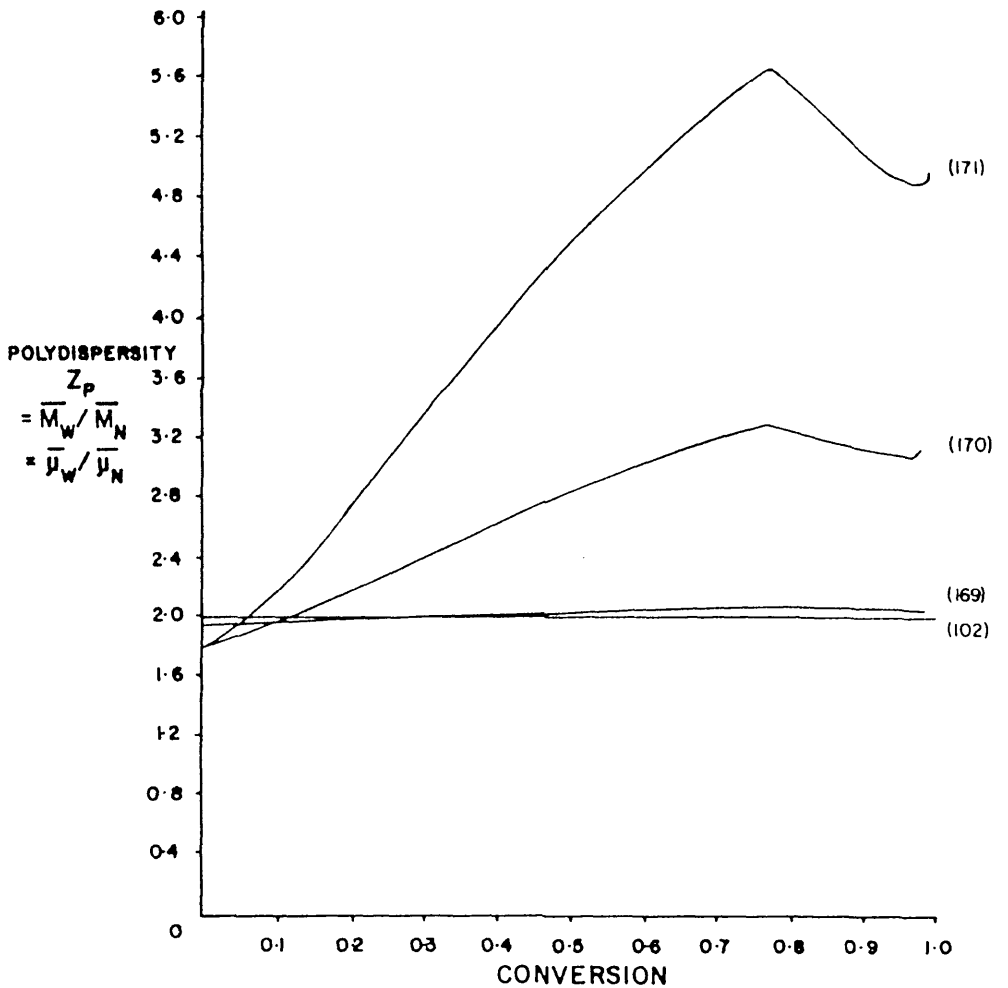

seen with lower values of k_{trm}, their absolute values no longer correspond to experiment. When k_{trm} is reduced by a factor of 10, $\bar{\mu}_n$ is increased by a roughly equivalent factor. In practical terms, the ratio k_p/k_{trm} determines $\bar{\mu}_n$. Therefore if $\bar{\mu}_n$ is to be accurately predicted it is most important to determine this ratio accurately. In Table 6.6, the chain transfer coefficients, C_M, reported by Abdel-Alim and Hamielec (44) and Kuchanov and Bort (45) are compared with those calculated from data of Smallwood (86). Regression of his data showed C_M to be equal to $3.0925 \times 10^{-2} \exp(-21731/RT)$. Note that $C_M^{-1} \simeq \bar{\mu}_n$.

Using Kuchanov's value for k_{trm} in the model yielded a rise in $\bar{\mu}_n$ of only 3% at 100% conversion from an initial value of $\bar{\mu}_n = 875$, at 50°C. Abdel-Alim, however, measured a 16% increase in $\bar{\mu}_n$ from an initial value of 720 at zero conversion and 50°C, whereas Smallwood reports $\bar{\mu}_n$ increasing by between 11 and 15% as conversion increases from 20% to 80% at similar temperatures.

TABLE 6.6

CHAIN TRANSFER TO MONOMER CONSTANTS, C_M

T	Smallwood		Abdel Alim		Bort		Mean	Standard Deviation	Coefficient of Variation
(°C)	C_M	C_M^{-1}	C_M	C_M^{-1}	C_M	C_M^{-1}	(C_M^{-1})		
50	9.4607×10^{-4}	1057	1.097×10^{-3}	911.9	1.057×10^{-3}	946.3	971.73	75.82	7.80%
60	1.2140×10^{-3}	823.7	1.418×10^{-3}	705.0	1.494×10^{-3}	669.2	732.63	80.87	11.04%
70	1.526×10^{-3}	655.2	1.807×10^{-3}	553.3	2.071×10^{-3}	482.9	563.78	86.85	15.37%

Table 6.6 highlights how important experimental precision is, for the differences between the different predictions of C_M^{-1} ($\simeq \bar{\mu}_n$) made by the different workers correspond to the claimed rises in $\bar{\mu}_n$ with conversion. There is, therefore, no significant reason for choosing a particular model for C_M from Table 6.6; all give an estimate of $\bar{\mu}_n$ within experimental accuracy. Despite this observation, a more suitable value of C_M may be given in the average of <u>all</u> the

observations recorded in Table 6.6. This is:

$$C_M = \frac{k_{trm}}{k_p} = 11.693 \exp\left[\frac{-25075}{RT}\right] \qquad (6.25)$$

and although it has not been used in this study, its subsequent use is recommended.

Optimisation of the parameters of the model, as more accurate experimental evidence becomes available, may yield improved prediction of the conversion dependencies of the molecular weight and its distribution. Indeed it is a particular feature of this model, that parameters may be changed without compromising the basis of MWD predictions; a generalised MWD is assumed. This is certainly not the case for the model of Abdel-Alim who has assumed an a priori form for the MWD, nor is it the case for the model of Kuchanov who has completely ignored molecular weight.

The measurement of molecular weight, its distribution and its conversion dependence and comparison with model's predictions offers a potentially sensitive diagnostic tool for mechanism. The use of caution is essential, for not only is accurate experimental data required, but an understanding of the functional form of the kinetic models is imperative.

For example consider the Mayo equation for the kinetic chain length, x_n, in a homogeneous free radical polymerisation:

$$\frac{1}{x_n} = \frac{1+p}{k_p}(f\, k_t\, k_d[I])^{1/2}\,\frac{1}{[M]} + C_M \;;\; C_M = \frac{k_{trm}}{k_p} \qquad (6.26)$$

where p is the proportion of termination due to disproportionation and all the other symbols have been defined previously. When chain transfer to monomer dominates termination reactions,

$$\left.\begin{aligned} &C_M >> \frac{1+p}{k_p}(f\, k_t\, k_d[I])^{1/2}\,\frac{1}{M} \\ &\text{and } \bar{x}_n = C_M^{-1} \end{aligned}\right\} \qquad (6.27)$$

Rearranging the Mayo expression and using the binomial expression yields:

$$\bar{x}_n = C_M^{-1} \left[1 - \frac{1}{k_p} \frac{+ p}{} \left(f \, k_t \, k_d [I] \right)^{1/2} \frac{1}{[M]} \right] \qquad (6.28)$$

If 'average' values are taken for k_p, k_{trm}, p, f etc in a multiphase system, the conversion behaviour of molecular weight in the PVC/VCM system can be seen qualitatively. C_M^{-1} is clearly the limiting (upper) value of number average chain length. More significantly any of the following phenomena will contribute to an increasing kinetic chain length with conversion:

* initiator depletion.

* decreasing k_t as segmental radical chain end diffusion is reduced by the gel or Trommsdorf effect.

* decreasing the efficiency of initiation, f.

* increasing the contribution of the combination of radicals to termination (decreasing p).

The real problem is to distinguish uniquely between the effects due to each factor. Such differentiation may ultimately prove impossible, although the form of the model should ease parametric optimisation. Further work should concentrate on the Trommsdorf effect and the value of k_t throughout the polymerisation. Physically a decreasing value of k_t represents an increasing resistance to the segmental diffusion of radical chain ends for mutual termination. Not only does it lead to increasing kinetic chain length - experimentally observed - it can signficantly increase autoacceleration, leading to peakier rate profiles at or near pressure drop.

Its experimental verification must therefore be the highest priority in PVC polymerisation kinetics.

6.2.8 Porosity

In Section 5.1(iii) a model for porosity was proposed which depended on the conversion, x_{set}, at which subgrains stop contracting to accommodate the density difference between monomer and polymer. When x_{set} is exceeded, further polymerisation leads to the development of pore spaces within the subgrains. At x_{set} the pore spaces will be completely occupied by the free liquid monomer phase: thereafter saturated monomer vapour will increasingly occupy the free space, as liquid monomer is consumed by polymerisation.

It has already been demonstrated in this study that vinyl chloride monomer is so mobile that equilibrium is easily maintained between the monomeric and polymeric phases (Section 6.2.3). Under these circumstances, the relationships derived in Appendix 5 show how phase volumes and therefore how porosity change with conversion x_{set}. The results are summarised in Figures 6.14A and 6.14B.

The distinction between the two graphs is the state of the polymer when the porosity is measured. The family of curves in Figure 6.14A are for polymer which is completely swollen with monomer. Inside the reactor this will indeed be the case upto pressure drop. However in making experimental measurements any monomer remaining is generally stripped out. The definition of porosity can account for this by taking the volume occupied by unswollen polymer as its basis in equation 5.6. The family of curves in Figure 6.14B are based on the assumption that the polymer phase is unswollen. On both graphs experimental porosity-conversion data of Smallwood (86) has been plotted for comparison.

In Figure 6.14 , curves (i) and (ii) show how the monomer phase depletes, (i), as the swollen polymer phase grows, (ii). Curve (iii) shows how the system volume (ie (i) and (ii)) behaves. Beyond $x = \alpha_5 = \alpha_6 = \alpha_7 = .77$ the free monomer phase has disappeared: further polymerisation is at the expense of the monomer swelling the polymer. The polymer phase becomes more dense and contracts in volume.

FIGURE 6.14 Relative phase volumes of diluent monomer phase and precipitated polymer phase for the PVC/VCM system as a function of conversion.

(i)(Volume of monomer phase + dissolved polymer)/V_0
(ii)(Volume of Precipitated polymer phase swollen by monomer)/V_0
(iii) ((i)+(ii))

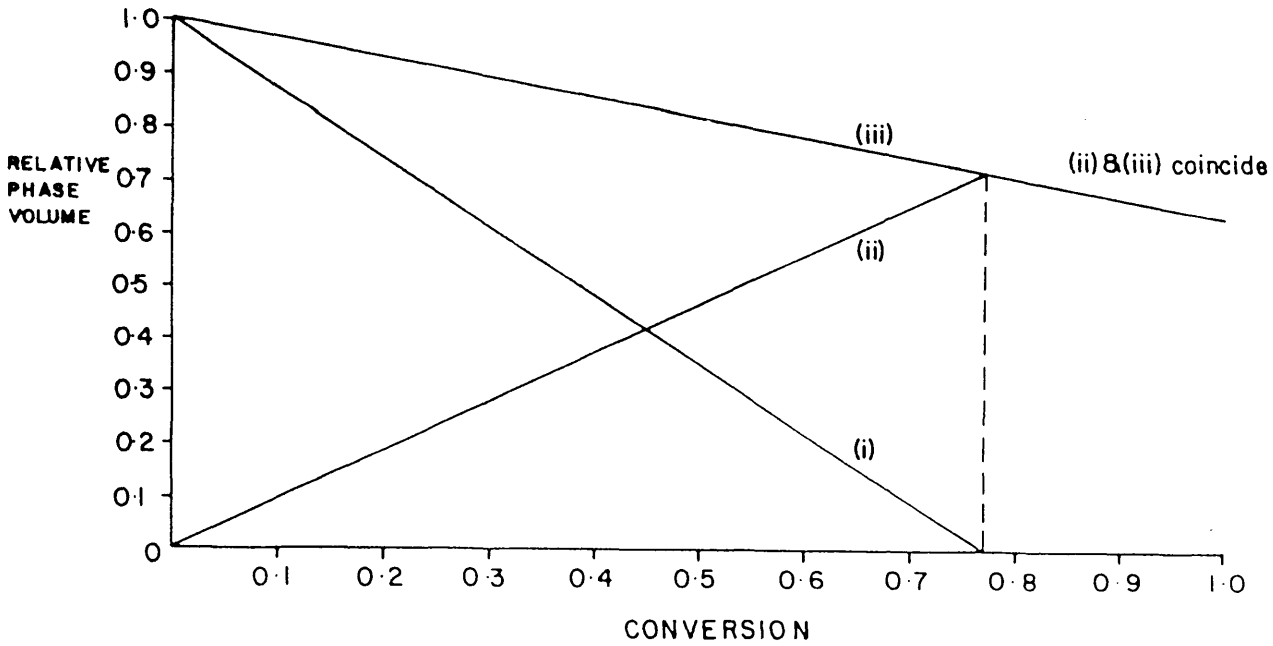

FIGURE 6.14 A) Porosity of PVC subgrains as a function of conversion when the PVC is considered to be completely swollen by VCM.

(iv) Porosity for non-contracting swollen polymer system, i.e. (1-(ii))

(v) Maximum attainable porosity for fully contracting model of a PVC subgrain with PVC primary particles completely swollen by VCM, i.e. ((i)/(iii))

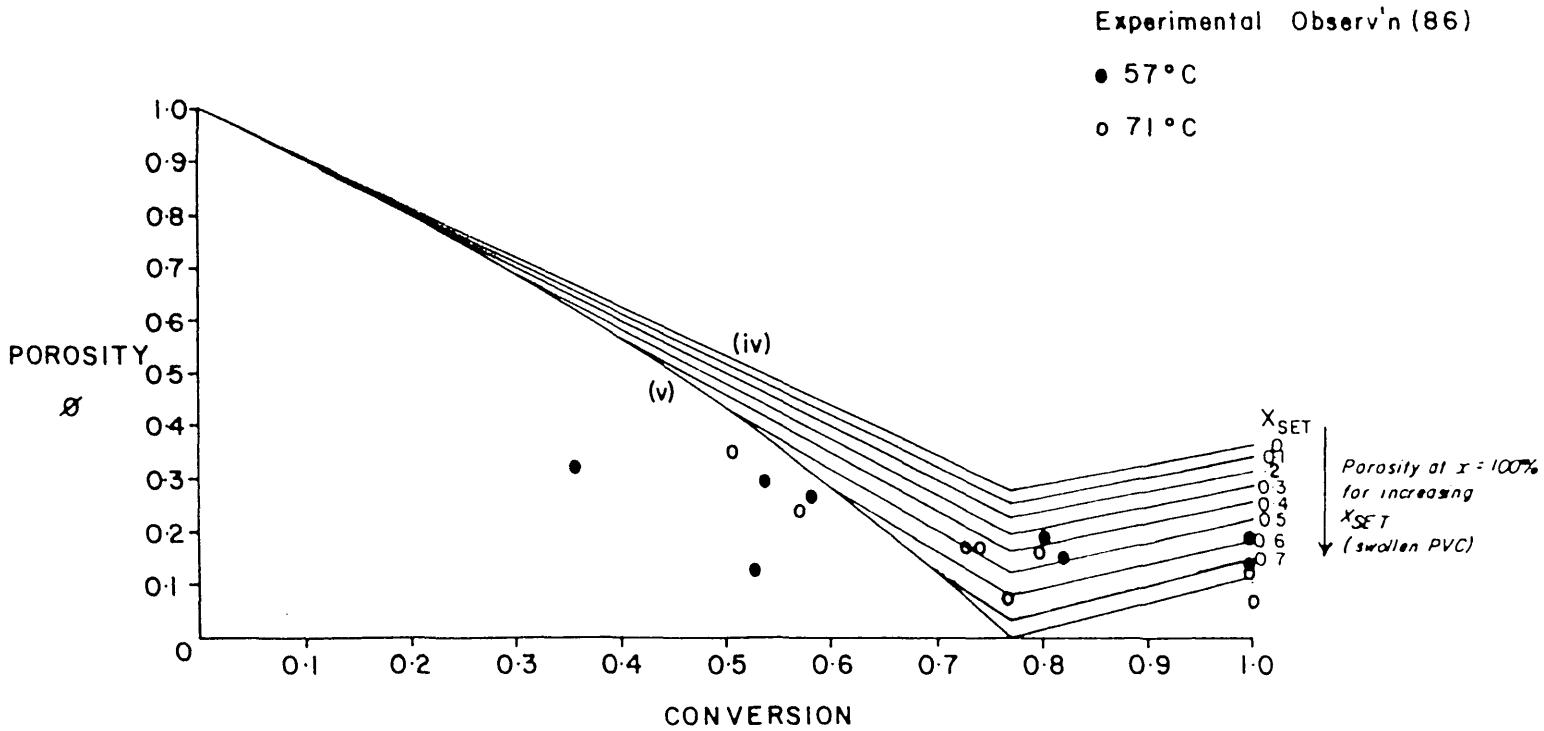

FIGURE 6.14 B) Porosity of PVC subgrains as a function of conversion when the PVC is considered not to be swollen by VCM.

(vi) Volume fraction of monomer in the PVC/VCM system for a continually contracting droplet.(porosity created when VCM is stripped from subgrains post-reaction)

(vii)Porosity when Subgrains do not contract during polymerisation, with PVC not swollen by monomer, $\emptyset = 1 - V_{polymer,unswollen}/V_0$

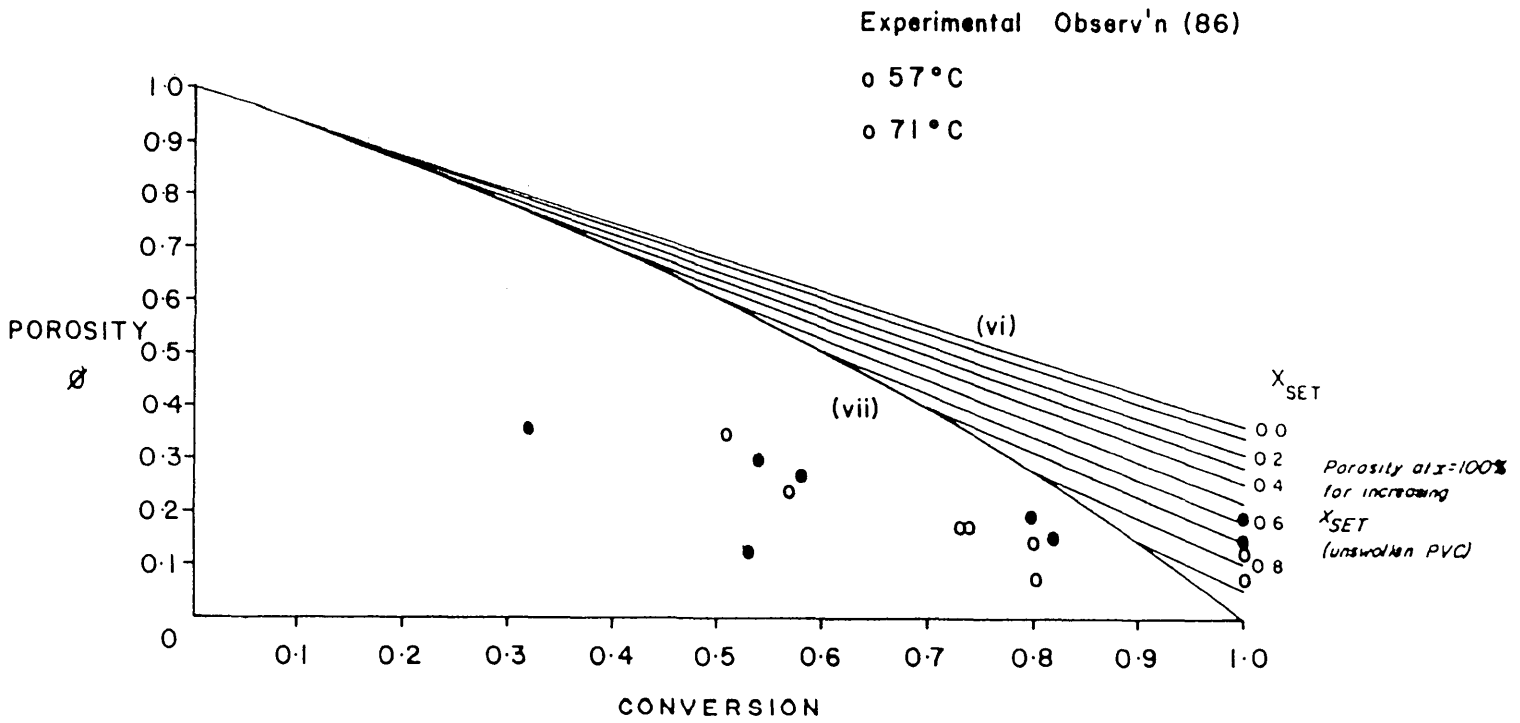

Curve (iv) shows the porosity for a non-contracting polymerising droplet occupied by swollen PVC. Since $x_{set} = 0$, the porosity at any conversion less than 100% represents the free space occupied by both the liquid monomer and any vapourised monomer. At $x = 0$ the system is entirely monomer and the porosity is therefore 100%.

The interesting feature of this model is the prediction of a minimum porosity at, 'pressure drop' conversion ~77%. At this conversion all the available monomer completely swells the formed polymer. Above it, this monomer is itself polymerised. The increasing density of the polymer phase is reflected in the rising porosity.

Curve (v) shows the porosity of a continuously contracting subgrain occupied by swollen PVC primary particles. It is obtained by dividing the locus of curve (i) by curve (iii). At 77% conversion it predicts zero porosity. Between the extremes of the two models for droplet contraction ((iv) (non-contracting) and (v) (continuously contracting)) a family of curves is obtained for the different values of x_{set}. All display a minimum porosity at pressure drop conversion. As an example of intermediate behaviour, if x_{set} is 50%, at 50% conversion the porosity is 43%, at 77% it is 12% and at 100% it is 28%.

At 100% conversion the porosity predicted by the swollen polymer model equals that predicted by the unswollen model. Figure 6.14B shows the porosity when the PVC is unswollen. Curve (vi) is the non-contracting model and curve (vii) the continuously contracting model. As with the swollen model, there is a family of curves which represents the different values of x_{set}. Table 6.7 gives the porosity at 100% conversion for various values of x_{set}.

TABLE 6.7

POROSITY AT 100% CONVERSION - SWOLLEN AND UNSWOLLEN POLYMER

Conversion x	Volume Fraction of VCM in System	Porosity at 100% Conversion for $x_{set} = x$
0	1.000	0.364
0.1	0.934	0.340
0.2	0.863	0.314
0.3	0.786	0.286
0.4	0.702	0.256
0.5	0.611	0.223
0.6	0.512	0.186
0.7	0.403	0.147
0.8	0.282	0.103
0.9	0.149	0.054
1.0	0.0	0.0

$\rho_p = 1400\ kgm^{-3}$ $\rho_m = 890 kgm^{-3}$

Porosity at intermediate conversions given by (unswollen model):-

$$\phi(x) = \frac{(V_M + V_p)|_{set} - V_p|_{unswollen}}{(V_M + V_p)_{set}} = \frac{1 - x_{set}\left[\frac{\rho_p - \rho_M}{\rho_p}\right] - x\frac{\rho_M}{\rho_p}}{1 - x_{set}\left[\frac{\rho_p - \rho_M}{\rho_p}\right]}$$

As with molecular weight behaviour, one of the problems of comparing theory with experiment is the sparsity of accurately recorded, openly available, experimental results. Smallwood (86) has, however, measured voidage and pore size distribution as a function of conversion. Despite his isolation techniques, which subject the PVC subgrains to severe mechanical strain and rupture, as entrapped VCM is stripped from the subgrains when they are withdrawn from the reactor, and despite the disruption which mercury porisimetry must cause, it is significant that his observations are consistent with a contracting swollen PVC porosity model. This is clear from Figures 6.14A and B where his data has been plotted for comparison with the swollen and unswollen models respectively. The

swollen model gives much closer agreement, although there is clearly a wide scatter in the data. Furthermore his observations are consistent with an x_{set} of 60-70%, subgrains continue to contract upto that conversion.

Analysing Smallwood's data in this manner has serious implications. Since monomer equilibrates rapidly with the gel phase the state of the PVC stripped of monomer is brought into question. The evidence suggests that the stripped polymer retains its swollen dimensions. As the monomer swelling the polymer is stripped, microvoids must be left within the PVC polymer network to maintain its expanded state. Such microvoids are not penetrated or disrupted by the measurement techniques. Hence although the model for PVC primary particles swollen by monomer is a considerable simplification of the true state, it is nevertheless a good approximation.

A real benefit of either model for porosity is the establishment of a link between porosity and x_{set}. At x_{set} flocculated primary particles have formed a coherent close-packed space filling structure within the droplet. Further inward contraction of the graft co-polymer droplet skin is prevented. The close-packing of primaries within the droplet is accelerated at the surface by the retreating VCM/water interface of the contracting droplet. It sweeps up primary particle nucleation sites before it. The earlier surface close-packing occurs the lower x_{set} is and the higher the resulting voidage or porosity is.

x_{set} is dependent on the mechanism for primary particle flocculation. Where the primaries flocculate rapidly to their limiting number, N_{∞}, at low conversions (ϵ high), their uniform growth and random packing, ensure x_{set} is approximately 70%. The slower the rate of flocculation (ϵ low) is, the longer their original identity is retained, and the earlier close packing occurs at the surface of the subgrain as the nucleation sites are swept up. Such slowly flocculating aggregates give rise to lower values of x_{set}, and ergo, higher values of ultimate (100% conversion) porosity. The conditions which cause such a lowering of x_{set} will involve higher concentrations of stabilising surfactant (more graft

copolymerisation); increased agitation (section 2.5(A)); and lower temperatures. This is confirmed, in part, by Table 6.4 where ϵ took values of 6.07 at 55°C and 10.39 at 70°C. The corresponding porosities (86) are .16 and .09. (low $\epsilon \equiv$ low $x_{set} \equiv$ high porosity).

Can a more detailed model be proposed for porosity?

It is reasonable to expect porosity to behave according to a model of a form

$$\phi(x) = \phi(\epsilon, We, x) \qquad (6.29)$$

where ϵ is the rate parameter for primary flocculation (equations 5.1 and 5.2) and We is the Weber number for suspended VCM/PVC droplets (2.5(A)). Furthermore, since this study has shown in equation 5.6, that

$$\phi(x) = \phi'(x_{set}, x) \qquad (6.30)$$

the desired relationship is

$$x_{set} = x_{set}(\epsilon^{+a}, We^{b}) \qquad (6.31)$$

The coefficients, a,b take different signs (in the different agitation zones (Section 2.5(A))).

This study has revealed a clear link between primary particle flocculation rate, ϵ, x_{set} and porosity, based upon fully swollen primary particles. Given the absence of accurate experimental observations, any number of semi-empirical models of the type 6.31 could be proposed. It would be unwise to suggest just one.

There is a clear need for a complete series of carefully controlled and monitored experiments to look at the influence of temperature, surfactant type and concentration under varying geometric and agitation conditions. By specifically recording porosity and pore size distribution, values of x_{set} can be determined from Figure 6.14A for correlation with ϵ and We. Only in this way

will more reasonable models for the macromechanism for average porostiy be deduced.

Semi-empirical models reveal little about the micromechanism of primary particle flocculation and pore formation. The model proposed by Ray and Jain (Equation 2.6.26) remains in this respect the best description of the agglomeration processes.

6.2.9 Reactor Pressure

A model was developed in Section 5.1(iv) for predicting reactor pressure behaviour: equation 5.24. In this section the suitability of that model is assessed.

Figure 6.15 shows how well it predicts 'pressure drop' for the different rates of VCM mass transfer between the vapour phase and the polymerisation sites within the subgrains. A reactor pressure profile for an actual polymerisation carried out under similar conditions as for the model calculation is shown too. The section of the profile of interest is upto the seven hour mark, when the reactor is subjected to controlled venting to end the polymerisation which has virtually stopped. Figure 6.15 also shows the real and computed rate profiles for comparison.

At high mass transfer rates (K_{OG} <10^{-8}mol/Ns) the pressure is predicted by the Flory-Huggins expression, the thermodynamic limit. While at low mass transfer rates (K_{OG} < 10^{-10}mol/Ns) there is no effective pressure drop: as the VCM saturated vapour pressure is maintained. The transition between the two limiting conditions occurs over just two orders of magnitude and, within that range, the modelled pressure approximates well to the observed experimental pressure profiles. Indeed it is reassuring to find that the mass transfer coefficients predicted by the models 5.25 and 5.26 lie within the range and differ by less than an order of magnitude. The k^{o}_{L} are predicted as $5.04 \times 10^{-4}ms^{-1}$ and $9.06 \times 10^{-5}ms^{-1}$ respectively. With a Henry's Law constant of $7.27 \times 10^{-4}Jmol^{-1}$, those correspond to values of K_{OG} of 6.93×10^{-9}mol/Ns and

FIGURE 6.15 Pressure profiles in an autoclave for the manufacture of PVC for different rates of mass transfer of gaseoue VCM from the vapour phase to the loci of polymerisation, (the rate of polymerisation profiles are also shown).

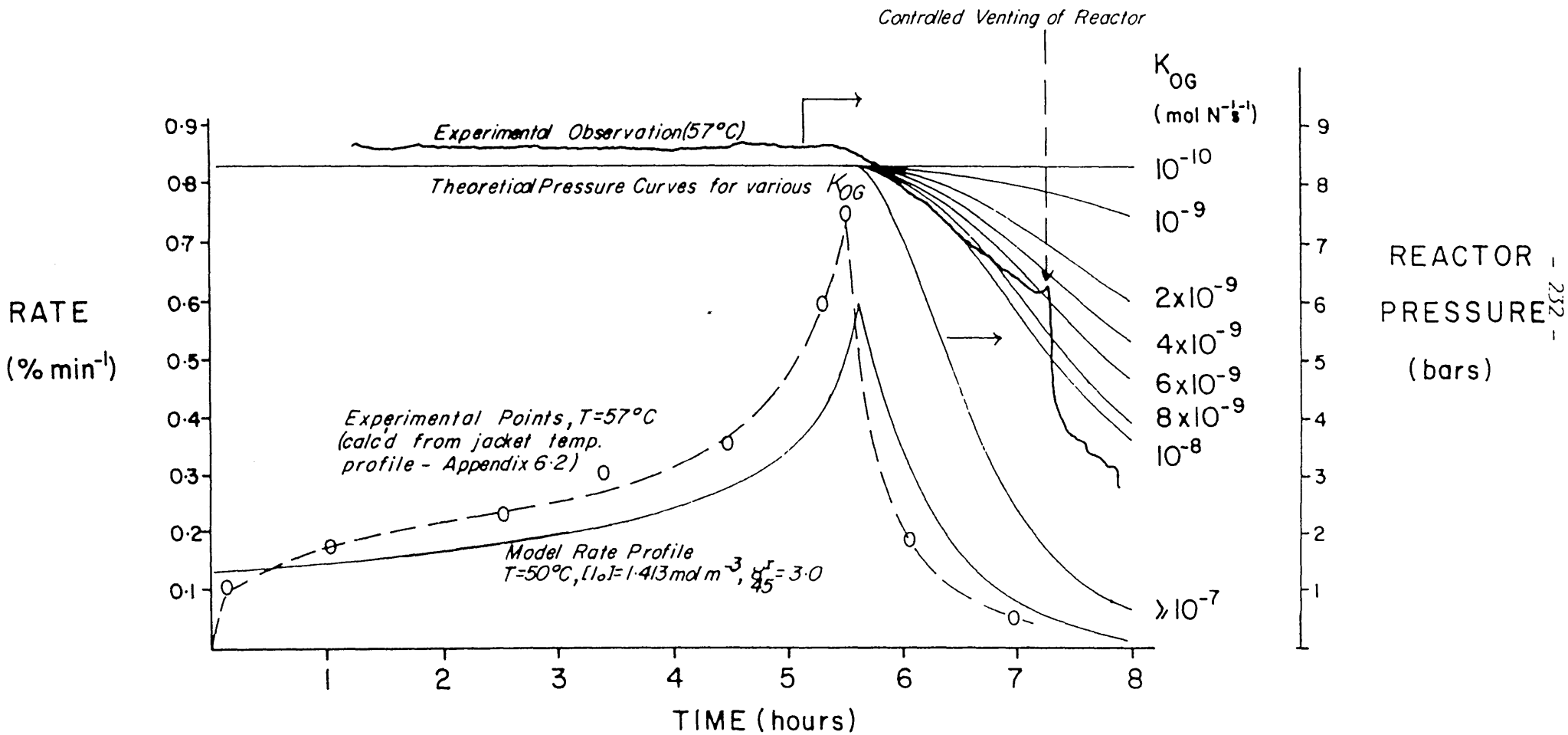

1.245×10^{-9}mol/Ns respectively. (The Henry's Law constant was calculated assuming that at 50°C the VCM s.v.p. is 8 bars, and its solubility in water is 11 mol m^{-3}).

It is important to realise that K_{OG} is quite dependent on the agitation conditions within the reactor. In a quiescent reactor K_{OG} may be so small that no pressure drop is observed, whereas with fierce agitation the pressure profile will be given by the thermodynamic limit. The correlation for k^{o}_{L} must therefore be chosen with care. For example, equation 5.26 reflects the effect of agitation:

$k^{o}_{L} \alpha \sqrt{N_S}$ where N_S is the agitator speed.

Whereas although equation 5.25 apparently takes agitation into account through the diameter of the suspended polymerising particle (predicted by equation 5.4), the suspended particle sizes however cancel out. This particular correlation therefore predicts no link between agitation and the rate of pressure drop.

Another correlation, for forced convection around a submerged body, given by equation 21.2-25 in reference (55) is:

$$Sh = 2.0 + .6\ Re^{1/2}\ Sc^{1/3} \qquad (6.32)$$

Thus predicts that,

$k^{o}_{L} \alpha N_S^{0.6}$

when combined with equation 5.4. (it gives a higher value of K_{OG} at 5.94×10^{-8}mol/N_S).

Using equation 5.24 to predict pressure drop necessitates the use of a correlation for mass transfer coefficients. However, as is clear, from figure 6.15 although the experimental pressure profile lies within the bounds of K_{OG} predicted by the correlations 5.25, 5.26 and 6.32, it follows none of them. While the experimental profile errs towards higher predictions for K_{OG} (ie 5.25 and 6.32),

practically any correlation could be used.

In not knowing precisely how k^{o}_{L} is affected by agitation, the weakness of using the degree of pressure drop as an estimate of conversion is demonstrated. This common industrial practice can only be applied, with confidence, for a particular reactor with particular agitation conditions: the same degree of pressure drop in another reactor may indicate a completely different conversion. A more suitable method for measuring conversion is to measure the heat load generated by the reaction exotherm.

Regression of experimental data using equation 5.24, with the conversion measured by the heat output and with a suitable thermodynamic expression for the vapour pressure above the polymer-monomer mixture, offers the ideal method for measuring K_{OG}. The subsequent correlation for K_{OG} would contribute further to the understanding of the behaviour of agitated systems.

6.3 SUMMARY

The model for polymerisation of vinyl chloride developed in this thesis has been applied to the study of various aspects of the kinetic and morphogenetic mechanism and, to assess the influence of process conditions on polymerisation. In general, each section of this chapter has concentrated on the contributions made to the overall polymerisation by individual model parameters. Some of those parameters were analysed using the analytic solution whereas others had to be analysed with the numerical solution, or model. The advantage offered by the analytic solution is its cheap cost; its solutions are computed in one thousandth of the time required for the numerical solutions. The two solutions coincide in their predictions when radicals terminate at the point of their initiation without diffusing into any of the precipitated polymer phase. The disadvantage of the analytic solution is its inability to model the resistance to the mass transfer for any species.

By varying most of the parameters of the model, all the

significant features of experimental profiles have been reproduced. Though in qualitative agreement with experiment, quantitative agreement was not always possible. This was due in part to the coarse nature of the sensitivity analysis for each parameter. (Though a large number of parameters were covered). The other reason was the accuracy of the available experimental data. An example of this appears in Section 6.2.7. The apparent increase in molecular weight with conversion is of the order of the deviations in the value of k_{trm} reported by different workers.

The parameters varied during this study were:

* termination rate constant, k_t
* initiator distribution coefficient, γ^I
* temperature
* initiator efficiency in the polymer phase, f
* monomer mass transfer coefficient, k_{AM}
* initiator mass transfer coefficient, k_{AI}
* radical mass transfer coefficient, $k_{A\sigma i}$
* rate of primary particle nucleation, ϵ
* transfer to monomer rate constant, k_{trm}
* conversion at which subgrains assume rigidity, x_{set}
* overall mass transfer coefficient between vapour phase and polymerisation sites, K_{OG}

The wide scope of the study has revealed a number of important features of the vinyl chloride polymerisation process. The principal findings are summarised below.

Initiator

When initiator is more soluble in the vinyl chloride monomer phase, a lower initial, and overall, rate is observed. However at the transition from heterogeneous monomer and polymer phase polymerisation to purely polymer phase polymerisation at ~77% conversion, there is increased 'peakiness' of the rate profile. γ^I is clearly an important parameter of the model, an observation which

has not been made in previous studies.

Termination Rate

The literature values for k_t used in most of this study are too high and give lower rates of polymerisation than are observed in practice (Figure 6.2). The monomer and polymer phase values of k_t should be reduced as suggested in Table 6.8 to give higher rates for all conversions.

Molecular Chain Length

The model predicted that μ_n increased with conversion (by 3%) in qualitative but not quantitative agreement with experimental observation, where it rises by approximately 15%. The dominance of chain transfer was supported by the observed values for Zp of ~2.0 and by the insensitivity of Zp and μ_n to changes in parameters other than k_{trm}. The value of k_{trm} due to Bort underestimated chain lengths (see Table 6.6): a new value of C_M is given in Table 6.8.

Mass Transfer

The assumption that there is no resistance to monomer and initiator mass transfer is a starting point for all other models. By considering the effect of its presence, this assumption has been shown to be valid.

For radical mass transfer, the picture is quite different. As the resistance is reduced from infinity ($k_{Aoi} = 0$) when radicals initiate, propagate and terminate in the same location, the most significant observation is the behaviour of the rate profiles at maximum rate. They become rounded, contrasting with the peaky profiles observed with the analytic solution. At very high mass transfer rates, the rate decelerates to the maximum rate, rather than continuously autoaccelerating to it (Figure 6.9).

The vinyl chloride vapour passing from vapour phase to polymerisation sites meets its principal resistance at the interface between the vapour and liquid. The specific area available for mass transfer through the interface is much smaller than that offered by the suspended VC/PVC droplets.

Primary Particle Development

The rate of primary particle agglomeration has a significant effect on the overall rate of reaction. Deviations in ϵ from its normal value can give rise to a ±10% difference in the time taken to reach pressure drop conversion (Table 6.4).

If the nature of the precipitated PVC is considered, porosity values are consistent with subgrains continually contracting upto 60-70% conversion, when the primary particles have completed a contiguous internal skeleton. Stripping VCM from PVC grains appears to leave them with their fully swollen dimensions (Figure 6.14(A)). A link was postulated in equation 6.31 between x_{set}, ϵ and We.

Temperature

The model predicts the experimentally observed transition from 'peaky' auto-accelerating rates at low temperatures, to reactions which have high initial rates and die off continuously from the start at high temperatures. At critical intermediate temperatures, plateau polymerisations are observed (Figure 6.5).

Pressure

In Section 6.2.9 this was shown to be purely dependent on the mass transfer of vinyl chloride form the vapour phase to the site of polymerisation. Although reactor pressure can indicate conversion, it is strongly dependent on the magnitude of K_{OG}.

Agitation

Agitation is crucial in determining the PVC grain and subgrain internal structure, droplet size distribution and K_{OG}. It has an insignificant effect on observed kinetics and only causes changes in rate when it has a large effect on ϵ. Even so, rates would change by no more than ±10%.

Rules of Thumb

In sections 6.1.5 and 6.1.6 some useful rules of thumb were developed from the analytic solution for calculator use, to determine:

(i) whether polymerisation will exhibit peak reactions, or not,
(ii) what amount of initiator to use to obtain a given maximum rate
(iii) how much initiator to use based on just one experimental test recipe.

Resulting from this study, values for kinetic and morphogenetic parameters are recommended in Table 6.8. Only k_p has remained the same as the value used by Kuchanov and Bort.

The parameters have strongly interdependent effects on the predictions made by the model. The variation in the values of γ^I and k_t will be particularly important in any future optimisation of the model. It will be possible, at least in principle, to optimise the model parameters subject to the concurrent experimental constraints imposed by observed rate and molecular weight profiles as functions of time or conversion.

In the final chapter the overall success of the model is discussed, with the recommendations and suggestions for further work.

TABLE 6.8

RECOMMENDED VALUES FOR KINETIC AND MORPHOGENETIC PARAMETERS

PARAMETER	PHASE	
	MONOMER (M)	POLYMER (P)
Propagation Rate Constant, $k_p/[m^3mol^{-1}s^{-1}]$	$50 \times 10^3 \exp\left[\frac{-27627.6}{RT}\right]$	
Termination Rate Constant, $k_t/[m^3mol^{-1}s^{-1}]$	$6.5 \times 10^8 \exp\left[\frac{-17588}{RT}\right]$	$3.5 \times 10^8 \exp\left[\frac{-34338}{RT}\right]$
Chain Transfer Coefficient, $C_m = k_{trm}/k_p$	$11.693 \exp\left[\frac{-25075}{RT}\right]$	
Initiator Decomposition Constants, k_D	Table 5.2(b)	
Initiator Efficiency, f	.7	.5
Initiator Mass Transfer Coefficient, k_{AI}^{MP}	$10^{-3}ms^{-1}$ ($\simeq\infty$)	
Monomer Mass Transfer Coefficient, k_{AM}^{MP}	$10^{-3}ms^{-1}$ ($\simeq\infty$)	
Radical Mass Transfer Coefficient, $k_{A\sigma i}^{MP}$	$2 \times 10^{-7}ms^{-1}$	
Primary Particle Flocculation $\frac{N(x) - N_\infty}{N_o - N_\infty} = e^{-\epsilon x}$	$\epsilon = 1.337 \times 10^6 \exp\left[\frac{-33550}{RT}\right]$ $N_o \propto f\, k_D[I]_M$ - Figure 5.2 $N_\infty = 5 \times 10^{17}m^{-3}$	
Porosity	equation 5.6; $x_{set} = .6 - .7$ equation 6.30	
Initiator Distribution Coefficient, $\gamma^I_{MP}=[I_M][I_P]$	3.0	
Monomer Mass Transfer Coefficient, k^o_L	equations 5.24, 5.25, 5.26	

CHAPTER SEVEN

SUCCESS OF THE MODEL

The principal aim of this thesis has been to develop a new process mathematical model for the polymerisation of vinyl chloride capable of predicting the effect of changes in process variables on the nature of the polymer produced in commercial reactors. This has indeed been achieved.

The development of such a model has required detailed consideration of all the physical and chemical kinetic processes involved in initiation, propagation and termination of free radicals, precipitation of macromolecules and the growth and development of supramolecular species. The model was initially expressed as an infinite set of differential conservation equations describing the mass conservation of each molecular species. A generating function was used to transform those equations to a tractable number. However the transformed equations contained the transform variable, s, which could only be removed by differentiation with respect to s, and setting s = 1. The set of equations produced by this differentiation expressed the time-variation of the moments of the molecular weight distributions. When integrated in the time domain, these equations were solved to give the rate of reaction and the behaviour of the number average and the weight average molecular weights as functions of time. Attempts to invert the transform equations directly to the molecular weight distribution proved unsuccessful.

Any form of mathematical model is, of course, only an approximation to the real process it describes. More sophisticated models try to represent nature more realistically and accurately. Increasing the degree of the sophistication of the description offered by a model brings certain disadvantages.

(a) The model may be too complex for meaningful solutions to be obtained, either analytically or numerically;

(b) the cost for computation of a numerial solution may be too high

and,

(c) the model may have too many parameters for experimental verification of each one.

None of these disadvantages are sufficient reason for not setting down a model. With the passage of time, and the development of new mathematical or experimental techniques, and cheaper and faster computers, difficult problems today may be solved more straightforwardly in the future. Where mathematical difficulties exist, some simplification of the model is usually necessary. This has been the case in this work. The solutions generated retain the essential features of the underlying physics but with some loss of accuracy. Much of the work in chapters three and four has been concerned with approximations necessary for tractable solution.

The model developed in this thesis represents the most detailed description to date of the physical process involved in vinyl chloride polymerisation.

It retains the two phase nature of the polymerisation similarly to the models of Bengough and Norrish, Mickley et al, Cotman et al, Talamini, Abdel-Alim et al, and Kuchanov et al. However it extends the simple view of interphase transport of radicals offered by the models of Mickley and of Ugelstad to allow <u>any</u> species (initiator, monomer growing or dead polymer) to be transported. Although Thiele et al consider general interphase transport, their model limits this to precipitation and neglects to account for the difference in equilibrium conditions which exist for different species between the polymer and monomer phases. These limitations do not apply to the current model.

An analytic solution has been derived which retains the functional form of those due to Talamini and Abdel-Alim, while allowing initiator to have different concentrations in the monomer and polymer phases. Kuchanov's model is the only one to have initiator distributed between phases, yet his model is so unwieldy that it needs numerical solution.

The current model unlike any other also predicts molecular weight

and its distribution directly from the chemical kinetic conservation scheme, avoiding the need to assume the form of the distribution.

Although the model is not as advanced in its description of particle size distribution as that of Ray and Jain (who ignore the chemical rate processes to a large extent) it does describe their number variation with conversion.

Thus by considering the polymerisation from first principles a model has been derived which is most general in its description: a model for which most previous models are a subset. In particular the model can predict a priori the autaccelerating nature of the rate profile over the entire conversion range and has identified its fundamental dependence on the dual effects of initiator distribution and radical mass transfer between phases. It is also able to predict, unlike most other models, rate behaviour beyond pressure drop and can therefore be applied to industrial situations.

The model nevertheless successfully mimics the principal features of vinyl chloride polymerisation. Although the results are in qualitative agreement with the experimental observations, strict quantitative agreement has not always been possible. Indeed this work has highlighted the need for accurate reproduceable experimental observations: examples of conflicting values are seen in Section 6.2.7 with molecular weights, and in Table 2.5 with kinetic parameters.

In addition to the model's ability to reproduce the principal features of the polymerisation, significant contributions to knowledge and understanding of the vinyl chloride polymerisation process and its modelling have been made in the following areas:

(a) the detailed investigation of the effect of changes in parameters of the model;
(b) the comprehensive discussion of the mathematical techniques;
(c) the determination of deficiencies in existing experimental results and theoretical understanding of the polymerisation, and

(d) the provision of a framework for future improvements in understanding to be incorporated in the model.

Each of these points is amplified below.

(a) The effect of parametric changes on model predictions

In Section 6.3 the predictions made by the model, as various parameters were changed independently, were summarised. Table 6.8 contained recommendations for the values of various parameters. Perhaps the most important observations concern mass transfer effects and morphological development.

The model treated mass transfer effects by using one dimensional film theory models: mass transfer coefficients were directly related to the diffusion coefficients for each species by the relationships 5.19, 5.25 and 5.26. This contrasted sharply to the approaches of Bort, Ugelstad and Olaj who have all previously lumped any mass transfer effects into a single parameter for radicals. They could not therefore access the influence of initiator or monomer mass transfer limitation.

However use of this model has demonstrated unequivocally, that any initiator or monomer mass transfer limitation to reaction in precipitated polymer particles is unlikely. The omissions of mass transfer made in previous models have been finally justified in this work.

Radical mass transfer from monomer to polymer phases can lead to increased rate and significant variation in the predicted rate profile. Experiments must be devised to verify whether this is occurring in reality.

Perhaps the most important finding is related to initiator distribution between the phases. It does not appear to have been considered by previous models. Yet the solubility of initiator in the different phases has considerable importance in determining the

rate profile. The greater it is in the monomer phase relative to the polymer phase, the lower the initiated rate, the longer the reaction takes before the rate peak and the 'peakier' the profile relative to the average rate. Experimentation in the field of initiator solubility, especially with respect to polymers, should be seriously considered.

By considering a simple model for primary particle flocculation, equation 5.1, it was found that the rate of reaction might be affected by up to 10%, but with no significant change in the general shape of the rate profile. If primary particle flocculation can be prevented in practice, by chemical means it would mean that specific surface area available for mass transfer is retained, and reaction rates would be marginally improved. Rapid flocculation reduces the rate of reaction.

Like primary particle flocculation, subgrain agglomeration is one of the important phenomena in determining ultimate polymer characteristics such as density. Whereas this model has shown an evident interaction between primary particle flocculation and rate of polymerisation (one affects the other and vice versa) subgrain agglomeration can only be a consequence of the changing interaction between agitation (physical forces) and stabilising surfactant (chemical forces). The rate of polymerisation may affect the rate of destabilisation of the surfactant, not vice versa. The secondary importance of subgrain agglomeration to the crucial (economically important) rate processes is further demonstrated by the contribution made to pressure drop: that is principally limited by interactions at the interface between the vapour and liquid phases (section 5.1(vi)). The topic of multiphase flow in agitated systems is an active area of research (see eg 93): a study of this type can only highlight the need for further experimental and theoretical studies on the VC/PVC/water/surfactant system. There is a dearth of experimental data on this particular system: only the most empirical of treatments is warranted (section 5.1(ii)).

(b) Mathematical techniques

In Chapter 4 the techniques applied to the solution of the model equations were carefully outlined as a guide to future workers in this field. Forming the model equations in conservative form is an essential first step. Thereafter stiffness in the solution of the model equations is a very real problem. It does not appear to be generally acknowledged in the literature, although both West (67) and Bosworth (68) have devoted considerable time to overcoming its effects. Their theses do not reflect this investment in time.

Past computers and specialised methods are also essential for the solution of stiff equations. Even so, timescales of 300–400 cp seconds on CDC Cyber 6600 computers have been the rule in this study. Carrying out any sensitivity analysis on a parameter is clearly very expensive. These costs will of course diminish as computers become cheaper in real terms.

Apart from any lack of a sufficient number of accurately recorded experimental observations, numerical optimisation of any of the numerous parameters of the model is unlikely in the forsee–able future. Such techniques are highly iterative and would rapidly increase the consumption of computer time.

Table 6.8 does however give initial estimates for starting any search in an optimisation procedure. Any optimisation is likely to be limited to trial and error methods around these values.

Numerical inversion of the generating functions used in this thesis is often talked about in the literature. The two attempts shown in Chapter 4 demonstrate the difficulty in achieving such an inversion.

(c) Deficiencies in experimental results and theoretical understanding of polymerisation

The results of computer analysis can be printed out to several decimal places: the computer models confer a false sense of increased accuracy. The emphasis on accuracy and model predictions can be misguided because the experimental evidence, especially for experiments on large process plants, is usually only accurate to 5 or 10 percent. On a process plant, temperature recorders are generally only accurate to 1°C and pressure gauges to ±(0.3 - 5.0) bars, depending on type, if they have been recently calibrated.

Any mathematical model potentially capable of accurate prediction is thus effectively limited by the parameters used by the program. It is, for example, pointless to calculate rate parameters to high precision, if those calculations rely on thermodynamic properties (such as specific molar volume) which have been measured inaccurately. Providing the user is aware of these limitations, he can begin to use a model more profitably in determining the range of values a parameter may take. (This was an important element of Chapter 6). After which he may be able to design better experiments for verifying the value of a parameter.

Mathematical models are aids to experimental studies, not replacements for it.

Even today model predictions of Suresh, Kuchanov and Abdel-Alim are compared with the experimental observations of, for example, Cotman et al, Bengough and Norrish, Breitenbach and Schindler and Mickley et al. The ultimate accuracy of many of the predictions of these models is therefore limited by the accuracy of the work performed by those workers and the accuracy of its presentation in the literature.

Advances in experimental techniques over the last 20 years, especially with the advent of relatively inexpensive computer control and monitoring systems, makes the repitition of some of the experiments necessary if the model is ever to be 'optimised'. Such

verification of the model requires the generation of a complete reaction surface, ie rate-time profiler, for difference amounts of initiator and different temperatures in the range 50 to 80°C, otherwise using a standard recipe for mnomer, surfactant and water concentrations.

With five or six initial initiator concentrations and five or six temperatures within the specified range, given a typical duration of eight hours per polymerisation, a minimum of six laboratory reactor weeks would be required per set of results. For more initiators, more investment is required. This represents an ideal solution. A much more economic method would be to chart reaction profiles at a given temperature with varying initiator charges. Adjust the parameters of the model to produce a best fit, and finally compare predictions with higher and lower temperatures and initiator concentrations against experimental observation. Such a strategy would require only a dozen polymerisations per initiator studied.

It is important too that when these experiments are performed, techniques are developed and improved for the on-line monitoring of:

1) the exothermic heat of reaction (to give direct measures of conversion and rate)

2) molecular weight and its distribution, and

3) particle size distribution.

(Smallwood (86) has already developed techniques for offline measuring of molecular weight: these methods suffer because the conversion at which samples are withdrawn is not known, nor is the effect of sample withdrawal understood.

Ultrasonic techniques (108) appear to have enormous potential for studying the behaviour and motion of 10 micron sized particles and larger. Light scattering techniques are useless in the PVC/VC/Water system; it is essentially opaque.)

The final areas where work must be done to resolve differences between theoretical studies and experimental results are:-

(i) primary particle flocculation

and (ii) subgrain agglomeration.

This study has shown that the simplest of flocculation models (eg 5.1) describes the behaviour of an average particle well. Unfortunately it gives no indication of the distribution of primary particle size. The improved kinetic model produced in this study, is suitable for its analytic form, as a source term for equation 2.6.26. Development of the work of Ray and Jain is probably the best way of determining primary particle size distribution.,

Subgrain agglomeration fits into the broader category of multiphase flow. The topic, and this particular polymerising system, with the destabilisation of sterically stable subgrains, is worthy of much deeper study than is possible in this thesis.

(d) Framework for future study

Isolation of the principal deficiencies in the knowledge of vinyl chloride polymerisation is the key to determining what research needs to be done. As new techniques and results become available, their incorporation in the model to reflect current thinking is straightforward.

RECOMMENDATIONS FOR FUTURE WORK

In addition to the general call for more experimental work made above, there are some specific recommendations to be made:

(i) to optimise the parameter set in table 6.8 by trial and error methods as more accurate consistent experimental

evidence becomes openly available in the literature;

(ii) to agree a standard form for the presentation of experimental results. Ideally the conversion-time curve should be supplemented by the rate-time curve, so that the behaviour of the derivative dx/dt can be observed, and the molecular weight-time curves.

(iii) to attempt to make measurements of the solubility of initiators in monomer and polymer phases.

(iv) to use the model to optimise the temperature control strategy to give greater control over molecular weight characteristics. Various ramp functions can be applied to give desired molecular weight range, rather than producing polymer at a fixed temperature, ie given Mn, Mw and Zp.

(v) to apply the rapid estimation methods of Chapter 6.1 (the analytic solution) to estimate initiator charges and polymerisation times more accurately and quickly than is presently performed.

(vi) to increase the utility of the model as a process simulation model by incorporating models for the particular reactor control mechanism. (For many heating/cooling water systems, the jacket temperature profile can be estimated directly from equation 6.1. However the difference in initial slopes between predicted and experimental rate curves (figure 6.4) is due to the influence of the control system: some may regard it as important to predict this behaviour accurately).

(vii) to carry out further studies similar to those of G R Johnson to study subgrain agglomeration, especially noting porosity and pore size distribution and relating it to x_{set} (Section 6.2.8).

(viii) to develop ultrasonic/radar techniques to study primary

particle flocculation.

(ix) to increase the sophistication of the model's description of radical diffusion to a shell model, in space and time, in the precipitated polymer phase. This is a particularly long term aim in view of the stiffness associated with solving higher order moment equations and the large amount of computer time required.

REFERENCES

1. BURGESS, R H (Editor)
Manufacture and Processing of PVC
Applied Science Publishers Ltd, 1982

2. CAMERON, J B; LUNDEEN, A J; McCULLEY, Jr J H
Trends in Suspension PVC Manufacture
Hydrocarbon Processing (39), March 1980

3. JOHNSTON, C W
Chapter 3 in Encyclopedia of PVC
Vol 1, Chap 3 (Ed L I Nass), Marcel Dekker 1976

4. SCHLEGEL, W F
Polymer Plant Engineering: Reaction, Polymer Recovery
Chemical Engineering, p 88, March 1972

5. ALBRIGHT, L F
Polymerisation of Vinyl Chloride
Chemical Engineering, p 151, May 1967

6. WINSLOW, F H; MATREYEK, W
Particle Size in Suspension Polymerisation
Ind Eng Chem 43 1108 (1951)

7. BILLMEYER, F W
Textbook of Polymer Science
Second Edition, John Wiley & Sons, Inc (1972)

8. FOWLER, J R; HARVEY, D J
Dynamic Simulation of a PVC Process
CEP p 61 January 1978

9. TERWIESCH, B
Suspension PVC in Large Reactors
Hydrocarbon Processing p 117 November 1976

10. BECKMANN, G
Design of Large Polymerisation Reactors
Advances in Chemistry, 128

11. THOMAS, J C
Preparation of Vinyl Chloride Polymers
US Pat 3, 562, 237, Feb 9 1971 (Filed Nov 30, 1964)

12. HARKINS, W D

J Amer Chem Soc 70 3695 (1948)

13. SMITH, W V; EWART, R H
Kinetics of Emulsion Polymerisation
J Chem Phys 16 (6) 592 (1948)

14. UGELSTAD, J; MORK, P
A Kinetic Study of the Mechanism of Emulsion Polymerisation of Vinyl Chloride
Brit Poly J (1970) 2 Jan

15. UGELSTAD, J; LERVIK, H; GARDINOVACKI, B; SUND E
Radical Polymerisation of Vinyl Chloride Kinetics and Mechanism of Bulk and Emulsion Polymerisation
P.A.C 26/2 B (1971)

16. UGELSTAD, J; FLOGSTAD, H; HANSEN, F K; ELLINGSEN
Studies on the Emulsion Polymerisation of Vinyl Chloride by Seed Polymerisation
J Poly Sci Sym no 42 473-85 (1975)

17. UGELSTAD, J
Model for Kinetics of Vinyl Chloride Polymerisation
J Macromol Sci - Chem A11 1281 (1977)

18. UGELSTAD, J; MORK, P C; HANSEN, F K
Kinetics and Mechanism of Vinyl Chloride Polymerisation
P.A.C. 53 323-363 Jan 1981

19. TREGAN, R; BONNEYMAYRE, A
Microstructure du Chlorure de Vinyle Polymerise en Masse
Plastiques Modernes et Elastomeres Septembre 1971

20. JOHNSON G R
The Effect of a Modified Weber Number on Resin Properties During VCM Suspension Polymerisation
AI Ch E 71st Annual Meeting

21. ALLSOP, M W
The Development and Importance of Suspension PVC Morphology
P.A.C. 53 (2) 449 (1981)

22. TERSELIUS, B; RANBY
Phase Structure of Polyvinyl Chloride (PVC) and PVC Polymer Blends
P.A.C. 53 (2) 421 (1981)

23. WENIG, W
The Microstructure of PVC as Revealed by X-Ray and Light Scattering
J Poly Sci Poly Phys Ed 16 (1635-49) 1978

24. GERRENS, H; FINK, W; KOHLEIN, E
Zur Kinetik der Emulsion-Polymerisation von Vinylchlorid
J Poly Sci C 16 2781-2793 (1967)

25. LIEGEOIS, J M
In General Discussion
J Macromol Sci-Chem, A11(8) pp 1449-1460

26. RANCE, D G; ZICHY, E L
The Life Cycle of the Two Phase System in Vinyl Chloride Polymerisation
P.A.C. 53 (2) 377 (1981)

27. BOISSEL, O; FISHER, N
Bulk Polymerisation of Vinyl Chloride: Nucleation Phase
J Macromol Sci-Chem A11(7) pp 1249-1269 (1977)

28. ZICHY, E L
Studies of Nascent Polymer Morphology in Inertially Suspended Vinyl Chloride Droplets
J Macromol Sci-Chem A11(7) pp 1205-12221 (1977)

29. BORT, D N; RYLOV, Ye Ye; OKLADNOV, N A; SHTARKMAN, B P; KARGIN, V A
Morphology of Bulk Polyvinyl Chloride
Poly Sci USSR 7 50 (1965)

30. BORT, D N; RYLOV, Ye Ye; OKLADNOV, N A; KARGIN, V A
Certain Features of the Heterophase Polymerisation of VC
Poly Sci USSR 9 334 (1967)

31. BORT, D N; MARININ, V G; KALININ, A I; KARGIN, V A
Certain Kinetic Parameters of the Bulk Polymerisation of VC and Their Effect on the Structural-Morphological Features of PVC
Poly Sci USSR 10 2984 (1968)

32. DAVIDSON, J A; WITENHAFER, D E
Particle Structure of Suspension Poly(Vinyl Chloride) and its Origin in the Polymerisation Process
J Poly Sci 18 51-69 (1980)

33. GEIL, P H
Morphology Terminology
J Macromol Sci-Chem, A11(8) 1461-1462 (1977)

34. WILSON, J C; ZICHY, E L

Polymer 20 264 (1979)

35. COOPER, W D; SPEIRS, R M; WILSON, J C; ZICHY, E L

Polymer 20 265 (1979)

36. RANCE, D G; ZICHY, E L

Polymer 20 266 (1979)

37. BENGOUGH, W I; NORRISH, R G W
The Mechanism and Kinetics of the Heterogeneous Polymerisation of Vinyl Monomers
Proc Roy Soc A220 301 (1950)

38. MAGAT, M
Contribution a la Cinetique de Polymerisation dans les Milieux Precipitants
J Poly Sci 16 491-504 (1955)

39. BREITENBACH, J W; SCHINDLER, A

Monatsh Chem 86 437 (1955)

39a. SCHINDLER, A; BREITENBACH, J W

Ric Sci (Suppl) 25A 34 (1955)

40. MICKLEY, H A; MICHAELS, A S; MOORE, A L
Kinetics of Precipitation Polymerisation of Vinyl Chloride
J Poly Sci 60 121-140 (1962)

41. TALAMINI, G
The Heterogeneous Bulk Polymerisation of Vinyl Chloride
J Poly Sci 4 535-537 (1966)

42. CROSATI-ARNALDI, A; GASPARINI, P; TALAMINI, G
The Bulk and Suspension Polymerisation of Vinyl Chloride
Makromol Chem 117 140-152 (1968)

43. COTMAN, J D; GONZALES, H M F; GLAVER, G C
Studies on Poly(vinyl chloride)
J Poly Sci 5 (A-1) 1137 (1967)

44. ABDEL-ALIM, A H; HAMIELEC, A E
Bulk Polymerisation of Vinyl Chloride
J Appl Poly Sci 16 783-799 (1972)

45. KUCHANOV, S I; BORT, D N
Kinetics and Mechanism of Bulk Polymerisation of VC
Poly Sci USSR A15 (10) 2393-2412 (1973)

46. OLAJ, O F

Angew Makromol Chem 47 1-14 (1975)

47. OLAJ, O F
Kinetic Models of Bulk Polymerisation of Vinyl Chloride and Their Rate Expressions
J Macromol Sci-Chem A11(7) 1307-1317 (1977)

48. OLAJ, O F
Estimation of the Characterisitc Ratio $K_p(f/k_t)^{1/2}$ and its Temperature Dependence in Bulk Polymer of Vinyl Chloride
J Macromol Sci-Chem A11(7) 1319-13331 (1977)

49. RAY, W H; JAIN, S K
On the Modeling of Bulk Poly(vinyl chloride) Reactors
J Appl Poly Sci 19 1297-1315 (1975)

50. UGELSTAD, J; FLOGSTAD, H; HERTZBERG, T; SUND, E
On the Bulk Polymerisation of Vinyl Chloride
Makromol Chem 164 171-181 (1973)

51. UGELSTAD, J
Model for Kinetics of Vinyl Chloride Polymerisation
J Macromol Sci-Chem A11(7) 1281-1305 (1977)

52. THIELE, R; NELLES, J; RAUCHSTEIN
Modellierung der Massepolymerisation von Vinylchlorid mit Einem Zweiphasenmodell
Plate und Kautschuk 25 (7) 395-397 (1978)

53. SURESH, A K; CHANDA, M
A New Kinetic Model for Bulk Polymerisation of Vinyl Chloride Based on Two Phase Hypothesis
Eur Polym J 18 607-616 (1982)

54. BUECHE, F J
Physical Properties of Polymers
Interscience, New York (1962)

55. BIRD, R B; STEWART, W E; LIGHTFOOT, E N
Transport Phenomena
John Wiley (1960)

56. CARACULACU, A A

P.A.C 53 (2) 385 (1981)

57. PERRY, R H; CHILTON, C H
The Chemical Engineers Handbook
McGraw Hill Koga Kusha Limited (1973)

58. CLIFT, R; GRACE, J R; WEBER, M E
Bubbles, Drops and Particles
Academic Press (1978)

59. ROGERS, G F C; MAYHEW Y R
Thermodynamic and Transport Properties of Fluids
(Third Edition)
Basil Blackwell Oxford (1980)

60. Vinyl Chloride Physical Properties
ICI Process Design Data

61. ENRIGHT, S
SDBASIC in "Optimal Second Derivative Methods for Stiff Systems" p 95
Stiff Differential Systems, R A Willoughby (Ed) Plenum Press (1973)

62. LINDBERG, B
IMPEX - A Stiff System Package Based on the Implicit Mid-Point Method with Smoothing and Extrpolation
Stiff Differential Systems, R A Willoughby (Ed) Plenum Press (1973)

63. HINDMARSH, A C; PAINTER J F
LSODI - Livermore Solver for ODE's (Implicit Form)
Mathematics and Statistical Division, L-316, Lawrence Livermore Laboratory, Livermore CA 94550

64. GEAR, C W
The Automatic Integration of Ordinary Differential Equations
Comm ACM 14 (3) p 176 (1971)

65. GEAR, C W
DIFSUB for Solution of Ordinary Differnetial Equations
Comm ACM 14 (3) p 185 (1971)

66. ROUTINE D02QBF
NAG FORTRAN Library Mark 8

67. WEST, M
Anionic Polymerisation of Dienes
PhD Thesis, Leeds (1980)

67a. BAMFORD, C H; TOMPA, H

Trans Faraday Soc 50 1097 (1954)

68. BOSWORTH, D J
The Mathematical Modelling of Gas Phase Polymerisation Reactors
PhD Thesis, Imperial College (1983)

69. LAMBERT, J D
Computational Methods in Ordinary Differential Equations
John Wiley (1973)

69a. HENRICI P
Discrete Variable Methods in Ordinary Differential Equations
John Wiley and Sons (1962)

70. GEAR, C W
Numerical Initial Value Problems in Ordinary Differential Equations
Prentice-Hall Inc (1971)

71. WEAST, R C (Ed)
Chemical Rubber Corporation Handbook of Chemistry and Physics
62nd Edition CRC (1981)

72. RAY, W H; LAURENCE, R L
"Polymerisation Reaction Engineering"
in Lapidus, L and Amundson, N R
Chemical Reactor Theory - A Review
Prentice-Hall (1977)

73. RAY, W H
On the Mathematicsl Modelling of Polymerisation Reactions
J Macromol Sci - Revs Macromol Chem C8 (1) 1-56 (1972)

74. ABRAHAM, W H
Path Dependent Distribution of Molecular Weights in Linear Polymers
I and E C Fundaments 2 (3) 221-4 (1963)

75. ABRAHAM, W H
Transient Polycondensation Calculations - An Analytic Solution
Chem Eng Sci 21 327-336 (1966)

76. SORNETTE, D; OSTROWSKY, N
Numerical Inversion of the Laplace Transform
NATO Adv Studyt Inst 75 755 (1981)

77. PIESSENS, R
Gaussian Quadrature Formulas for the Numerical Integration of Bromwich's Integral and the Inversion of the Laplace Transform
J Eng Maths 5 (1) 1-9 (1971)

78. PIESSENS, R
Gaussain Quadrature Forulas for Bromwich's Integral
Comm ACM 16 (8) 486-7 (1973)

79. BELLMAN, R E; KALABA, R E; LOCKET, J
(Book) Numerical Inversion of the Laplace Transform
American Elsevier Publishing Co, New York (1966)

80. JURY, E I
Theory and Application of the Z-Transform Method
R E Kreiger, New York, 1964 and 1973

81. GRABBE, E M; RAMO, S; WOOLDRIDGE, D E (Editors)
Handbook of Automation, Computation and Control
Volume 1, John Wiley, (1958)

82. KORN; KORN
Mathematical Handbook for Scientists and Engineers
McGraw Hill (1961)

83. CARNAHAN, B; LUTHER, H A; WILKES, J O
Applied Numerical Methods
John Wiley (1969)

84. BARRETT, K E J (Editor)
Dispersion Polymerisation in Organic Media
John Wiley & Sons (1975)

85. FITCH, R M; TSAI, C H
In Polymer Colloids
(ed Fitch, R M) Plenum Press, New York pp 73-103 (1971)

86. SMALLWOOD, P V
Unpublished data.

87. HOPFF, H; LUSSI H; HAMMER E
On the Agitation of Suspension Polymerisations
Macromol Chem 84 274 (1965)

88. CHATELAIN, J

Brit Polymer J, 5 457 (1973)

89. SHINNAR, R; CHURCH J M
Predicting Particle Size in Agitated Dispersions
Ind Eng Chem 52 3 pp 253-6 (1960)

90. SCHRODER R; PIOTROWSKI, B
On the Particle Formation During Suspension Polymerisation of Styrene
Ger Chem Eng 5 pp 139-146 (1982)

91. LAUGNER, F; MORITZ, H U; REICHERT, K H
On Particle Size of Suspension Polymers II Polymerising Two-Phase System
Ger Chem Eng 2 329 (1979)

92. CALDERBANK, P H
Physical Rate Processes in Industrial Fermentation
Trans Inst Chem Engrs (London) 36 443 (1958)

93. NAGATA, S
Mixing: Principles and Applications
John Wiley, New York (1975)

94. LEWIS, M H; JOHNSON, G R
Agitation Scale-Up Effects During VCM Suspension Polymerisation
J Vinyl Technol 3 102 (1981)

95. DANCKWERTS, P V
Significance of Liquid-Film Coefficients in Gas Adsorption
Ind Eng Chem 43 1460 (1951)

96. Akzo Chemie UK Limited Company Literature. 12-14 St Ann's Crescent, Wandsworth, London SW18

97. STEPHENSON, R
"The Effect of Agitation on Stirred Suspension Drop-Size: A Model Study" in 'Multiphase Flow Systems'
I Chem E Symp Ser 38 C4 (1974)

98. KELSALL, D G; MAITLAND, G C
"The Interaction of Process Conditions and Product Properties for PVC" in Polymer Reaction Engineering.
K H Reichert and W Geiseler (Editors). Published by Carl Hanser Verlag, Munich (1983) / MacMillan Publishing, New York

99. TOBOLSKY, A V; RODGERS, C E; BRICKMAN, R D
Dead-End Radical Polymerisation II
J Am Chem Soc 82 1277-1280 (1960)

100. BERENS, A R
The Solubility of Vinyl Chloride in Poly(Vinyl Chloride)
Polymer Preprints 15 (2) 197 (1974)

101. BERENS, A R
The Diffusion of Vinyl Chloride in Poly(Vinyl Chloride)
Polymer Preprints 15 (2) 203 (1974)

102. BERENS, A R
Vinyl Chloride Monomer in PVC: From Problem to Probe
P.A.C. 53 365-375

103. CRANK, J
The Mathematics of Diffusion (Second Edition)
O.U.P. (1975)

104. International Polymerisation Workshop on
POLYMER REACTION ENGINEERING
Berlin, Germany, Oct 5-7, 1983
Reported in:
POLYMER REACTION ENGINEERING
Influence of Reaction Engineering on Polymer Properties
edited by K H Reichert and W Geiseler
Pub Catl Hanser Verlag, Munich 1983

105. TIRRELL, M; TULIG, T J
Diffusion-Controlled Reactions in Polymers: The Influence of Polymer Concentrative and Molecular Weight in the Reaction Environment.
in (104)

106. ALLSOP, M W
Effect of Vinyl Chloride Injection on the Morphology of Suspension-Polymerised PVC
J Macromol Sci-Chem A11 (7) pp1223-34 (1977)

107. ABDEL ALIM, A H; HAMIELEC, A E
Bulk Polymerisation of VC - Commercial Initiator Systems
J Appl Poly Sci 18 1603-1609 (1974)

108. SLADKY, P; PELANT, I; PARMA L
Ultrasonic Monitoring of Suspension Polymerisation of VC
ULTRASONICS 17 (1) 32-6 (1979)

APPENDIX 3.1

SUMMARY OF LIQUID THERMODYNAMIC PROPERTIES

(SOURCES, REFS 59,60)

		20°C	50°C	70°C
Heat Capacity	Cp_{VCM}	1.418	1.461	1.494
$kJkg^{-1}K^{-1}$	Cp_{H_2O}	4.183	4.182	4.191
	$\bar{C}p$	3.738	3.744	3.757
Density	ρ_{VCM}	915.	860.	820.
kgm^{-3}	ρ_{H_2O}	998.2	988.1	977.5
	$\bar{\rho}$	985	967	952
Viscosity	μ_{VCM}	$.184 \times 10^{-3}$	$.136 \times 10^{-3}$	$.116 \times 10^{-3}$
$kgm^{-1}s^{-1}$	μ_{H_2O}	1.002×10^{-3}	$.544 \times 10^{-3}$	$.400 \times 10^{-3}$
	$\bar{\mu}$	$.870 \times 10^{-3}$	$.478 \times 10^{-3}$	$.354 \times 10^{-3}$
Thermal	k_{VCM}	$.121 \times 10^{-3}$	$.104 \times 10^{-3}$	$.091 \times 10^{-3}$
Conductivity	k_{H_2O}	$.603 \times 10^{-3}$	$.643 \times 10^{-3}$	$.662 \times 10^{-3}$
$kWm^{-1}K^{-1}$	$\bar{k}$	$.525 \times 10^{-3}$	$.556 \times 10^{-3}$	$.536 \times 10^{-3}$
Diffusivity of VCM in Water	D_{VCM,H_2O}	13.900	24.6	35.6
$10^{-10}m^2s^{-1}$				

Mean Properties given by $\bar{\rho} = \sum_i x_i P_i$, where x_i is mol fraction

For charge 1.5:1 Water:Monomer w/w $x_{VCM} = .161$

SUMMARY OF HEAT TRANSFER COEFFICIENTS

		20°C	50°C	70°C
Autoclave side $kWm^{-2}K^{-1}$	h_i	13.520	16.950	18.110
Jacket side $kWm^{-2}K^{-1}$	h_o	.869–1.504	.999–1.730	1.067–1.848
Overall $kW^{-2}K^{-1}$	U_o	.721–1.111	.819–1.253	.867–1.320
VCM droplets to Water $kWm^{-2}K^{-1}$		~87.66	~60.24	~49.00

Notes

(1) Diffusivity calculated according to Wilke–Chang Correlation (p 515, ref 55)

Diffusivity of A in B $D_{AB} = 7.4 \times 10^{-8} \frac{(\psi_B M_B)^{1/2} T}{\mu (V_A)^{.6}}$

where ψ_B = 2.6 for water

μ = solution viscosity in centipoises

M_B = molar mass of B

T = absolute temperature

V_A = molar volume of A in $cm^3 gmol^{-1}$ as liquid at the normal boiling point

(2) Autoclave side heat transfer coefficient calculated according (Equation 4-100, p 4-37, ref 57)

$$\frac{h_i d}{k}\left[\frac{\mu_s}{\mu}\right]^{.14} = .87\left[\frac{P^2 N\rho}{\mu}\right]^{2/3}\left[\frac{c\mu}{k}\right]^{1/3}$$

where d is the diameter of the autoclave

h_i is the the autoclave heat transfer coefficient

μ is the viscosity of the autoclave bulk

μ_s is the viscosity of autoclave contents at autoclave wall

P is the length of the agitator

N is the shaft speed (revolutions/unit time)

ρ is the density of the autoclave contents

C is the heat capacity of autoclave contents

and k is the thermal conductivity of the autoclave contents

(3) Jacket side heat transfer coefficient calculated according to

$$Nu = .332\ Re^{1/2}\ Pr^{1/2}$$

$$\frac{h_o d}{k} = .332\left[\frac{\rho\ u d}{\mu}\right]^{1/2}\left[\frac{\mu\ c_p}{k}\right]$$

where symbols have their conventional meaning.

(4) Overall heat transfer coefficient given by

$$\frac{1}{U_o} = \frac{1}{h_o} + \frac{b}{k}\frac{S_o}{S_{lm}} + \frac{S_o}{h_i\ S_i}$$

where S_o, S_i are the external and internal surface areas of the reactor, b is the reactor wall thickness, k is the thermal conductivity of the reactor wall and S_{lm} is the log mean area of reactor.

$$S_{lm} = (S_o - S_i)/\ln(S_o/S_i)$$

(5) Heat transfer from suspended VCM to continuous medium, calculated according to equation 5.38, reference (58).

$$K = \frac{\mu_{VCM}}{\mu_{H_2O}}$$

$$Nu = \frac{h_o\, do}{k}\left[1 - \frac{1}{Re^{1/2}}\left(2.89 + 2.15K^{0.64}\right)\right]^{1/2}(Re\ Pr)^{1/2}$$

$$Re > 10$$

$$K < 2$$

where Re,Pr are the Reynold's and Prandtl numbers of the suspended droplet. Re ~ 20.

APPENDIX 4.1

DEFINITIONS RELATING TO NUMERICAL INTEGRATION TECHNIQUES (69,70)

Convergence

A linear multistep method (4.3) is said to be convergent for all initial value problems (4.1), subject to the existence of a unique solution y(x), if

$$\lim_{\substack{h\to 0 \\ nh = x - a}} y_n = y(x_n)$$

holds for all $x \in [a,b]$ where a,b are finite real constants and for all solutions $\{y_n\}$ of the difference equation (4.3) satisfying the starting conditions

$$y_\mu = \eta_\mu(h) \text{ for which } \lim_{h\to 0} \eta(h) = \eta \quad \mu = 0(1)k - 1$$

Order and Error Constant

Define a linear difference operator, L

$$L[y(x);h] = \sum_{j=0}^{k} [\alpha_j\, y(x + jh) - h\, \beta_j\, y'(x + jh)]$$

where y(x) is an arbitrary function differentiable on [a,b]. Expanding the test functions in y,y' about (x) and collecting terms

$$L[y(x);h] = C_0\, y(x) + C_1\, h\, y'(x) + ... + C_q\, h^q\, y^q(x) + ...$$

The operator (and its associated LM method) is said to be of order p if $C_0 = C_1 = ... = C_p = 0$, $C_{p+1} \neq 0$. Through this definition, construction of specific LM methods may be achieved.

C_{p+1} is known as the error constant.

Local Truncation Error (LTE)

L.T.E. = $L[y(x_n);h]$ when $y(x)$ is the theoretical solution of the initial value problem.

The term $C_{p+1}\ h^{p+1}\ y^{p+1}(x_n)$ is called the principal location truncation error.

Global Truncation Error

The implementation of L.T.E. at a point requires that no previous truncation errors have been made: this is rarely the case, and global trunction error is defined as the difference between theoretical solution and actual solution.

$$e_{n+k} = y(x_{n+k}) - y_{n+k}$$

≡ starting error + accumulated roundoff error + accumulated local truncation error

Consistency

A linear multistep method is said to be consistent if it has order $p \geq 1$.

The First and Second Characteristics Polynomials of an LM method are defined by

$$\rho(\xi) = \sum_{j=0}^{k} \alpha_j\ \xi^j$$

$$\sigma(\xi) = \sum_{j=0}^{k} \beta_j\ \xi^j$$

A LM method is consistent if, and only if

$$\rho(1) = 0$$

$$\rho'(1) = \sigma(1)$$

Zero-Stability

A LM method is said to be zero stable if no root of the first characteristic polynomical $\rho(\xi)$ has modulus greater than one, and every root with modulus one is simple.

Convergence Theorem

The necessary and sufficient conditions for a LM method to be convergent are that it is consistent and zero stable.

(Consistency controls the magnitude of the local error test committed at each stage in the calculation, with zero stability controlling error propagation as calculation proceeds. Both are essential if convergence is to be achieved).

Absolute Stability

Absolute stability governs choice of minimum steplength required for global error to be damped out as computation proceeds, and for local truncation error to remain acceptably small. It is guaranteed for a given $\bar{h}=h\partial f/\partial y$ (with $y' = f(x,y)$) if all the roots of the stability polynomial, $\pi(r,h) = \rho(r) - h\sigma(r) = 0$, satisfy the condition $|r_s| < 1$, $s = 1(1)k$. The interval of stability (α,β) on the real line exists for a LM method if the method is stable for all $\bar{h} \in (\alpha,\beta)$.

Relative Stability

At small positive $\bar{h}$ every consistent zero-stable linear multistep method is absolutely unstable. However weak stability theory (69) tells us that the solution of the error equation:

$$\sum_{j=0}^{k} (\alpha_j - h\lambda\beta_j)\, \tilde{e}_{n+j} = \Phi_{n+k}$$

where $\phi_{n+k} \equiv T_{n+k} - R_{n+k}$

$T_{n+k} \equiv L(y(x_n);h)$ is the local truncation error

$R_{n+k} \equiv$ roundoff error made at the nth application of the method

$\tilde{e}_{n+j} \equiv y(x_n) - \tilde{y}_n$ is the global error

and $\tilde{y}_n$ is the solution when roundoff error has been made

is usually dominated by a term in r_1^n.: the error grows at a rate similar to the rate of growth of the solution.

A linear multistep is said to be relatively stable for a given $\bar{h} = h\,\partial f/\partial y$ if the roots of the stability polynomial $\pi(r,h) = \rho(r) - h\,\sigma(r)$ satisfy $|r_s| < |r_1|$ $s = 2(1)k$.

An interval (α,β) of the real line is said to be an interval of relative stability if the method is relatively stable for all $h \in (\alpha,\beta)$.

Lipschitz Condition and Constant (69a)

For

$$\frac{dy}{dx} = f(x,y) \qquad y(a) = \eta \tag{A}$$

let $f(x,y)$ be defined and continuous for all points (x,y) in the region D defined by $a \leq x \leq b$, $-\infty < y < \infty$, a and b finite, and let there exist a constant L such that, for every x,y,y^* where (x,y) and (x,y^*) are both in D.

$$|f(x,y) - f(x,y^*)| \leq L(y - y^*)$$

Then if η is any given nunmber, there exists a unique solution $y(x)$ of the initial value problem (a) where $y(x)$ is continuous and differentiable for all (x,y) in D. The constant L is known as the Lipschitz constant.

APPENDIX 5.1

PART I

CONSERVATION RELATIONSHIPS FOR PRECIPITATED POLYMER SWOLLEN BY MONOMER

When the PVC precipitates from the monomer during polymerisation, there are a number of useful relationships we can derive for both the diluent and precipitated phases.

If M_i, P_i represent the number of moles of monomer and number of moles of monomer converted to polymer respectively in phase i, the phase volumes are given by:

$$V_4 = \bar{V}_4^M M_4 + \bar{V}_4^P P_4 \qquad V_5 = \bar{V}_5^M M_5 + \bar{V}_5^P P_5 \qquad (1)$$

where the subscripts 4,5 have been retained from Chapter 3 to describe the monomeric and polymeric phases and

V_i^M, V_i^P represent the specific molar volumes of monomer and polymer respectively.

The solubilities of polymer in each phase are given by

$$\alpha_4 = \frac{P_4}{M_4 + P_4} \qquad \alpha_5 = \frac{P_5}{P_5 + M_5} \qquad (2)$$

From an overall mass balance and a definition of conversion, x

$$M_4 + M_5 + P_4 + P_5 = M_O \qquad (3)$$

$$x = \frac{P_4 + P_5}{M_O} \qquad (4)$$

where M_O is the initial number of moles of monomer in the system.

The following relationships may be deduced for the heterogeneous stage of the polymerisation.

$$M_4 = \frac{M_O(1 - \alpha_4)(\alpha_5 - x)}{(\alpha_5 - \alpha_4)} \qquad M_5 = \frac{M_O(1 - \alpha_5)(x - \alpha_4)}{(\alpha_5 - \alpha_4)} \tag{5}$$

$$P_4 = \frac{M_O\,\alpha_4\,(\alpha_5 - x)}{(\alpha_5 - \alpha_4)} \qquad P_5 = \frac{M_O\,\alpha_5\,(x - \alpha_4)}{(\alpha_5 - \alpha_4)} \tag{6}$$

and

$$V_4 = \frac{M_O\{(1 - \alpha_4)\,\bar{V}_4^M + \alpha_4\,\bar{V}_4^P\}(\alpha_5 - x)}{(\alpha_5 - \alpha_4)} \tag{7}$$

$$V_5 = \frac{M_O\{(1 - \alpha_5)\,\bar{V}_5^M + \alpha_5\,\bar{V}_5^P\}(x - \alpha_4)}{(\alpha_5 - \alpha_4)}$$

$$\alpha_4 \cong 0.0$$

Beyond $x = \alpha_5$ when the monomer phase has disappeared, the relationships become

$$M_5 = M_O(1 - x) \qquad P_5 = M_O\,x \tag{8}$$

$$V_5 = M_O\{(1 - x)\bar{V}_5^M + x\,\bar{V}_5^P\} \tag{9}$$

PART II

NERNST DISTRIBUTION CONSTANTS FOR MONOMER AND POLYMER

From equations (5), (6) and (7), the Nernst Distribution Coefficients between monomer phase (subscript 4) and basic particles (subscript 5) are easily deduced:

For monomer $\gamma_M^{45} = \frac{[M_4]}{[M_5]}$

$$= \frac{(1 - \alpha_4)/\{(1 - \alpha_4)\,\bar{V}_4^M + \alpha_4\,\bar{V}_4^P\}}{(1 - \alpha_5)/\{(1 - \alpha_5)\,\bar{V}_4^M + \alpha_5\,\bar{V}_5^P\}} \simeq 3.03 \text{ for } \alpha_4 = 10^{-3},\ \alpha_5 = .77$$

For polymer $\gamma_P^{45} = \frac{[P_4]}{[P_5]}$

$$= \frac{\alpha_4/\{(1 - \alpha_4)\,\bar{V}_4^M + \alpha_4\,\bar{V}_4^P\}}{\alpha_5/\{(1 - \alpha_5)\,\bar{V}_5^M + \alpha_5\,\bar{V}_5^P\}} \simeq 9.05 \times 10^{-4}$$

Summary

Distribution Between	Monomer and Basic Particles	Monomer and Primary Particle Surface	Primary Particle Surface and Bulk
Monomer	γ_M^{45}	$\gamma_M^{46} = \gamma_M^{45}$	$\gamma_M^{67} = 1.0$
Polymer	γ_P^{45}	$\gamma_P^{46} = \gamma_P^{45}$	$\gamma_P^{67} = 1.0$

PART III

NUMBER OF PRIMARY PARTICLES VERSUS CONVERSION

The number of primary particles, N_p, is given by

$$N_p = \frac{\text{total volume of swollen polymer at conversion, } x}{\text{volume of primary particle}} = \frac{V_5}{\frac{4}{3}\pi r^3}$$

$$= \frac{M_o\{(1 - \alpha_5)\,\bar{V}_5^M + \alpha_5\,\bar{V}_5^P\}\,(x - \alpha_4)}{(\alpha_5 - \alpha_4)\,\frac{4}{3}\pi r^3} \qquad (12) \text{ from } (7)$$

With a knowledge of the primary particle radius (from electron micrographs) and the conversion at which this is measured, the number of primary particles in the polymerising system can be calculated.

The number concentration of primary particles is given by

$$[N_p] = \frac{N_p}{V_4 + V_5} = \frac{N_p}{M_o\{p\,\bar{V}^P + (1 - p)\bar{V}^M\}} \qquad (13)$$

APPENDIX 6.1

SUMMARY OF EXPERIMENTS PERFORMED WITH THE NUMERICAL MODEL

Series	Aim of Experiment and Means of Achievement
A	Assessing Initiator Mass Transfer Effects between Primary Surface and Primary Bulk. By:- starving primary particle bulk of initiator by lowering m.t.c. between primary surface and bulk ($10^{-7}ms^{-1}$ to $10^{-15}ms^{-1}$) with (i) Fast m.t. of monomer ($10^{-3}ms^{-1}$) (ii) No m.t. of radicals ($0ms^{-1}$)
B	Assessing Initiator M.T. Effects between Monomer and Basic/Primary Surface By:- Lowering m.t.c. between monomer and basic particle or primary particle surface ($10^{-7}ms^{-1}$ to $10^{-15}ms^{-1}$) with (i) Fast m.t. of monomer ($10^{-3}ms^{-1}$) (ii) No m.t. of radicals ($0ms^{-1}$)
C	Assessing monomer M.T. effects between monomer and basic/primary surface By:- Lowering m.t.c. between monomer and basic particle or primary particle surface ($10^{-7}ms^{-1}$ to $10^{-15}ms^{-1}$) with (i) Fast m.t. of initiator ($10^{-3}ms^{-1}$) (ii) No m.t. of radicals ($0ms^{-1}$)
D	B and C combined with (i) Fast m.t. of initiator and monomer from primary surface to bulk ($10^{-3}ms^{-1}$) (ii) No m.t. of radicals ($0ms^{-1}$)

Series	Aim of Experiment and Means of Achievement
F	Assessing Radical M.T. effects between monomer and basic/ primary surface by:- lowering m.t.c. between monomer and basic particule or primary particle surface ($10^{-3}ms^{-1}$ to $10^{-13}ms^{-1}$) with (i) Fast m.t. of initiator and monomer ($10^{-3}ms^{-1}$) (ii) No m.t. of radicals from surface to bulk of primary.
H	Assessing influence of the mode of termination on molecular weight by increasing the proportion of termination due to combination. $k_t = k_{tc} + k_{td}$ (a) $k_{tc} = f\ k_t$ $f \leq 1$ (b) with (i) Fast m.t. of initiator and monomer ($10^{-3}ms^{-1}$) (ii) No m.t. of radicals (iii) Rate of chain transfer constant.
I	Assessing influence of change in rate of termination by chain transfer to monomer on molecular weight $k_{trm}^{j} = 10^{n}\ k_{trm}^{j}\|_{standard}$ (Section 5.2) with (i) Fast m.t. of initiator and monomer ($10^{-3}ms^{-1}$) (ii) No m.t. of radicals (iii) Rate of termination by combination and disproportionation constant.

Series	Aim of Experiment and Means of Achievement
K	Assessing influence of primary particle flocculation according to rule $N(x) = N_\infty + (N_O - N_\infty)e^{-\epsilon x}$ $N_O = F\ N_\infty$ with (i) Fast m.t. of initiator and monomer ($10^{-3}ms^{-1}$) (ii) Radical m.t.c. (monomer to basic particle or primary surface) $2 \times 10^{-7}ms^{-1}$ $n_\infty = 5 \times 10^{17}m^{-3}$ $F = 10,100$ $\epsilon = 0,1,10,30,50,70$
M	Effect of Variation in Initiator Distribution Coefficient (Monomer/basic particle or primary surface) coupled with initiator m.t.c. variation, with ($2 \times 10^{-7}ms^{-1}$) and without ($0ms^{-1}$) radical transfer, and with fast m.t. of monomer ($10^{-3}ms^{-1}$)

RESULTS

SERIES:- A

RUN NUMBER	MASS TRANSFER COEFFICIENTS (M/s)			INITIATOR DISTRIBUTION COEFFICIENTS			TOLERANCE IN NUMERICAL ROUTINES	CONVERSION FOR			TIME P.D. COMMENCES T_{pd} (mins)	NUMBER AVERAGE CHAIN LENGTH $\bar{\mu}_n$	WEIGHT AVERAGE CHAIN LENGTH $\bar{\mu}_w$	POLY-DISPERSITY z_p	VOIDAGE (POROSITY)	OTHER COMMENTS
								PRIMARY FORMATION $X_{p,SEG}$	PERICELLULAR MEMBRANE X_{set}	PRESSURE DROP X_{pd}						
100	10^{-3} 10^{-3} 0	10^{-3} 10^{-3} 0	10^{-7} 10^{-3} 0	1.538	1.538	1.0	10^{-8}	.5 (arbitrarily chosen)	.08 (arbitrarily chosen)	.77	257					
101			10^{-8}	"	"	"	"	"	"	"	257					
102			10^{-9}	"	"	"	"	"	"	"	257					
103			10^{-10}	"	"	"	"	"	"	"	258					
104			10^{-11}	"	"	"	"	"	"	"	262					
105			10^{-12}	"	"	"	"	"	"	"	262					
106			10^{-13}	"	"	"	"	"	"	"	262					
107			10^{-14}	"	"	"	"	"	"	"	262					
108			10^{-15}	"	"	"	"	"	"	"	262					

RESULTS

SERIES:- B

RUN NUMBER	MASS TRANSFER COEFFICIENTS (M/s)			INITIATOR DISTRIBUTION COEFFICIENTS			TOLERANCE IN NUMERICAL ROUTINES	CONVERSION FOR PRIMARY FORMATION $X_{p,SEG}$	CONVERSION FOR PERICELLULAR MEMBRANE X_{set}	CONVERSION FOR PRESSURE DROP X_{pd}	TIME P.D. COMMENCES T_{pd} (mins)	NUMBER AVERAGE CHAIN LENGTH $\bar{n}$	WEIGHT AVERAGE CHAIN LENGTH $\bar{w}$	POLY-DISPERSITY Zp	VOIDAGE (POROSITY)	OTHER COMMENTS
109	10^{-7}	10^{-7}	10^{-3}	1.538	1.538	1.0	10^{-8}	.5	.08	.77	257	875	1750	2.00		
	10^{-3}	10^{-3}	10^{-3}													
	0	0	0													
110	10^{-8}	10^{-8}		"	"	"	"	"	"	"	257	875	1750	2.00		
111	10^{-9}	10^{-9}		"	"	"	"	"	"	"	257	875	1750	2.00		
112	10^{-10}	10^{-10}		"	"	"	"	"	"	"	275	870	1740	2.00		
113	10^{-11}	10^{-11}		"	"	"	"	"	"	"	>>400	860	1720	2.00		56% conversion maximum
114	10^{-12}	10^{-12}		1.538	1.538	1.0	10^{-8}	.5	.08	.77	-	850	1700	2.0		40% maximum conversion
115	10^{-13}	10^{-13}		"	"	"	"	"	"	"	-	850	1700	2.00		"
116	10^{-14}	10^{-14}		"	"	"	"	"	"	"	-	850	1700	2.00		"
117	10^{-15}	10^{-15}		"	"	"	"	"	"	"	-	850	1700	2.00		"

RESULTS

SERIES:- C

T = 50°C

RUN NUMBER	MASS TRANSFER COEFFICIENTS (M/s)			INITIATOR DISTRIBUTION COEFFICIENTS			TOLERANCE IN NUMERICAL ROUTINES	CONVERSION FOR PRIMARY FORMATION $X_{p,SEG}$	CONVERSION FOR PERICELLULAR MEMBRANE X_{set}	CONVERSION FOR PRESSURE DROP X_{pd}	TIME P.D. COMMENCES T_{pd} (mins)	NUMBER AVERAGE CHAIN LENGTH $\bar{J}n$	WEIGHT AVERAGE CHAIN LENGTH $\bar{J}w$	POLY-DISPERSITY Z_p	VOIDAGE (POROSITY)	OTHER COMMENTS
119	10^{-3} 10^{-7} 0	10^{-3} 10^{-7} 0	10^{-3} 10^{-7} 0	1.538	1.538	1.0	10^{-6}	.5	.08	.77	257	841.4	1750	2.08		
118	10^{-8}	10^{-8}		"	"	"	"	"	"	"	257	841.4	1750	2.08		
120	10^{-9}	10^{-9}		"	"	"	"	"	"	"	269	841.4	1750	2.08		
121	10^{-10}	10^{-10}		"	"	"	"	"	"	"	-	841.5	1750	2.08		(time limit) 60% maximum conversion
122	10^{-11}	10^{-11}		"	"	"	"	"	"	"	-	834.7	1730	2.08		(time limit) 36% maximum conversion
123	10^{-12}	10^{-12}		1.538	1.538	1.0	10^{-6}	.5	.08	.77	-	822.1	1710	2.08		30% maximum conversion
124	10^{-13}	10^{-13}		"	"	"	"	"	"	"	-	822.1	1710	2.08		
125	10^{-14}	10^{-14}		"	"	"	"	"	"	"	-	822.1	1710	2.08		
126	10^{-15}	10^{-15}		"	"	"	"	"	"	"	-	822.1	1710	2.08		

RESULTS

SERIES:- D

T = 50°C

RUN NUMBER	MASS TRANSFER COEFFICIENTS (K/s)			INITIATOR DISTRIBUTION COEFFICIENTS			TOLERANCE IN NUMERICAL ROUTINES	CONVERSION FOR PRIMARY FORMATION $X_{p,SEG}$	CONVERSION FOR PERICELLULAR MEMBRANE X_{set}	CONVERSION FOR PRESSURE DROP X_{pd}	TIME P.D. COMMENCES T_{pd} (mins)	NUMBER AVERAGE CHAIN LENGTH $\bar{D}n$	WEIGHT AVERAGE CHAIN LENGTH $\bar{D}w$	POLY-DISPERSITY Z_p	VOIDAGE (POROSITY)	OTHER COMMENTS
127	10^{-7}	10^{-7}	10^{-3}	1.538	1.538	1.0	10^{-6}	.5	.08	.77	258	892.3	1807	2.029	37.96	
	10^{-7}	10^{-7}	10^{-3}													
	0	0	0													
128.1	10^{-8}	10^{-8}		"	"	"	"	"	"	"	258	892.3	1807	2.029	37.76	
	10^{-8}	10^{-8}														
129	10^{-9}	10^{-9}		"	"	"	"	"	"	"	257	891.3	1799	2.023	37.78	time limit Ox = .99
	10^{-9}	10^{-9}														
130.1	10^{-10}	10^{-10}		"	"	"	"	"	"	"	388	888.7	1784	2.008	37.06	
	10^{-10}	10^{-10}														
131.2	10^{-11}	10^{-11}		"	"	"	"	"	"	"	-	873.4	1744	1.996	63.68	maximum conversion 52%
	10^{-11}	10^{-11}														
132.1	10^{-12}	10^{-12}		1.538	1.538	1.0	10^{-6}	.5	.08	.77	-	870.9	1738	1.996	72.87	46%
	10^{-12}	10^{-12}														
133	10^{-13}	10^{-13}		"	"	"	"	"	"	"	-	870.7	1738	1.996	74.10	
	10^{-13}	10^{-13}														
134	10^{-14}	10^{-14}		"	"	"	"	"	"	"	-	870.7	1738	1.996	74.25	
	10^{-14}	10^{-14}														
135	10^{-15}	10^{-15}		"	"	"	"	"	"	"	-	870.7	1738	1.996	74.27	
	10^{-15}	10^{-15}														

RESULTS

SERIES:- F

T = 50°C

RUN NUMBER	MASS TRANSFER COEFFICIENTS (M/s)			INITIATOR DISTRIBUTION COEFFICIENTS			TOLERANCE IN NUMERICAL ROUTINES	CONVERSION FOR			TIME P.D. COMMENCES T_{pd} (mins)	NUMBER AVERAGE CHAIN LENGTH $\bar{n}$	WEIGHT AVERAGE CHAIN LENGTH $\bar{w}$	POLY-DISPERSITY z_p	VOIDAGE (POROSITY)	OTHER COMMENTS
								PRIMARY FORMATION $X_{p,SEG}$	PERICELLULAR MEMBRANE X_{set}	PRESSURE DROP X_{pd}						
161	10^{-3}	10^{-3}	10^{-3}	1.538	1.538	1.0	10^{-6}	.17%	.08	.77	158	903.1	1804	1.997	36.28	
	10^{-3}	10^{-3}	10^{-3}													
	10^{-3}	10^{-3}	0													
160				"	"	"	"	.34%	"	"	152	904.1	1806	1.997	36.25	
	10^{-4}	10^{-4}														
159.1				"	"	"	"	.43%	"	"	145	905.2	1808	1.997	36.23	
	10^{-5}	10^{-5}														
158				"	"	"	"	.42%	"	"	171	901.8	1801	1.997	36.24	
	10^{-6}	10^{-6}														
180				"	"	"	"	.40%	"	"	176	901.2	1800	1.997	36.23	
	8×10^{-7}	8×10^{-7}														
179				1.538	1.538	1.0	10^{-6}	.40%	.08	.77	189	900.1	1798	1.997	36.25	
	9×10^{-7}	9×10^{-7}														
178				"	"	"	"	.41%	"	"	214	898.1	1794	1.997	36.24	
	2×10^{-7}	2×10^{-7}														

RESULTS

SERIES 1 - F (CONT)

T = 50°C

RUN NUMBER	MASS TRANSFER COEFFICIENTS (M/s)			INITIATOR DISTRIBUTION COEFFICIENTS			TOLERANCE IN NUMERICAL ROUTINES	CONVERSION FOR PRIMARY FORMATION $X_{p,SEG}$	CONVERSION FOR PERICELLULAR MEMBRANE X_{set}	CONVERSION FOR PRESSURE DROP X_{pd}	TIME P.D. COMMENCES T_{pd} (mins)	NUMBER AVERAGE CHAIN LENGTH $\bar{l}n$	WEIGHT AVERAGE CHAIN LENGTH $\bar{l}w$	POLY-DISPERSITY Z_p	VOIDAGE (POROSITY)	OTHER COMMENTS
157.1				"	"	"	"	.40%	"	"	231	897.1	1792	1.997	36.21	
	10^{-7}	10^{-7}														
156.1				"	"	"	"	.41%	"	"	254	896.1	1790	1.997	36.22	
	10^{-8}	10^{-8}														
141	10^{-9}	10^{-9}	10^{-9}	"	"	"	"	"	"	"	257	892.5	1806	2.029	37.96	
	10^{-9}	10^{-9}	10^{-9}													
	10^{-9}	10^{-9}	0													
142				"	"	"	"	"	"	"	258	892.6	1806	2.028	37.91	
	10^{-10}	10^{-10}	0													
143				"	"	"	"	"	"	"	258	892.6	1806	2.028	37.90	
	10^{-11}	10^{-11}	0													
144				"	"	"	"	"	"	"	258	892.7	1806	2.028	37.93	
	10^{-12}	10^{-12}	0													
145				"	"	"	"	"	"	"	258	892.6	1806	2.028	37.88	
	10^{-13}	10^{-13}	0													

RESULTS

SERIES:- H

T = 50°C

RUN NUMBER	MASS TRANSFER COEFFICIENTS (M/s)			INITIATOR DISTRIBUTION COEFFICIENTS			TOLERANCE IN NUMERICAL ROUTINES	CONVERSION FOR			TIME P.D. COMMENCES T_{pd} (mins)	NUMBER AVERAGE CHAIN LENGTH $\bar{\nu}_n$	WEIGHT AVERAGE CHAIN LENGTH $\bar{\nu}_w$	POLY-DISPERSITY Z_p	VOIDAGE (POROSITY)	OTHER COMMENTS
								PRIMARY FORMATION $X_{p,SEG}$	PERICELLULAR MEMBRANE X_{set}	PRESSURE DROP X_{pd}						
162	10^{-3}	10^{-3}	10^{-3}	1.538	1.538	1.0	10^{-6}	.4%	.08	.77	258	883.6	1766	1.998	36.23	$k_{tc} = 0k_t$
	10^{-3}	10^{-3}	10^{-3}													
	0	0	0													
163				"	"	"	"	"	"	"	258	888.4	1775	1.998	36.22	$k_{tc} = .2k_t$
164				"	"	"	"	"	"	"	258	893.3	1785	1.998	36.23	$k_{tc} = .4k_t$
165				"	"	"	"	"	"	"	258	898.3	1794	1.997	36.21	$k_{tc} = .6k_t$
166				"	"	"	"	"	"	"	258	903.4	1804	1.996	36.21	$k_{tc} = .8k_t$
167				"	"	"	10^{-8}	"	"	"	258	908.5	1813	1.996	36.23	$k_{tc} = k_t$

RESULTS

SERIES:- I

T = 50°C

RUN NUMBER	MASS TRANSFER COEFFICIENTS (K/s)			INITIATOR DISTRIBUTION COEFFICIENTS			TOLERANCE IN NUMERICAL ROUTINES	CONVERSION FOR			TIME P.D. COMMENCES T_{pd} (mins)	NUMBER AVERAGE CHAIN LENGTH $\bar{n}$	WEIGHT AVERAGE CHAIN LENGTH $\bar{w}$	POLY-DISPERSITY z_p	VOIDAGE (POROSITY)	OTHER COMMENTS
								PRIMARY FORMATION $X_{p,SEG}$	PERICELLULAR MEMBRANE X_{eet}	PRESSURE DROP X_{pd}						
168	10^{-3}	10^{-3}	10^{-3}	1.538	1.538	1.0	10^{-6}	.4%	.08	.77	255	94.72	187.4	1.979	36.27	10 x k_{trm}]
	10^{-3}	10^{-3}	10^{-3}													
	0	0	0													
102	10^{-3}	10^{-3}	10^{-3}	"	"	"	"	"	"	"	258	895		1.979		k_{trm}]
	10^{-3}	10^{-3}	10^{-3}													
	0	0	0													
169				"	"	"	"	"	"	"	258	6410	13010	1.979	36.27	$10^{-1}k_{trm}$]
		168														
170				"	"	"	"	"	"	"	258	19810	57800	2.595	36.23	$10^{-2}k_{trm}$]
		168														
171				"	"	"	"	"	"	"	258	26390	125500	3.815	36.27	$10^{-3}k_{trm}$]
		168														

RESULTS

SERIES:- K

$T = 50°C$

RUN NUMBER	MASS TRANSFER COEFFICIENTS (M/s)			INITIATOR DISTRIBUTION COEFFICIENTS			TOLERANCE IN NUMERICAL ROUTINES	CONVERSION FOR PRIMARY FORMATION $X_{p,SEG}$	CONVERSION FOR PERICELLULAR MEMBRANE X_{set}	CONVERSION FOR PRESSURE DROP X_{pd}	TIME P.D. COMMENCES T_{pd} (mins)	NUMBER AVERAGE CHAIN LENGTH $\bar{\mu}_n$	WEIGHT AVERAGE CHAIN LENGTH $\bar{\mu}_w$	POLY-DISPERSITY z_p	VOIDAGE (POROSITY)	OTHER COMMENTS
181	10^{-3} / 10^{-3} / 2×10^{-7}	10^{-3} / 10^{-3} / 2×10^{-7}	10^{-3} / 10^{-3} / 0	1.538	1.538	1.0	10^{-6}	.98%	.08	.77	194	899.7	1797	1.997	36.25%	F = 10 ϵ = 0
182	"	"	"	"	"	"	"	1.0%	"	"	195	899.7	1797	1.997	36.27%	F = 10 ϵ = 1
183	"	"	"	"	"	"	"	.98%	"	"	207	898.8	1796	1.997	36.23%	F = 10 ϵ = 10
184	"	"	"	"	"	"	"	.83%	"	"	212	898.14	1795	1.997	36.21%	F = 10 ϵ = 30
185	"	"	"	"	"	"	"	.86%	"	"	213	898.2	1794	1.997	36.23	F = 10 ϵ = 50
186	"	"	"	"	"	"	"	.70%	"	"	214	898.2	1794	1.997	36.25	F = 10 ϵ = 70
187	"	"	"	"	"	"	"	.82%	"	"	174	901.5	1801	1.997	36.25	F = 100 ϵ = 0
188	"	"	"	"	"	"	"	.79%	"	"	176	901.4	1801	1.997	36.21	F = 100 ϵ = 1
189	"	"	"	"	"	"	"	.51%	"	"	192	900.3	179.8	1.997	36.24	F = 100 ϵ = 10
190	"	"	"	"	"	"	"	3.4%	"	"	206	899.0	1796	1.997	36.22	F = 100 ϵ = 30
191	"	"	"	"	"	"	"	2.7%	"	"	210	898.6	1795	1.997	36.22	F = 100 ϵ = 50
192	"	"	"	"	"	"	"	2.15%	"	"	211	898.4	1795	1.997	36.24	F = 100 ϵ = 70

RESULTS

SERIES:- M

T = 50°C

RUN NUMBER	MASS TRANSFER COEFFICIENTS (M/s)			INITIATOR DISTRIBUTION COEFFICIENTS			TOLERANCE IN NUMERICAL ROUTINES	CONVERSION FOR PRIMARY FORMATION $X_{p,SEG}$	CONVERSION FOR PERICELLULAR MEMBRANE X_{set}	CONVERSION FOR PRESSURE DROP X_{pd}	TIME P.D. COMMENCES T_{pd} (mins)	NUMBER AVERAGE CHAIN LENGTH $\bar{l}n$	WEIGHT AVERAGE CHAIN LENGTH $\bar{l}w$	POLY-DISPERSITY Zp	VOIDAGE (POROSITY)	OTHER COMMENTS
193	10^{-3}	10^{-3}	10^{-3}	1.0	1.0	1.0	10^{-6}	.41	.08	.77	205	898.9	1796	1.997	36.24	M1
	10^{-3}	10^{-3}	10^{-3}													
	2×10^{-7}	2×10^{-7}	0													
194				1.3	1.3	1.0	"	.42	"	"	211	898.4	1795	1.997	36.22	M1
195				1.9	1.9	1.0	"	.40	"	"	219	897.8	1793	1.997	36.25	M1
196				2.2	2.2	1.0	"	.40	"	"	223	897.6	1793	1.997	36.21	M1
197	0.5×10^{-3}	10^{-10}	10^{-3}	1.0	1.0	1.0	10^{-6}	.40	.08	.77	224	897.4	1793	1.997	36.21	M2
	10^{-3}	10^{-3}	10^{-3}													
	2×10^{-7}	2×10^{-7}	0													
198				1.3	1.3	1.0	"	.41	"	"	226	897.3	1792	1.997	36.25	M2
199				1.9	1.9	1.0	"	.41	"	"	230	897.0	1792	1.997	36.25	M2
200				2.2	2.2	1.0	"	.40	"	"	231	897.0	1797	1.997	36.22	M2

RESULTS

SERIES:- M

T = 50°C

RUN NUMBER	MASS TRANSFER COEFFICIENTS (M/s)			INITIATOR DISTRIBUTION COEFFICIENTS			TOLERANCE IN NUMERICAL ROUTINES	CONVERSION FOR			TIME P.D. COMMENCES T_{pd} (mins)	NUMBER AVERAGE CHAIN LENGTH μ_n	WEIGHT AVERAGE CHAIN LENGTH μ_w	POLY-DISPERSITY Z_p	VOIDAGE (POROSITY)	OTHER COMMENTS
								PRIMARY FORMATION $X_{p,SEG}$	PERICELLULAR MEMBRANE X_{set}	PRESSURE DROP X_{pd}						
201	.8 x 10^{-3}	10^{-10}	10^{-3}	1.0	1.0	1.0	10^{-6}	.40	.08	.77	218	897.7	1793	1.997	36.26	M3
	10^{-3}	10^{-3}	10^{-3}													
	2 x 10^{-7}	2 x 10^{-7}	0													
202				1.3	1.3	1.0	"	.40	"	"	222	897.6	1793	1.997	36.23	M3
203				1.9	1.9	1.0	"	.40	"	"	226	897.3	1792	1.997	36.28	M3
204				2.2	2.2	1.0	"	.41	"	"	228	897.1	1792	1.997	36.25	M3
205	.2 x 10^{-3}	10^{-8}	10^{-3}	1.0	1.0	1.0	10^{-6}	.41	.08	.77	211	898.3	1794	1.997	36.23	M4
	10^{-3}	10^{-3}	10^{-3}													
	2 x 10^{-7}	2 x 10^{-7}	0													
206				1.3	1.3	1.0	"	.41	"	"	216	898.0	1794	1.997	36.18	M4
207				1.9	1.9	1.0	"	.41	"	"	222	897.6	1793	1.997	36.25	M4
208				2.2	2.2	1.0	"	.40	"	"	225	897.4	1793	1.997	36.25	M4

RESULTS

SERIES:- M

T = 50°C

RUN NUMBER	MASS TRANSFER COEFFICIENTS (M/s)			INITIATOR DISTRIBUTION COEFFICIENTS			TOLERANCE IN NUMERICAL ROUTINES	CONVERSION FOR PRIMARY FORMATION $X_{p,SEG}$	CONVERSION FOR PERICELLULAR MEMBRANE X_{set}	CONVERSION FOR PRESSURE DROP X_{pd}	TIME P.D. COMMENCES T_{pd} (mins)	NUMBER AVERAGE CHAIN LENGTH $\bar{P}n$	WEIGHT AVERAGE CHAIN LENGTH $\bar{P}w$	POLY-DISPERSITY Z_p	VOIDAGE (POROSITY)	OTHER COMMENTS
209	$.7 \times 10^{-3}$	10^{-9}	10^{-3}	1.0	1.0	1.0	10^{-6}	.41	.08	.77	225	898.7	1795	1.997	36.26	MS
	10^{-3}	10^{-3}	10^{-3}													
	2×10^{-7}	2×10^{-7}	0													
210				1.3	1.3	1.0	"	.41	"	"	212	898.2	1793	1.997	36.24	MS
211				1.9	1.9	1.0	"	.41	"	"	220	897.7	1793	1.997	36.25	MS
212				2.2	2.2	1.0	"	.41	"	"	223	897.5	1793	1.997	36.22	MS

RESULTS

SERIES:- N

T = 50°C

RUN NUMBER	MASS TRANSFER COEFFICIENTS (M/s)			INITIATOR DISTRIBUTION COEFFICIENTS			TOLERANCE IN NUMERICAL ROUTINES	CONVERSION FOR			TIME P.D. COMMENCES T_{pd} (mins)	NUMBER AVERAGE CHAIN LENGTH $\bar{\nu}_n$	WEIGHT AVERAGE CHAIN LENGTH $\bar{\nu}_w$	POLY-DISPERSITY z_p	VOIDAGE (POROSITY)	OTHER COMMENTS
								PRIMARY FORMATION $X_{p,SEG}$	PERICELLULAR MEMBRANE X_{set}	PRESSURE DROP X_{pd}						
217	.5 x 10^{-3}	10^{-10}	10^{-3}	1.0	1.0	1.0	10^{-6}	.40	.08	.77	278	894.9	1788	1.997	36.24	M2A
	10^{-3}	10^{-3}	10^{-3}													
	2 x 10^{-7}	2 x 10^{-7}	0													
218				1.3	1.3	1.0	"	.40	"	"	286	894.6	1787	1.997	36.24	M2A
219				1.9	1.9	1.0	"	.41	"	"	301	894.0	1786	1.997	36.21	M2A
220				2.2	2.2	1.0	"	.40	"	"	308	893.9	1786	1.998	36.21	M2A
221	.8 x 10^{-3}	10^{-10}	10^{-3}	1.0	1.0	1.0	10^{-6}	.40	.08	.77	264	895.5	1789	1.997	36.25	M3A
	10^{-3}	10^{-3}	10^{-3}													
	2 x 10^{-7}	2 x 10^{-7}	0													
222				1.3	1.3	1.0	"	.40	"	"	274	895.5	1788	1.997	36.25	M3A
223				1.9	1.9	1.0	"	.40	"	"	290	894.4	1787	1.997	36.25	M3A
224				2.2	2.2	1.0	"	.4	"	"	298	894.1	1786	1.997	36.23	M3A

RESULTS

SERIES:- M

T = 50°C

RUN NUMBER	MASS TRANSFER COEFFICIENTS (M/s)			INITIATOR DISTRIBUTION COEFFICIENTS			TOLERANCE IN NUMERICAL ROUTINES	CONVERSION FOR			TIME P.D. COMMENCES T_{pd} (mins)	NUMBER AVERAGE CHAIN LENGTH $\bar{l}_n$	WEIGHT AVERAGE CHAIN LENGTH $\bar{l}_w$	POLY-DISPERSITY I_p	VOIDAGE (POROSITY)	OTHER COMMENTS
								PRIMARY FORMATION $X_{p,SEG}$	PERICELLULAR MEMBRANE X_{set}	PRESSURE DROP X_{pd}						
225	.2 x 10^{-6}	10^{-5}	10^{-5}	1.0	1.0	1.0	10^{-6}	.43	.08	.77	248	896.4	1791	1.997	36.23	M4A
	10^{-5}	10^{-5}	10^{-5}													
	2 x 10^{-7}	2 x 10^{-7}	0													
226				1.3	1.3	1.0	"	.40	"	"	260	895.8	1789	1.997	36.24	M4A
227				1.9	1.9	1.0	"	.41	"	"	279	894.9	1788	1.997	36.24	M4A
227.1				2.2	2.2	1.0	"	.41	"	"	287	894.5	1787	1.997	36.23	M4A
228	.7 x 10^{-6}	10^{-5}	10^{-5}	1.0	1.0	1.0	10^{-6}	.40	.08	.77	240	896.8	1791	1.997	36.24	M5A
	10^{-5}	10^{-5}	10^{-5}													
	2 x 10^{-7}	2 x 10^{-7}	0													
229				1.3	1.3	1.0	"	.40	"	"	252	896.2	1790	1.997	36.26	M5A
230				1.9	1.9	1.0	"	.41	"	"	273	895.1	1788	1.997	36.21	M5A
231				2.2	2.2	1.0	"	.40	"	"	282	894.7	1787	1.997	36.21	M5A

APPENDIX 6.2

Conditions of Temperature and Pressure observed in practice in autoclaves manufacturing PVC by a suspension process

(i) Autoclave 1

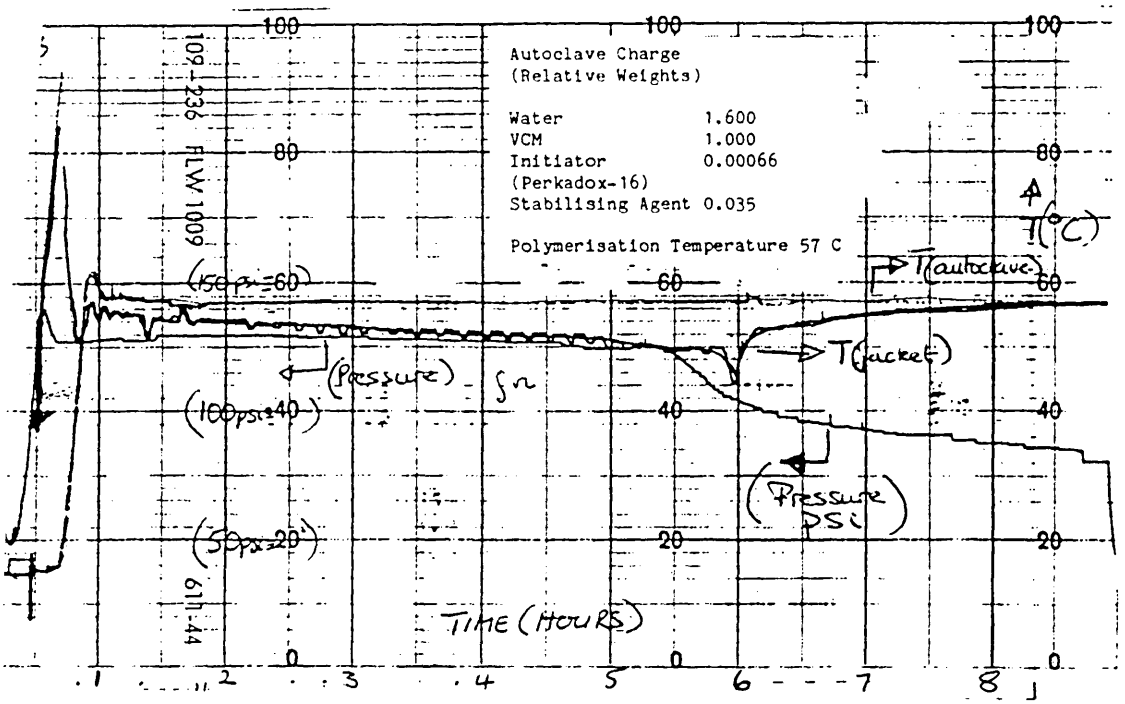

(ii) Autoclave 2

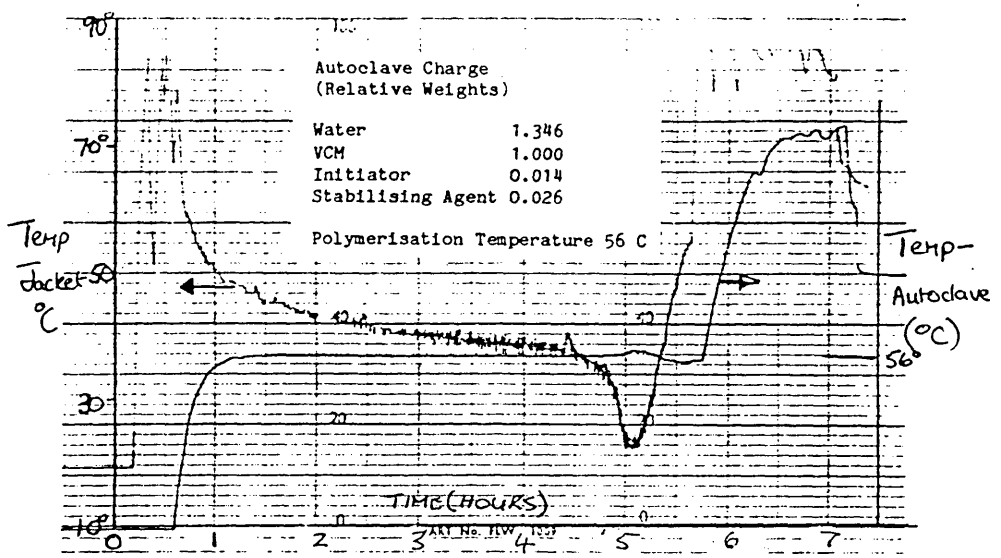

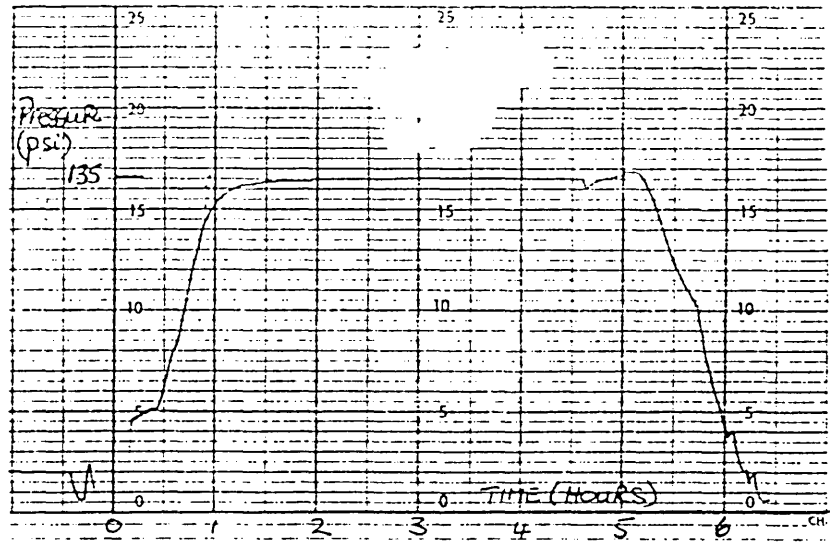
Pressure
(psi)
135
25
20
15
10
5
0
TIME (HOURS)
0
1
2
3
4
5
6
CH.

LIST OF SYMBOLS

Subscripts or Superscripts

l,L	liquid phase
m,M	monomer phase
p,P	polymer phase
pd	pressure drop
s	surface value
1	Vapour Phase
2	Aqueous (Continuous Phase)
3	VCM Droplet Surface Phase
4	Continuous Monomer Phase with droplet/subgrain
5	Microgel Phase (Basic Particles)
6	Primary Particle Surface Phase
7	Primary Particle Bulk PHase
0	initial condition

Dimensionless Groups

Gr	Grashoff Number	(eq 5.25, p153)
Sc	Schmidt Number	(eq 5.25, p153)
Sh	Sherwood Number	(eq 5.25, p153)
We	Weber Number	(p45)

α, β, γ, δ, ϵ, ϕ, η, τ, defined and used in Chapter 3.5

[] denotes concentration of species

a	distance between primary particle centres (m)
A	interfacial area (m^2)
c	coordination number
c_p	specific heat capacity ($Jkg^{-1}K^{-1}$)
c_m	chain transfer coefficient (k_{trm}/k_p)
c_{ij}	concentration of species i in phase j ($kmolm^{-3}$)
d	particle or vessel diameter (m)
D	diffusion coefficient (m^2s^{-1})
D_L', D_L	diffusion coefficients for radical absorption/desorption
E_A	activation energy ($Jmol^{-1}$)
Ep	activation energy for propagation rate constant ($Jmol^{-1}$)

E_{trm}	activation energy for transfer to monomer rate constant ($Jmol^{-1}$)
f	initiator efficiency
f	arbitrary function
F	mass flowrate (kgs^{-1})
G	Gibbs Free Energy
$G_p(s,t)$	generating function for dead polymer M.W.D.
$G_R(s,t)$	generating function for growing radicals M.W.D.
h	local heat transfer coefficient, steplength
H	Henry's Law Constant
H(t)	Heaviside Function
I	Initiator
I	Unit Matrix
j_i	mass flux of species i
J	Jacobian matrix
k,K	arbitrary constants
k_D, k_i	Initiator decomposition rate constant ($kmols^{-1}$)
k_p, k_{wo}	Propagation rate constant ($m^3kmol^{-1}s^{-1}$)
k_t, k_{ao}	termination rate constant ($m^3kmol^{-1}s^{-1}$)
k_{td}	termination by disproportionation rate constant
k_{tc}	termination by combustion rate constant
k_{trm}, k_{uo}	termination by transfer to monomer rate constant
k_{trp}	termination by transfer to polymer
k_a, k_{a-1}	absorption/desorption coefficients for radicals
k_I, k_o	mass transfer coefficient
k	thermal conductivity ($Wm^{-2}K^{-1}$)
k_j	integration functions
k_{Ai}^{jk}	mass transfer coefficient for species i passing from phase j to phase k (ms^{-1})
K_{OG}	overall mass transfer coefficients
L	Lipschitz constant
m	degree of polymerisation (chain length) or polymer
M	Monomer
N	number of particles
$n_{i(j)}$	number of moles of species i (in phase j)
$\underline{N_i}$	flux of i through surface of phase
$\underline{n}$	unit normal vector to phase surface

$\underline{n_j}$ vector representating mass of species in each phase
$= [n_{ij}, n_{mj}, n_{\sigma oj}, n_{\sigma 1j}, n_{\sigma 2j}, n_{\lambda oj}, n_{\lambda 1j}, n_{\lambda 2j}]^T$

Ns stirrer speed (rpm)

p proportion of termination reactions due to disproportionation

P conversion

P_A, P_l solution vapour pressure

P_{AO}, P_{lO} saturated vapour pressure of pure substance

P dead polymer of chain length x monomer units

q heat flux (Wm^{-2})

R Universal Gas Constant (8.314 $Jmol^{-1}k^{-1}$)

r,R radius

r_i rate of formation of i

r_r rate per unit volume

R_p rate of polymerisation in polymer phase

R_m rate of polymerisation in monomer phase

$R_x\cdot$ Radical of chain length x

S surface area

s generating function variable

T temperature

t time

u overall heat transfer coefficient

V_p rate of polymerisation (eq 2.6.1)

$V_{(j)}$ volume (of phase j)

$\underline{v}$ velocity

V_i^j partial molar volume of i in phase j (per monomer unit in polymer phases)

w_o^i rate of initiator

x conversion

x_b, x_i, x_i^* bulk, interface, equilibrium molefractions in phase being transferred to

x_{bppte} conversion when basic particles nucleate

x_{pseg} conversion when primary particles form

x_{set} conversion when droplets stop contracting with conversion

y_b, y_i, y_i^* bulk, interface, equilibrium mole fractions in phase transferred from

z_p polydispersity = weight average chain length/number average chain length

α_j	integration constants, mass fraction of polymer in phase j
β_j	integration constant
γ_{ij}	= $[C_i]/[C_j]$ local Nermst Equilibrium/Partition constant
δ	thickness of shell
ϵ	rate
λ_i	ith moment of dead polymer molecular weight distribution, eigenvalues
λ_0	zeroth moment of dead polymer M.W.D.
λ_1	first moment of dead polymer M.W.D.
λ_2	second moment of dead polymer M.W.D.
μ_w	weight average chain length = λ_2/λ_1
μ_n	number average chain length = λ_1/λ_0
ν_i	density ratio (monomer:polymer) in phase i
ρ_i	mass of species i
σ_0	zeroth moment of growing chain M.W.D.
σ_1	first moment of growing chain M.W.D.
σ_2	second moment of growing chain M.W.D.
ϕ	porosity, volume fraction
χ	Flory Interaction Parameter

Other symbols may be more locally defined in the text.